Studies on polymer derived SiC based ceramics and ceramic matrix composites for high temperature applications

Thesis submitted to
Cochin University of Science and Technology
in partial fulfilment of the requirements for
the award of the degree of

Doctor of Philosophy
in
Chemistry

Under the Faculty of Science

by

Ganesh Babu T.
Reg. No. 4941

Ceramic Matrix Products Division
Analytical Spectroscopy and Ceramics Group
Propellants, Polymers, Chemicals & Materials Entity
Vikram Sarabhai Space Centre
Indian Space Research Organisation
Thiruvananthapuram, Kerala, India-695 022

December 2017

Studies on polymer derived SiC based ceramics and ceramic matrix composites for high temperature applications

Ph. D. Thesis under the Faculty of Science,
Cochin University of Science and Technology

Author:

GANESH BABU T.
Senior Research Fellow
Ceramic Matrix Products Division
Propellants, Polymers, Chemicals & Materials Entity
Vikram Sarabhai Space Centre
Thiruvananthapuram-695 022
E mail: ganeshbabut@gmail.com

Research Guide:

Dr. RENJITH DEVASIA
Scientist/Engineer-SF
Ceramic Matrix Products Division
Propellants, Polymers, Chemicals & Materials Entity
Vikram Sarabhai Space Centre
Thiruvananthapuram-695 022
E mail: renjithdevasia@gmail.com

Propellants, Polymers, Chemicals & Materials Entity
Vikram Sarabhai Space Centre
Thiruvananthapuram-695022, INDIA

December 2017

.....to, my parents

01 August 2018

CERTIFICATE

This is to certify that the work embodied in the thesis entitled "**Studies on polymer derived SiC based ceramics and ceramic matrix composites for high temperature applications**", submitted by **Mr. Ganesh Babu T.** in partial fulfilment of the requirements for the degree of Doctor of Philosophy in Chemistry to Cochin University of Science and Technology, is an authentic and bonafide record of the original research work carried out by him, under my supervision at the Ceramic Matrix Products Division (CMPD), Analytical Spectroscopy and Ceramics Group (ASCG), Propellants, Polymers, Chemicals & Materials Entity (PCM), Vikram Sarabhai Space Centre, Thiruvananthapuram. Further, the results embodied in this thesis, in full or in part, have not been submitted previously for the award of any other degree in any University/Institution. All the relevant corrections and modifications suggested by the audience during the Pre-synopsis Seminar and recommended by the Doctoral Committee have been incorporated in the thesis.

Dr. Renjith Devasia
Scientist 'SF'
Ceramic Matrix Products Division
Analytical Spectroscopy and Ceramics Group
Propellants, Polymers, Chemicals & Materials Entity
(Research Guide)

DECLARATION

I hereby declare that the work presented in this thesis entitled **"Studies on polymer derived SiC based ceramics and ceramic matrix composites for high temperature applications",** is the outcome of the original research work carried out by me under the guidance of Dr. Renjith Devasia., Scientist-SF, Ceramic Matrix Products Division (CMPD), Analytical Spectroscopy and Ceramics Group (ASCG), Propellants, Polymers, Chemicals & Materials Entity (PCM), Vikram Sarabhai Space Centre, Thiruvananthapuram. Further the results embodied in this thesis, in full or in part, have not been included in any other thesis/dissertation submitted previously for the award of any degree, diploma, associateship, or any other title, recognition from any University/Institution.

Thiruvananthapuram   **Ganesh Babu T.**

01 August 2018

smoothly paved my path towards the successful completion of this research work. Besides this, I bow my head to the people who has helped me knowingly and un-knowingly to reach this milestone in my life.

<div align="right">Ganesh Babu T.</div>

Table of Contents

Chapter 3 Studies on boron modified phenol-formaldehyde (BPF) as preceramic matrix resin for CMCs

Chapter 3.1 Synthesis, characterization and ceramic conversion studies of BPF resins

Chapter 3.2 Fabrication and characterization of CMCs using BPF as matrix resin.. 97

Chapter 4 Studies on silazane modified phenol-formaldehyde (SPF) as preceramic   matrix   resin   for CMCs...111

List of Figures

List of Tables

Symbols and Abbreviations

β	Full width at half maximum measured in radians
δ	Chemical Shift
θ	Bragg's angle
λ	Wavelength of X-ray radiation equal to 1.5406 Å
ρ	Density
σ_f	Flexural strength
$\bar{M}_w$	Weight average molecular weight
$\bar{M}_n$	Number average molecular weight
2D	Two dimension
BC	Boron-carbon containing ceramics
BCTS	Boron modified cyclotrisilazane
BPF	Boron modified phenol-formaldehyde
BPFSi	Boron modified phenol formaldehyde resin blended with silicon powder
CFRP	Carbon fiber reinforced polymer matrix composites
CMC	Ceramic matrix composite
CTS	1, 3, 5-trimethyl-1´, 3´, 5´-trivinylcyclotrisilazane
CVI	Chemical vapor infiltration
d	Interplanar distance
D	Average crystallite size
D-band	Distorted carbon band
DCP	Dicumyl peroxide
DMF	N, N-dimethylformamide
EBC	Environmental barrier coatings
EDX	Energy Dispersive X-ray
E_f	Flexural modulus
F/M	Fiber/matrix
F-CVI	Thermal gradient-forced flow-chemical vapor infiltration
FESEM	Felid emission Scanning electron microscopy
FFT	Fast Fourier Transformer
FTIR	Fourier Transform-Infra Red
FWHM	Full width at half maximum
G-band	Graphitic carbon band
GPC	Gel permeation chromatography
h-BN	Hexagonal-boron nitride
HM	High-modulus
HMTA	Hexamethylenetetramine
HRTEM	High-resolution Transmission electron microscopy
HT	High-tensile
I_A	Area of the interface
I_D	Intensity ratio of the D-band
IF-CVI	Isothermal-forced flow-chemical vapor infiltration
I_G	Intensity ratio of the G-band
IM	Intermediate-modulus

k	Coefficient, which is generally taken as 0.94
L_a	Size of carbon domains along the six-fold ring plane
LSI	Liquid silicon infiltration
m_o	Initial weight of ceramic or ceramic matrix composite
MTS	Methyltrichlorosilane
NMR	Nuclear Magnetic Resonance
PAN	Polyacrylonitrile
PCTS	Polycyclotrisilazane
P-CVI	Pulsed flow-chemical vapor infiltration
PF	Phenol-formaldehyde
PIP	Polymer impregnation/infiltration and pyrolysis
pph	Parts per hundred
PVC	Polyvinylchloride
PyC	Pyrocarbon
Py–GC–MS	Pyrolysis–gas chromatography–mass spectrometry
RBSC	Reaction bonded silicon carbide
RMI	Reactive Melt Infiltration
SAED	Selected area electron diffraction
SEM	Scanning electron microscopy
SiBCN	Silicon boron carbonitride
SiBOC	Silicon boron oxycarbide
SiC	Silicon carbide
SiCN	Silicon carbonitride
SPF	Silazane modified phenol formaldehyde
TBC	Thermal barrier coatings
TGA	Thermogravimetric analysis
TG-CVI	Temperature gradient-chemical vapor infiltration
THF	Tetrahydrofuran
UHM	Ultra-high-modulus
V	Volume of composite
V_f	Fiber volume fraction
VLS	Vapor-liquid-solid
VS	Vapor-solid
VV	Vapor-vapor
XRD	X-Ray Diffraction

Chapter 1

Introduction

Ceramic Matrix Composite (CMC)

Fiber

Interphase coating

Matrix
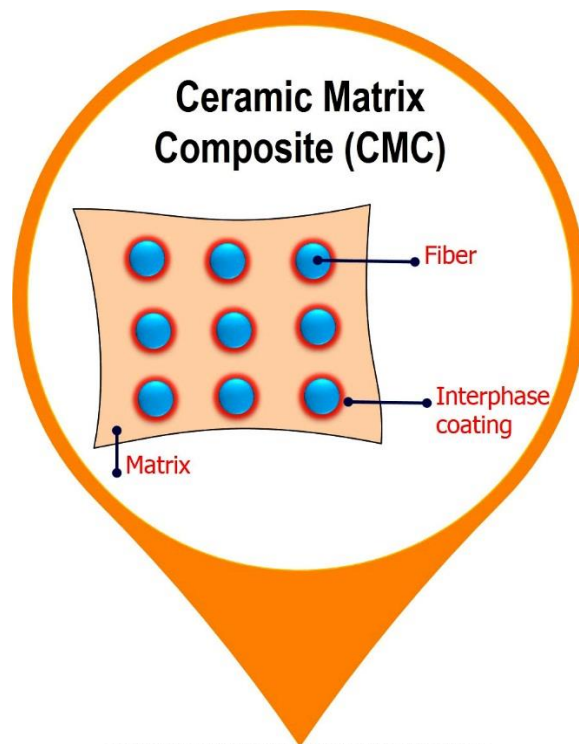
This chapter gives a general introduction on CMCs such as,

- Design and selection of constituents in CMCs

- Processing techniques involved to fabricate CMCs

- Role of boron in the protection of CMCs

The introductory chapter concludes with the discussion on the scope and objective of the present investigation

Composite materials have played vital role in development of aeronautic, military and spatial industries [Abdalla *et al.* 2003, Peters 2013]. With years of focused research, significant advancements have been made in terms of quality and performance level of composite materials which has substantially widened their applications [Mouritz *et al.* 2001, Dong-Xiao 2006, Gibson 2010, Gay 2014]. Today, sustainable development forms the main pre-occupations of governments and industries. Towards this, different research programs have been launched, new standards and measures have been placed with national and international scope to mitigate the environmental impacts [Shanyi 2007]. Intensive researches are being carried out aimed at the weight reduction of the structures by using composite materials, for which more and more materials were extensively explored that can survive in the extreme environments [Niihara 1991, Baldus *et al.* 1999, Cao *et al.* 2004]. Particularly, composites made of carbon or ceramic fibers combined with carbon or ceramic matrix called ceramic matrix composites (CMCs) are potential candidates for high-temperature applications such as rocket nozzles, aeronautic jet engines, heat shields and aircraft braking systems [Baldus *et al.* 1999, Cao *et al.* 2004, Naslain 2004]. They have the advantage of retaining their thermo-mechanical properties even at very high temperature, which highlights their usage for high-temperature applications [Schmidt *et al.* 2004, Krenkel 2008]. However, the production cost and the materials used can reach escalating prices depending on the targeted applications and the technologies required for their production. Hence, development of these materials with competitive and attractive methods gains tremendous significance for high-temperature application.

1.1. Ceramic Matrix Composites (CMCs)

Aeronautic, military and industrial applications require advanced materials that can survive extreme environments. Recently, ceramics have attracted enormous attention due to their superior properties, such as high-temperature stability, oxidation and corrosion resistance, as well as enhanced thermo-mechanical properties compared to that of metals and polymers [Baldus *et al.* 1999, Cao *et al.* 2004, Sanchez *et al.* 2013, Kalpakjian *et al.* 2014]. Monolitic ceramics (SiC, B_4C, Si_3N_4, SiB_4), ceramic coatings like thermal barrier coatings (TBC), environmental barrier coatings (EBC) and ceramic

matrix composites (CMCs) are some of the examples for high temperature ceramic materials that can be classified as advanced materials [Miller 1997, Cao *et al.* 2004]. Although monolithic ceramics possess desirable properties such as low density, high strength, high temperature resistance, chemical inertness, wear and erosion resistance, they exhibit extremely brittle behavior under thermal and mechanical loading conditions. In order to overcome this drawback, fiber-reinforcemented ceramics are used to increase toughness of the ceramic materials and are termed as CMCs [Ohnabe *et al.* 1999, Schmidt *et al.* 2004]. They received considerable attention for thermo-structural applications due to their low density, high modulus and good thermal shock resistance [Ohnabe *et al.* 1999]. CMCs represent the latest entry in the field of composites. They are largely suitable for the high temperature applications such as components in thrust providing parts of rocket or missile systems and thermal protection systems of the nose cap in re-entry vehicles [Triantou *et al.* 2017, Triantou *et al.* 2017].

1.1.1. Classification of CMCs

CMCs are broadly classified into two classes *viz.* oxide and non-oxide CMCs [Sun *et al.* 2006]. Oxide CMCs consist of oxide fibers combined with oxide matrices, while the non-oxide CMCs consist of non-oxide fibers combined with non-oxide matrices. Some of the most commonly used oxide and non-oxide fibers and matrices for high temperature applications are given in Table 1.1.

Table 1.1
Some of the most commonly used oxide and non-oxide ceramic fiber and matrices for high temperature applications

CMCs	FIBER	MATRIX
OXIDE	• Alumina (α-Al_2O_3) • Alumina silicate ($Al_2O_3.SiO_2$) • Alumina borosilicate ($Al_2O_3.SiO_2.B_2O_3$) • Alumina zirconate ($Al_2O_3.ZrO_2$) • Zirconium silicate ($ZrO_2.SiO_2$)	• Alumina (α-Al_2O_3) • Alumina silicate ($Al_2O_3.SiO_2$) • Zriconia (ZrO_2)

NON-OXIDE	- Carbon (C) - Silicon carbide (SiC) - Boron nitride (BN) - Silicon borocarbonitride (SiBCN)		- Carbon (C) - Silicon carbide (SiC) - Boron carbide (B_4C) - Silicon nitride (Si_3N_4) - Silicon carbonitride (SiCN) - Silicon borocarbonitride (SiBCN)

The oxide CMCs have distinctive properties such as good oxidation resistance, alkali corrosion resistance and low dielectric constants [Levi *et al.* 1998]. This makes them potential candidate for applications which requires long-term service in oxidizing environments, such as hot gas filters and exhaust components of aircraft engines [Di Salvo *et al.* 2015]. However, the operating temperature for the oxide CMCs are limited to 1000°C due to their poor creep resistance [Chermant *et al.* 2002, Hackemann *et al.* 2010]. For the CMCs to be used for long-term thermo-structural applications, non-oxide CMCs are the ideal candidate due to their exclusive properties such as high thermal conductivity, lower thermal expansion, oxidation resistance and high creep resistance as compared to the oxide CMCs [Naslain 2004, Krenkel 2008]. This makes them highly suitable for high temperature applications such as aeronautic jet engines [Zhao *et al.* 2003], heat shields [Zhao *et al.* 2003], heat exchangers [Sommers *et al.* 2010], aircraft braking systems [Sommers *et al.* 2010] and gas turbine [Morrison *et al.* 2004] applications where the oxide CMCs are unsuitable. Hence, the scope of this investigation is limited to non-oxide CMCs.

1.2. Design and selection of constituents in CMCs

When designing a CMCs, there are a number of factors that affects the performance of the material. In particular, the mechanical behavior and chemical composition of the individual components (reinforcement and matrix), and the interaction between these components (the interface) is of vital importance. A number of characteristics must be considered when selecting the reinforcement and matrix materials including temperature capability, density, strength, coefficient of thermal expansion, creep behavior and fracture toughness.

In general, CMCs are made of three major components (Figure 1.1):

(i)   a reinforcing material such as carbon fiber, silicon carbide fiber, etc.,

(ii)   an interphase coating such as pyrocarbon (PyC), hexagonal-boron nitride (hex-BN), etc.,

(iii)   a matrix such as silicon carbide (SiC), boron carbide (B_4C), etc.,

Fiber [C, SiC]
• Carries load

Interphase coating [BN ,PyC]
• Weak F/M interface
• Increased toughness
• Non-catastrophic failure

Matrix [SiC, B_4C]
• Transfers the load
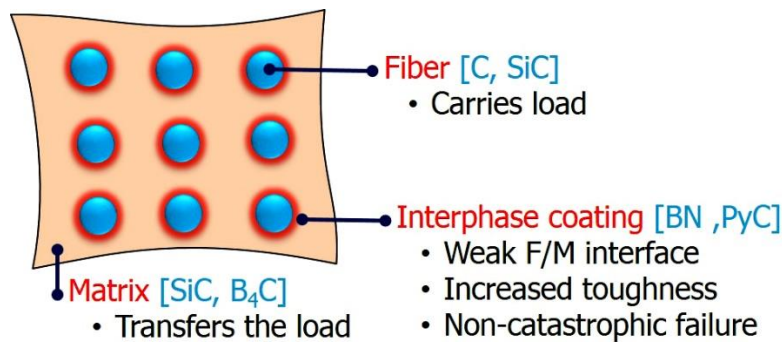
Figure 1.1 Basic components of CMCs

Each of the above components play a vital role in tailoring the properties of CMCs, which are described in detail as follows.

1.2.1 Reinforcing Material

Ceramic reinforcements can be produced in the form of continuous fiber, short fiber, whisker, or particle (Figure 1.2). Among these, continuous non-oxide ceramic fibers (SiC, C, BN, etc.) are very attractive as reinforcement for the ceramic materials due to their unique properties such as high tensile strength and elastic modulus, high creep resistance and oxidation resistance as compared to the oxide ceramic fibers, making them an ideal candidate for CMC to use it for long-term applications [Christin 2002, Flores *et al.* 2014, Agarwal *et al.* 2017].

Among the non-oxide ceramic fibers shown in the Figure 1.2, carbon and SiC fiber as reinforcement are most commonly utilized in CMC fabrications due to their high strength, stiffness and thermal stability.
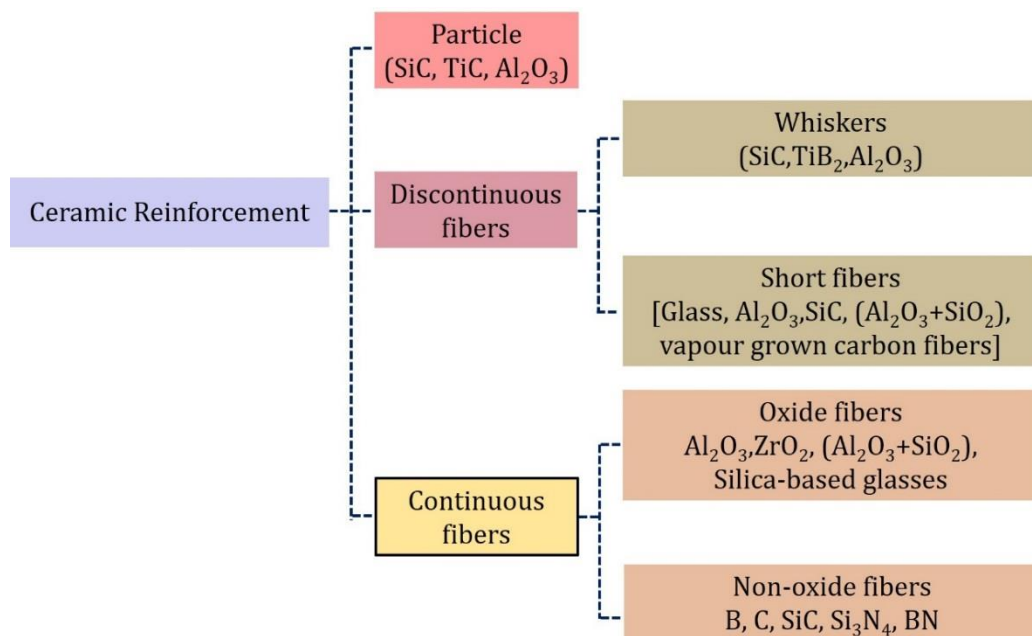
Figure 1.2 Types of ceramic reinforcements

1.2.1.1 Silicon Carbide fiber as reinforcement

The discovery of SiC fiber has revolutionized the field of ceramic reinforcements during the last quarter of the 20th century [Naslain 2005, Takeda *et al.* 2009]. In particular, a process, developed by the late Professor Yajima [Yajima *et al.* 1978], involving controlled pyrolysis of polycarbosilane precursor to yield a flexible fine diameter SiC fiber must be considered the harbinger of the making ceramic fibers from polymeric precursors. The first generation of SiC-based fibers are, Si–C–O fibers [Nicalon (from Nippon Carbon, Japan) fiber]. This is made of SiC nano-crystals in the size of 1 to 2 nm and free carbon embedded in an amorphous SiC_xO_y matrix. As a result, their stiffness (E= 220 GPa) is much lower than that of pure SiC (E= 400 GPa) and more importantly, they decompose beyond 1100-1200°C with a strength degradation. Hence, CMCs fabricated with these fibers should be processed by low temperature techniques and their use is limited within this temperature range. The second generation of SiC-based fibers are oxygen-free fibers (Hi- Nicalon) consisting of a mixture of SiC-nano-crystals in the size of 5 nm and free carbon embedded in the SiC matrix. Since, they do not possess oxygen, their thermal decomposition temperature will be shifted to higher temperature. Also, they creep at moderate temperature (1200°C), however their

creep resistance can be improved (1400°C) on subsequent heat treatment at 1400-1600°C which stabilizes the fiber microstructure. The third generation of SiC-based fibers are oxygen-free and quasi-stoichiometric in nature (Hi-Nicalon S, Tyranno SA or Sylramic) and are prepared at very high temperature (1600 to 2000°C) with crystallite size is in the range of 20 to 200 nm. The third generation of the SiC-based fibers exhibit superior thermal stability as compared to the first and second generation SiC fibers. There are other potential SiC-based fiber reinforcements, e.g. the amorphous Si-B-C-N fibers but which are still at an experimental stage. In spite of the great significance of SiC-based fibers in the field of CMCs, all these fibers are very stiff in nature and has high crystallite size. This leads to poor weave-ability and difficulties in fabricating the CMCs with complex shapes which limits their applicability. Also, most of the SiC fibers are very expensive and their availability is less as compared to carbon fibers.

In this regards, only carbon fiber has reached the stage in which they have been used to reinforce different high-temperature CMC systems [Sambell *et al.* 1972, Figueiredo *et al.* 2013, Gay 2014]. Although these fibers degrade in an oxidizing atmosphere above 450°C, they are stable under non-oxidizing conditions up to temperatures of 2800°C [Lamouroux *et al.* 1999]. Carbon fibers have unique properties such as good mechanical and thermal properties at elevated temperature, low density and moderate cost. In addition, the diameter of the carbon fiber is in the range of 7 µm to 10 µm giving them good weaving ability and they can be used to produce nD-preforms of complex shapes make it very popular in aerospace, civil engineering and military applications [Chawla 1998, Krenkel *et al.* 2002].

1.2.1.2 Carbon fiber as reinforcement

Carbon fibers have been described as the fibers containing at least 90% carbon obtained by the controlled pyrolysis of appropriate fibers [Fitzer 1987]. The carbon atoms are bonded together in microscopic crystals that are more or less aligned parallel to the long axis of the fiber [Peebles Jr 1995]. The crystal alignment makes the fiber very strong for its size. Several thousand carbon fibers are twisted together to form a yarn, which may be used by itself or woven into a fabric [Buckley *et al.* 1993]. Carbon

fiber has many different weave patterns and can be combined with a ceramic materials and wound or molded to form CMCs, such as carbon fibers reinforced silicon carbide composite (C/SiC), to provide high strength-to-weight ratio materials [Camus *et al.* 1996, Su *et al.* 2004, Longbiao *et al.* 2013, Zhang *et al.* 2013].

1.2.1.2.1 Manufacture of carbon fibers

Carbon fibers are manufactured by controlled pyrolysis of an organic fiber precursor. Some of the commercially important precursors, their chemical structure and the carbon fiber yield are given in Table 1.2.

Table 1.2
Some carbon fiber precursors and their yields [Fitzer 1989, Chand 2000]

Sl. No.	Precursor	Chemical structure	Yield (wt. %)
1.	Rayon	$(C_6H_{10}O_5)$	20-25
2.	PAN	$(CH_2\text{-}CH)_n$	45-50
3.	Mesophase pitch	CN	75-85

Depending on the precursor and processing, a variety of carbon fibers with different strength and modulus can be obtained. The most important sources for the production of carbon fibers are from PAN and pitch precursors [Figueiredo *et al.* 2013] which are discussed in detail in the following.

(a) Carbon fibers from PAN precursors

The flow chart and the structural changes of PAN precursor during the various processing steps involved in the fabrication of carbon fiber are given in Figure 1.3 and 1.4, respectively. The PAN precursor has a flexible polymer chain structure made of polar nitrile groups in the backbone of carbon [Figure 1.4 (a)]. During the stabilization process, the PAN precursor fiber is heat treated to 200-220°C under tension. During this process, the nitrile groups react to form a ladder structure, which is a rigid and thermally stable structure [Figure 1.4 (b)]. Also, when PAN is heat treated under air at 220°C, the absorbed oxygen crosslinks the chains and a stable ladder structure is obtained. This process is also done under tension which helps in maintaining the orientation of the ring structure. During the carbonization process, the carbon fiber is heat treated in between 1000°C and 1500°C. This will lead to the development of hexagonal network structure of carbon and the evolution of gases. This gas evolution is

partly responsible for some crack formation in the carbon fiber, resulting in a lower tensile strength. In order to increase the tensile strength, the carbon fiber is heat treated under tension between 2000°C to 3000°C to form graphite fiber.
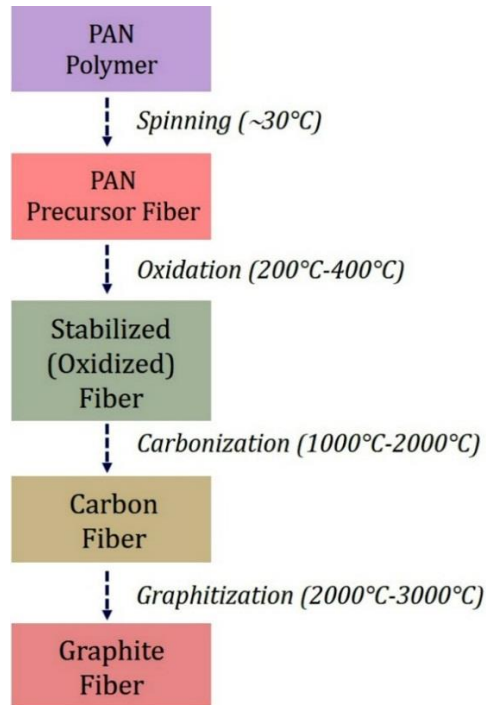
Figure 1.3 Flow chart for the fabrication of PAN based carbon fiber [Fitzer 1989]
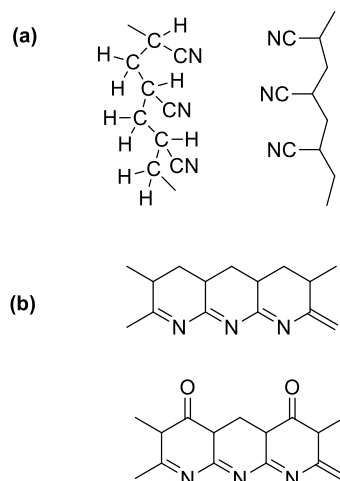
Figure 1.4 (a) the carbon backbone chain structure of PAN and (b) the ladder structure of PAN after stabilization

(b) Carbon fibers from Pitch precursors

Pitches form an important and low-cost raw material for producing carbon fibers.

There are three common sources of pitch:

(i)   Petroleum asphalt

(ii)   Coal tar

(iii)   Polyvinyl chloride (PVC)

Pitches are thermoplastic in nature and are difficult to carbonize without being first stabilized against fusion during pyrolysis. A flow chart of the process for the fabrication of carbon fibers from a pitch is shown in Figure 1.5.
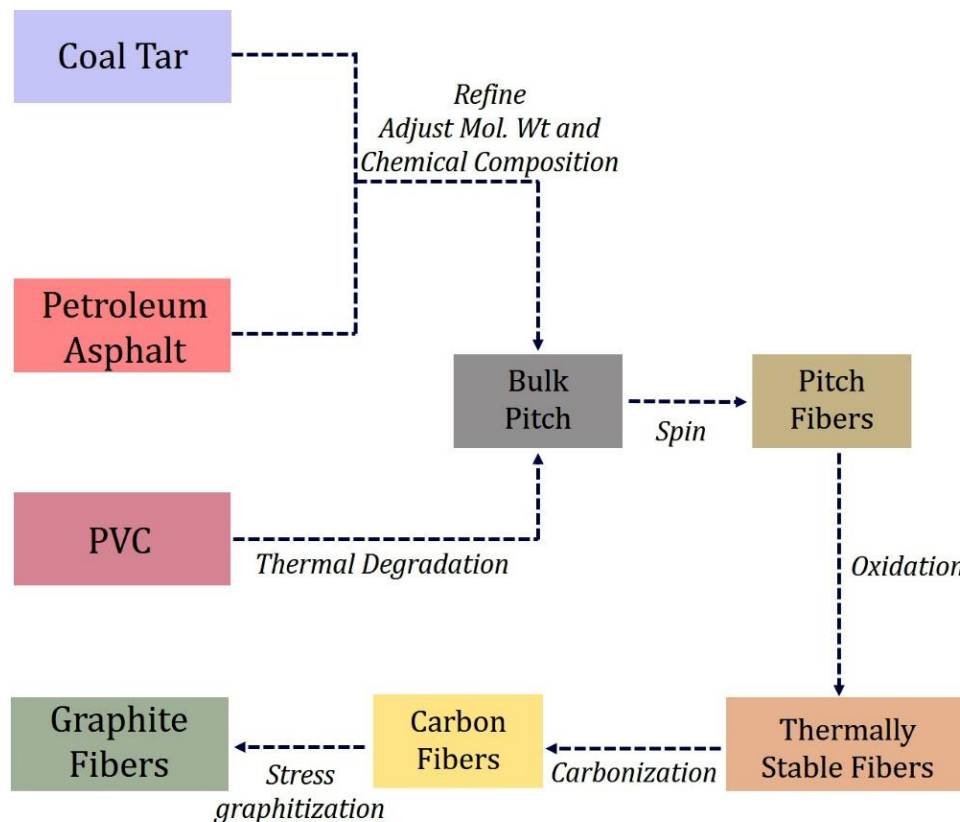
Figure 1.5 Flow chart for the fabrication of Pitch based carbon fiber [Chawla 1998]

It involves the following steps:

(i)   *Fiberization,* i.e. extrusion of a polymer melt or solution into a precursor fiber.

(ii)   *Stabilization* (oxidation or thermosetting) is done at relatively low temperatures (200-450°C), usually in air. This renders the precursor infusible during the subsequent high-temperature processing.

(iii)   *Carbonization* is carried out under nitrogen atmosphere at the temperature of 1000-2000°C. At the end of this step the fiber has 85-99% of carbon content.

(iv)   *Graphitization* is done under argon or nitrogen atmosphere at a temperature greater than 2500°C. This step increases the carbon content to more than 99% and imparts a very high degree of preferred orientation to the fiber.

1.2.1.2.2   Classification of Carbon fibers

Based on modulus, strength, and final heat treatment temperature, carbon fibers can be classified into the following three categories:

Based on properties of carbon fibers, they can be grouped into:

(i)   Ultra-high-modulus (UHM) having modulus of >450 GPa

(ii)   High-modulus (HM) having modulus between 350–450 GPa

(iii)   Intermediate-modulus (IM) having modulus between 200–350 GPa

(iv)   Low modulus and high-tensile (HT) having modulus of <100 Gpa; tensile strength of >3.0 GPa

Based on precursor materials, carbon fibers are classified into:

(i)   Polyacrylonitrile (PAN) based carbon fibers

(ii)   Pitch based carbon fibers

(iii)   Rayon based carbon fibers

Based on final heat treatment temperature, carbon fibers are classified into:

   (i)   Type-I, high-heat-treatment carbon fibers (HTT), where final heat treatment temperature should be above 2000°C and can be associated with high-modulus type fiber.

   (ii) Type-II, intermediate-heat-treatment carbon fibers (IHT), where final heat treatment temperature should be around or above 1500°C and can be associated with high-strength type fiber.

   (iii) Type-III, low-heat-treatment carbon fibers, where final heat treatment temperature not greater than 1000°C. These are low modulus and low strength materials.

1.2.1.2.3   Commercially available products of carbon fibers

There are a number of companies producing carbon fibers commercially and each has a number of carbon fiber products with different fiber properties and yarn counts [Krenkel 2008]. Also, they are offered in a wide range of tensile strengths and moduli having wide range of filament bundles in the range of 1000 (1 K) to 400 000 (400 K) [Frank *et al.* 2016]. Table 1.3 shows a survey of carbon fibers mostly used as reinforcement for CMCs fabrications.

Table 1.3
Types of carbon fiber reinforcement most commonly used for CMCs (manufacturer Toray, Japan)

Sl. No.	Trade name	Diameter (µm)	Density (g/cm^3)	Tensile Strength (MPa)	Tensile Modulus (GPa)
1.	T-300	7	1.76	3530	230
2.	T-300J	7	1.78	4210	230
3.	T-400H	7	1.80	4410	250
4.	T-700G	7	1.80	4900	240
5.	T-700S	7	1.80	4900	230
6.	T-800H	5	1.81	5490	294
7.	T-800S	5	1.80	5880	294
8.	T-1000G	5	1.80	6370	294
9.	M-35J	5	1.75	4700	343
10.	M-40J	5	1.77	4410	377
11.	M-46J	5	1.84	4120	436
12.	M-50J	5	1.88	4120	475
13.	M-55J	5	1.91	4020	540
14.	M-60J	5	1.93	3920	588

Among the carbon fibers given in the Table 1.3, T-300 carbon fiber was selected in this study due to its availability and moderate cost. T-300 carbon fiber are available in four types of filament bundles such as 1K, 3K, 6K and 12K. It is to be noted that, on increasing the number of filaments, the strength of fiber increases whereas wettability of the matrix resin decreases and hence an optimum strength and wettability is desired for the CMCs fabrications. This will lead to low coefficient of thermal expansion (CTE) mismatch between the fiber and matrix. Hence, among the carbon fiber filaments (1K, 3K, 6K and 12K) T-300 3K was selected for the further investigations. In addition, the diameter of the T-300 3K carbon fiber is of 7 µm making their weaving quite facile and can be used to produce nD-preforms of complex shapes.

1.2.2 Fiber/Matrix Interface

The fiber/matrix interfacial domain is a decisive constituent of fiber reinforced CMCs [Kerans *et al.* 1989]. Depending on the characteristics of the domain, the composite will be either a brittle ceramic or a damage tolerant composite as shown in Figure 1.7.

Thus, several requirements, which may seem to oppose to each other, have to be met the requirements [Budiansky *et al.* 1986, Evans *et al.* 1989, Figueiredo *et al.* 2013, Rajan *et al.* 2014]:

(i)   Fibers have to be bonded to the matrix, in order to ensure material integrity and to obtain a continuous medium.

(ii) Fiber failures have to be prevented when the matrix cracks which is achieved by crack deviation.

(iii) Once deviation of matrix cracks has occurred, the loads still have to be transferred efficiently through the interfaces, so that a certain amount of the applied load is still carried by the matrix.

(iv) Then, in aggressive environments, the fibers should not be exposed to species conveyed by the matrix cracks.

Meeting all of above requirements will lead to high-performance composite materials.
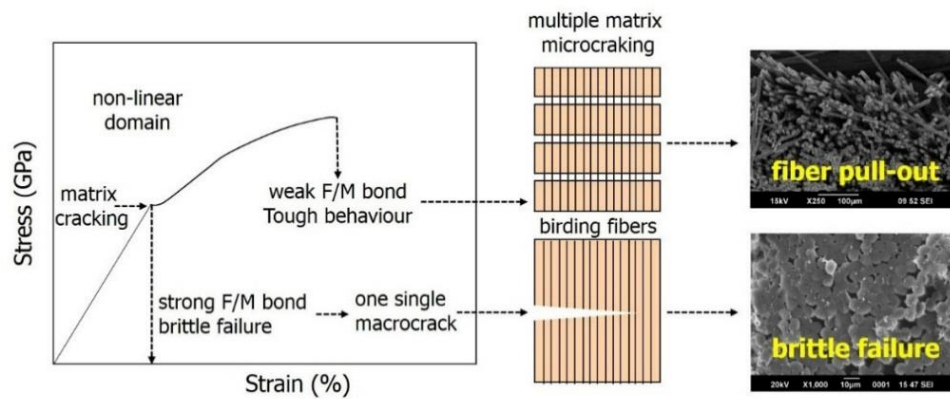
Figure 1.7 Mechanical behaviour under tension loading of CMCs and their correlation with the F/M bonding

The fiber/matrix interfacial domain may consist of an interface or an interphase [Curtin 1991]. An interface between two phases, or between the fiber and the matrix, can be defined as a surface across which a discontinuity occurs in one or more material properties [Naslain 1998]. On the other hand, an interphase is a thin film of material bonded to the fiber and to the matrix [Naslain 1993]. An interphase also implies the presence of at least two interfaces: one with the matrix and one with the fiber, and more when the interphase consists of a multilayer. The total area of the interface in composites is extremely large. It can be easily shown that it varies inversely with the fiber diameter:

$$I_A = 4V_f \frac{V}{d}$$

where 'V$_f$' is fiber volume fraction, 'V' is the volume of composite, and 'd' is fiber diameter.

Interface properties are dictated by the fiber and the matrix that have been selected, since bonding results from chemical reactions during processing or thermal shrinkage during cooling. Therefore, the number of routes, which are permitted to meet the above mentioned requirements for the interfacial domain, is limited by the number of constituents that are compatible. The concept of *interphase* allows these limitations to be overcome, and the interfacial characteristics to be tailored with respect to

composite properties [Naslain 1993].

1.2.2.1 Interphase concept in CMCs

The interphase is a thin film having a low shear strength (typically, 0.1–1 µm in thickness), which is deposited on the fiber surface prior to the deposition of the matrix and whose main function is to arrest or/and deflect the matrix micro-cracks formed under load, hence protecting the fibers from an early failure by notch effect (mechanical fuse function) [Tressler 1999]. In addition, the interphase has a load transfer function (as in any fiber composite) and may act as diffusion barrier during composite processing, when necessary [Feng *et al.* 2017].

1.2.2.1.1 Types of interphase

There are four types of interphase is been suggested and tested in a variety of CMCs [Naslain 1998, Morrison 2010] and are schematically shown in Figure 1.8, the main objective is to introduce a weak interface between a strongly bonded F/M system.
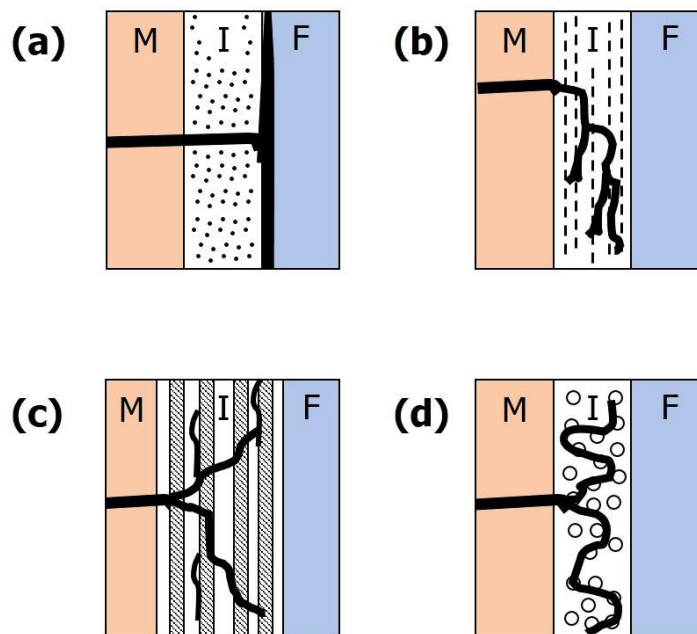
Figure 1.8. Crack deflection pathways for different types of interphases in CMCs: (a) Type I interphase: weak fiber/interphase interface, (b) Type II interphase: interphase with a layered crystal structure, (c) Type III interphase: multilayer $(X-Y)_n$ interphase and (d) Type IV interphase: porous interphase.

a)   *Type I interphase*

In type I interphases, a simple weak interface is introduced in the F/M interfacial zone to act as mechanical fuse [Figure 1.8 (a)]. Examples of such weak interfaces are:

(i)   Silica glass/anisotropic pyrocarbon (PyC) interface

(ii)   Lanthanum phosphate $LaPO_4$/ alumina interface.

b)   *Type II interphase*

In type II interphases are most commonly employed interphase for the CMCs. These interphase is made of a layered crystal structure, which are deposited parallel to the fiber surface and provide a weak bond to the F/M interface [Figure 1.8 (b)]. Examples of such interphases are:

(i)   Anisotropic turbostratic PyC

(ii)   Hexagonal-boron nitride

(iii)   Phyllosilicates, such as the fluorophlogopite mica, $KMg_3 (AlSi_3)O_{10}F_2$

(iv)   Hexaluminates, such as hibonite $CaAl_2O_{19}$

c)   *Type III interphase*

In type III interphases, the concept used in type II interphases is extended to the micro- or nano-structure. These interphases consist of a stack of layers of different nature [say, $(X-Y)_n$], strongly bonded to the fiber surface, but with weak internal interfaces which can be either the *X/Y* interfaces or even atomic planes if one of the layers, say *X*, has a layered crystal structure, as for the type II interphase [Figure 1.8 (c)]. With respect to the latter, type III interphases can be widely tailored, the adjustable parameters being the nature of *X* and *Y*, the number of *X -Y* sequences, *n*, and the thicknesses of *X* and *Y* layers in the sequence. As an example, layer *X* can act as mechanical fuse and layer *Y* as diffusion barrier. At least two interphases of this type have been extensively studied:

(i)   The dual BN-SiC (*n*=1) interphases used in silica based glass-CMCs

(ii)   The (PyC-SiC)$_n$ multilayer interphases (with typically, 1 , n , 10) used in SiC/SiC composites.

d)   *Type IV interphase*

In type IV interphases, the interphase is a layer of a porous material [Figure 1.8 (d)]. Examples of such interphases are:

(i)   Porous alumina (or) zirconia layers in alumina fiber/alumina matrix composites.

One simple way to form such porous oxides is first to deposit a carbon/oxide mixture on the fibre surface, then to embed the coated fibres in the matrix and finally, to burn out the carbon of the interphase. Other approaches have been proposed to weaken the F/M bonding in CMCs but have not been applied yet to real composites or have not yielded improved mechanical properties or/and lifetimes.

Although different types of interphase concepts have been suggested as shown above, it has been postulated that the best interphase materials might be those with a layered crystal structure on the fiber surface, such as pyrocarbon (PyC), hexagonal boron nitride (h-BN), can transfer load and protect fiber effectively [Carrère *et al.* 2000, Naslain *et al.* 2004].

BN interphase

The h-BN interphase coating is deposited via chemical vapor infiltration (CVI) technique using BCl_3 and NH_3 as precursor at 850°C for 4h under nitrogen atmosphere [Naslain *et al.* 1991]. There are many reports available on the utilization of BN as interphase coating for the CMC fabrication and have resulted in very good thermo-mechanical properties [Kerans *et al.* 2002, Kiser *et al.* 2016]. However, the use of h-BN as an interphase material raises several difficulties. Firstly, the most common gaseous precursor of BN, i.e., BF_3-NH_3-Ar or BCl_3-NH_3-H_2 are corrosive and hygroscopic. Hence, their use in CVI may damage carbon fibers and introduce, at their surface, oxygen-containing species yielding low fiber/interphase bonding. Further, BN when deposited from BCl_3-NH_3-H_2 under CVI conditions, i.e., at low temperature (900-1000°C) and low pressure (a few KPa) with an excess of NH_3 is amorphous (or poorly

crystallized) and not stable in air at room temperature [decompose into boria (B_2O_3)]. Post-deposition heat treatments can be applied to remove the moisture, but they are limited in temperature by the thermal stability of fibers. Hence, research has been performed to find other potential interphase materials with a layered crystal structure.

PyC interphase

On the other hand, PyC as interphase found to be a promising candidate for the CMC applications in spite of its poor oxidation resistance. The PyC interphase coating is deposited on carbon fabric via an isothermal/isobaric CVI technique using CH_4 as precursor at 1200°C for 3h under argon atmosphere. The structure of PyC is similar to that of graphite but includes disorder as shown in Figure 1.9, graphene layers have limited extent and may include C-5 or C-7 arrangements responsible for some waviness; they may furthermore be stacked with rotational disorder (turbostratic graphite) and contain screw dislocations. Also, it is highly refractory and chemically compatible with SiC matrix. Further, its atomic graphene planes can be deposited parallel to the fiber surface and are weakly bonded to one another. This weak bonding between F/M Interface leads to an energy dissipative mechanism such as fiber pull-out and debonding. Further, this will increase the energy required for the propagation of the cracks leading to a high mechanical property as shown in Figure 1.7.
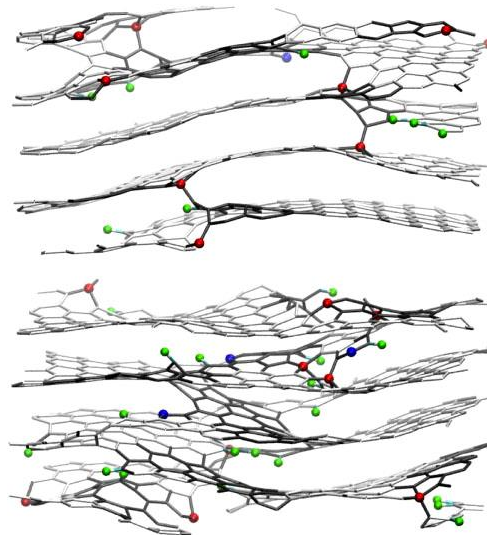
Figure 1.9. Atomistic model of pyrocarbon (PyC)

However, CMCs being used at high temperatures and in oxidizing atmospheres, the interphase should be preferably resistant to oxidation. This last requirement is especially important if one remembers that CMCs are often micro-cracked, the micro-crack network facilitating the in-depth diffusion of oxygen towards the interphases and the fibres. Hence, attempts have been made in this thesis to improve the oxidation resistance of CMCs through the alteration of the matrix composition to have *self-healing* properties.

1.2.3 Matrix

The matrix is the last necessary component of a CMC, and is vital since the intrinsic properties of the matrix play a critical role in the functionality of the finished composite [Wilson *et al.* 2001]. Matrix materials are selected with several important properties in mind such as high melting temperature, oxidation resistance and chemical inertness, low coefficient of thermal expansion. The most important ceramic materials used as matrix for CMCs along with their physical and mechanical properties are given in Table 1.4.

Table 1.4
Physical and mechanical characteristics of ceramic materials

Sl. No.	Ceramic materials	Density (g/cm^3)	Melting point (°C)	Young's modulus (GPa)	Coefficient of thermal expansion $(10^{-6}K^{-1})$	Fracture toughness $(MPa.m^{1/2})$
1.	SiC	3.21	2830	410	4.0	4.6
2.	Si_3N_4	3.17	1900	310	3.3	6.1
3.	B_4C	2.54	2445	450-470	5.0	2.9-3.7
6.	TaC	13.9	3880	450	4.3	4.1
7.	ZrC	6.6	3530	430	6.8	3.0
8.	HfC	12.2	3890	510	6.7	2.9
9.	TiC	4.93	3160	400	4.1	4.1

Among the various ceramic materials listed Table 1.4, silicon carbide (SiC) is the most commonly used ceramic material for high-temperature applications [Chamberlain *et al.* 2014, Jiménez *et al.* 2016]. This is due to their unique properties such as high melting point, excellent mechanical properties at high temperatures related to its covalent character and relatively good oxidation resistance up to about 1500°C in oxygen-rich atmospheres [Brennan *et al.* 1982, Naslain 2005, Bansal 2006]. Also, SiC

can be easily deposited in a fiber preform by a variety of techniques.

1.3. State of the art for the fabrication of CMCs

The current scenario for the fabrication of CMCs are

(i)   Chemical vapor infiltration (CVI) technique

(ii)   Polymer impregnation/infiltration and pyrolysis (PIP) technique

(iii)   Liquid silicon infiltration (LSI) also called reactive melt infiltration (RMI) technique

(iv)   The ceramic route

(v)   Reaction bonded silicon carbide (RBSC) technique

For all the above routes three main steps are commonly adopted for the fabrication of CMCs:

(i)   Production of the carbon fiber preform

(ii)   Building up a weak fiber/matrix interface

(iii)   Densification using matrix
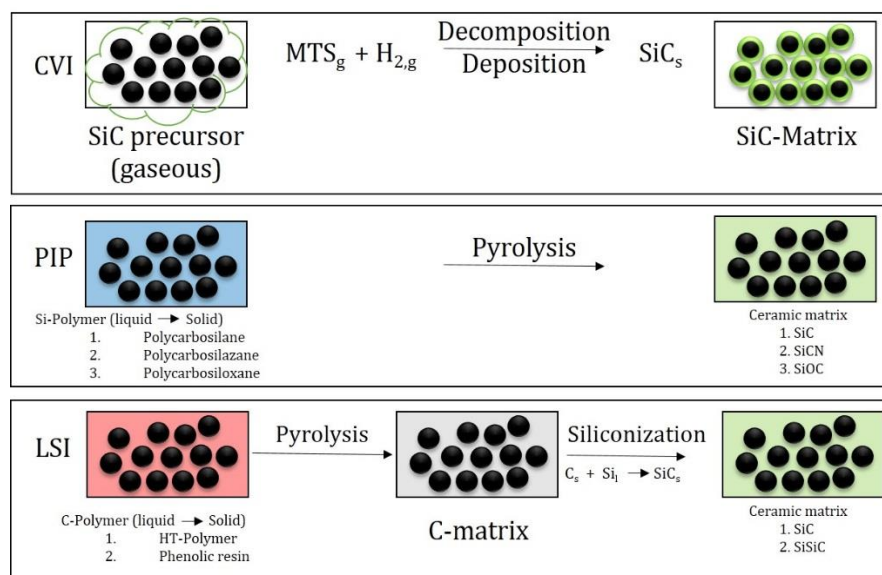
Figure 1.10 Schematic overview of the different methods used for manufacturing of CMCs.

1.3.1   Chemical Vapor Infiltration (CVI) technique

CVI is widely used and mostly matured technique for the development of CMCs [Naslain *et al.* 1989, Naslain 1993, Kiser *et al.* 2016]. This method is used to deposit ceramic materials like carbon, silicon carbide, boron nitride and other refractory materials in a porous structure by the decomposition of vapors. CVI is similar to chemical vapor deposition (CVD) as CVD implies deposition onto a surface, whereas CVI implies deposition within a body.

Processing involved for the fabrication of CMCs via CVI technique

A ceramic continuous fiber structure (porous preform) is prepared and placed in the reactor to act as the reinforcement phase. Reactant gases or vapors are supplied to the reactor which flow around and diffuse into the preform (Figure 1.11). The decomposition of the reactants fills the space between the fibers, forming composite material in which matrix is the deposited material and dispersed phase is the fibers of the preform. The diameter of the fibers gradually increases as the reaction progresses as shown in Figure 1.12.
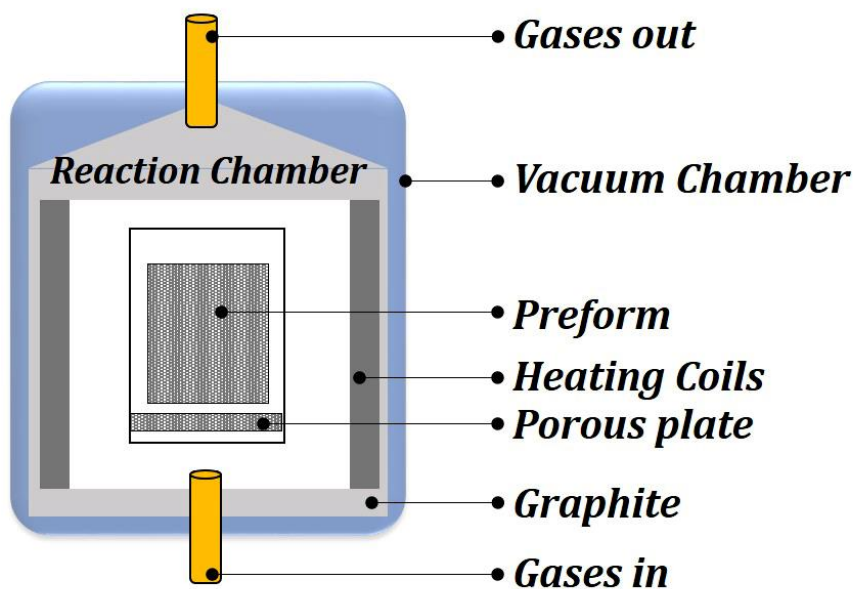
Figure 1.11 Chemical Vapor Infiltration (CVI) reactor
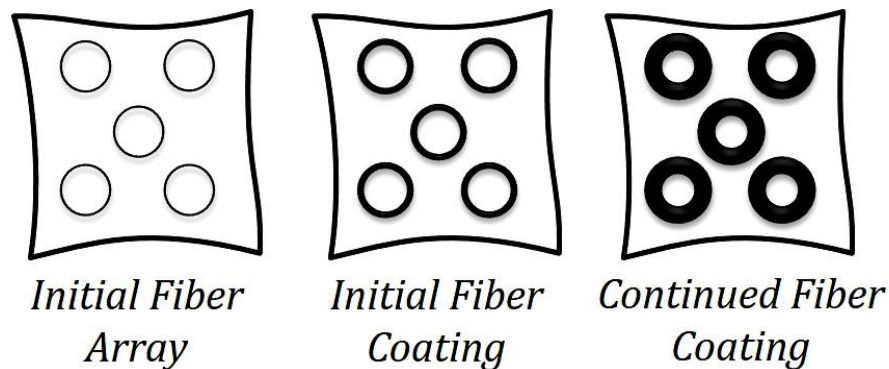
Figure 1.12 Densification of matrix in CMCs *via* CVI technique

The schematic representation of CVI process for the fabrication of C/SiC composite is shown in Figure 1.13. In order to prevent possible chemical reaction between matrix material and the fiber and to obtain a weak interphase between the fibers and the matrix, fiber coating is necessary. CH_4 gas is introduced into the preform to obtain pyrocarbon (PyC) interphase as the interlayer between fiber and the matrix. The PyC thickness in the process must be in the range of 0.1 - 0.8 μm. In order to deposit SiC as a matrix material, a gas mixture of hydrogen and methyltrichlorosilane (MTS) is exposed to carbon fiber preform in an infiltration furnace at temperatures approximately 800-1000°C under the pressure of 1 kPa.

Chemistry of the process is described by the following reaction:

$$Cl_3SiCl\,(g) + H_2 \longrightarrow SiC\,(s) + 3HCl$$
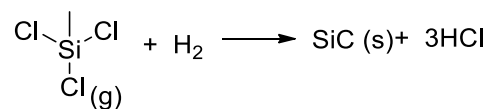
Hydrogen acts as a catalyst and at the end of the process β-SiC is produced. To obtain the better quality of SiC matrix three parameters, namely, pressure, temperature and volume ratio of hydrogen and MTS have to be taken into consideration. CVI method is suitable to produce not only for the simple plates but also for very large and complex structure since it is possible to form a carbon fiber preform in complex shape. In this process, use of low temperature and pressure conditions gives less damage to fibers and thus, complex shapes can be produced. Moreover, by controlling the

composition of the gases, pure and uniform fine grained SiC matrix which directly affects the mechanical properties of the composite can be obtained.
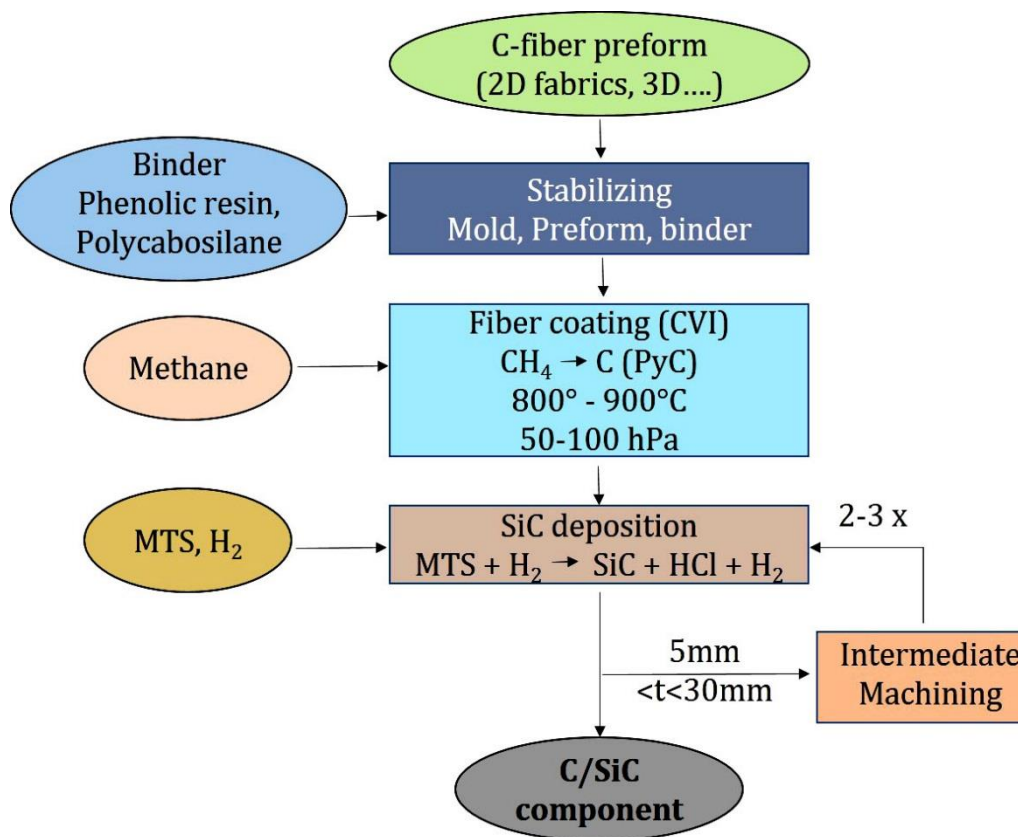
Figure 1.13. Schematic view of CVI process

Different types of CVI processes:

(i) *Isothermal/isobaric CVI process:* The reactant gas is supplied to the preform at a uniform temperature and pressure. It is a very slow process as it has a low rate of diffusion.

(ii) *Temperature gradient (TG-CVI):* In this process the vapor diffuses initially to the hotter surface of the preform and then to the cooler surface. The temperature difference enhances the gas diffusivity. The vapors decompose mostly in the hot inner surface as the rate of the chemical reaction increases with increase in temperature. Due to the prevention from early closure of the surface pores, this method allows

better densification of the ceramic matrix.

(iii)   *Isothermal-forced flow (IF-CVI):* In this process, vapors are forced into the uniformly heated preform. The rate of the deposition is increased by the increase in infiltration of the forced reactant gas.

(iv)   *Thermal gradient-forced flow (F-CVI):* This process is the combination of the both TG-CVI and IF-CVI processes which enhances the infiltration of the vapors. This process also reduces the densification time. Temperature difference in preform is achieved by heating the above region while the bottom region is cooled. Forced flows are determined by the difference in the pressure of the entering and exhaust gases.

(v)   *Pulsed flow (P-CVI):* In this process, the surrounding gas pressure changes rapidly. The pressure changes repeatedly during each cycle. Each cycle consists of the evacuation of the reactor vessel followed by its filling with the reactant gas.

Advantages

(i)   Low residual stress due to low infiltration temperature

(ii)   Large, complex shape product can be produced in a near-net shape

(iii)   Enhanced mechanical properties, corrosion resistance and thermal shock resistance

(iv)   Various matrices can be fabricated

(v)   Very low fiber damage

Disadvantages

(i)   Matrix deposition rate is very low

(ii)   Time consuming process

(iii)   Residual porosity is very high (10-15%)

(iv)   High capital and production costs

1.3.2 Polymer Impregnation/Infiltration and Pyrolysis (PIP) technique

Polymer impregnation/infiltration and pyrolysis (PIP) process can be defined as the conversion of the preceramic precursor into ceramic matrix via pyrolysis. The main advantage of this route is flexibility of selection of preceramic resins to obtain different types of CMCs [Jones *et al.* 1999, Riedel *et al.* 2006, Lee *et al.* 2008]. The important criteria for the preceramic resin to be used as matrix resin for the fabrication of CMCs through PIP route is,

(a)   The preceramic resin should wet the fibers and should have low enough viscosity to flow in the pore network between the fiber filaments.

(b)   Upon pyrolyzing preceramic resin should yield a high ceramic yield.

The most commonly used preceramic polymers are as follows,

(i)   Silicon containing preceramic polymers such as polysilane, polycarbosilane and polysiloxane

(ii)   Silicon and nitrogen containing preceramic polymers such as polysilazane, perhydridopolysilazane and polycarbosilazane

(iii)   Silicon and boron containing preceramic polymers such as polyborosilane and polyborosiloxane

(iv)   Silicon, boron and nitrogen containing preceramic polymers such as polyborosilazane

All the above mentioned resins can be used as preceramic matrix resin for the fabrication of CMCs through PIP route which is unique advantage of this route. After selection of the preceramic resin, PIP process contains four different steps (Figure 1.14):

(i)   Deposition of fiber coating by CVI technique (Section 1.2.2.1),

(ii)   Manufacture of CFRP preform,

(iii)   Pyrolysis of the CFRP preform,

(iv)   Densification via repeated polymer infiltration and pyrolysis
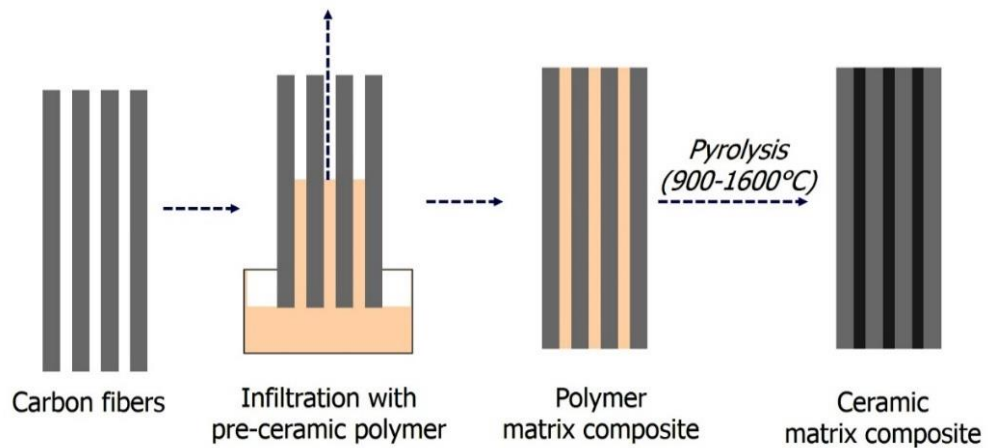
Figure 1.14. Steps of polymer infiltration and pyrolysis process
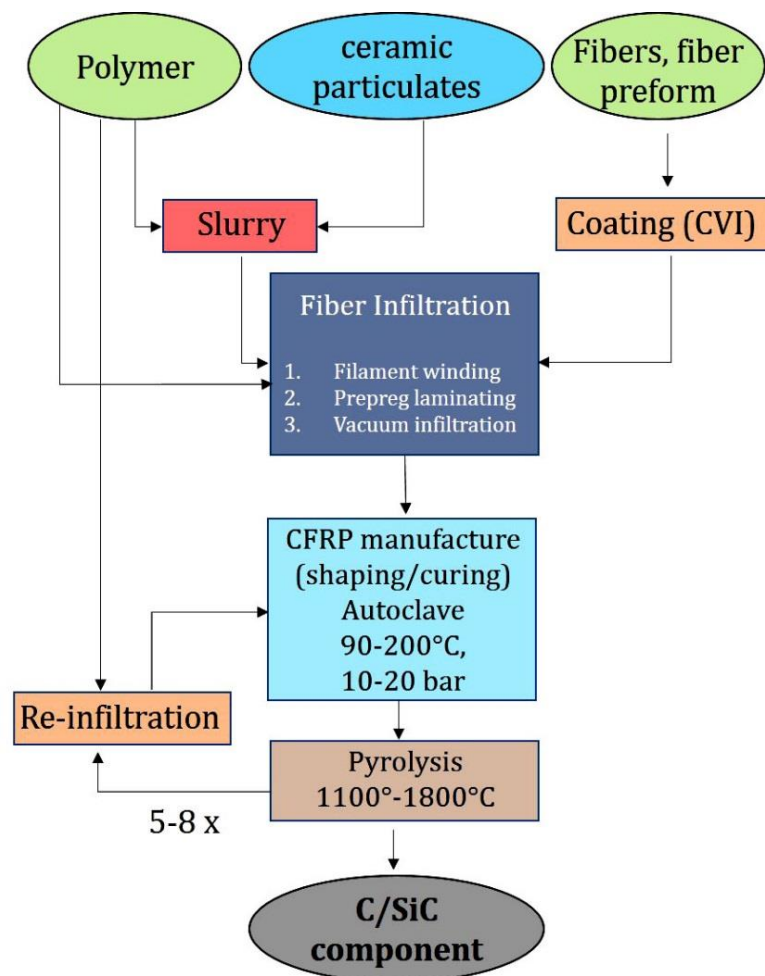
Figure 1.15 Polymer infiltration and pyrolysis process [Krenkel 2008]

Firstly, in order to achieve weak fiber-matrix interphase the carbon fiber or fiber preforms are coated via continuous or discontinuous CVD or CVI processes. Thickness of the PyC layer may change between 0.1–0.8 μm. The second step is manufacturing of a CFRP preform via wet filament winding, vacuum assisted polymer (VAP), or resin transfer molding (RTM). These techniques are very common for ordinary polymer matrix composites; however, usage of the preceramic precursors necessitates higher curing temperatures and inert atmosphere for elimination of oxidation during curing. In the third step, CFRP preform is pyrolyzed in inert gas atmosphere. During pyrolysis, organic compounds are eliminated, the network of the polymer is decomposed and it turns into amorphous ceramic matrix. The percentage of the resultant ceramic depends on the type of preceramic polymer utilized and the pyrolysis conditions (temperature and atmosphere). The last step is the ceramization by pyrolysis which is applied at high temperature under vacuum or in inert atmosphere. Re-infiltration and pyrolysis steps are done 5-8 times in order to decrease residual porosity and increase the density of the matrix material and to obtain crystalline SiC (Figure 1.15).

Advantages

(i)   Fibers damage is prevented due to the processing at a relatively low temperature

(ii)   Good control of the matrix composition and the microstructure

(iii)   Reinforcing phase of different types (particulate, fibrous) may be used

(iv)   Net shape parts may be fabricated

(v)   Matrices of various compositions (silicon carbide, silicon nitride, silicon carbonitride) may be obtained

(vi)   No residual silicon is present in the matrix

Disadvantages

(i)   The fabrication time is relatively long due to the multiple infiltration-pyrolysis cycle

(ii)   There is a residual porosity decreasing the mechanical properties of the composite

(iii)   Relatively high production cost (higher than in Liquid Silicon Infiltration method)

1.3.3 Liquid Silicon Infiltration (LSI)/ Reactive Melt Infiltration (RMI) technique

Liquid Silicon Infiltration (LSI) process is a type of Reactive Melt Infiltration (RMI) technique, in which the ceramic matrix forms as a result of chemical interaction between the liquid metal infiltrated into a porous reinforcing preform and the substance (either solid or gaseous) surrounding the melt. LSI is used for fabrication of C/SiC composites. The process involves infiltration of carbon (C) micro-porous preform with molten silicon (Si) at a temperature exceeding its melting point 1414°C (Figure 1.16).
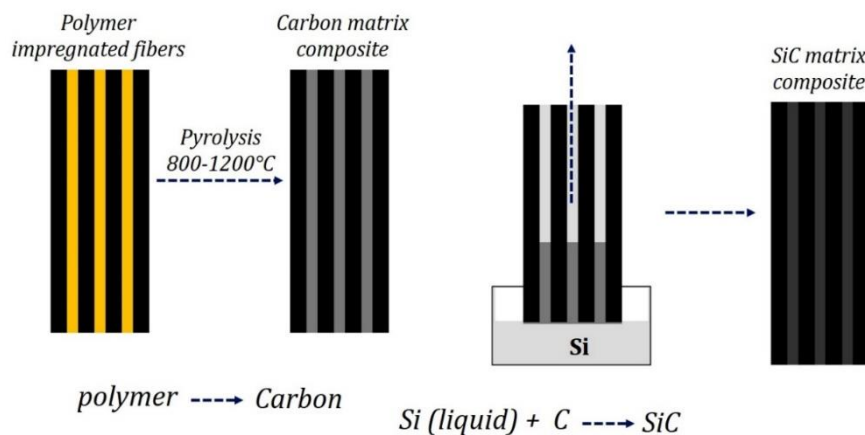
Figure 1.16 Steps involved in LSI process [Krenkel *et al.* 2002]

The liquid silicon wets the surface of the carbon preform. The melt soaks into the porous structure driven by the capillary forces. The melt reacts with carbon forming silicon carbide according to the reaction:

$$C_{(s)} \; + \; Si_{(l)} \longrightarrow SiC_{(s)}$$
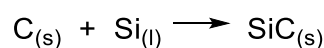
SiC produced in the reaction fills the preform pores and forms the ceramic

matrix. Since the molar volume of SiC is less than the sum of the molar volumes of silicon and carbon by 23%, the soaking of liquid silicon continues in course of the formation of silicon carbide. The initial pore volume fraction providing complete conversion of carbon into silicon carbide is 0.562. If the initial pore volume fraction is lower than 0.562 the infiltration results in entrapping residual free silicon. Commonly at least 5% of residual free silicon is left in SiC matrix. The porous carbon is synthesized by pyrolysis of a polymerized resin. The most commonly used polymer is phenol-formaldehyde resin [Odeshi *et al.* 2006].
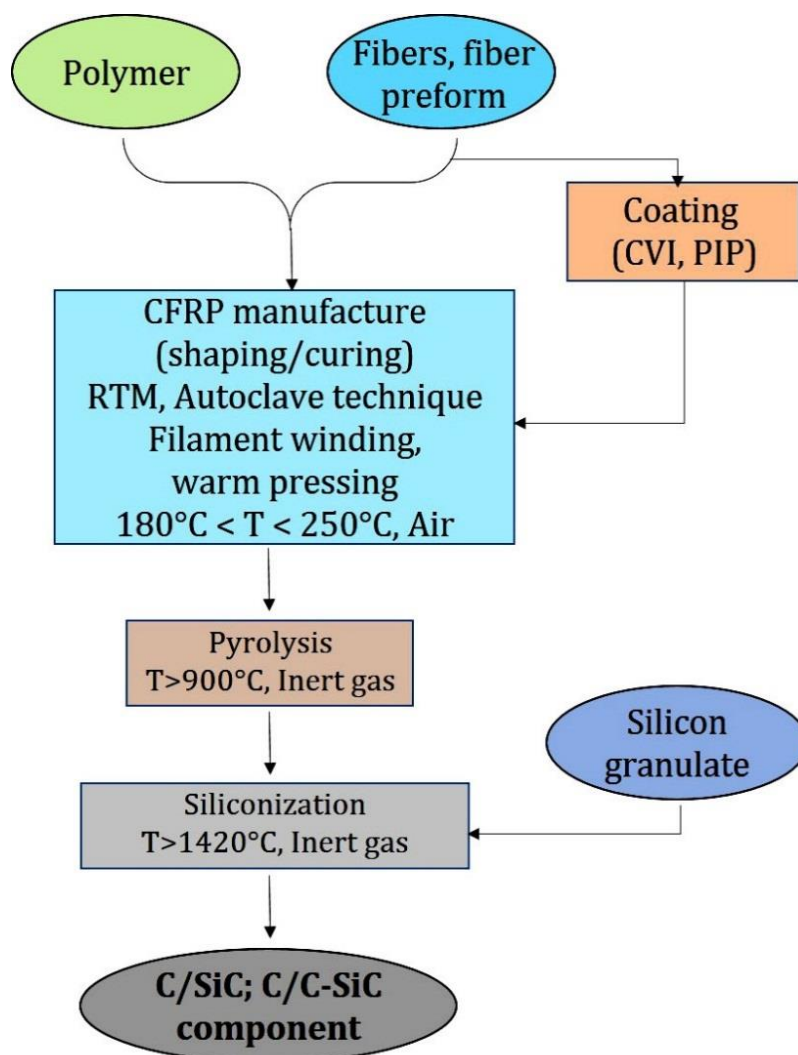
Figure 1.17. Schematic overview of the manufacture of C/SiC materials via LSI [Krenkel *et al.* 2005]

LSI process

Processing of C/C-SiC composites via LSI contains three main steps (Figure 1.17),

(i)   Production of carbon fiber reinforced polymer matrix composites (CFRP)

(ii)   Pyrolysis of CFRP to C/C preform

(iii)   Liquid silicon infiltration of C/C preform

Composites manufactured by LSI contain lower amount of porosities which results in higher shear strength and thermal conductivity. It is a near net shaping process and its main advantage is its in-situ joining capability and the possibility of manufacturing large and complex shape components with the help of near net shaping. Moreover, this process has lower component fabrication time and thus, manufacturing cost is reduced considerably compared to other manufacturing techniques.

Advantages

(i)   Low cost

(ii)   Short production time

(iii)   Very low residual porosity

(iv)   High thermal conductivity

(v)   High electrical conductivity

(vi)   Complex and near-net shapes may be fabricated

Disadvantages

(i)   High temperature of molten silicon may cause a damage of the fibers

(ii)   Residual silicon is present in the carbide matrix

(iii)   Lower mechanical properties of the resulting composite: strength, modulus of elasticity

1.3.4 **The ceramic route**

In the ceramic route, the matrix precursor is a slurry, i.e. a stable suspension of a β-SiC powder in a liquid which also contains sintering additives and a fugitive binder. The reinforcement is impregnated with the slurry and wound on a drum, yielding a 1D-prepreg-type intermediate product [Rosso 2006]. After drying, the layers are stacked in the die of a unidirectional press and the composite sintered at high temperature under pressure.

Disadvantages

(i)   The sintering of SiC powder is very difficult and requires very high temperatures, even in the presence of sintering aids.

(ii)   Since, it is performed here under pressure (to achieve low residual porosity), the combined effect of high temperature and high pressure was considered for a long time as a source of too severe fiber degradation and this route more or less disregarded.

1.3.5 **Reaction Bonded Silicon Carbide (RBSC) technique**

In comparison to CVI, PIP and ceramic route, the LSI process is relatively economical [Krenkel 2009]. However, in this process, reaction of liquid silicon with carbon is not restricted to the carbon of the matrix, but it also reacts with the carbon fiber leading to poor mechanical properties [Odeshi *et al.* 2006, Magnant *et al.* 2012].

To overcome the disadvantages of LSI technique, while retaining the cost advantage, fine silicon powder was added to the polymeric precursor. Before silicon-carbon reaction occurs, silicon and carbon are distributed homogeneously within the matrix and hence the reaction is restricted mainly to the matrix. This method has been termed as 'Reaction Bonded Silicon Carbide method' (RBSC) which is modified LSI route [Magnant *et al.* 2012].

Figure 1.18 content
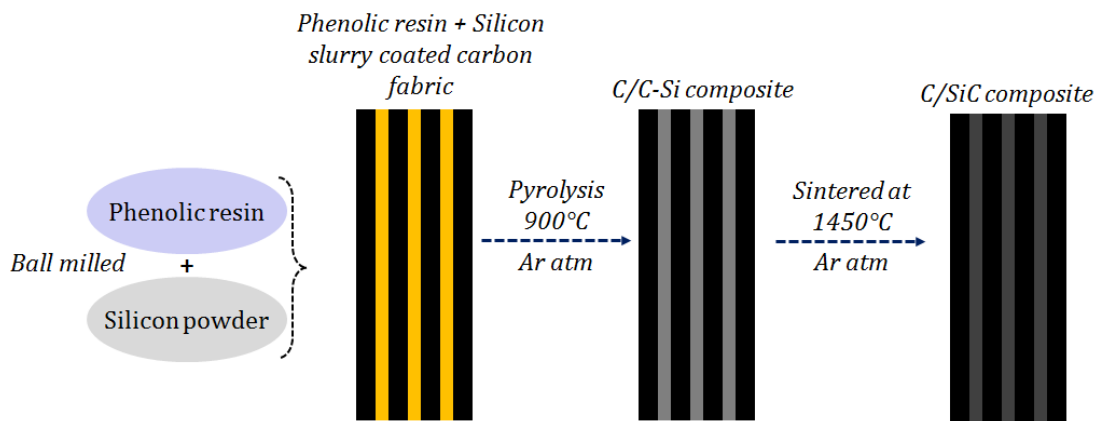
Figure 1.18 Schematic overview of the manufacture of C/SiC materials via RBSC [Ganesh Babu *et al.* 2016]

In the developed processing method, RBSC, a matrix suspension consisting of silicon powder in phenolic resin is prepared first. The fiber bundle is impregnated with the suspension as shown in Figure 1.18. After drying, the prepregs are cut and stacked in a mould. Curing of the resin is performed in a heatable press at a maximum temperature of 200°C under a pressure of 20 MPa. A component of carbon-fiber-reinforced plastic (CFRP) is formed. During carbonization up to 900°C in argon atmosphere, the phenolic resin is transformed into glassy carbon. This is accompanied by a weight loss of 45% (i.e. volume reduction 54%). Thus, due to a low shrinkage of the composite (approx. 5%) the porosity increases up to a value of 15-20 %. After carbonization the matrix consists of silicon and carbon in stoichiometric ratio homogeneously distributed within the matrix. In the final thermal treatment step-the silicon-carbon reaction-the reaction of liquid silicon and solid carbon to form silicon carbide within the matrix is carried out at a temperature slightly above the melting point of silicon (1450°C, under argon atmosphere). Silicon carbide is of higher density than silicon and carbon, but the shrinkage of the composite due to the reaction is again hindered by the fiber reinforcement. This leads to a further increase of the composite's porosity to a value of more than 30% with a corresponding low total density of

approximately 1.5 g/cm^3. The final product of carbon-fiber-reinforced silicon carbide (C/SiC) is achieved.

1.4. The key issues with C/SiC composites

The important properties for the CMCs are,

(i) It should have good mechanical properties that can be retained even at high temperature (>1200°C)

(ii) It should possess good oxidation resistance.

The mechanical property can be improved through a proper design of the F/M interface arresting and deflecting cracks formed under load in the brittle matrix and preventing the catastrophic failure of the CMCs. This crack deflection is controlled *via* the deposition of a thin layer of a compliant material with a low shear strength, on the fiber surface, referred to as the *interphase* as explained in *Section 1.2.2.1* which acts as a mechanical fuse.

However, in terms of oxidation resistance, the interphase coating used for the CMCs should be preferably resistant to the oxidation [Naslain 2004]. Further, it is observed that when SiC is used as a matrix in either C/SiC or SiC/SiC composites, SiC undergoes multiple micro-cracking when loaded in tension beyond a relatively low stress level (100-200 MPa). These micro-cracks, facilitate the in-depth diffusion of oxygen towards the oxidation-prone interphases and the fibers, when the composite is exposed to an oxidizing atmosphere at medium or high temperatures [Ruggles-Wrenn *et al.* 2013, Al Nasiri *et al.* 2016]. Hence, for the long-term applications, the objective of CMCs is to engineer or tailor the SiC-matrix in order to impede or at least to slow down oxygen diffusion in the material and to increase its durability in corrosive environments. Towards this, *self-healing* matrix plays a vital role in the protection of CMCs from oxidizing environment [Low 2014, Luan *et al.* 2016].

1.5. Concept of Self-healing matrix

For long-term high temperature applications, CMCs has to be highly engineered in order to improve their oxidation resistance, particularly at the level of the interphase and the matrix. In this field, boron-bearing species are reported to be highly efficient [Naslain *et al.* 2004, Ganesh Babu *et al.* 2016, Bertrand *et al.* 2017]. They can form fluid oxide phases (B_2O_3 or –Si-O-B-C- multi phase) over a broad temperature range (600–1200°C) when heated in an oxidizing atmosphere as shown in eqns. (1.1) to (1.5) [Ganesh Babu *et al.* 2016].

$$SiB_{4(s)} + 4O_2 \xrightarrow{600°C} B_2O_3(l) + xSiO_{2(l)} \qquad (1.1)$$

$$B_2O_{3(l)} \xrightarrow{900°C} B_2O_{3(g)} \qquad (1.2)$$

$$SiC + 3O_{2(g)} \xrightarrow{1200°C} 2SiO_{2(l)} + 2CO_{(g)} \qquad (1.3)$$

$$B_2O_{3(l)} + xSiO_{2(l)} \xrightarrow{1000\text{-}1200°C} B_2O_3.xSiO_{2(l)} \qquad (1.4)$$

$$B_2O_3.xSiO_{2(l)} \xrightarrow{>1300°C} B_2O_{3(g)} + xSiO_{2(l)} \qquad (1.5)$$
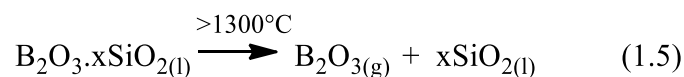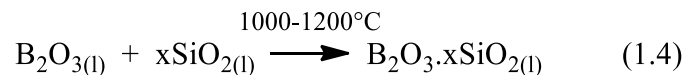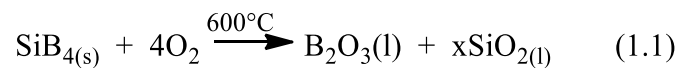
These B-bearing species, if introduced in the interphase or ceramic matrix of non-oxide CMCs or as fillers, could be used to design *self-healing* materials which form fluid oxide phases during oxidation to fill cracks. This will slow down the in-depth diffusion of oxygen imparting self-healing properties as shown in Figure 1.19 to improve the lifetimes of the CMCs [Tong *et al.* 2008].

Despite many relevant studies regarding the role of substitutional boron in protection of CMCs [Quemard *et al.* 2007, Cluzel *et al.* 2009], controversy still remains, and many more experimental results must be discussed. Indeed, different approaches have been used to produce B-doped carbon materials. Although each study used different materials and experimental conditions, the final goal for each was to improve the oxidation stability by introduction of boron into system.
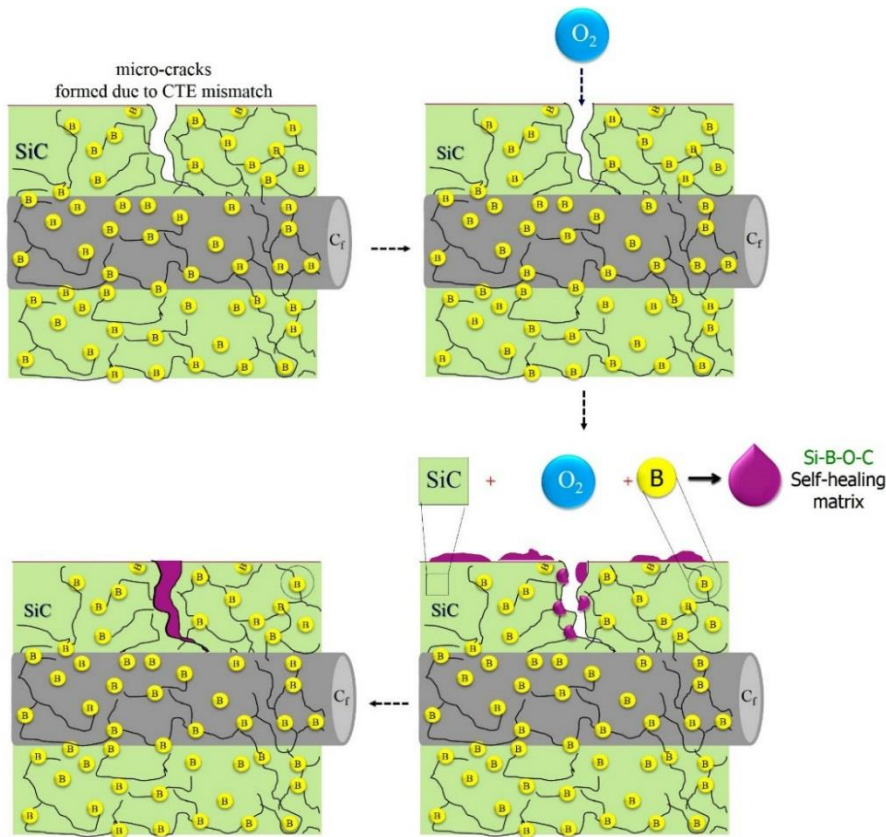
Figure 1.19 Schematic representation of Self-healing mechanism in CMCs

1.5.1 Methodologies to achieve self-healing property

1.5.1.1 Boron containing interphase

In this methodology, the elemental boron will be doped in interphase to obtain a layered crystal structure or microstructure which act as a mechanical fuse (matrix crack deflection), as well as a better oxidation resistance. So far researchers have developed three kinds of boron doped interphases, namely boron-doped PyC [PyC (B)], h-BN [BN (B)], and (BN-SiC)$_n$ multilayers [Naslain 1998, Naslain 1999]. For all these materials, the oxidation resistance improvement is related to the formation of a B_2O_3 or B_2O_3-SiO_2 fluid phase resulting from the oxidation of the boron and silicon-bearing species, according to the following eqns (1.6) to (1.9). B_2O_3 has a low melting point (~450°C) and its viscosity decreases as temperature is raised. It remains in the liquid state up to a temperature of about 900°C in a dry atmosphere but it is readily gasified at low temperatures in the presence of moisture. However, the viscosity and thermal

stability of the fluid oxide phase can be tailored if the oxide phase contains both B_2O_3 and SiO_2.

$$2B + 3/2O_{2(g)} \longrightarrow B_2O_{3(l)} \tag{1.6}$$

$$2BN_{(s)} + 3/2O_{2(g)} \longrightarrow B_2O_{3(l)} + N_{2(g)} \tag{1.7}$$

$$SiC(s) + 2O_{2(g)} \longrightarrow SiO_{2(s,l)} + CO_{(g)} \tag{1.8}$$

$$SiC(s) + 3/2O_{2(g)} \longrightarrow SiO_{2(s,l)} + CO_{(g)} \tag{1.9}$$
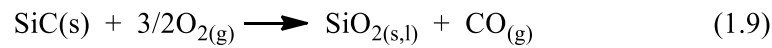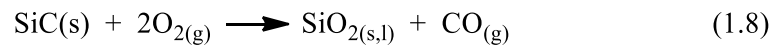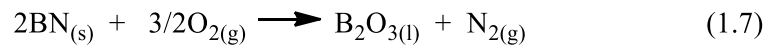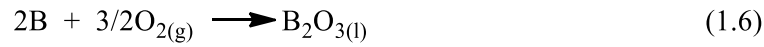
1.5.1.2 Boron containing ceramic additives

In this methodology, boron containing ceramics such as B_4C, SiB_4 or boron itself will be added as additive or mixed with SiC ceramic to achieve *self-healing* matrix as shown in eqns. (1.10) to (1.13) [Wang *et al.* 2010].

$$B_4C(s) + 4O_{2(g)} \longrightarrow 2B_2O_{3(l)} + CO_{2(g)} \tag{1.10}$$

$$B_4C(s) + 7/2O_{2(g)} \longrightarrow 2B_2O_{3(s,l)} + CO_{2(g)} \tag{1.11}$$

$$SiB_{4(s)} + 4O_2 \longrightarrow B_2O_3(l) + xSiO_{2(l)} \tag{1.12}$$

$$2B + 3/2O_{2(g)} \longrightarrow B_2O_{3(l)} \tag{1.13}$$
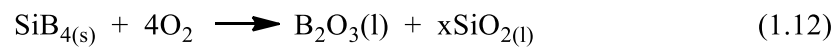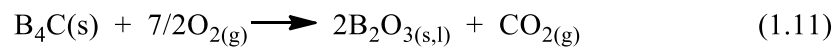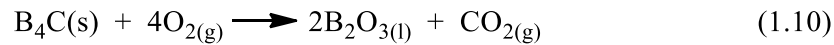
However, by the addition of boron containing ceramic additive to the polymeric precursors suffers from several disadvantages such as poor homogeneity, adhesion and processing difficulties. Also, by loading the liquid precursor with a ceramic additive considerably increases its viscosity and may render impossible the complete impregnation of a complex nD-fiber preform.

1.5.1.3 Boron containing ceramic matrix

This methodology is the most advanced technique for achieving *self-healing* properties for the CMCs. The boron-containing ceramic will be introduced in the SiC-matrix itself, which will overcome the limitation created by the additives. Further, it will improve the oxidation resistance of CMCs through the *in-situ* formation of fluid

oxide phases based on borosilicate glass ($SiO_2.B_2O_3$). Researchers have reported the introduction of a multi-layered *self-healing* matrix based on boron in the SiC matrix [Carrère *et al.* 2003, Quemard *et al.* 2007]. Compared to multi-layered self-healing matrix fabricated by CVI method, synthesizing boron as back bone of the polymer resin has a shorter processing time and is a cost effective route [Ganesh Babu *et al.* 2016].

In this regard, synthesis of boron, silicon and nitrogen containing polymers has gained importance due to their superior thermo-chemical properties compare to boron free preceramic polymer [Ionescu *et al.* 2012]. These polymers upon pyrolysis at higher temperatures gives silicon, boron and nitrogen containing ceramics such as silicon boride (SiB_4 or SiB_6), SiC/B_4C, boron nitride (BN), silicon-boron-oxycarbide (SiBOC) ceramics [Riedel *et al.* 2006], silicon carbonitrides (SiCN) ceramic [Bahloul *et al.* 1993, Golczewski *et al.* 2004], silicon boron carbonitrides (SiBCN) ceramics [Tang *et al.* 2016]. These ceramic materials, when exposed to oxidizing environment at high temperature, forms a protective borosilicate glassy layer on the surface, which prevents further oxidation of the CMCs by forming *self-healing* matrix. The general classes of boron, silicon and nitrogen containing polymers used as precursors for CMCs are polyborosilanes, polysilazane, polyborosiloxane and polyborosilazane.

In spite of the great importance of such class of novel ceramic materials, relatively fewer studies have been reported on their synthesis. Silicon, boron and nitrogen containing ceramics are commonly prepared by the pyrolysis of polymeric precursors such as dimethyldiethoxysilane, dialkyldichlorosilanes, polyorganoborosilazane [Kong *et al.* 2015, Zhang *et al.* 2017], hydridopolysilazane [Lee *et al.* 2003], silazane-substituted borazines [Luo *et al.* 2013], etc. In almost all these methods, the preparation of polymeric precursor requires several intermediate steps involving complex synthesis procedures and handling of hazardous chemicals (borane dimethyl sulfide, chlorosilanes) and their by-products (ammonium chloride) [Lee *et al.* 2003, Luo *et al.* 2013]. This makes the overall preparation of these ceramic process very complex, laborious and expensive. Also, the most of the polymeric precursors will be insoluble in common solvents, which limits further processability and impedes its use as a preceramic resin for high-temperature applications. This

difficulty in further processing of preceramic resins can be overcome by its modification with organic resins.

Among various organic resins, phenol-formaldehyde (PF) resin can easily be modified with inorganic moieties such as boron [Ganesh Babu *et al.* 2016], silicon [Nason 1939], titanium [Zhang *et al.* 2013] and phosphorus [Hsiue *et al.* 2001]. In addition to feasibility of modification, PF resin are relatively inexpensive which makes them potential candidate for producing cost effective ceramics.

1.6. Need for the modification of phenol-formaldehyde (PF) resin

Phenol-formaldehyde (PF) resin is a thermoset polymer which are most attractive materials in the marketplace and has hundreds of industries benefit from their use [Knop *et al.* 1979, Knop *et al.* 2013]. Their primary use is for aircraft interior structures because of their low flammability and smoke production [Nair 2004]. They are also used for high-temperature heat shields due to their excellent ablative resistance and as the starting material for C/C composites because of their high char yield during graphitization [Fitzer 1987]. The PF upon pyrolyzing under inert atmosphere produce a porous carbon matrix which are mainly used for the fabrication of C/C and C/SiC composites. PF resins are prepared by the reaction of phenol or substituted phenol with an aldehyde, especially formaldehyde, in the presence of an acidic or basic catalyst. PF resins are broadly classified into Novolacs and Resols based on the type of catalyst used and nature of crosslinks [Lee *et al.* 2003]. The structure of these two types of PF resins are given in Figure 1.20.
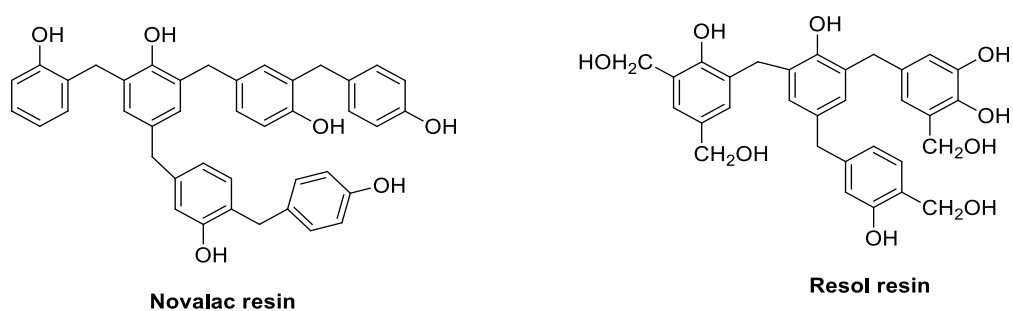
Figure 1.20. Structure of phenolic resins

a. *Novolac resin*

Novolac resins are synthesized from a monomer feed with excess phenol in the presence of an acid catalyst. The final novolac resin is unable to react further without the addition of a crosslinking agent like hexamethylenetetramine (HMTA). Novolac resins are amorphous thermoplastics, which are solid at room temperature and soften and flow in the temperature range 65-105°C. The number average molecular weight of a standard phenol novolac resin is between 250°C and 900°C. Novolac resins are soluble in polar organic solvents (e.g., alcohols, acetone), but not in water.

b. *Resol resin*

A base (alkaline) catalyst and, usually but not necessarily, a molar excess of formaldehyde is used to make resole resins. When an excess of formaldehyde is used, sufficient number of methylol and dibenzyl ether groups remain reactive to complete the polymerization and cure the resin without incorporation of a curing agent. The typical number average molecular weight of a resol resin is between 200 and 450. The commonly used alkaline catalysts are NaOH, $Ca(OH)_2$, and $Ba(OH)_2$.

Resol resin can easily be modified with inorganic moieties such as boron, silicon, titanium and phosphorus as compared to that of novalac resin [Chiang *et al.* 2004, Kawamoto *et al.* 2010, Zhang *et al.* 2013]. This is due to the presence of free methylol groups in resol resin which helps in feasibility of the modification. These modified resins are widely used in the process of polymer infiltration and pyrolysis technique to prepare refractory carbide modified carbon/carbon composites (C/C). However, similar to the disadvantages associated with other polymeric materials, the application of PF resin at high temperatures is restricted due to its thermal degradation above 200°C [Li *et al.* 2016]. For the development of advanced ceramics based on modification of preceramic resin with organic resin such as PF, it is particularly attractive to utilize the best properties of each component to develop new materials with tailor made properties. Hence, attempts were made in this thesis to synthesize phenol formaldehyde resin modified with boron, silicon and nitrogen which are expected to be potential preceramic matrix resin for CMCs to achieve improved oxidation resistance

property.

1.7. Application of CMCs

It is convenient to divide the general applications of CMCs in terms of aerospace and non-aerospace applications. In the aerospace area, performance is the foremost consideration while in the non-aerospace fields cost effectiveness is the prime consideration.

1.7.1 Aerospace applications

Aerospace applications, in general, demand high thrust-to-weight ratios, faster cruising speeds, increased altitudes and improved flight performance [Naslain *et al.* 2004]. These goals translate into material requirements involving increased strength-to-density, stiffness-to-density and improved damage tolerance all at significantly higher temperatures. High-temperature structural composites represent a key technology for advanced aerospace systems [Triantou *et al.* 2017]. CMCs potentially offer higher specific mechanical properties which can be utilized in a variety of high-temperature aerospace applications. SiC coated C/C composites are used as a thermal protection material in the Ceramic Matrix Products Division of Vikram Sarabhai Space Centre, Indian Space Research Organization (ISRO). C/SiC composites are candidate materials for a variety of space plan programs in ISRO. Besides the space plane, other applications for CMCs include a variety of high speed airplane, various defense related projects such as Advanced Tactical Fighter (ATF), many existing fighters, missiles, hypersonic flights, hard armor and turbine engines [Halbig *et al.* 2013, Kalaiyarasan *et al.* 2016, Kiser *et al.* 2016, Luo *et al.* 2017].

1.7.2 Non-aerospace applications

Among the non-aerospace applications of CMCs, engine components at high temperatures and in corrosive environments [Low 2014], cutting tool inserts [Liu *et al.* 2014], wear resistant parts [Wang *et al.* 2017], nozzles [Halbig *et al.* 2013] and exhaust ducts [Hynes *et al.* 2016], energy related applications such as heat exchanger tubes [Zhou *et al.* 2013], etc. are the prime areas. For such applications, the components can range from simple to complex and tend to be smaller in size. Thus, it is not surprising

that for applications related to wear, cutting tool inserts, and heat engines, there are commercially available dense, wear-resistant, particle- and whisker-reinforced ceramic matrix composites.

Scope and objectives

The survey of pertinent literature reveals that, the field of CMCs have been intriguing technologists for diverse high temperature applications such as rocket nozzles, aeronautic jet engines, heat shields and aircraft braking systems. There has been concerted developments and innovations reported in this field over the last two decades. The search for more and more advanced materials that can survive the extreme environments clearly shows the ever rising interest and un-tapped potential of this field for further technological advancement of CMCs. However, the production cost and the materials used can reach escalating price depending on the targeted applications and the technologies required for their production which continues to be a major obstacle to widespread application of CMCs. Hence, development of these materials with competitive and attractive methods gains tremendous significance for high-temperature application.

The main objective of this study is to develop new class of cost effective preceramic polymer to employ it as matrix resin for CMCs to achieve *self-healing* properties and to investigate its effect on mechanical properties. Covering these aspects, the research work is divided into the following chapters.

Chapter-1 gives a general introduction on CMCs, design and selection of constituents in CMCs, processing techniques involved to fabricate CMCs and the role of boron in protection of CMCs for the long-term aerospace applications.

Chapter-2 provides the details on materials, experimental procedures and the analytical techniques used in the present study.

Chapter-3 deals with the investigation of boron modified phenol-formaldehyde (BPF) resins as preceramic matrix resin for CMCs. This chapter comprises of two parts;

- In the first part, synthesis, characterization and ceramic conversion studies of BPF resins are discussed in detail. The aim of the work is to evaluate BPF as a potential *self-healing* matrix resin for the fabrication of CMC.

- In the second part, CMCs are fabricated using BPF resin blended with elemental silicon as preceramic matrix resin, PyC as interphase and 2D carbon fabric as reinforcement. The study focusses on the optimization of fiber/matrix (F/M) volume ratio and the influence of PyC interphase coating on the flexural properties of CMCs.

In Chapter-3, silicon is added as additive to the preceramic polymer and used as matrix resin for CMCs. In Chapter-4, attempt was made to incorporate silicon as back bone of preceramic polymer and used as matrix resin for CMCs. This work has been divided into two parts;

- In the first part, synthesis, characterization and ceramic conversion studies of silazane modified phenol-formaldehyde (SPF) resins are discussed in detail. The principle objective of the study is to select an appropriate pyrolysis condition (pyrolysis) to achieve desired ceramic in high yield (>60 wt. %).

- In the second part, CMCs are fabricated using SPF as matrix resin *via* polymer impregnation and pyrolysis (PIP) techniques. The study focusses on the investigation of fracture behavior and failure mechanism of the obtained CMCs.

In Chapter-4, the work was focused on the improvement of mechanical properties of the CMCs derived from SPF. However, for the long-term use superior oxidation resistance of CMCs are highly desired. Hence, in Chapter-5, synthesis of single source preceramic matrix resins containing silicon, boron and nitrogen are attempted to get SiBCN based ceramics. This work has been divided into two parts;

- In the first part, synthesis, characterization and ceramic conversion studies of boron modified cyclotrisilazane (BCTS) resins are discussed in detail. The principle objective of this work is to assess BCTS resin as potential preceramic resin and to attain oxide free SiBCN ceramic.

- In the second part, CMCs derived from BPF and SPF resins were screened based on the mechanical properties and were infiltrated with

BCTS resin to achieve cost-effective CMCs with improved oxidation resistance property.

Chapter-6 summarizes the findings of the present investigation together with concluding remarks and scope for future work.

Chapter 2

Materials and Methods
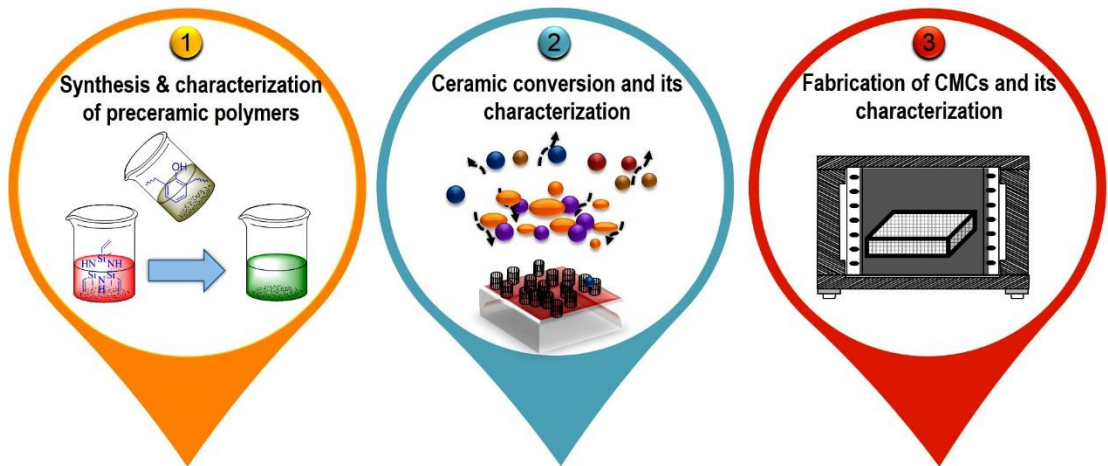
- This chapter provides the details on the materials and experimental procedure for the synthesis and ceramic conversion process of preceramic polymers.

- Analytical techniques used for the characterization of the preceramic polymers and the ceramic materials.

- Procedure for the fabrication of CMCs and the evaluation of mechanical and oxidation resistance properties of the CMCs.

2.1. Materials

The materials used for the synthesis of preceramic polymers and fabrication of CMCs are given in Table 2.1.

Table 2.1
List of chemicals and materials

Sl. No.	Materials	Source
1.	Phenol-formaldehyde (PF) resin (properties are given in Table 2.2)	Produced in-house [Propellant Fuel Complex (PFC), VSSC]
2.	Silicon powder (99.5% purity, 7.5 μm particle size)	MEPCO, India
2.	Boric acid (99.5 % purity)	Qualigens, India
3.	N, N-dimethylformamide (DMF) (99.9% purity)	Sigma Aldrich, India
4.	Toluene (99.9% purity)	Sigma Aldrich, India
5.	Silicon powder (99.5% purity, 7.5 μm particle size)	MEPCO, India
6.	1, 3, 5-trimethyl-1', 3', 5'-trivinylcyclotrisilazane (CTS) (99.5 % purity)	Sigma Aldrich, India
7.	Dicumyl peroxide (DCP) (98% purity)	SD fine-Chem Ltd., India
8.	Acetone, 99.0 %	Sisco Research Laboratory, India
8.	Distilled water	N.A.
9.	dichloromethane (99.5 % purity)	Sigma Aldrich, India
10.	$CaSO_4$ (99.5 % purity)	Sigma Aldrich, India
11.	2D carbon fabric (T300 3K, 8H, satin weave)	Toray, Japan

Table 2.2
Properties of PF resin (Synthesized in-house)

Sl.No.	Property	Phenol-Formaldehyde Resin
1.	Type	Resol
2.	Specific Gravity	1.18-1.20
3.	Viscosity at 30°C (cps)	600
4.	Free formaldehyde (%)	0.1
5.	Cure Time	120 min. at 175°C

2.2. Synthesis of preceramic polymers

2.2.1. Synthesis of BPF resin

BPF resins were synthesized by using the procedure given below:

In a typical experiment, 100g of phenol formaldehyde (PF) resin was taken in a four-necked round bottom flask equipped with a mechanical stirrer, condensor and Dean Stark apparatus and an inlet and outlet for argon gas. In the first step, the PF resin was heated in an oil bath to 80°C under argon atmosphere for 1h. In the second step, 5 g of boric acid in DMF was added drop-wise to the PF resin and refluxed at 120°C for 4h under argon atmosphere. In order to remove the reaction by product (water) using a Dean Stark system, 35ml of toluene was added to the reaction mixture and distilled. Finally, greenish yellow viscous BPF resin was obtained which is designated as BPF-5 [boric acid is 5 parts per hundred (pph) w.r.t. PF]. Similarly, BPF-10, BPF-15, BPF-20, BPF-25 and BPF-30 resins were also prepared by varying the concentration of boric acid from 10 pph to 30 pph w.r.t. PF, respectively (as shown in Table 2.3). However, the concentration of boric acid could not be increased beyond 30 pph as it precipitated in solution. PF resin is soluble in acetone whereas the BPF resin synthesized was insoluble in acetone. The schematic representation of BPF resin is shown in Figure 2.1.

Table 2.3
Different composition of BPF resin

Sl. No.	Sample	PF (g)	Boric acid (g)
1.	PF	100	-
2.	BPF-5	100	5
3.	BPF-10	100	10
4.	BPF-15	100	15
5.	BPF-20	100	20
6	BPF-25	100	25
7.	BPF-30	100	30
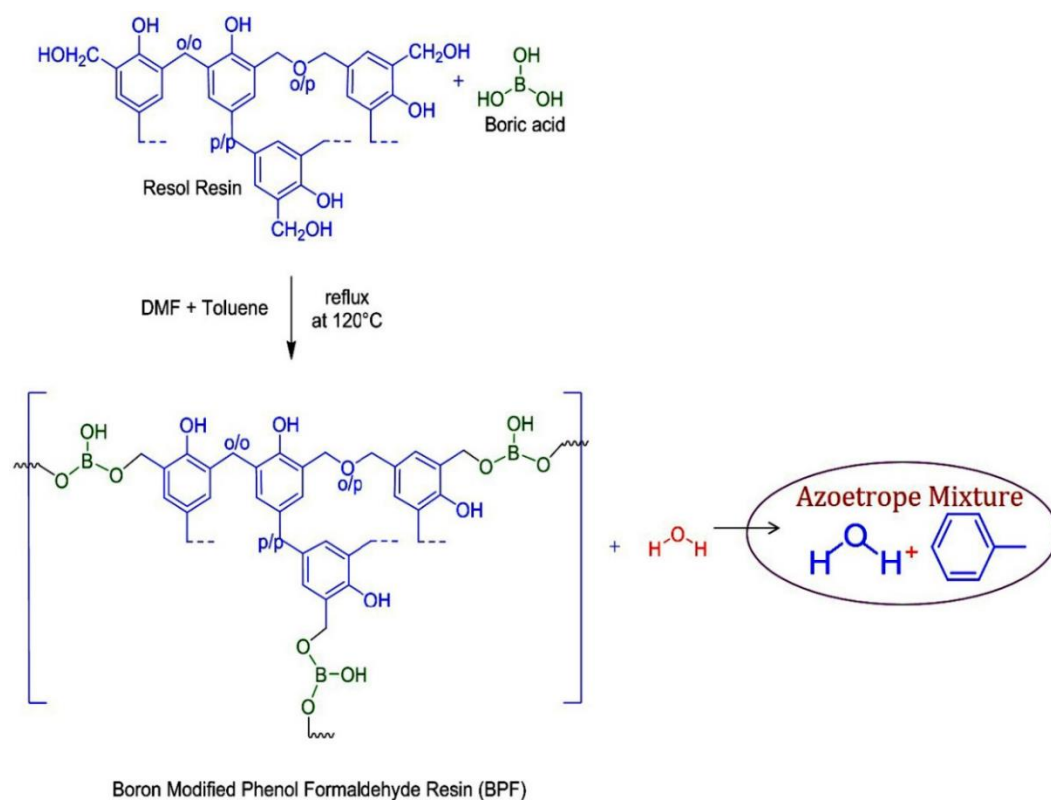
Figure 2.1 Synthesis of BPF resin

2.2.2. Synthesis of SPF resin

SPF resins were synthesized *via* a facile two step reaction by using the procedure given below:

SPF resins with different concentration of silazane were synthesized *via* a facile two step reaction. In the first step, preparation of polycyclotrisilazane (PCTS) was carried out according to a previously reported procedure [Toreki *et al.* 1990]. As a typical example, 5 g of CTS was taken in four-necked round bottom flask equipped with a mechanical stirrer, condensor and an inlet and outlet for nitrogen gas. 0.06 g of DCP (CTS: DCP= 90: 1 molar ratio) in dry toluene was added drop-wise to the CTS. The reaction mixture was refluxed at 135°C for 12h under nitrogen atmosphere to form viscous PCTS resin. In the second step, 100 g of PF resin in DMF was added drop-wise to the obtained PCTS resin and refluxed at 120°C for 4h under nitrogen atmosphere.

Finally, yellowish viscous SPF resins was obtained which is designated as SPF-5 [CTS is 5 parts per hundred (pph) w.r.t. PF]. Similarly, SPF-10, SPF-15, SPF-20, SPF-25 and SPF-30 resins were also prepared by varying the concentration of CTS from 10 pph to 30 pph w.r.t. PF, respectively (as shown in Table 2.4). However, the concentration of CTS could not be increased beyond 30 pph due to incomplete reaction of PCTS with PF resulting in the formation of separate phase in the reaction medium. The schematic representation of SPF resin is shown in Figure 2.1.
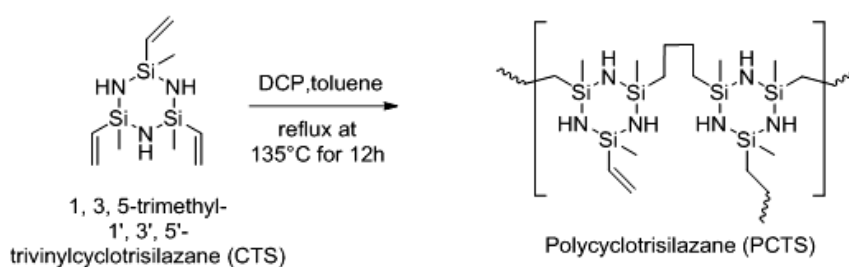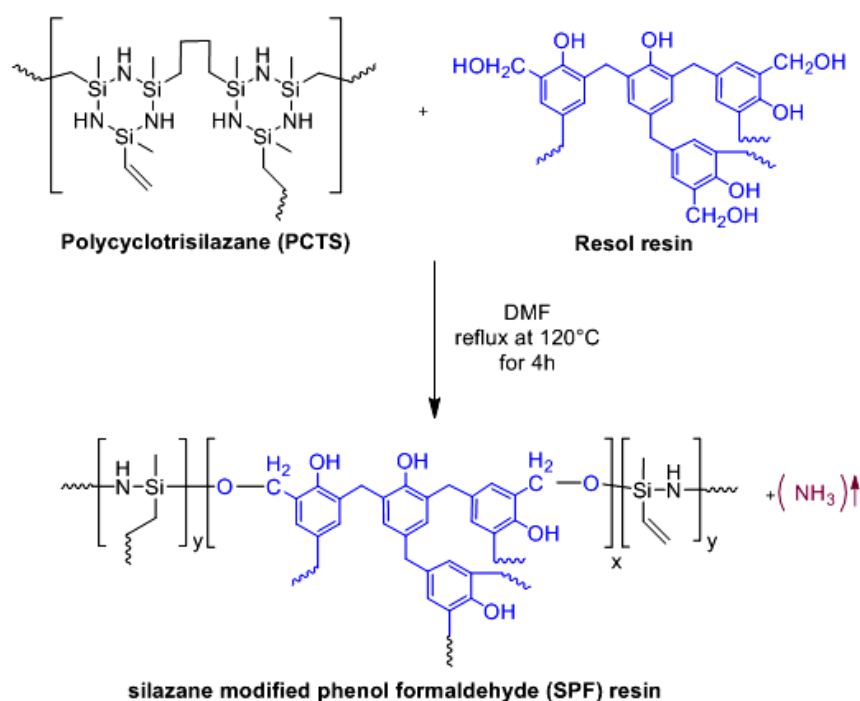
Figure 2.2 Synthesis of SPF resin

Table 2.4
Different composition of SPF resin

Sl.No	Sample	Conversion of CTS to polycyclotrisilazane (PCTS)		PF-106 (g)
		CTS (g)	DCP (g)	
1	PF	-	-	100
2	SPF-5	5	0.06	100
3	SPF-10	10	0.12	100
4	SPF-15	15	0.17	100
5	SPF-20	20	0.23	100
6	SPF-25	25	0.29	100
7	SPF-30	30	0.35	100

2.2.3. Synthesis of BCTS resin

BCTS resins were synthesized by reacting boric acid with 1, 3, 5-trimethyl-1', 3', 5'-trivinylcyclotrisilazane (CTS) in the molar ratio of 1:1, 1:3 and 1:5 as shown in Table 2.5. In a typical procedure, 3.65 g (0.059 mole) of boric acid in distilled water was taken in four-necked round bottom flask equipped with a mechanical stirrer, condensor and an inlet and outlet for nitrogen gas. 15 g (0.059 mole) of CTS was added drop-wise to the boric acid solution at 80°C, followed by refluxing at 105 °C for 11h under nitrogen atmosphere. The reaction was cooled to room temperature and the water layer was removed by fractionation using dichloromethane followed by drying it in $CaSO_4$ for 24h. The residual solvent was removed under vacuum to obtain a clear colourless resin, which is designated as BCTS11 (molar ratio of H_3BO_3: CTS is 1:1). Similarly, BCTS13 and BCTS15 resins were also prepared by varying the concentration of boric acid with CTS in molar ratio of 1:3 and 1:5, respectively as shown in Table 2.5.

Table 2.5
Different composition of BCTS resin with viscosity and molecular weight

Sl. No.	Sample	Molar ratio of Boric acid: CTS	CTS (g)	Boric acid (g)
1	CTS	-	-	-
2	BCTS11	1:1	15.08	3.65
3	BCTS13	1:3	45.23	3.65
4	BCTS15	1:5	75.38	3.65
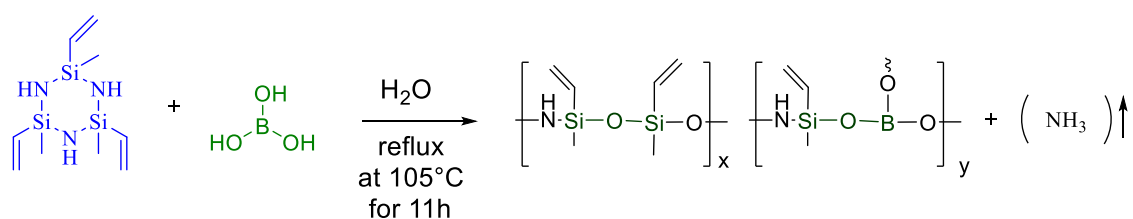
Figure 2.3 Synthesis of BCTS resin

2.3. Characterization of preceramic polymer

2.3.1. Gel permeation chromatography (GPC)

Molecular weights ($\bar{M}_w$ and $\bar{M}_n$) were determined by Waters 'Alliance' gel permeation chromatograph (GPC) instrument using HR1 and HR2 microstyragel columns and tetrahydrofuran (THF) as the eluent with a flow rate of 1 mLmin^{-1}. Water 410RI detector was used. The system was managed with millennium 32 GPC software. The molecular weights reported were based on polystyrene standards.

2.3.2. Viscosity measurements

Using HBDT Brookfield viscometer (Model Visco II+), the viscosity of preceramic polymer at 25°C was determined. The viscosity of the oligomer was measured in terms of the resistance to rotation experienced by rotor blade, which was rotated with in the fluid under consideration, for a particular duration and temperature.

2.3.3. Fourier Transform-Infra Red (FT-IR) spectroscopy

The structural characterization of preceramic polymer was done using FT-IR spectroscopy. Samples were recorded in KBr pellets using Perkin Elmer Spectrum GX-A FTIR spectrometer in the wave number range of 4000-400 cm^{-1}. The instrument employed a pyroelectric detector for scanning the samples and it generated the spectra depicting the percentage of transmittance versus wave number, by averaging 5 scans at a resolution of 0.5 cm^{-1}.

2.3.4. Nuclear Magnetic Resonance (NMR) spectroscopy

^{1}H-, ^{29}Si- and ^{11}B- NMR spectra were measured at 300, 59.6 and 96.3 MHz respectively, on Brucker DMX 300 Spectrometer. For ^{1}H- and ^{29}Si-NMR, the chemical shifts were recorded using CDCl$_3$ as solvent and tetramethylsilane as an internal

standard. In the case of ^{11}B-NMR spectra, deuterated THF was used as solvent and the chemical shifts were reported with respect to an external standard viz., borontrifluoride etherate.

2.3.5. Thermogravimetric analysis (TGA)

Thermogravimetric analysis (TGA) of preceramic polymers were performed on TA Instruments SDT 2960 at a heating rate of 10°C min^{-1} under nitrogen atmosphere over a temperature range of 25°C to 1200°C.

2.3.6. Pyrolysis–gas chromatography–mass spectrometry (Py–GC–MS)

Pyrolysis-gas chromatography-mass spectrometry (Py–GC–MS) studies were conducted using a Thermo Electron Trace Ultra GC directly coupled to a Thermo Electron Polaris Q (Quadruple ion trap) mass spectrometer and SGE pyrolyzer (Pyrojector II, SGE Analytical Science Pty Ltd, Ringwood, Victoria, Australia).

2.4. Polymer to Ceramic conversion

2.4.1. Pyrolysis of BPF resin

The synthesized BPF resins (Table 2.3) were cured at 175°C for 2 h in air oven. 15 g of the cured BPF was taken in alumina crucible and pyrolyzed at 1450°C under argon atmosphere at a heating rate of 3°C/min and gas flow rate of 50 mL/min. The furnace temperature was maintained at 1450°C for 3 h and then it was cooled to room temperature at a heating rate of 3°C/min to obtain boron and carbon (BC) containing ceramics.

2.4.2. Pyrolysis of BPF resin with silicon as additive

The synthesized BPF resin (Table 2.3) was blended with stoichiometric amount of silicon powder (designated as BPFSi) with respect to carbon obtained at 1450°C during pyrolysis of PF, i.e. ratio of Si: C = 2.33:1. The mixture was ball milled for 120 min to obtain uniform slurry, followed by curing at 175°C. 15 g of cured mix was taken in alumina crucible and sintered at 1450°C under argon atmosphere at a heating rate of 3°C/min and gas flow rate of 50 mL/min. The furnace temperature was maintained at 1450°C for 3 h and then it was cooled to room temperature at a heating rate of 3°C/min

to obtain silicon, carbon and boron-containing ceramics (designated as SiBOC).

2.4.3. Pyrolysis of SPF resin

The synthesized SPF resins (Table 2.4) were cured at 200°C for 2 h under vacuum oven. 15 g of the cured SPF was taken in alumina crucible and pyrolyzed at 1450°C and 1650°C separately under argon and nitrogen atmosphere. Ceramic conversion studies were carried out by heating the sample at a rate of 3°C/min and maintained at pyrolysis temperature (1450°C or 1650°C) for 3 h. The furnace was then cooled back to room temperature at a rate of 3°C/min. Both the heating and cooling process were carried out under argon or nitrogen atmosphere at a flow rate of 50 mL/min.

2.4.4. Pyrolysis of BCTS resin

The synthesized BCTS resins (Table 2.5) were cured at 200°C for 2 h under vacuum oven. 15 g of the cured BCTS was taken in alumina crucible and pyrolyzed at 1450°C and 1650°C under nitrogen atmosphere. Ceramic conversion studies were carried out by heating the sample at a rate of 3°C min^{-1} and maintained at pyrolysis temperature (1450°C or 1650°C) for 3 h. The furnace was then cooled back to room temperature at a rate of 3°C min^{-1}. Both the heating and cooling process were carried out under nitrogen atmosphere at a flow rate of 50 mL/min.

2.5. Characterization of ceramics obtained from preceramic polymer

2.5.1 X-Ray Diffraction (XRD) analysis

The structural evolution of ceramics was studied using X-ray diffraction (XRD) analysis. The sample were recorded on a Bruker D8 discover using Cu-Kα radiation (40 kV, 40 mA; step scan of 0.051, counting time of 5 s/step and 1.5460 A°). The crystallite size of ceramics was calculated from the line broadening of diffraction peak using Scherrer equation.

$$D= \frac{k\lambda}{\beta \cos\theta} \tag{2.1}$$

where D is the average crystallite size, k is the coefficient, which is generally taken as 0.94, λ is the wavelength of X-ray radiation equal to 1.5406 Å, β is full width at half maximum (FWHM) measured in radians, and θ is the Bragg's angle.

2.5.2 Raman spectroscopy

The nature of free carbon in the ceramics was understood using Raman spectra recorded with WITec alpha 300R confocal Raman microscope using frequency doubled Nd: YAF laser of excitation wavelength 532 nm. The parameters such as variations in position and intensity of D and G band were derived using Gaussian curve fitting of the Raman bands. The intensity ratio of the D and G bands (I_D/I_G) were used to calculate the cluster size (La) of the free carbon using the formula reported by Ferrari and Robertson [Ferrari *et al.* 2004].

$$\frac{I_D}{I_G} = C'(\lambda)\,\mathrm{L}_a^2 \qquad (2.2)$$

where L_a is the size of carbon domains along the six-fold ring plane, and C' is a coefficient that depends on the excitation wavelength (λ) of the laser. The value of C' of the wavelength of 532 nm of the Nd: YAG laser used here is 0.6195 nm.

2.5.3 Scanning electron microscopy (SEM) / Energy Dispersive X-ray (EDX) analysis

The morphological features were analyzed using scanning electron microscopy (SEM) analysis. The analysis was done using JEOL Model JSM - 6390LV. This instrument has a resolution of 3 nm at an accelerating voltage of 20 KV and ultimate vacuum of 10^{-7} Torr. The specimen surface was made electrically conductive by coating a thin layer of gold by the plasma vapor deposition in a Fine Coat Ion Sputterer JF-1100. For EDX analysis, an OXFORD INCA system was used.

2.5.4 Felid emission Scanning electron microscopy (FESEM) / Energy Dispersive X-ray (EDX) analysis

In order to obtain high-resolution and magnified image the ceramic sample,

Field Emission Scanning Electron Microscopy (FESEM) was carried out. The ceramic samples were imaged using a Carl Zeiss, Supra 55, FESEM instrument. SUPRA 55 FE-SEM is an ultra-high resolution FESEM based on the unique GEMINI Technology. It provided excellent imaging properties combined with analytical capabilities. This instrument has a resolution of 1 nm at an accelerating voltage of 30 KV and ultimate vacuum of 10^{-7} Torr. The sample surface was made electrically conductive by coating a thin layer of gold by the plasma vapor deposition in a Fine Coat Ion Sputterer JF-1100. For EDX analysis, an OXFORD INCA system was used.

2.5.5 High-resolution Transmission electron microscopy (HRTEM) analysis

High-resolution transmission electron microscope analysis was used to study the crystal structure and topographical features such as shape/dimensions of the surface structures present in the ceramic sample. The samples were recorded using Technai 30 G2, S-TWIN instrument. For this samples were prepared by finely powdering the ceramics into sub-micron sizes and dispersing these in acetone to form a uniform slurry. A drop of the slurry was transferred to a carbon-film coated TEM grid.

2.5.6 Elemental Analysis

2.5.6.1 Estimation of silicon

Silicon content of the ceramic were determined by gravimetric analysis [1966]. The silicon containing ceramic sample was converted to its sodium salt by sodium carbonate fusion. The extract was dehydrated with perchloric acid, ignited, and then volatilized after adding hydrofluoric acid. The residue obtained was ignited and weighed. The loss in weight represents the quantity of silica formed. Percentage of silicon in the sample is then estimated as:

$$\text{Silicon}\,(\%) = \frac{\text{Weight of silica in grams} \times 28.08 \times 100}{\text{Weight of the ceramic sample in grams} \times 60.08}$$

2.5.6.2 Estimation of boron

Boron content of ceramic sample was also determined by volumetric analysis

[1966]. About 1 to 2 g of the sample and 5 g of anhydrous sodium carbonate were taken in a platinum crucible and heated in a furnace to 1000°C. The melt was dissolved in water followed by digestion. The solution was filtered through a filter paper. The pH of the filtrate was adjusted to 3.5 with dilute sulphuric acid and heated for some time to remove any carbonic acid formed. The filtrate was titrated against standard sodium hydroxide solution. Mannitol solution was added and the titration was continued till mannitol borate equivalent point (near pH = 8.1) was reached. Boron percentage in the sample is then estimated as:

$$\text{Boron (\%)} = \frac{\text{Volume of NaOH} \times \text{Normality of NaOH} \times 10.8 \times 100}{\text{Weight of the ceramic sample in grams}}$$

2.5.6.3 Estimation of carbon and nitrogen

The percentage of carbon and nitrogen present in ceramic samples were determined using a Perkin Elmer Elemental Analyzer (Model PE 2400). The analyzer was based on the Flash dynamic catalytic combustion of samples into simple gases. The system used a steady state wave-front chromatographic approach to separate the mixture of gases. The separated gases were detected as a function of thermal conductivity.

2.5.6.4 Estimation of oxygen

The oxygen content in the ceramic samples was analyzed by LECO TC 436 O-H-N analyzer. The ceramic powder was fused in a graphite crucible in Helium atmosphere and the liberated oxygen is reacted with carbon from the crucible to form CO_2, which was estimated by a non-dispersive infra-red detector (NDIR).

2.5.7 Determination of ceramic residue

The ceramic residue was experimentally determined as shown below

$$\text{Ceramic residue (\%)} = \frac{\text{Weight of the ceramic obtained at } 1450°C \text{ or } 1650°C \text{ in grams x } 100}{\text{Weight of the cured preceramic polymer in grams}}$$

2.6. Preparation of ceramic matrix composites (CMCs)

In the present investigation, CMCs were fabricated using 2D carbon fabric (Toray, T300 3K, 8H, satin weave) as reinforcement, PyC as an interphase, two different matrix resin namely, slurry of PF or BPF resin with silicon powder and SPF resin as matrix precursors and BCTS resin as oxidation protection coating.

2.6.1 Deposition of PyC interphase coating

The PyC interphase coating of thickness 0.2-0.5 μm was deposited on carbon fabric via an isothermal/isobaric CVI technique using CH_4 as precursor at 1200°C for 3hr under argon atmosphere.

2.6.2 Preparation of CMCs using slurry containing PF or BPF resin with silicon powder as matrix precursor

CMCs were fabricated from carbon fabric (Toray, T300 3K, 8H, satin weave) as reinforcement and slurry containing PF or BPF resin with silicon powder as matrix resin via RBSC technique (Figure 2.4).

In the typical experiment, carbon fabric was cut into square pieces of 200×200 mm^2 size and the slurry was applied on to the pieces. The coated fabric pieces were dried at 80°C for 1 h and stacked in 0°/90° fiber orientation to form the desired thickness of the preform. The whole assembly was covered with Teflon sheet and kept in a steel mold. The mold was then placed in a hydraulic press and was cured at 175°C in a programmed heating as given in Table 2.6. The precursor composite was then allowed to cool to room temperature and removed from the hydraulic press. The cured preforms were pyrolyzed at 900°C followed by sintering at 1450°C (slightly above the melting point of silicon) in a programmed heating rate as given in Table 2.6 under argon atmosphere at a flow rate of 50 mL/min. Thus obtained CMCs were machined to evaluate the flexural and oxidation resistance properties.
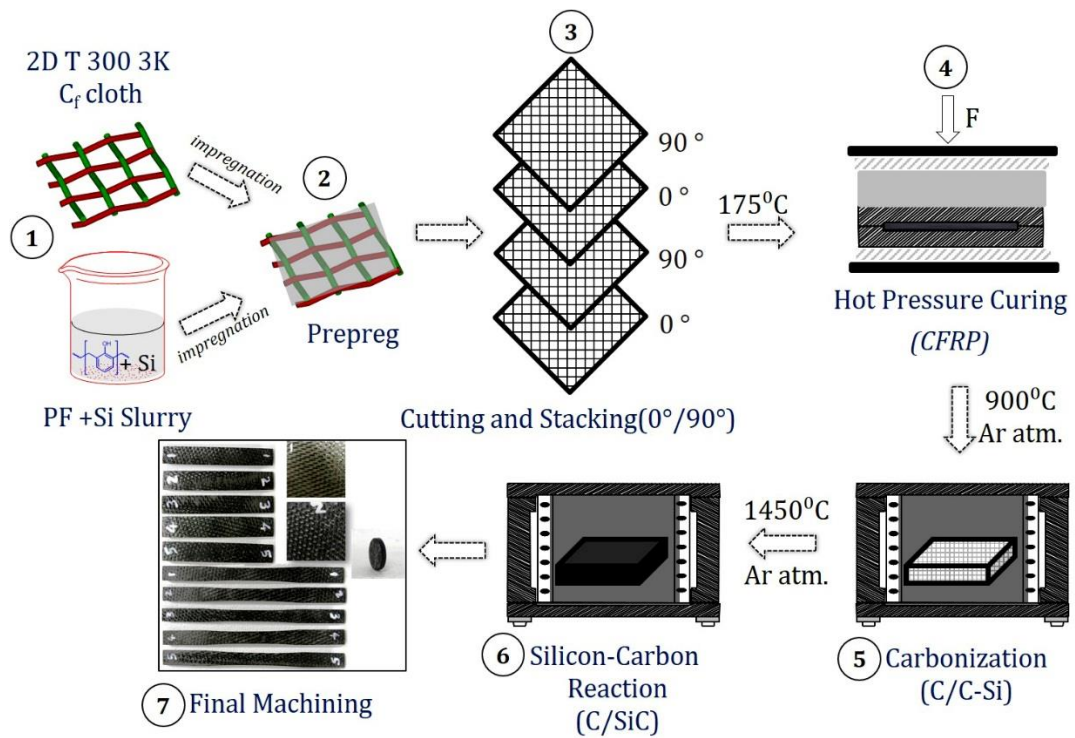
Figure 2.4 Schematic view for the fabrication of CMCs using slurry containing PF or BPF resin with silicon powder as matrix precursor *via* RBSC method

Table 2.6
Hot press curing profile programme for CMC

Sl. No.	Outside Temperature (°C)	Inside Temperature (°C)	Time (h)	Pressure(lb/in^2)
1.	105	95	1	
2.	145	125	1	
3.	165	150	1	200
4.	190	175	3	

Table 2.7
Pyrolysis and sintering profile programme for CMC

Sl. No.	Temperature (°C)	Heating rate (°C/min)	Dwell
1.	25 to 400	2	1h at 400°C
2.	400-900	2	1h at 900°C
3.	900-1450	3	3h at 1450°C
4.	1450-25	3	-

2.6.3 Preparation of CMCs using SPF resin as matrix precursor

CMCs were fabricated using different composition of SPF (SPF-5 to SPF-30) as preceramic matrix resin and 2D carbon fabric as reinforcement *via* PIP process as

shown in Figure 2.5.
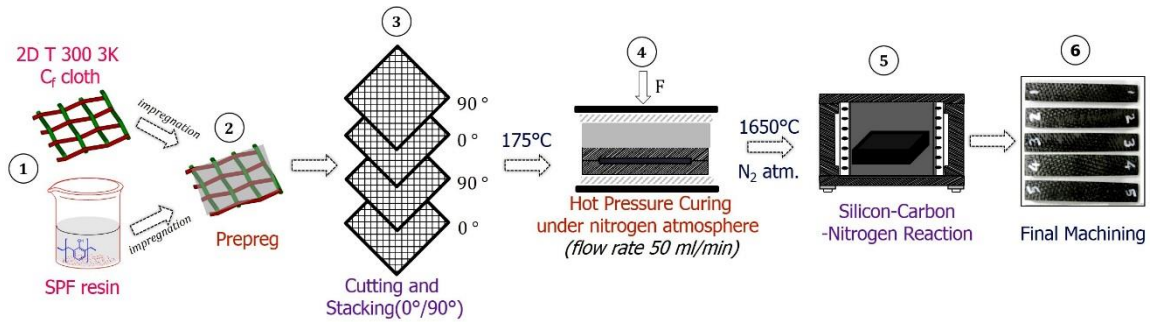
Figure 2.5 Schematic view for the fabrication of CMCs using SPF resin as matrix precursor *via* PIP method

In the typical experiment, SPF resin was coated over PyC coated carbon fabric pieces (150×150 mm^2) and the precursor composite were fabricated by following the procedure described in the previous section. The cured preform was pyrolyzed at 900°C followed by sintering at 1650°C in a programmed heating rate as given in Table 2.8 under nitrogen atmosphere at a flow rate of 50 mL/min. Three PIP cycles were repeated for further densification of the CMCs. Thus obtained CMCs were machined to evaluate the flexural properties.

Table 2.8
Pyrolysis and sintering profile programme for CMC

Sl. No.	Temperature (°C)	Heating rate (°C/min)	Dwell
1.	25 to 400	2	1h at 400°C
2.	400-900	2	1h at 900°C
3.	900-1650	3	3h at 1650°C
4.	1650-25	3	-

2.6.4 BCTS as oxidation protection coating for CMCs

CMCs derived from BPF and SPF resins were screened based on the mechanical properties and were infiltrated with BCTS resin to achieve cost-effective CMCs with improved mechanical and oxidation resistance properties. The schematic view for the vacuum infiltration of BCTS resin into CMCs are shown in Figure 2.6. In the typical procedure, CMCs with the dimension of $60\times9\times5$ mm^3 were taken and cleaned using emery paper to open-up the surface pores and infiltrated with the BCTS resin using

vacuum infiltration technique which involves the following steps,

1. Apply Vacuum < 1 torr for 30 mins

2. Infiltration of BCTS resin through vacuum infusion until CMCs are completely covered with resin

3. Kept under vacuum for 10 h

4. Allowing the CMCs to equilibrate to atmospheric pressure; vacuum cure at 200°C for 180 minutes
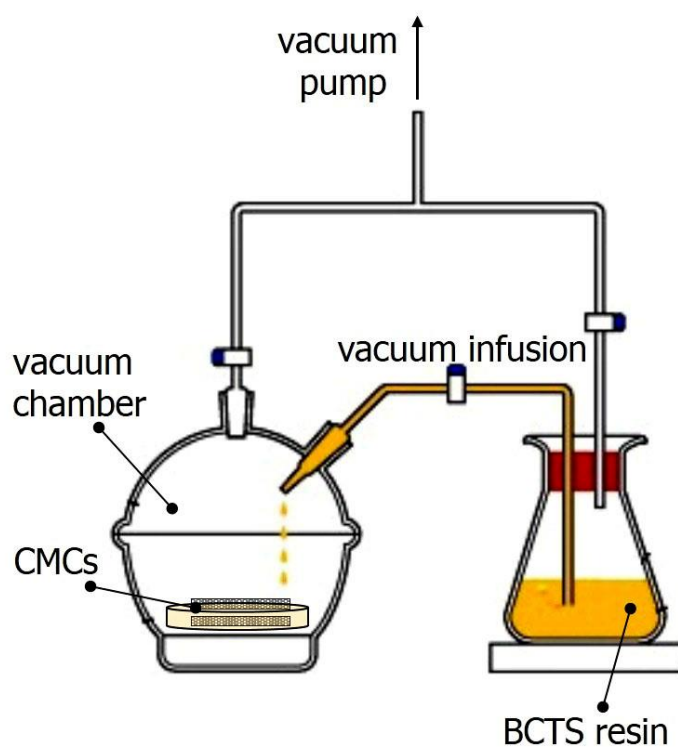
Figure 2.6 Schematic view for the vacuum infiltration of BCTS resin into CMCs

Thus obtained cured preforms were pyrolyzed at 900°C followed by sintering at 1650°C in a programmed heating rate as given in Table 2.8 under nitrogen atmosphere at a flow rate of 50 mL/min. Thus obtained CMCs were machined to evaluate the flexural and oxidation resistance properties.

2.7. Characterization of CMCs

2.7.1 Bulk density and open porosity

The bulk density and open porosity of the composites were measured by Archimedes method using distilled water as per ASTM C 20 [Kumar Mandal 2010].

$$\text{Bulk density} = \frac{D}{W - S} \text{ g/cm}^3 \tag{2.3}$$

$$\text{Open porosity} = \frac{(W - D)}{(W - S)} \times 100 \tag{2.4}$$

where, 'W' is saturated weight of the CMC, 'D' is the dry weight of the CMC and 'S' is suspended weight of the CMC

2.7.2 Evaluation of flexural strength

The flexural strength and modulus of the composites were measured by three-point-bending test at room temperature on a universal testing machine (INSTRON-5569) as per ASTM C 1341 [C1341 2013]. The dimension of the test sample was $60 \times 9 \times 5$ mm^3. The span length, L is 30 mm, and the crosshead speed is 0.5 mm/min. Flexural strength (σ_f) and flexural modulus (E_f) are calculated with the following equations:

$$\sigma_f = \frac{3PL}{2BH^2} \tag{2.5}$$

$$E_f = \frac{\Delta PL^3}{4BH^3 \Delta f} \tag{2.6}$$

where P is the maximum load, $\Delta P / \Delta f$ is the slope of the straight line in the load–deflection curve recorded during the test. All the flexural strength and modulus are the average values from five sample tests.

2.7.3 Optical microscopy analysis

After three-point-bending test, the crack propagation on the fractured surface of the CMCs was observed by an optical microscope. The fractured surface of the CMCs samples was recorded on Olympus BX51M optical microscopic instrument.

2.7.4 Scanning Electron Microscopy (SEM) analysis

The fracture surface of the composites was observed using a SEM technique as described in *Section 2.5.3*.

2.7.5 Oxidation resistance test

Isothermal oxidation of ceramics and the ceramic matrix composites were done in a raising hearth furnace (Fitzer Instruments India Pvt. Ltd). The ceramic samples were oxidized isothermally at three different temperatures 1000°C, 1250°C and 1500°C in a raising hearth furnace at an air flow rate of 100 cm^3/ min for 3hr with 30 mins interval. The change in weight was calculated using the formula

$$\frac{\Delta m}{m_0} = \frac{(m - m_0)}{m_0} \times 100 \qquad (2.7)$$

where, m_0 is the initial ceramic weight at time, $t = 0$ and m that at time, t) and the oxidation rate was calculated using the formula,

$$\text{oxidation rate} = \frac{(m - m_0)}{t} \qquad (2.8)$$

Chapter 3

Studies on boron modified phenol-formaldehyde (BPF) as preceramic matrix resin for CMCs

As discussed in *Chapter 1, Section 1.4*, the C/SiC composites are highly prone to oxidation in oxidizing environment. To enhance the application regime of C/SiC composite, the oxidation resistance of the composites have to be improved. In this regard, boron-bearing species are reported to be highly efficient. They can form fluid oxide phases (B_2O_3 or Si–B–O ternary phase) during oxidation to fill cracks which in turn slows down the in-depth diffusion of oxygen imparting *self-healing* properties. There are many methodologies to achieve *self-healing* properties for CMCs which are explained in *Chapter 1, Section 1.5*. It has been concluded that, compared to other methodologies, incorporating boron as back bone of the matrix resin has shorter processing time and is cost effective. To the best of our knowledge, there are no available reports on boron modified phenol formaldehyde (BPF) based preceramic precursor.

This chapter deals with the investigation of boron modified phenol-formaldehyde (BPF) resins as potential preceramic matrix resin for CMCs. This work has been divided into two parts;

- In the first part, synthesis, characterization and ceramic conversion studies of BPF resins are discussed in detail.

- In the second part, CMCs are fabricated using BPF as preceramic matrix resin. This study focused on the optimization of fiber/matrix (F/M) volume ratio and the influence of PyC interphase coating on the flexural properties of CMCs.

Chapter 3.1

Synthesis, characterization and ceramic conversion studies of BPF resins

Synthesis — 1

boron modified phenol-formaldehyde (BPF) resin

SiBOC Ceramic — 2

Self-healing matrix — 3

$SiC + O_2 + B \rightarrow$

SiC

Cr
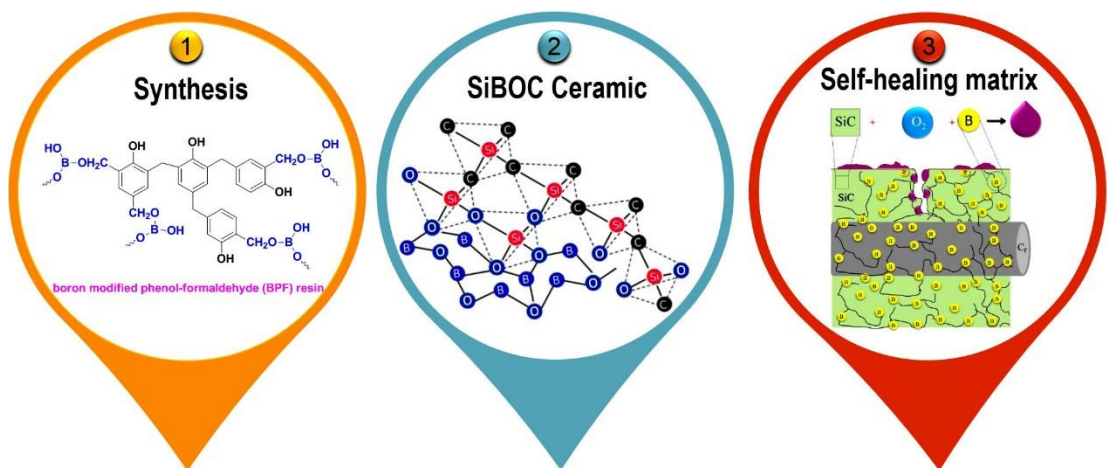
3.1.1. Introduction

This chapter reports synthesis and ceramic conversion of boron modified phenol formaldehyde (BPF) resins, with the aim to use it as preceramic matrix resin for CMCs. This preceramic polymer was synthesized by reacting varying concentrations of boric acid with phenol formaldehyde resin and the polymer to ceramic transformation were carried out at 1450°C under argon atmosphere, with and without silicon as reactive additive. The obtained ceramic phases, morphology and elemental composition were thoroughly investigated through XRD, SEM and HRTEM techniques. The objective of this study was to evaluate BPF resin as a potential *self-healing* matrix resin for CMCs. Hence, CMCs are fabricated using BPF as matrix resin *via* RBSC technique. The microstructures, mechanical properties as well as oxidation behaviour of CMCs are thoroughly investigated.

3.1.2. Experimental

3.1.2.1 Materials

Details of the chemicals and materials are given in *Chapter 2, Section 2.1*.

3.1.2.2 Synthesis of BPF resin

The procedure for the synthesis of BPF resins are given in *Chapter 2, Section 2.2.1*.

3.1.2.3 Characterization

Characterization methods employed include FT-IR, XRD, Raman spectroscopy, HRTEM, SEM, elemental analysis, three-point-bending test and oxidation resistance test. The detailed procedures of all these characterizations are given in *Chapter 2, Section 2.5 and 2.7*.

3.1.2.4 Polymer to ceramic conversion

The detailed procedure for the polymer to ceramic conversion process of BPF and BPFSi are given in *Chapter 2, Section 2.4.1 and 2.4.2*.

3.1.2.5 Fabrication of C_f/SiBOC composite

C_f/SiBOC composite were fabricated from 2D carbon fabric as

reinforcement and BPFSi as the matrix resin using standard RBSC procedure as detailed in *Chapter 2, Section 2.6.2*. Finally, the CMCs were machined to evaluate flexural strength and oxidation resistance test.

3.1.2.6 Oxidation tests

The detailed procedure for the oxidation test and the calculation of change in weight and oxidation rate of the CMCs are given in *Chapter 2, Section 2.7.5*.

3.1.3. Results and Discussion

3.1.3.1 Synthesis and characterization of BPF resin

The BPF resin was synthesized by reacting boric acid (5 to 30 pph) with PF resin. The PF resin consists of phenolic hydroxyl and methylol groups of which methylol groups are far more reactive functional groups as compared with phenolic hydroxyl groups [Kawamoto *et al.* 2010]. The reaction of boric acid with methylol groups precedes that of boric acid with phenolic hydroxyl groups, as shown in Figure 3.1.1.
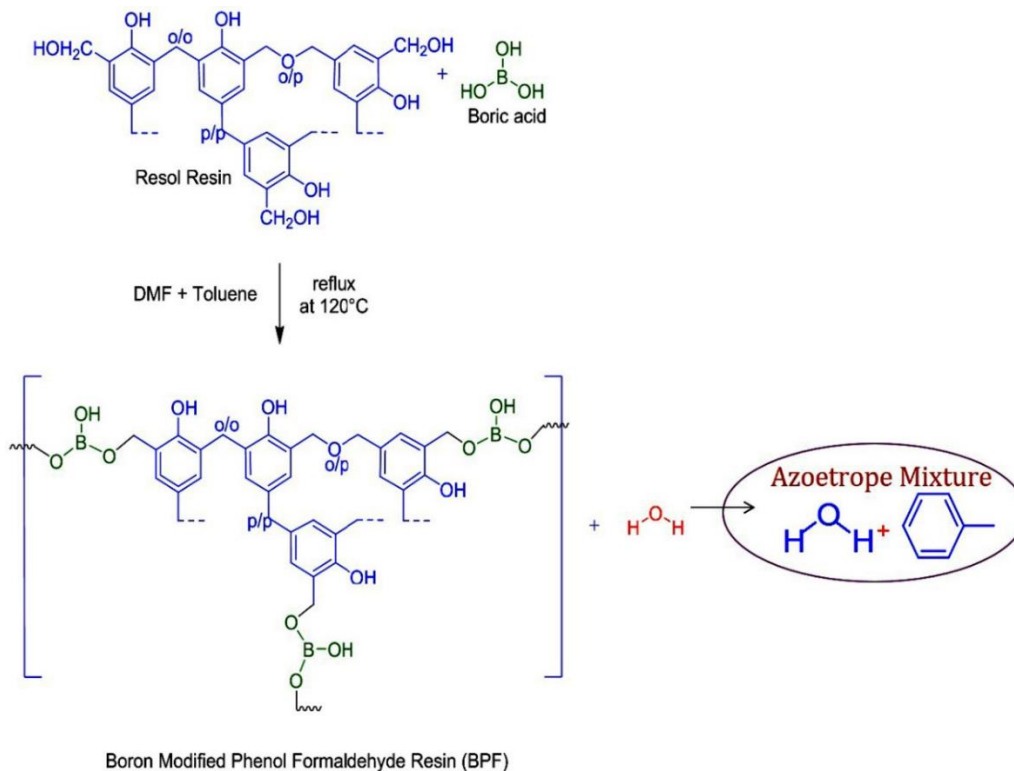
Figure 3.1.1 Synthesis of BPF resin
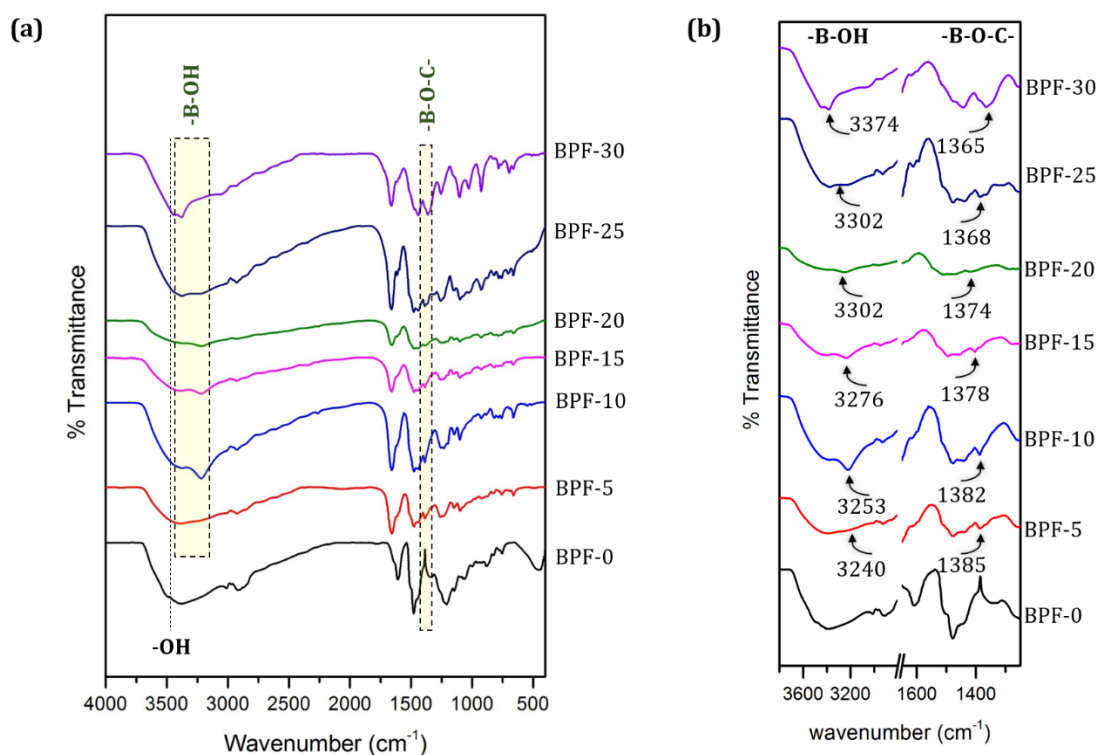
Figure 3.1.2 shows (a) FT-IR spectra of BPF resins (b) magnification in the range from 3800 to 2800 cm⁻¹ and 1650 to 1250 cm⁻¹

Figure 3.1.2 shows (a) FT-IR spectra of BPF resins (b) magnification in the range from 3800 to 2800 cm^{-1} and 1650 to 1250 cm^{-1}. The band which appears around 1098 cm^{-1}, 1385 cm^{-1}, 1475 cm^{-1} and 3250 cm^{-1} corresponds to C-O-C, B-O-C, C–H and B–OH stretching respectively. The formation of B–O–C linkage proves that boric acid has chemically reacted with PF resin by the condensation of boric acid with PF resin as reported earlier [Zmihorska-Gotfryd 2006]. In addition, the presence of B-OH group indicates that, all the -OH group in boric acid is not involved in the condensation reaction with methylol group which might be due to steric hindrance by phenolic groups [Gao *et al.* 2011]. It was also observed that, on increasing the concentration of boric acid, both B-OH and B-O-C stretching frequency shifted from 3240 cm^{-1} to 3374 cm^{-1} and 1385 cm^{-1} to 1365 cm^{-1} (Figure 3.1.2 (b)), respectively. This may be due to the interactions by the local electron density of the newly formed B-O-C group [Mondal *et al.* 2005, Barros *et al.* 2006]. Moreover, by increasing the concentration of boric acid, the intensity of B-O-C stretching band increases which proves beyond doubt that boric

acid has chemically reacted with PF resin.

3.1.3.2   Pyrolysis of BPF at 1450°C

As our objective was to make polymer derived ceramic matrices, we have subjected BPF to pyrolysis at 1450°C in argon atmosphere (*Section 3.1.2.4*) and the structural evolution of the resultant ceramics were studied by XRD, Raman spectroscopic and HRTEM techniques.

3.1.3.2.1 XRD of BPF resin pyrolyzed at 1450°C
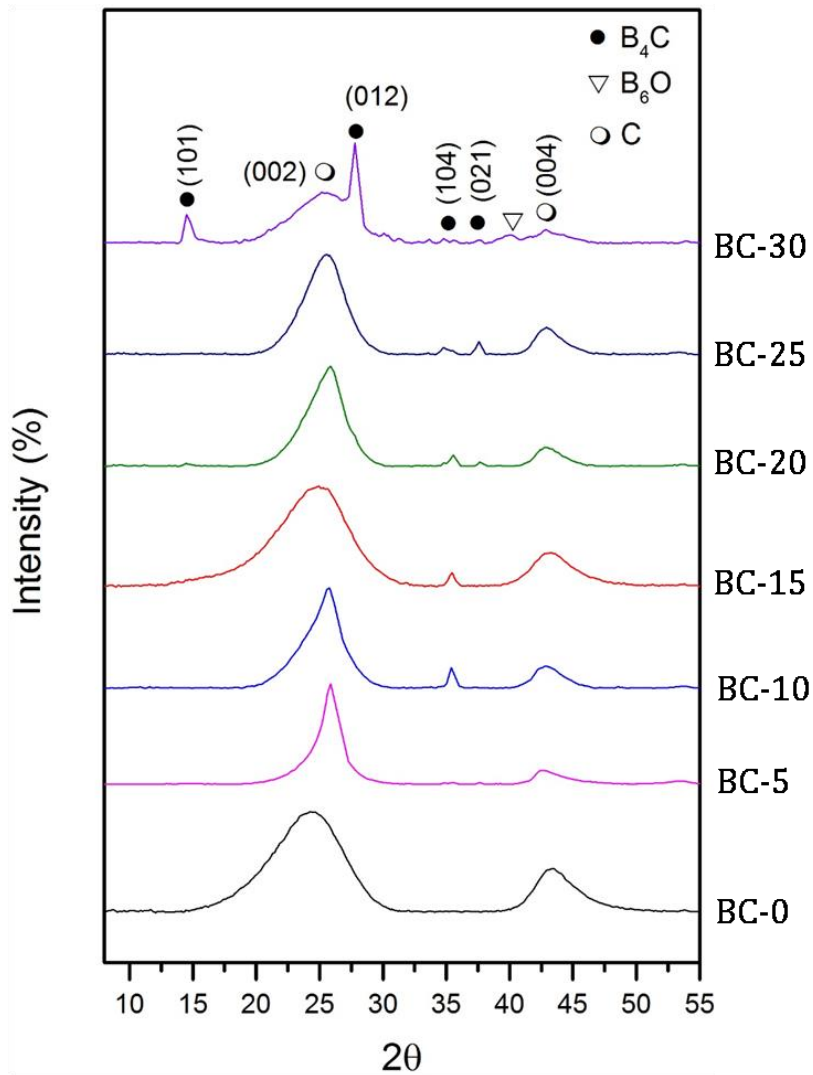
Figure 3.1.3 XRD of B-C ceramics derived for BPF

The XRD pattern of the ceramic samples obtained from BPF resins after pyrolysis at 1450°C in argon atmosphere is shown in Figure 3.1.3. For BC-0, two broad diffraction peaks centered at 2θ = 24.9° and 43.2° are present, which corresponds to (002) and (004) planes of glassy carbon (PDF 89-8493) respectively. In the presence of boron, for BC-5 to 25, in addition to the peaks at 2θ = 24.9° and 43.2°, two other peaks at 2θ = 35.5° and 37.6° were observed, which corresponds to (104) and (021) planes of boron carbide (PDF 65-6874) respectively. For BC-30, new peaks were observed at 2θ = 14.5°, 27.7° and 40.1° which is not observed in other systems. The peaks at 2θ = 14.5° and 27.7° represents (101) and (021) planes of boron carbide (PDF 65-6874) present in the matrix of the carbon [Ding *et al.* 2015] and the peak at 2θ =40.1° corresponds to boron oxide (PDF 06-0643).

As per the powder diffraction database (PDF 65-6874) for boron carbide, the intensity of the peak at 2θ = 35.5° (104) was higher than that of the peak at 2θ = 37.7° (021) which is true in the case of BC-10, BC-15 and BC-20, however in BC-25, a reverse trend was observed. This is due to a change in the location of boron in the lattice of carbon [Conde *et al.* 2000]. In BC-30, the additional peak of boron carbide at 2θ =27.7°, forms a shoulder peak with the main peak at 2θ = 24.9° corresponding to carbon, indicating the precipitation of boron carbide from the carbon matrix above the solubility limit of boron. This observation is further supported by HRTEM analysis (See Figure 3.1.6). Additionally, with increase in boron concentration, peak contraction of (004) plane of carbon is observed indicating increase in its crystallite size which is computed in Table 3.1.1. This difference was explained later with the support of Raman analysis.

3.1.3.2.2 Raman spectra of BPF resin pyrolyzed at 1450°C

Further, structural information on free carbon present in BC ceramics was understood using Raman spectral analysis. In B-C ceramics, there were two specific absorption peaks (as shown in Figure 3.1.4) within the ranges of ~1335cm^{-1} (D-band) and ~1565 cm^{-1} (G-band), respectively indicating the presence of free carbon. Ceramics are heterogeneous systems and hence in the case of BC-25 and BC-15, in addition to free carbon peaks, B$_4$C peaks were also observed. These low intensity peaks in the

range of 700 cm^{-1} to 1050 cm^{-1} can be attributed to stretching vibrations in the C-B-C chains of B$_4$C [Domnich *et al.* 2011].
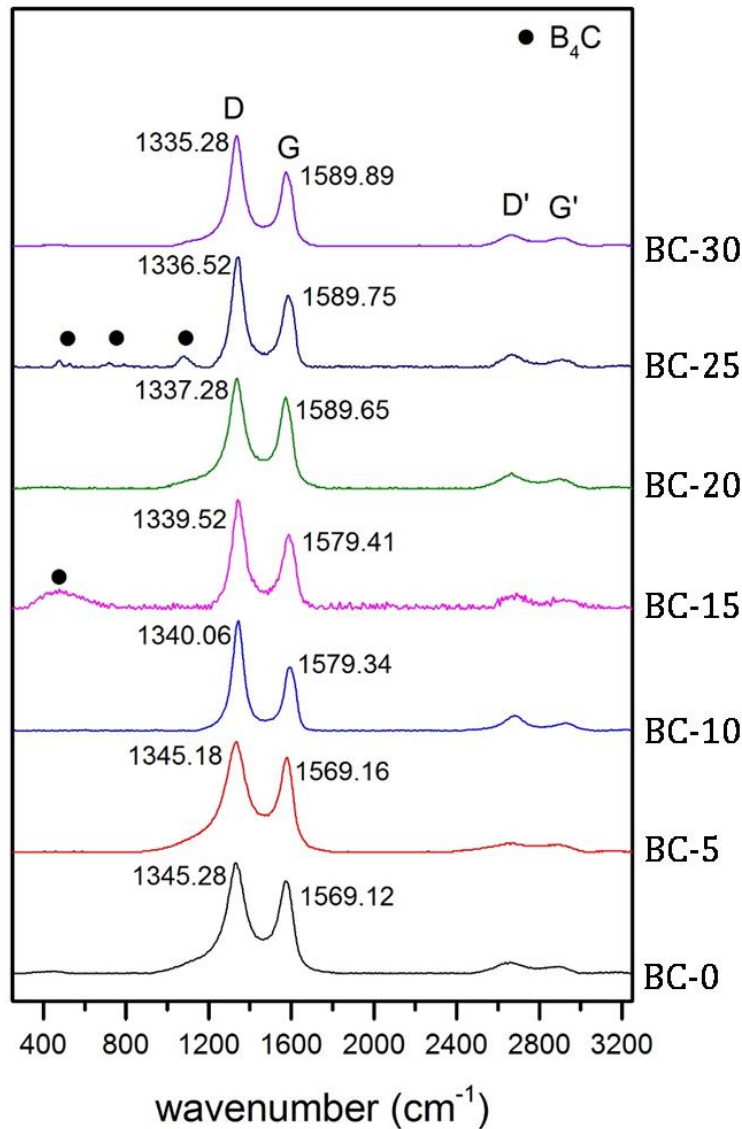
Figure 3.1.4 Raman spectra of the B-C ceramics derived for BPF

As per the literature [Inagaki *et al.* 1998], increase in frequency of G band or a decrease in frequency of D band reflects the degree of the order in carbon. It was observed that there was an increase in the G-band and a decrease in the D-band from BC-0 to BC-30 with the incorporation of boron (as shown in Table 3.1.1). In addition, the D-band shifted to 1335 cm^{-1} (BC-30) from 1345 cm^{-1} (BC-0). The changes observed in the Raman spectra of BC indicates the rearrangement of crystalline structure leading

to an increase in graphitic ordered structure followed by subsequent decrease in amorphous structure (Figure 3.1.4). These rearrangements leading to graphitic ordered structure provides superior mechanical strength and oxidation stability to ceramics [Jacobson *et al.* 2006].

Table 3.1.1 Parameters derived from Raman spectra and XRD of B-C ceramics

Sample	Position of D peak (cm^{-1})	Position of G peak (cm^{-1})	I_D/I_G	d_{002} (nm)	Crystallite size from Raman (nm)	FWHM C (004) plane	Crystallite size from XRD (nm)
BC-0	1345.28	1569.12	0.954	3.62	2.38	3.65	2.45
BC-5	1345.18	1569.16	0.748	3.56	2.43	3.63	2.46
BC-10	1340.06	1579.34	1.002	3.45	2.92	2.64	3.38
BC-15	1339.52	1579.41	1.237	3.44	3.01	2.51	3.56
BC-20	1337.28	1589.65	1.144	3.43	3.02	2.50	3.57
BC-25	1336.52	1589.75	1.083	3.41	3.26	2.41	3.70
BC-30	1335.28	1589.89	1.065	3.21	3.87	2.29	3.90

Further information on free carbon present in BPF derived BC ceramics can be obtained by calculating the ratio of intensities of D band (I_D) and G band (I_G). By increasing the concentration of boron, the I_D/I_G value shows an increase from BC-0 to BC-15 and then it shows a decrease from BC-15 to BC-30 (Figure 3.1.5).
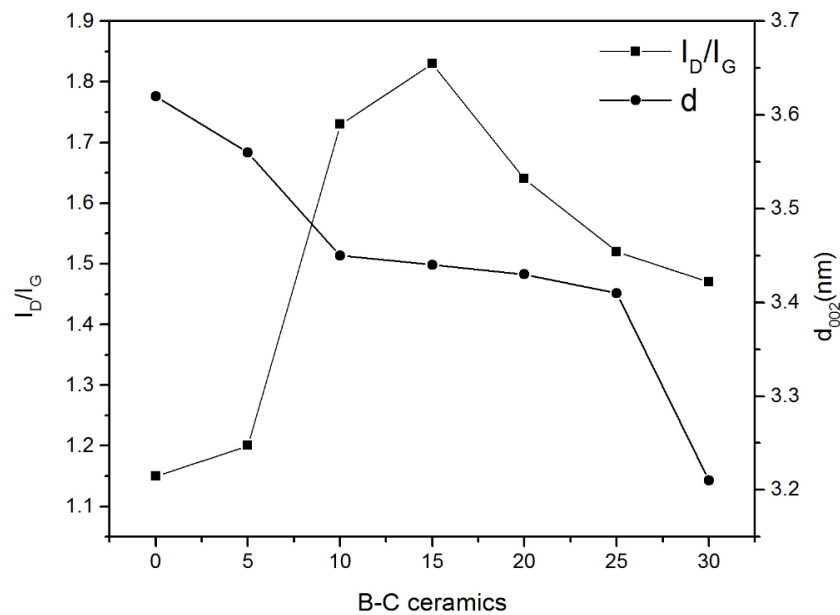
Figure 3.1.5 Variation of I_D/I_G with interplanar distance (d_{002}) of free carbon present in B-C ceramics

It is reported that [Tuinstra *et al.* 1970, Ferrari *et al.* 2004], for amorphous carbon (BC-0 to BC-15) the I_D/I_G value is directly proportional to the crystallite size (L_a), and for crystalline carbon (BC-20 to BC-30) the I_D/I_G value is inversely proportional to the crystallite size (L_a). From the trend in I_D/I_G value, it can be concluded that, the morphology of free carbon changes from BC-0 to BC-30. BC-15 is the critical point where the phase transformation has taken place from amorphous carbon to crystalline carbon and the results are fall in line with crystallite size obtained from XRD as well.

On correlating the interplanar distance (d) and crystallite size (L_a) with the concentration of boron, it can be seen that on increasing boron concentration, the crystallite size increases and the interplanar distance decreases. This results in the ordering of layers in plane and increase in stacking of the carbon layers leading to the formation of graphitic carbon.

From XRD and Raman spectral studies of B-C ceramics, it was clear that phase transformation has taken place from BC-0 to BC-30. Previous researchers have used XRD and Raman spectroscopy as a tool to explain the phase transformation of carbon in the presence of boron [Hagio *et al.* 1987, Inagaki *et al.* 1998, Ferrari *et al.* 2004, Wang *et al.* 2013].

3.1.3.2.3 HRTEM of BPF resin pyrolyzed at 1450°C

In this study, HRTEM was used as a tool to study the evolution of crystalline structure of ceramics. So, the phase evolution of four typical ceramics (BC-0, BC-10, BC-15 and BC-30) were studied using HRTEM. The empirical formula of the typical ceramics is shown in Table 3.1.2.

Table 3.1.2
Elemental Analysis for B-C ceramics obtained at 1450°C in argon atmosphere

SI. No.	Sample	Composition (mass %)			
		B	C	O	Empirical Formula
1.	BC-0	-	100	0	C
2.	BC-10	4.33	94.54	1.13	$B_{0.04} O_{0.01} C$
3.	BC-15	6.2	92.05	1.76	$B_{0.06} O_{0.01} C$
4.	BC-30	14.1	74.74	11.16	$B_{0.18} O_{0.14} C$
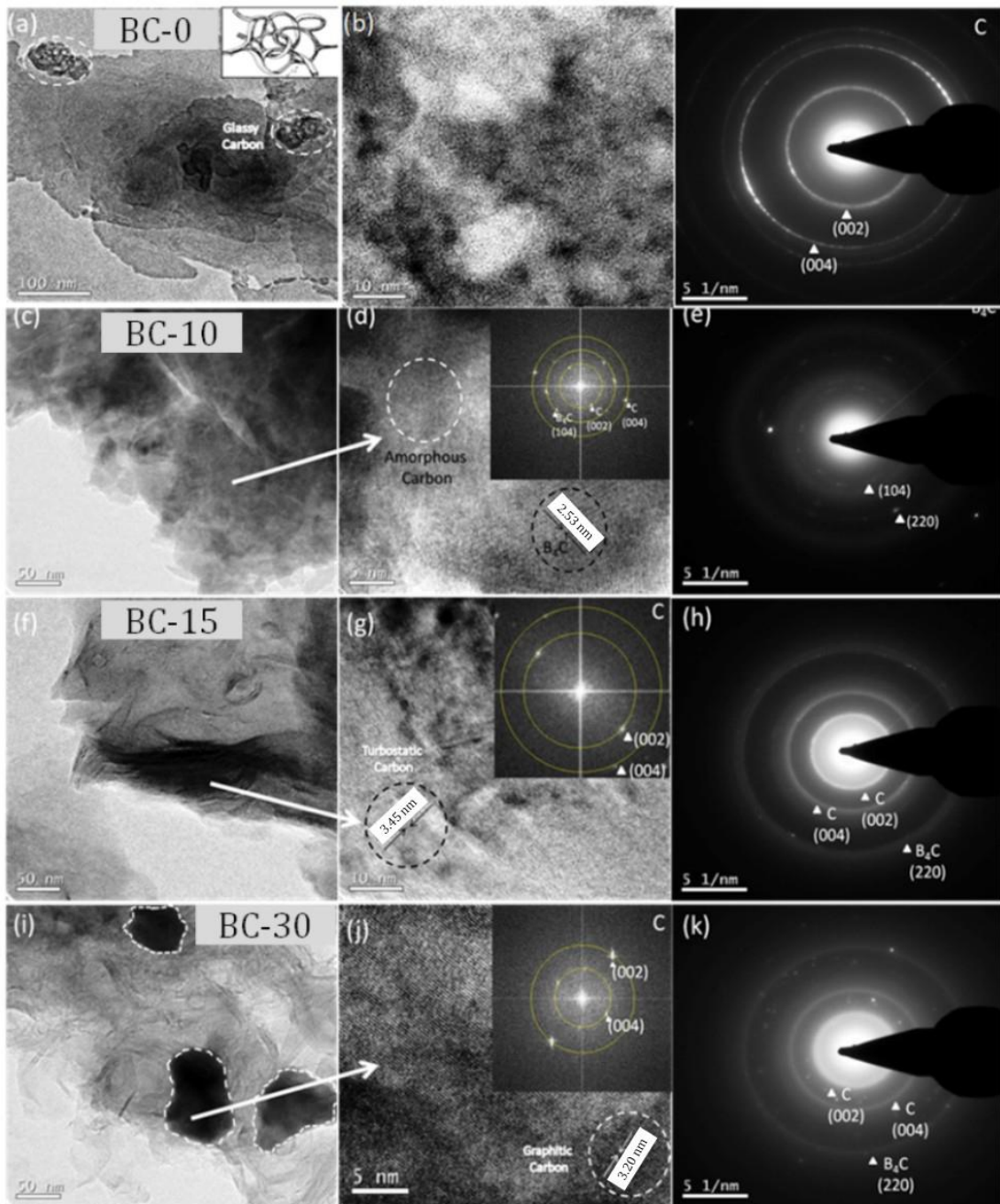
Figure 3.1.6 presents a HRTEM micrograph of (a) BC-0, (c) BC-10, (f) BC-15 and (i) BC-30 along with their corresponding selected area electron diffraction (SAED) and Fast Fourier Transformer (FFT) patterns

Figure 3.1.6 (a) represents HRTEM of BC-0, where the glassy carbon is clearly visible. Glassy carbon is a form of carbon that is produced by carbonizing a phenolic resin under carefully controlled conditions of temperature and pressure [Draper *et al.*

1976]. The glassy carbon is composed of fine ribbon like structures which are entangled and randomly inter weaved with each other. In the case of BC-10, the carbon was in amorphous form which was confirmed through SAED pattern (Figure 3.1.6-e). In addition, FFT pattern of BC-10 (Figure 3.1.6-d) confirms the presence of boron carbide lattice having d $_{(104)}$ spacing of 2.53 nm. HRTEM image of BC-15 (Figure 3.1.6-g) clearly shows the presence of turbostatic carbon having d_{002} spacing of 3.45 nm. In addition to these three distinct carbon structures, additional morphological features were also observed. In BC-30 ceramic, boron carbide nano-crystals with a size of less than 50 nm were observed (Figure 3.1.6-i) either on the edge of the granular particles or in the matrix of the graphitic structures, as indicated by circles. The existence of boron carbide in the BC-30 was identified by the SAED pattern (Figure 3.1.6-k) and the FFT pattern of BC-30 (Figure 3.1.6-j) which shows the graphitic carbon lattice having d_{002} spacing of 3.20 nm. From these results, the phase transformation of glassy carbon (BC-0) to graphitic carbon (BC-30) on incorporation of boron has been confirmed without any doubt. From HRTEM analysis of the BPF derived ceramic matrix it is evident that there is a gradual graphitization pattern from BC-0 to BC-30. This phenomenon may be attributed to the *catalytic effect of boron* [Yu *et al.* 2015].

From the XRD and HRTEM of BC 30, it was observed that boron carbide (012) has crystallized out from the carbon matrix. So, from the result of elemental analysis of boron (Table 3.1.2), it can be concluded that at boron wt% of 14.1 (BC 30), boron carbide has precipitated out from the carbon matrix. In the case of BC-10 (B wt%- 4.33) and BC-15 (B wt%. 6.2) , boron may exist at the interstitial position of carbon [Zhong *et al.* 2005]. On increasing boron concentration, boron promotes the graphitization of glassy carbon by means of 'bond breaking mechanism' and removes defects by replacing the carbon atoms in the graphite lattice [Chongjun *et al.* 1997]. As a result, interplanar distance decreases from d_{002}=3.62 to 3.20 nm and leads to a rearrangement of the glassy carbon into graphitic carbon.

3.1.3.3   Pyrolysis of BPFSi at 1450°C

Our objective was to design a boron containing preceramic matrix for CMC applications. For which silicon powder was blended with BPF (BPFSi) and pyrolyzed at 1450°C in argon atmosphere (*Section 3.1.2.4*) to obtain silicon and boron containing

ceramics. The phase evolutions of the ceramics were characterized by XRD. The empirical formula of the typical ceramics is shown in Table 3.1.3.

Table 3.1.3
Elemental Analysis for SiBOC ceramics obtained at 1450°C in argon atmosphere

SI. No.	Sample	Composition (mass %)				
		B	Si	C	O	Empirical Formula
1.	SiBOC-0	-	63.06	30.46	6.48	$Si_{2.07} O_{0.21} C$
2.	SiBOC-10	13.16	53.68	24.62	8.54	$Si_{2.18} B_{0.53} O_{0.34} C$
3.	SiBOC-15	16.35	47.62	23.81	12.22	$Si_{2.0} B_{0.68} O_{0.51} C$
4.	SiBOC-30	33.15	39.16	16.46	11.23	$Si_{2.01} B_{2.01} O_{0.68} C$

3.1.3.3.1   XRD of BPFSi pyrolyzed at 1450°C

Figure 3.1.7 shows the X-ray diffraction pattern of the ceramic samples obtained from BPFSi after pyrolysis at 1450°C in argon atmosphere. For SiBOC-0, peaks corresponding to β-SiC appeared at 2θ= 35.6°(111), 41.3°(200), 59.9°(220), 71.7°(311) and 75.4°(222) (PDF 74- 2307). In the presence of boron, for SiBOC-5 and SiBOC-30, in addition to the peaks observed for SiBOC-0 ceramic, new peaks corresponding to SiB_4 phase appeared at 2θ= 28.6° (110), 47.5° (205) and 56.3° (125). Moreover, on increasing the concentration of boron, the intensity of SiB_4 peaks at 2θ= 28.6° (110), 47.5° (205) and 56.3° (125) increases.

At elevated temperatures, Si atoms may replace 'C' atoms in the C–B–C chain of icosahedron B_4C, which leads to the formation of silicon boride. The replaced 'C' atoms may react with excess Si, leading to the formation of SiC [Shi *et al.* 2010] and the reactions are shown in eqn. (3.1.1) to (3.1.3). This explains the formation of SiB_4 phase in the ceramics.

$$3B_4C + 2Si \longrightarrow 2SiB_4 + 3C \qquad (3.1.1)$$

$$3B_4C + 3Si \longrightarrow 2SiB_4 + SiC + 2C \qquad (3.1.2)$$

$$3B_4C + 5Si \longrightarrow 2SiB_4 + 3SiC \qquad (3.1.3)$$
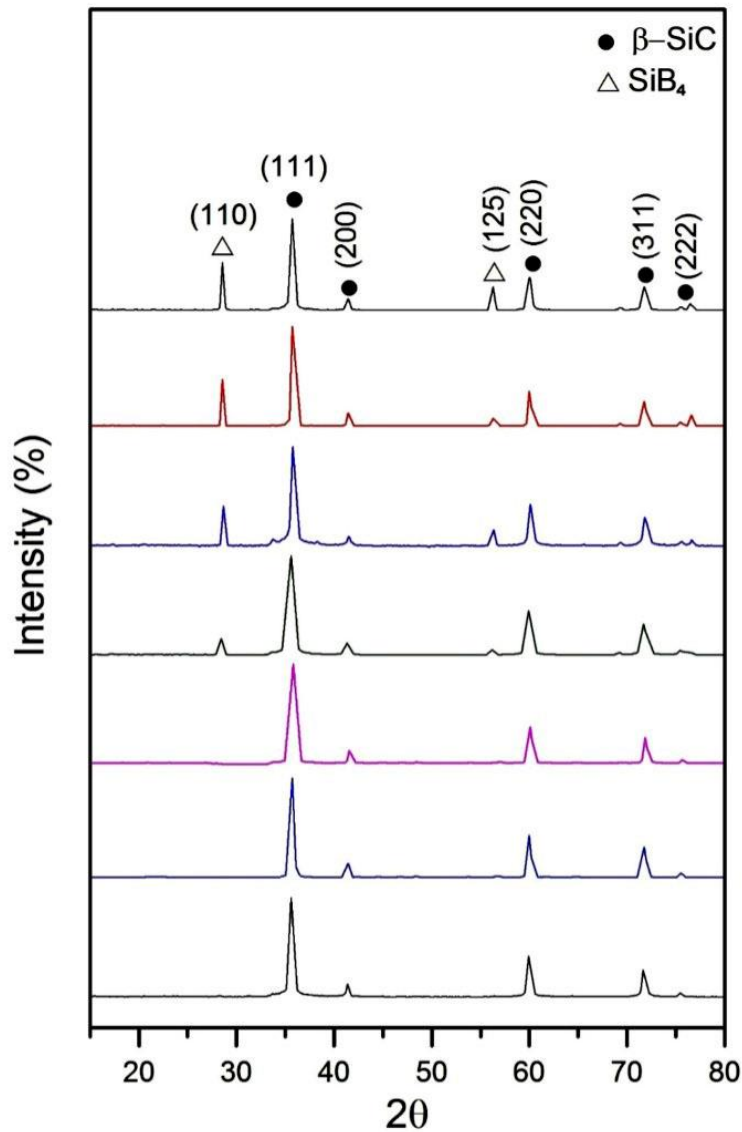
Figure 3.1.7 XRD of SiBOC mixed ceramics derived for BPFSi

3.1.3.3.2   Oxidation behaviour and Microstructural of SiBOC ceramics

In order to evaluate the oxidation behavior, typical ceramics (SiBOC-0, SiBOC-10, SiBOC-15, and SiBOC-30) were oxidized isothermally at 1000°C, the associated weight change and the oxidation rates were calculated (*See Section 3.1.2.6*).
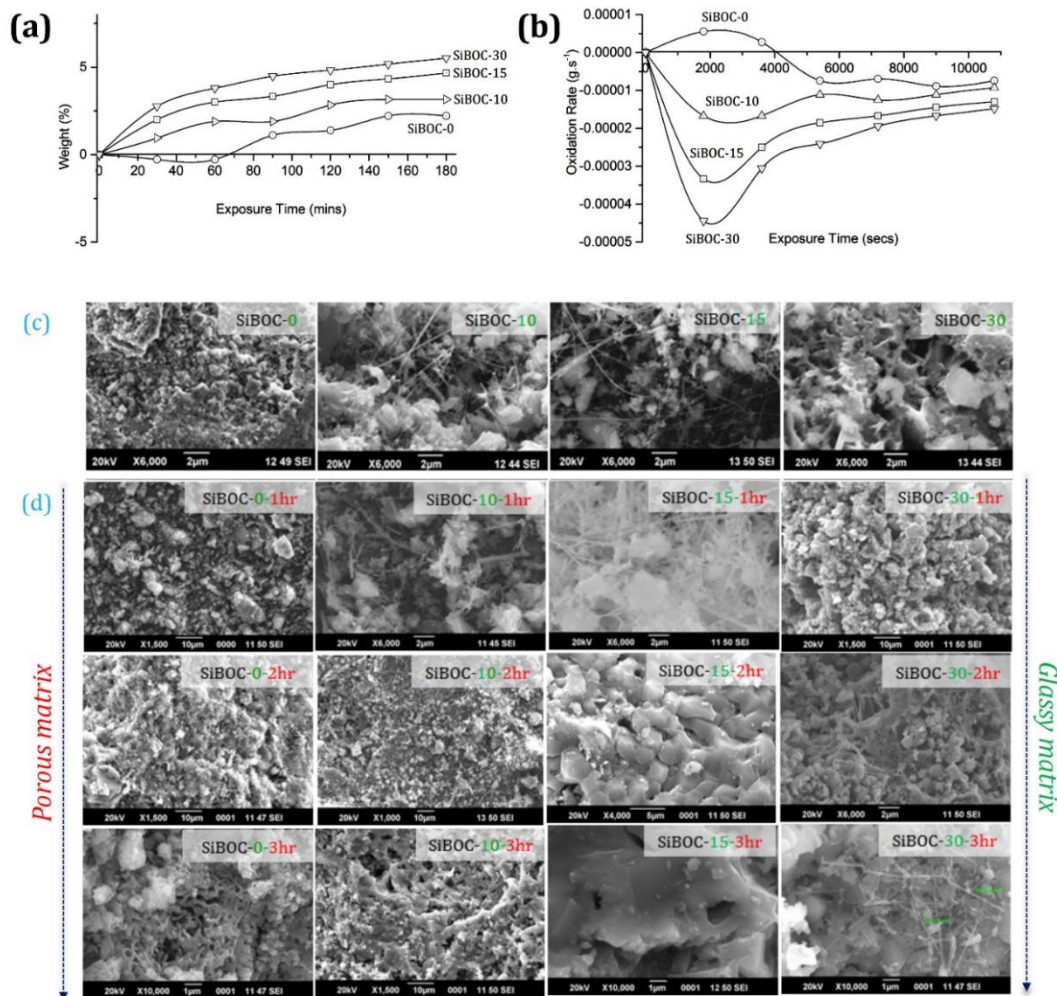
Figure 3.1.8 Isothermal oxidation at 1000°C in air for 3 hr, showing (a) Weight change (%) of oxidized SiBOC ceramic (b) Oxidation rate of SiBOC ceramic (c) SEM image of the SiBOC ceramic before oxidation (d) SEM image of oxidized SiBOC ceramics at the interval of 1hr, 2hr and 3hr.

Figure 3.1.8 (a) shows the weight change (%) of oxidized SiBOC ceramics. In the presence of boron, increase in weight was observed for all the formulations due to the possible chemical reaction as shown in eqn. (3.1.5) and (3.1.7). As the concentration of boron increases, the concentration of fluid oxide phase (B_2O_3 (l) and SiO_2 (l)) also increased leading further increase in weight. In the case of SiBOC-0, weight loss was observed initially followed by a slight weight gain. The weight loss may due to the presence of free carbon which gets oxidized at 400°C as shown in eqn. (3.1.4). In Figure

3.1.8-b, it can be seen that, in the presence of boron, the oxidation rate of the ceramics decrease. This is due to the formation of borosilicate glassy phase $B_2O_3.xSiO_2$ (eqn. (3.1.7)) from a solution of SiO_2 with B_2O_3 formed during the oxidation of SiB_4 (eqn. (3.1.5)) [Matsushita *et al.* 2001].

$$C + O_2 \xrightarrow{400°C} 2CO \qquad\qquad (3.1.4)$$

$$SiB_4 + O_{2(g)} \xrightarrow{600°C} B_2O_{3(l)} + xSiO_{2(l)} \qquad\qquad (3.1.5)$$

$$B_2O_{3(l)} \xrightarrow{900°C} B_2O_{3(g)} \qquad\qquad (3.1.6)$$

$$B_2O_{3(l)} + xSiO_{2(l)} \xrightarrow{1000°C} B_2O_3.xSiO_{2(l)} \qquad\qquad (3.1.7)$$
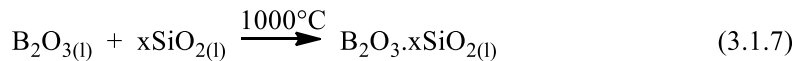
Figure 3.1.8-c shows the surface morphology of SiBOC ceramics before oxidation, where SiBOC-0 and 30 shows the presence of porosity in the matrix. It was observed that, as the oxidation exposure time for SiBOC-0 increases, the porosity level in the ceramic matrix also increases, this may be due to oxidation of free carbon present in the ceramics [Matsushita *et al.* 2001]. In the presence of boron, a glassy layer was formed on the surface of the ceramics which confirms the formation of fluid oxide material as per eqn. (3.1.5) & (3.1.7). As the oxidation time increases from 1hr to 3hr for SiBOC-30, the concentration of fluid oxide ($B_2O_3.xSiO_2$) also increases. This layer is responsible for protection of ceramic matrix composites under severe oxidative atmosphere [Matsushita *et al.* 1997, Tong *et al.* 2008].Volatilization of B_2O_3 phase can happen for ceramic matrix with low boron content as shown in eqn. (3.1.6) [Golovko *et al.* 1994, Tong *et al.* 2008]. Hence prolonged oxidation of SiBOC-10 leads to the formation of pores in the matrix (SiBOC-10-3hr) due to B_2O_3 volatilization. In SiBOC-10 and SiBOC-15 nano/micro-whisker formation was seen and the concentration of these nano/micro-whiskers increases with the oxidation time (Figure-3.1.8-d). Oxidative decomposition of SiB_4 results in formation of B_2O_3 and SiO_2 (eqn. 3.1.5). A liquid phase is formed due to miscibility of B_2O_3 with SiO_2 and this helps in bringing silica and carbon in close contact which subsequently reacts to generate SiBOC whiskers [čerović *et al.* 1995]. Thus, boron acts as a catalyst for the formation of SiBOC whisker. This observation suggests that, the whiskers may have grown by a vapour liquid solid (VLS) mechanism [Raman *et al.* 1997].

3.1.3.4   C$_f$/SiBOC composite fabrication

Our studies proved that SiBOC obtained from BPFSi shows self-healing behaviour and so it was of interest to use it as preceramic matrix resin for the fabrication of carbon fiber reinforced ceramic matrix composite (C$_f$/SiBOC). CMCs were fabricated using BPFSi-0, 10, 15 and 30 (*Section 3.1.2.5*) and preliminary mechanical properties were evaluated.

3.1.3.4.1   Evaluation of flexural strength
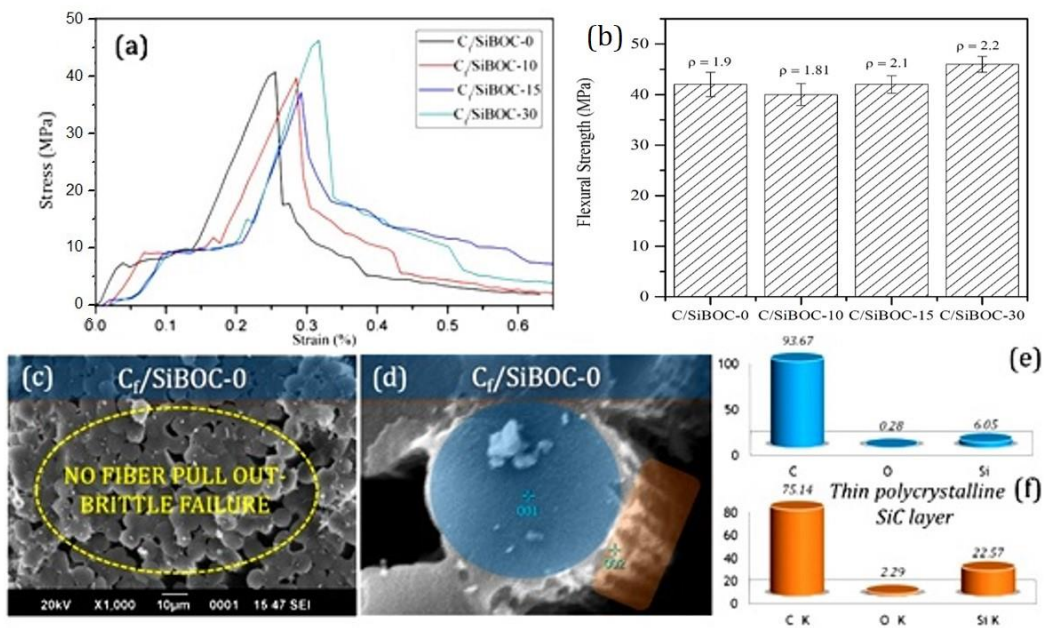
Figure 3.1.9 (a) stress-strain-diagram of C$_f$/SiBOC from a flexural strength (b) Comparison of average flexural strength of C$_f$/SiBOC along with its densities, (c) SEM image of fractured surface of C$_f$/SiBOC-0, (d) SEM image of the top surface (plateau) (blue) and side wall (orange) of carbon fibers, showing the thin polycrystalline SiC product layer on the side wall, (e) and (f) shows the EDX for top surface (plateau) and side wall of carbon fiber respectively.

Figure 3.1.9 (a) shows the typical stress-strain-curves for the flexural strengths of the CMCs. Figure 3.1.9 (b) shows the average flexural strength for carbon fiber reinforced with different matrix composition (C$_f$/SiBOC-0, C$_f$/SiBOC-10, C$_f$/SiBOC-15 and C$_f$/SiBOC-30). It is expected that BPFSi as matrix resin will improve the mechanical strength due to the formation of β-SiC and SiB$_4$ ceramics. However, it is

observed that the improvement is marginal i.e., maximum flexural strength obtained for C_f/SiBOC-30 was only 46 ± 1.6 MPa (ρ=2.2 g/cm^3) [Figure-3.1.9 (b)]. The major reason for the low mechanical properties is that, SiBOC matrix is very brittle and hence crack reaches the saturation point very fast and fiber fails in a brittle manner. The brittle failure of the composite was observed in the SEM image (Figure 3.1.9 (c)) which clearly shows lack of fiber pull out, indicating strong fiber-matrix bonding in the absence of an *interphase* coating [Buet *et al.* 2014]. Another reason can be that, the presence of elemental silicon (melting point ~1390-1410°C) and oxygen in the matrix can react with carbon fiber causing a reduction in strength of the fiber which has been proved with spot-EDX analysis (Figure-3.1.9 (d, e and f)). The EDX was recorded for the top surface (plateau) of the fractured carbon fiber (Figure 3.1.9 (e)) and the carbon fiber side walls (Figure 3.1.9 (f)) of C_f/SiBOC-0 composite. It reveals that, the side wall of the carbon fiber is enriched with silicon 22.57 wt% as compared to 6.05 wt% on the top surface (plateau) of carbon fiber. The morphology of the carbon fiber side walls (Figure 3.1.9 (d)) clearly indicated that, it has been damaged by reacting with elemental silicon to form thin polycrystalline SiC layer which has led to reduction in the flexural strength of the C_f/SiBOC composites. This phenomenon may not exist in the presence of an interphase coated carbon fiber (such as PyC or h-BN) which is reported to help in crack deflection and acts as a diffusion barrier [Naslain *et al.* 2004].

3.1.3.4.2 Oxidation of C_f/SiBOC composite and its microstructure

C_f/SiBOC composites were oxidized isothermally at three different temperatures 1000°C, 1250°C and 1500°C in raising hearth furnace at the flow rate of air 100 cm^3/ min for 3hr with 30 mins intervals. The weight change and oxidation rate were calculated. Figure 3.1.10 (a) and 3.1.10 (b) shows the percentage weight change and oxidation rate of C_f/SiBOC composite respectively. The weight loss was observed for the entire composite (Figure 3.1.10 (a)) and it increases with exposure time, indicating that oxygen has diffused into the C_f/SiBOC composite, resulting in the oxidation of the carbon phase (eqn. (3.1.8)). The weight loss is most predominant in the case of C_f/SiBOC-0 composite. Obviously, the increase of exposure time has led to the acceleration of the oxidation rate (Figure 3.1.10 (b)). Theoretically the formation of B_2O_3 and SiO_2 in the case of boron incorporated composite could lead to increase in

weight (eqn 3.1.9) [55] but loss in weight was observed experimentally due to predominant consumption of carbon. After oxidation for 1hr (Figure 3.1.10 (b)), the oxidation rate of the composite decreased due to the formation of B_2O_3, $B_2O_3.xSiO_2$ and SiO_2 phases at 1000°C, 1250°C and 1500°C respectively (as shown in eqn (3.1.9) to (3.1.13)) which acts as self-healing film and hence subsequently hinders the diffusion of oxygen into the intra-bundle pores of the composite.

$$C + O_2 \xrightarrow{400°C} 2CO \tag{3.1.8}$$

$$SiB_4 + O_{2(g)} \xrightarrow{600°C} B_2O_{3(l)} + xSiO_{2(l)} \tag{3.1.9}$$

$$B_2O_{3(l)} \xrightarrow{900°C} B_2O_{3(g)} \tag{3.1.10}$$

$$2SiC_{(s)} + 3O_{2(g)} \xrightarrow{1200°C} 2SiO_{2(l)} + 2CO_{(g)} \tag{3.1.11}$$

$$B_2O_{3(l)} + xSiO_{2(l)} \xrightarrow{1000-1250°C} B_2O_3.xSiO_{2(l)} \tag{3.1.12}$$

$$B_2O_3.xSiO_{2(l)} \xrightarrow{>1300°C} B_2O_{3(g)} + xSiO_{2(s)} \tag{3.1.13}$$
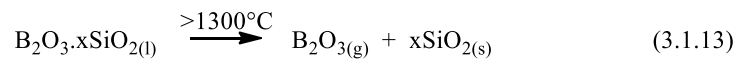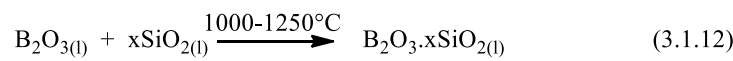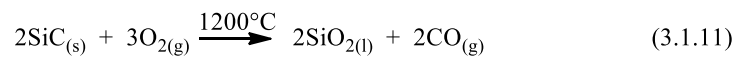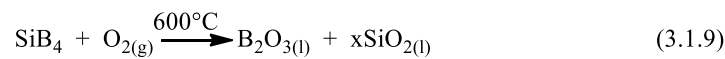
Further insight into the oxidation behavior of the composites can be obtained from SEM studies. The SEM images of $C_f/SiBOC$ composite before and after oxidation tests are shown in Figure 3.1.10 (c) and (d) respectively. In the case of $C_f/SiBOC$-0-1000°C composite, the exposed carbon fibers get oxidized leading to considerable weight loss, while the matrix remains intact. The voids present in $C_f/SiBOC$-0 at 1000°C, 1250°C and 1500°C composite are caused due to the oxidation of fibers (indicated in Figure 3.1.10 (c)) which becomes the path way for oxygen to enter into the composite and hence results in a damage. It was expected that $C_f/SiBOC$-0-1250°C composite will form SiO_2 layer which will protect the carbon fiber from oxidation. However, it is observed that the holes formed at 1000°C has become a path way for the oxygen to enter into the system [Raman *et al.* 1997], which leads to further weight loss at 1250°C and 1500°C. This is reflected in the percentage weight loss (Figure 3.1.10 (a)) where we can see two step weight losses in the case of $C_f/SiBOC$-0-1250°C composite. In the case of boron bearing composite ($C_f/SiBOC$-10, $C_f/SiBOC$-15 and $C_f/SiBOC$-30) SiBOC matrix oxidized to form B_2O_3, $B_2O_3.xSiO_2$ and SiO_2 phases at 1000°C, 1250°C and 1500°C respectively as per the eqn. (3.1.9) to (3.1.13). The

formation of these phases led to the healing of micro-crack in the SiBOC matrix and protected the carbon fiber from oxidation. Increasing the concentration of boron further increased the self-healing properties of C_f/SiBOC composite.
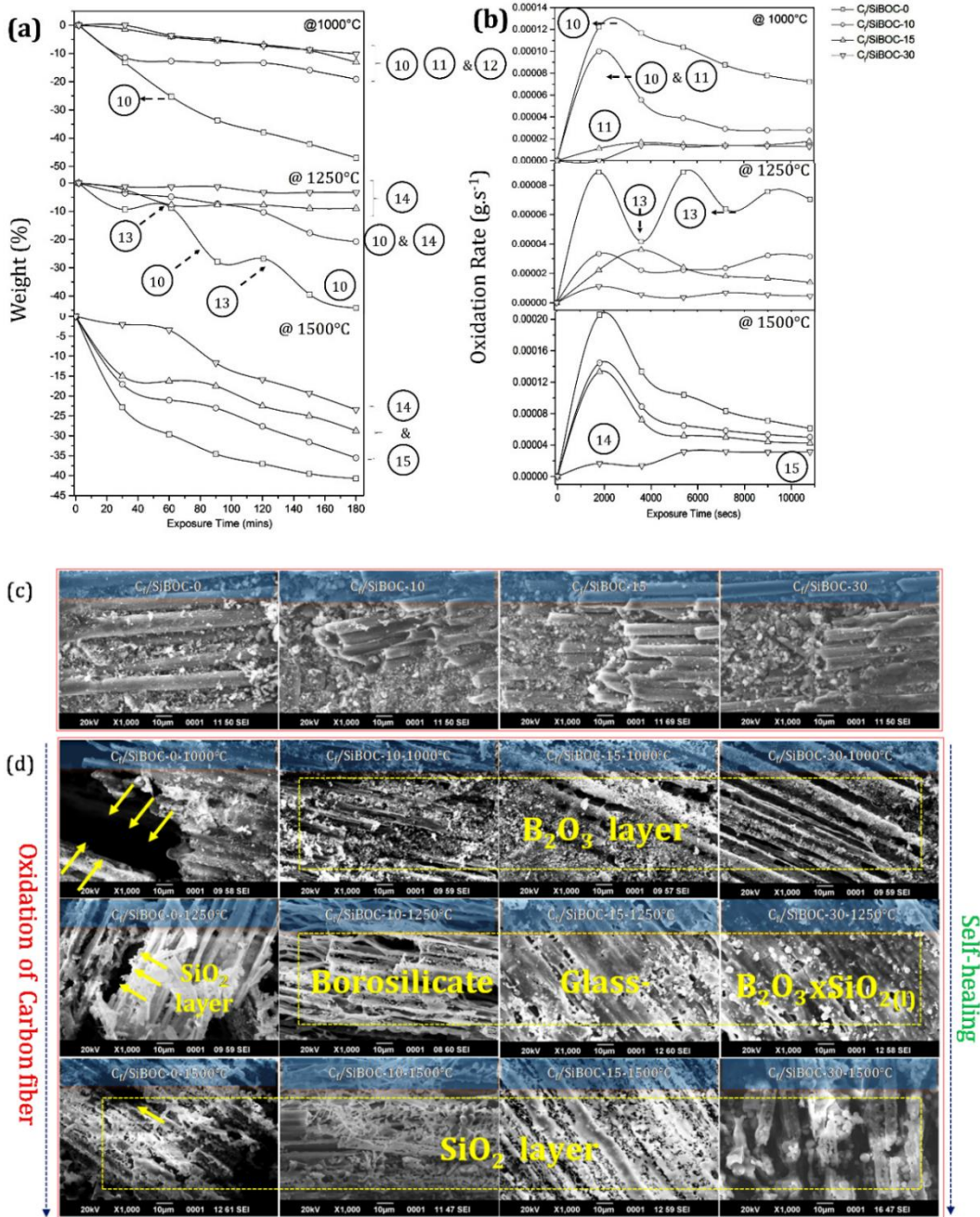
Figure 3.1.10 Isothermal oxidation at 1000°C, 1250°C and 1500°C in air for 3 hr, showing (a) percentage weight change of C_f/SiBOC composite, (b) oxidation rate of C_f/SiBOC composite, (c) The SEM image of the C_f/SiBOC composite before oxidation and (d) The SEM image of the C_f/SiBOC composite after oxidation.

From the above results, it is proved that boron incorporated i.e., C_f/SiBOC-10, 15 and 30 ceramic composites displayed better oxidation resistance compared to a C_f/SiBOC-0 due to the existence of SiB_4 ceramics. However, in order to improve the oxidation as well as the reusability of the C_f/SiBOC composite materials a suitable interphase coating on the fiber has to be employed in addition to a self-healing matrix.

3.1.4. Conclusions

The current work was aimed at developing a cost effective C_f/SiBOC composite using BPFSi as matrix resin and 2D carbon fabric as reinforcement by RBSC method. The study leads to following conclusions

(i)   Boron is incorporated in the back bone of phenol formaldehyde resin which is the carbonaceous precursor for the formation of reaction-bonded SiBOC mixed ceramics.

(ii)   Raman and HRTEM analysis revealed the morphology of free carbon in B-C ceramics which supports the transformation of glassy carbon (BPF-0) to graphitic carbon (BPF-30).

(iii)   Isothermal oxidation of SiBOC mixed ceramics at 1000°C leads to the formation of SiO_2-B_2O_3 phase proving boron bearing ceramics are more efficient at relatively low temperatures (500–1000°C) to protect CMCs.

(iv)   Flexural strength of C_f/SiBOC composites showed marginal improvements maximum of 46±1.6 MPa was achieved in the case C_f/SiBOC-30.

(v)   Fractured surface of C_f/SiBOC-0 composite was observed using SEM which showed brittle failure with no fiber pull out and this is attributed to the strong fiber-matrix bonding in the composite.

(vi)   Energy dispersive X-rays (EDX) of C_f/SiBOC-0 composite shows that, the side wall of the carbon fiber is enriched with silicon 22.57 wt% as compared to 6.05 wt% on top surface (plateau) of carbon fiber. This clearly indicated that it has been damaged by reacting with elemental

silicon leading to reduction in the flexural strength of the C_f/SiBOC composites.

(vii)   Evaluation of oxidation resistance for C_f/SiBOC composites at various temperatures (1000°C, 1250°C and 1500°C) proved the formation of borosilicate glass at relatively low temperature which is responsible for self-healing property of CMCs.

(viii) Significance of interphase coating on the flexural strength has to be understood and hence will be studied in detail in next Chapter.

Chapter 3.2

Fabrication and characterization of CMCs using BPF as matrix resin
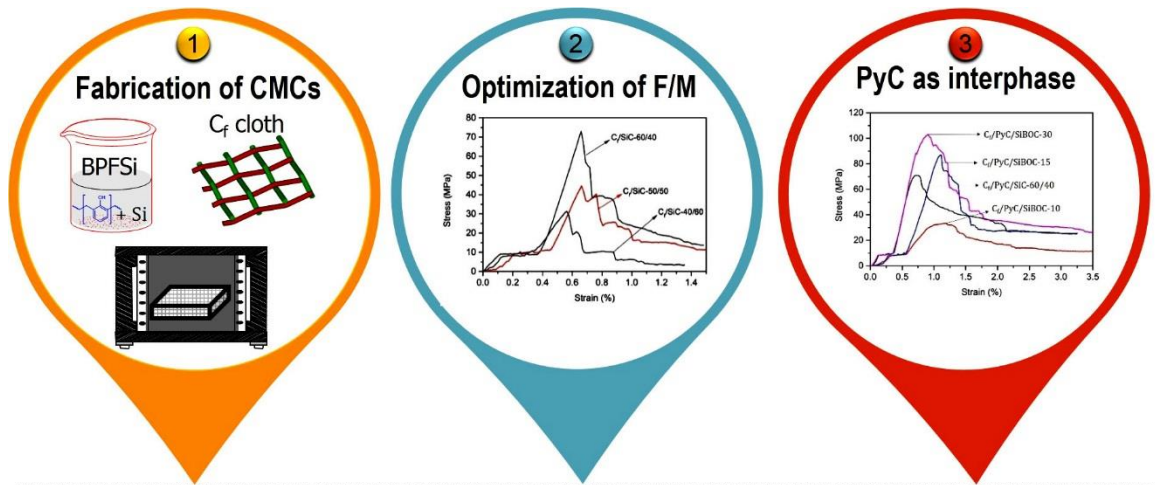
Results of this chapter has been published in:

3.2.1. Introduction

Chapter 3.1, has demonstrated that the boron modified C_f/SiBOC composites exhibit improved oxidation resistance compared to C_f/SiC composite by the formation of *self-healing* matrix. However, the flexural strength of C_f/SiBOC composites shows only marginal improvement (46±1.6 MPa) as compared to C_f/SiC composite (42±2.2 MPa) and it was attributed to the damage of carbon fiber on reaction with elemental silicon. This study imparts the significance of *interphase* coating and optimization of F/M volume ratio on the improvement of flexural strength. Also to enhance the application regime of C_f/SiBOC composites, the fracture behavior and mechanism should be investigated in detail.

Hence, in this chapter, the study focuses on the optimization of F/M volume ratio and the influence of PyC interphase coating on the flexural properties of C_f/SiBOC derived from BPF resin *via* RBSC method. At the same time, the flexural properties of C_f/SiBOC are compared with C_f/SiC composite derived from PF resin. Finally, the fracture behavior and mechanism of C_f/SiBOC and C_f/PyC/SiBOC composites are discussed based on the characterization of the fracture surface and its microstructure.

3.2.2. Experimental

3.2.2.1 Materials

Details of the chemicals and materials are detailed in *Chapter 2, Section 2.1*.

3.2.2.2 Synthesis of BPF resin

The procedure for the synthesis of BPF resins are detailed in *Chapter 2, Section 2.2.1*.

3.2.2.3 Preparation of preceramic matrix precursors

The procedure for the preparation of preceramic matrix precursors are given in *Chapter 2, Section 2.4.2*. The typical properties of the preceramic precursors are shown in Table 3.2.1.

3.2.2.4   Fabrication of C$_f$/SiC composites

In order to optimize the F/M volume ratio and to understand its effect on the flexural properties of the composites, three types of C$_f$/SiC composites were fabricated by varying the F/M volume ratio viz. 40/60, 50/50 and 60/40 using PFSi as matrix and 2D carbon fabric as reinforcement via standard RBSC techniques as described in *Chapter 2, Section 2.6.2*. Their CMCs were designated as C$_f$/SiC-40/60, C$_f$/SiC-50/50 and C$_f$/SiC-60/40. Finally, these composites were machined to evaluate flexural properties.

3.2.2.5   Fabrication of C$_f$/SiBOC composites

C$_f$/SiBOC composites were fabricated using BPFSi-10, BPFSi-15 and BPFSi-30 as matrix resin and 2D carbon fabric as reinforcement through RBSC method as described in *Chapter 2, Section 2.6.2*. The composites thus obtained are named as C$_f$/SiBOC-10, C$_f$/SiBOC-15 and C$_f$/SiBOC-30. Finally, these composites were machined to evaluate flexural properties.

3.2.2.6   Fabrication of CMCs with PyC interphase

To study the effect of PyC interphase coating on the flexural properties of the composites. CMCs with PyC interphase were fabricated as described in *Chapter 2, Section 2.6.1,* followed by densification with the above mentioned matrices *via* RBSC method and are denoted as C$_f$/PyC/SiBOC-10, C$_f$/PyC/SiBOC-15 and C$_f$/PyC/SiBOC-30. Finally, the obtained composites were machined to evaluate the flexural properties. The flexural properties were compared with C$_f$/PyC/SiC composite derived from PFSi also.

3.2.2.7   Characterization

Characterization methods employed include density and open porosity measurements, three-point-bending test, optical microscopy analysis and SEM analysis. The detailed procedures of all these characterizations are given in *Chapter 2, Section 2.5 and 2.7*.

3.2.3. Results and Discussions

Chapter 3.1, explored the fabrication of cost effective *self-healing* C_f/SiBOC composites. The composites were prepared using slurry containing boron modified phenol formaldehyde with elemental silicon as matrix and 2D carbon fabric as reinforcement via the RBSC method. The study showed improvement in the oxidation resistance properties of C_f/SiBOC as compared to C_f/SiC composite. However, the flexural strength of C_f/SiBOC composites showed only marginal improvements, which was attributed to the detrimental reaction of elemental silicon with the carbon fibers. In order to overcome this and to enhance the flexural properties of C_f/SiBOC composites, the present study focuses on the optimization of F/M volume ratio and the influence of PyC interphase coating on the flexural properties of C_f/SiBOC composites.

Table 3.2.1
Properties of the Preceramic matrix precursors

SI. No.	Sample	Ceramic residue at 1450°C (%)	Empirical Formula
1.	PFSi	75.54	$Si_{2.07} O_{0.21} C$
2.	BPFSi-10	76.46	$Si_{2.18} B_{0.53} O_{0.34} C$
3.	BPFSi-15	79.44	$Si_{2.0} B_{0.68} O_{0.51} C$
4.	BPFSi-30	87.51	$Si_{2.01} B_{2.01} O_{0.68} C$

3.2.3.1 Studies on optimization of F/M volume ratio in C_f/SiC composites

C_f/SiC composites with three different F/M volume ratio viz. 40/60, 50/50 and 60/40 were fabricated and its properties are given in Table 3.2.2.

Table 3.2.2
Properties of the C_f/SiC composites

SI. No.	Samples	Open Porosity (%)	Density (g/cm³)	Flexural strength (MPa)	Flexural Modulus (GPa)
1.	C_f/SiC-40/60	37.2	1.37	25.96 ± 3.9	7.5 ± 2.1
2.	C_f/SiC-50/50	33.2	1.41	36.62 ± 5.0	10.75 ± 1.4
3.	C_f/SiC-60/40	28.2	1.46	63.2 ± 9.9	15.96 ± 3.9

It is observed that the open porosity of the composite is decreased on increasing the fiber vol. % (Table 3.2.2). It is well known that the pores formed in the polymer derived CMCs are due to the thermal transformation of polymer matrix composite to CMCs. During this process polymer gets decomposed resulting in the formation of many gaseous species which escape as volatile product imparting porosity

in the final composites. As a result, on decrease in the matrix vol. % and increase the fiber vol. % in CMCs, porosity is decreased.

3.2.3.1.1 Evaluation of flexural strength
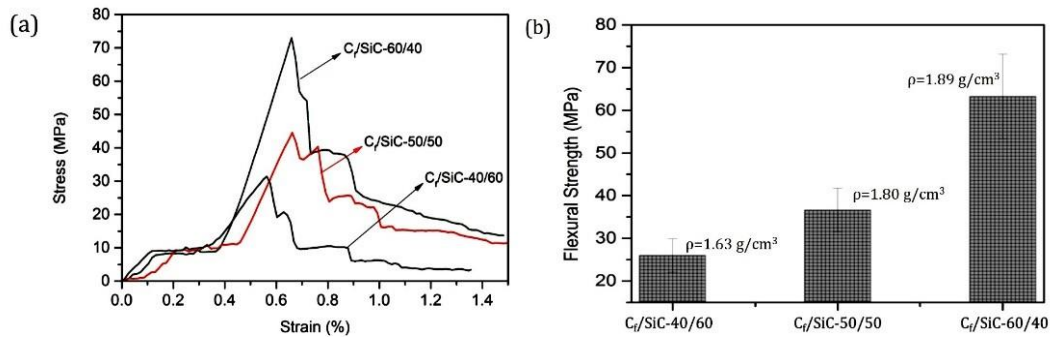
Figure 3.2.1 (a) stress-strain-curves and (b) the average flexural strength of C_f/SiC-40/60, C_f/SiC-50/50 and C_f/SiC-60/40 composites.

Figure 3.2.1 (a) and (b) shows the typical stress-strain-curves and the average flexural strength of C_f/SiC-40/60, C_f/SiC-50/50 and C_f/SiC-60/40 composites. The values of flexural strength and flexural modulus are summarized in Table 3.2.2. The results clearly validate the changes observed in stress-strain behaviour, flexural strength and flexural modulus with the change in fiber content of the composites. In the case of C_f/SiC-40/60 and C_f/SiC-50/50 composites, the flexural modulus were quite low i.e., 7.5 ± 2.1 and 10.75 ± 1.4 GPa respectively and exhibited low flexural strength of 25.9 ± 3.9 MPa and 36.6 ± 10.7 MPa respectively. In the case of C_f/SiC-60/40 composite, the flexural modulus has increased to 15.96 ± 3.9 GPa and shows highest flexural strength of 63.2 ± 9.9 MPa. The reason for the high modulus and high flexural strength in C_f/SiC-60/40 composite is due to its low open porosity (28.2 %) and high fiber content (60 vol. %). This composite can transfer the stress very effectively from the matrix to fiber as compared to the C_f/SiC-40/60 and C_f/SiC-50/50 composites having higher vol. % of pores (37.2 % and 33.2 %) and low fiber content (40 and 50 vol. %) [Tong *et al.* 2008].
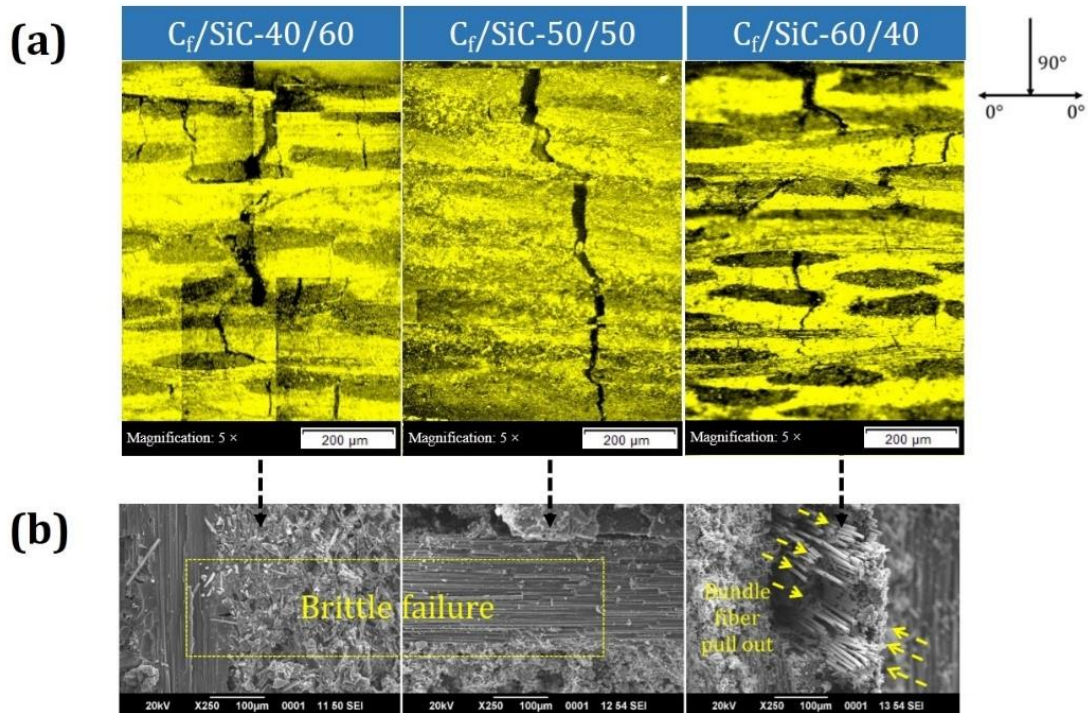
Figure 3.2.2 (a) Optical Image of lateral view on the development of cracks in a flexural specimen and (b) SEM image of the fractured surface of C$_f$/SiC-40/60, C$_f$/SiC-50/50 and C$_f$/SiC-60/40 composites

Further, studies on the crack propagation and fracture surface of these composites has revealed the reason for high flexural strength in the case of high fiber content. Figure 3.2.2 (a) and (b) shows lateral view of the development of cracks in a flexural specimen and the fractured surface of C$_f$/SiC-40/60, C$_f$/SiC-50/50 and C$_f$/SiC-60/40 composites. In the case of C$_f$/SiC-50/50 composite, the cracks run in a relatively straight path through the specimen and propagates through 90° plies with no crack bridging of 0° bundles. In contrast C$_f$/SiC-40/60 and C$_f$/SiC-60/40 composites shows, more segmentation cracks along 0°/90° directions. This phenomenon is expected to show fiber pull-out with high flexural value. However, the SEM image of fractured surface (Figure 3.2.2 (b)) reveals that C$_f$/SiC-40/60 composite has failed in a brittle manner with a lowest flexural strength of 25.9 ± 3.9 MPa. This may be due to low fiber content (40 vol.%) and high porosity (37.2 %) which leads to premature failure of the composite [Tong *et al.* 2008]. On the contrary, C$_f$/SiC-60/40 exhibited a non-catastrophic fracture leading to fiber bundle pull-out. This reveals that the

reinforcement of 'C' fiber is effective in preventing catastrophic fracture, especially for the composites with a high volume fraction of fiber reinforcement.

From the above results, it is proved that C_f/SiC-60/40 composite demonstrated better flexural properties compared to a C_f/SiC-40/60 and C_f/SiC-50/50. So, we have chosen an F/M volume ratio of 60/40 for our all further studies. In the second part of the investigation, the effect of PyC interphase was studied using CMCs prepared from BPF resin with F/M volume ratio of 60/40.

3.2.3.2 Studies on effect of PyC interphase coating on flexural properties of CMCs

To study the effect of PyC interphase coating on the flexural properties, CMCs were fabricated with and without PyC interphase coating. The properties of CMCs are shown Table 3.2.3.

Table 3.2.3
Properties of the CMCs with and without PyC interphase

SI. No.	Samples	Open Porosity (%)	Density (g/cm³)	Flexural strength (MPa)	Flexural Modulus (GPa)
		(a) Without PyC interphase			
1.	C_f/SiC-60/40	28.2	1.46	63.2 ± 9.9	15.96 ± 3.9
2.	C_f/SiBOC-10	31.4	1.39	19.74 ± 6.0	8.32 ± 3.9
3.	C_f/SiBOC-15	25.9	1.50	24.38 ± 7.6	18.53 ± 3.2
4.	C_f/SiBOC-30	25.6	1.53	38.7 ± 4.4	22.18 ± 3.1
		(b) With PyC interphase			
5.	C_f/PyC/ SiC-60/40	27.6	1.49	70.6 ± 5.2	16.23 ± 1.9
6.	C_f/PyC/SiBOC-10	30.9	1.40	32.86 ± 10.7	9.3 ± 3.2
7.	C_f/PyC/SiBOC-15	23.4	1.56	86.86 ± 3.2	23.15 ± 2.9
8.	C_f/PyC/SiBOC-30	21.8	1.59	102.72 ± 11.5	26.4 ± 3.1

3.2.3.2.1 Without PyC interphase

Figure 3.2.3 (a) and (b) shows the typical stress-strain-curves and the average flexural strength of C_f/SiC-60/40, C_f/SiBOC-10, C_f/SiBOC-15 and C_f/SiBOC-30 composites. The average flexural strength and flexural modulus are summarized in Table 3.2.3.
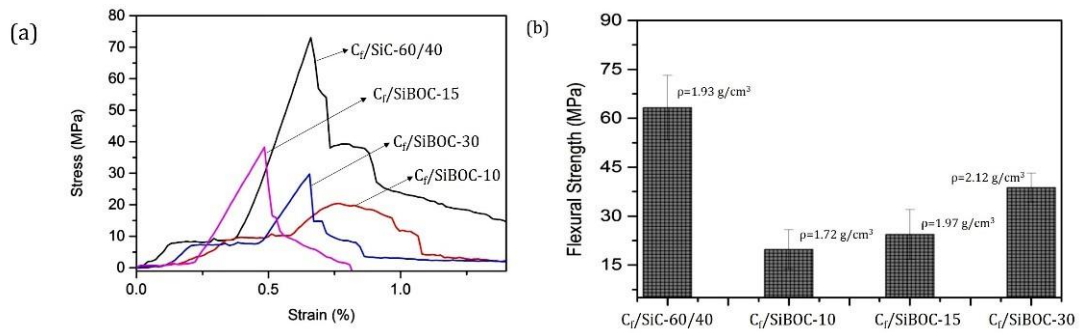
Figure 3.2.3 (a) stress-strain-curves and (b) the average flexural strength of C_f/SiC-60/40, C_f/SiBOC-10, C_f/SiBOC-15 and C_f/SiBOC-30 composites.

It is expected that BPFSi as matrix resin and high fiber content will improve the flexural strength of the composites. However, the maximum flexural strength was obtained for C_f/SiC-60/40 (63.2 ± 9.9 MPa) which was derived from PFSi. Furthermore, the stress-strain curve of C_f/SiBOC-10 exhibit a pseudo-ductile fracture behaviour which is normally expected to show high flexural strength [Cao *et al.* 2014]. However, it is found to exhibit the lowest flexural strength (19.7 ± 6.0 MPa) among the other composites. The reason for lack of improvement in flexural strength in the case of C_f/SiBOC-10, C_f/SiBOC-15 and C_f/SiBOC-30 composites were understood by studying the crack propagation and fracture surface of these composites.
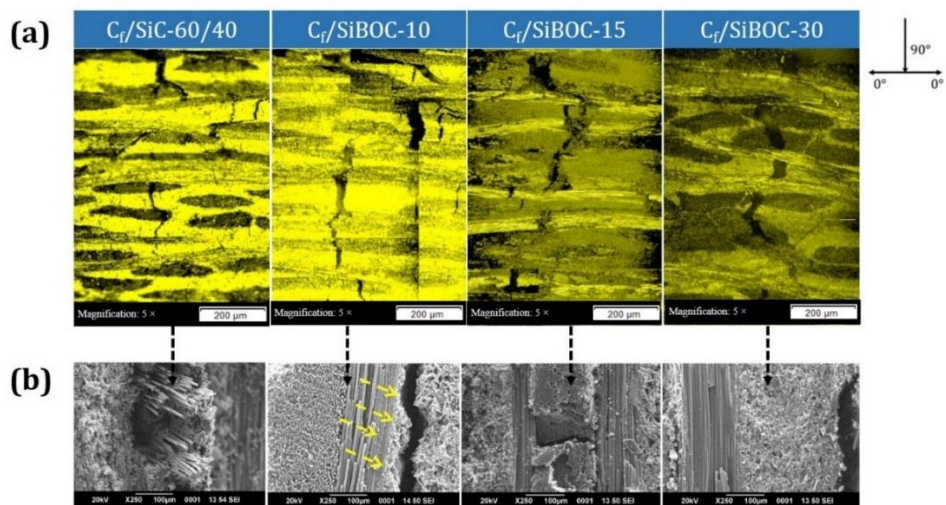
Figure 3.2.4 (a) Optical image of lateral view on the development of cracks in a flexural specimen and (b) SEM image on the fractured surface of C_f/SiC-60/40, C_f/SiBOC-10, C_f/SiBOC-15 and C_f/SiBOC-30 composites.

Figure 3.2.4 (a) and (b) shows lateral view of the development of cracks in a flexural specimen and the fractured surface of C_f/SiC-60/40, C_f/SiBOC-10, C_f/SiBOC-15 and C_f/SiBOC-30 composites. In the case of C_f/SiC-60/40, C_f/SiBOC-15 and C_f/SiBOC-30 composites, though the development of cracks exhibits similar phenomenon (Figure 3.2.4 (a)), i.e., cracks run in a relatively straight path through the specimen with some segmentation cracks, but its fracture surface was not same (Figure 3.2.4 (b)). The fracture surface of C_f/SiC-60/40 composite shows fiber pull out phenomenon in contrast to C_f/SiBOC-15 and C_f/SiBOC-30 composites which have shown no fiber pull out. This results in a catastrophic failure which has been reflected in their flexural properties as well (Table 3.2.3). The major reason behind the catastrophic failure was that, SiBOC as matrix leads to a strong bonding in F/M interface and hence crack reaches the saturation point very fast and fiber fails in a brittle manner. The brittle failure of the composite was observed in the fractured surface of SEM image (Figure 3.2.4 (b)) which clearly shows the lack of fiber pull out, indicating the strong bonding in F/M interface. Another reason can be that, during the fabrication of CMCs using RBSC technique, carbon fiber gets attacked by the elemental silicon. This will lead to reduction in the flexural properties which was proved in the previous chapter (Chapter 3.1). On contrast, the crack propagation and fracture surface behaviour of C_f/SiBOC-10 composite shows more segmentation cracks along 0°/90° directions and leads to partial delamination of the composite. The delamination has occurred between fiber and the matrix, as indicated by arrows (Figure 3.2.4 (b)) which says that F/M interface is too low in this composite. This is due to the structurally weak points like high property of pores (31.4 %) or cracks in the matrix which may lead to a premature failure of the composite and has resulted in lowering of flexural strength (19.7 ± 6.0 MPa) among other composites.

3.2.3.2.2 With PyC interphase

As our main objective was to overcome the above mentioned problems and to enhance the flexural properties of C_f/SiBOC composites, a thin layer of PyC interphase coating was deposited on the carbon fiber using CVI followed by densification of the composite using RBSC method.
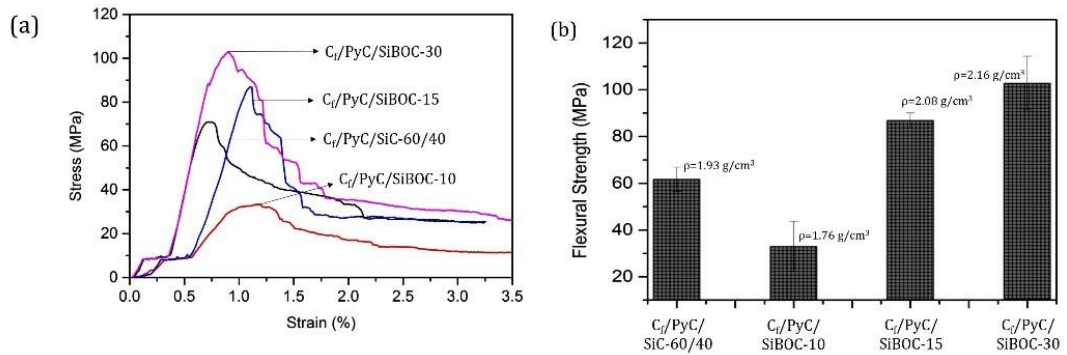
Figure 3.2.5 (a) stress-strain-curves and (b) the average flexural strength of C$_f$/PyC/SiC-60/40, C$_f$/PyC/SiBOC-10, C$_f$/PyC/SiBOC-15 and C$_f$/PyC/SiBOC-30 composites.

Figure 3.2.5 (a) and (b) shows the typical stress-strain-curves and the average flexural strength of C$_f$/PyC/ SiC-60/40, C$_f$/PyC/SiBOC-10, C$_f$/PyC/SiBOC-15 and C$_f$/PyC/SiBOC-30 composites. The average flexural strength and flexural modulus are summarized in Table 3.2.3. The results clearly shows the changes in stress-strain behaviour and flexural properties of the CMCs having PyC Interphase. In the case of CMCs without PyC Interphase, the stress-strain curve exhibited a linear increase in stress followed by a quick drop after reaching maximum (Figure 3.2.3 (a)). In contrast, the stress-strain curves of CMCs with PyC Interphase are divided into three stages: at the initial stage, a linear increase in stress followed by a curve at middle stage and a gradual drop at the final stage. This phenomenon is typical for the CMCs having weak F/M bonding which leads to good mechanical properties [Cao *et al.* 2014]. As expected, CMCs with PyC interphase has shown high flexural and modulus values as compared to the CMCs without PyC interphase (Table 3.2.3). The reason for the high flexural strength and modulus in the presence of PyC is explained with the help of studies on crack propagation and fracture surface of the composites.

Figure 3.2.6 (a) and (b) shows lateral view of the development of cracks in a flexural specimen and the fractured surface of C$_f$/PyC/ SiC-60/40, C$_f$/PyC/SiBOC-10, C$_f$/PyC/SiBOC-15 and C$_f$/PyC/SiBOC-30 composites.
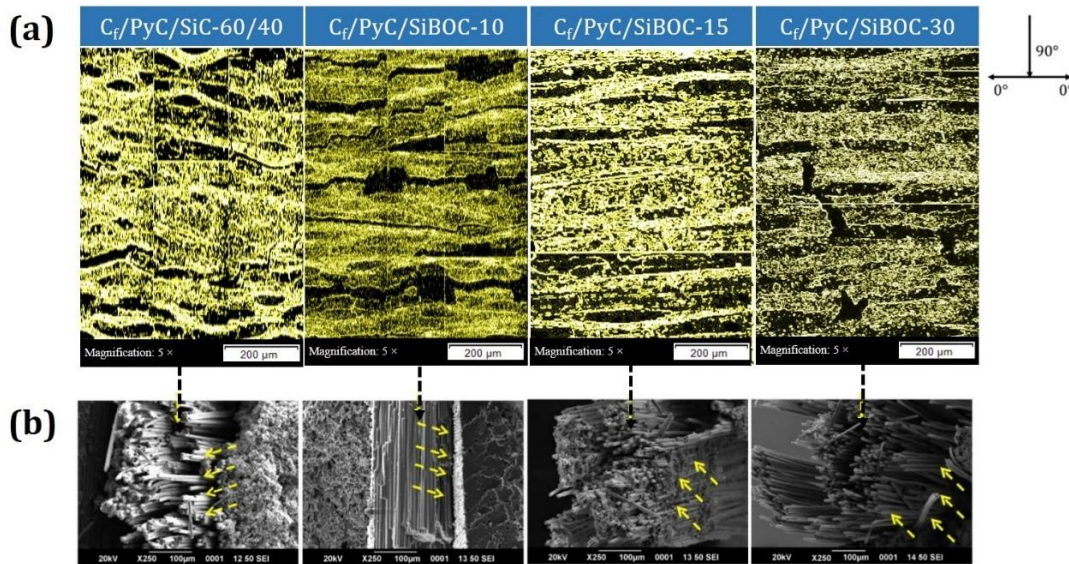
Figure 3.2.6 (a) Optical image of lateral view on the development of cracks in a flexural specimen and (b) SEM image on the fractured surface of C$_f$/PyC/SiC-60/40, C$_f$/PyC/SiBOC-10, C$_f$/PyC/SiBOC-15 and C$_f$/PyC/SiBOC-30 composites.

Optical image of C$_f$/PyC/ SiC-60/40, C$_f$/PyC/SiBOC-15 and C$_f$/PyC/SiBOC-30 composites revealed that, the presence of PyC interphase has helped in propagation of cracks along 0°/90° directions. This states that the existence of weak bonding between F/M Interface leads to an energy dissipative mechanism such as fiber pull-out and debonding (Figure 3.2.6 (b)). Further, this will increase the energy required for the propagation of the cracks leading to a high flexural properties as compared to the CMCs without PyC (Table 3.2.3). In contrast, C$_f$/PyC/SiBOC-10 composite has shown similar trend as observed for C$_f$/SiBOC-10 composite and has led to the lowest flexural strength (32.86 ± 10.7 MPa) among other composites. In addition, the flexural properties has increased with increase in concentration of boron and the maximum flexural strength and flexural modulus was achieved for C$_f$/PyC/SiBOC-30 composite of about 102.7 ± 11.5 MPa and 26.4 ± 3.1 GPa.

3.2.4. Conclusions

To enhance the flexural properties of C$_f$/SiBOC composites, the present study focuses on the optimization of F/M volume ratio and the influence of PyC interphase coating on the flexural properties of C$_f$/SiBOC composites.

To understand the effect of F/M volume ratio on the flexural properties of the composites, three types of C_f/SiC composites were fabricated by varying the F/M volume ratio viz. 40/60, 50/50 and 60/40 using PFSi as matrix precursor. The results show that, the flexural strength has increased from 25 ± 3.9 MPa (fiber content-40%) to 63 ± 9.9 MPa (fiber content-60%) on increasing the fiber vol. %. Additionally, C_f/SiC-40/60 and C_f/SiC-50/50 composites has failed in a brittle manner while C_f/SiC-60/40 composite exhibited a non-catastrophic fracture leading to fiber bundle pull-out. This reveals that the reinforcement of 'C' fiber is effective in preventing catastrophic fracture, especially for the composites with a high volume fraction of fiber reinforcement.

In the second part of investigation, CMCs were prepared with and without PyC interphase using BPFSi as matrix. The study proves that, PyC as interphase in the CMCs has played an important role in the load-carrying capability of the final composite. CMCs with PyC interphase shows an improvement in flexural strength from 32.86 ± 10.7 MPa (C_f/PyC/SiBOC-10) to 102 ± 11.5 MPa (C_f/PyC/SiBOC-30) while CMCs without interphase has shown no trend in improvement of flexural properties and the maximum flexural strength obtained was 38 ± 4.4 MPa (C_f/SiBOC-30). Further, the fractography of CMCs without interphase shows no fiber pull-out, indicating a strong fiber-matrix bonding. CMCs with PyC interphase coating shows fiber pull-out phenomenon and hence fails in a ductile manner. The study has proved the importance of optimization of F/M volume ratio and the need of PyC interphase coating to fabricate CMCs with better mechanical properties.

Chapter 4

Studies on silazane modified phenol-formaldehyde (SPF) as preceramic matrix resin for CMCs

In the previous chapter, it was understood that carbon fiber has been damaged by reacting with molten silicon to form thin polycrystalline SiC layer which has led to a reduction in the flexural property of the CMCs. So, in this chapter, silicon as additive was avoided and we have incorporated in the back bone of PF resin to prevent the silicon attack of carbon fiber to achieve improved mechanical properties of the CMCs. In this regard, PF modified with silazane is expected to result in an advanced preceramic resin for CMCs. As explained in *Chapter 1, Section 1.5.1.3 and 1.6*, many reports are available on PF resin based preceramic matrix resin, of which organometallic polymers, such as polysiloxane [Najafi *et al.* 2015, Noparvar-Qarebagh *et al.* 2016] and polyborosiloxane [Li *et al.* 2016], were widely studied for improving the thermo-structural properties of high-performance materials. To the best of our knowledge, there are no available reports on silazane modified phenol formaldehyde (SPF) based preceramic resin.

Hence, this chapter deals with the investigation of SPF as a potential preceramic matrix resin for CMCs. This work has been divided into two parts;

- In the first part, synthesis, characterization and ceramic conversion studies of SPF resin is discussed in detail.

- In the second part, CMCs are fabricated using SPF as matrix resin via polymer impregnation and pyrolysis (PIP) techniques.

Chapter 4.1

Synthesis, characterization and ceramic conversion studies of SPF resins
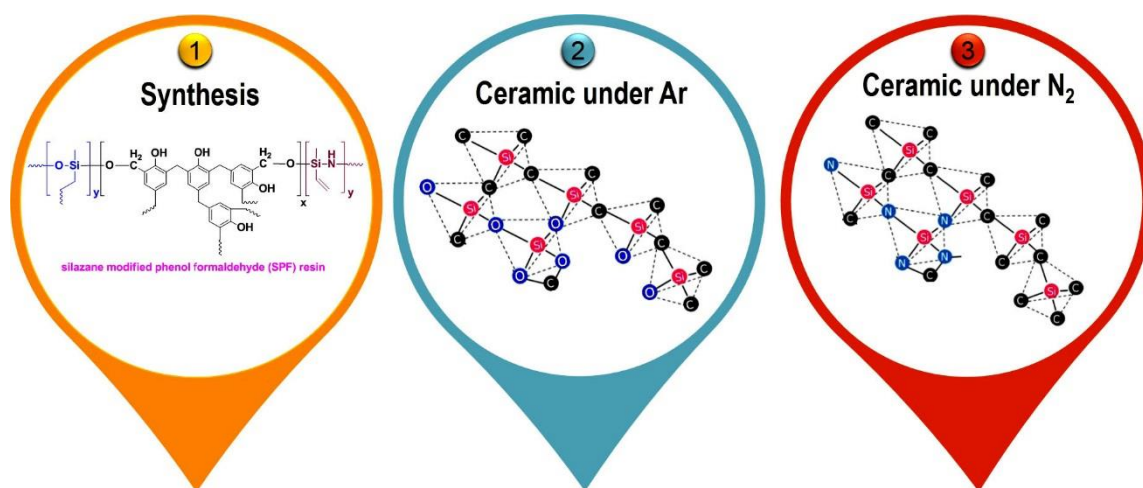
4.1.1. Introduction

This chapter reports synthesis and ceramic conversion of a novel preceramic polymer system based on SPF resins. This resins were synthesized by reacting varying amounts of 1, 3, 5-trimethyl-1', 3', 5'-trivinylcyclotrisilazane (CTS) with phenol formaldehyde (PF) resin. The conversion of preceramic resin to ceramics with high yield (>60 wt. %) and tailor-ability to obtain the desired ceramics are important criteria for the preceramic matrix resin. These criteria are highly dependent on the molecular structure and the pyrolysis conditions (temperature and atmosphere) of the preceramic resin, which significantly alters their properties for high-temperature applications [Bahloul *et al.* 1993, Bahloul *et al.* 1993]. Furthermore, the aim of this chapter is to employ SPF as matrix resin for CMCs. In this regard, the most commonly employed pyrolysis gas atmospheres are argon and nitrogen. Though, ammonia is another suggested pyrolysis atmosphere, the degradation of the reinforcement like carbon fiber is quite feasible under corrosive ammonia atmosphere [Chawla 1998] which may result in the deterioration of the CMCs strength, making ammonia atmosphere highly unsuitable for CMCs. Hence, this study was carried out under argon and nitrogen atmosphere for the final intended application and to select the most suitable pyrolysis condition to achieve the desired ceramics in high yield. The effect of pyrolysis conditions on ceramic yield, structural evolution and preceramic crystallization behavior was thoroughly investigated through XRD, Raman and FESEM techniques. The objective of this study is to assess the potential of SPF as a preceramic resin for CMCs and selection of an appropriate pyrolysis condition in order to achieve desired ceramic in high yield (>60 wt. %).

4.1.2. Experimental

4.1.2.1. Materials

Details of the chemicals are described in *Chapter 2, Section 2.1*.

4.1.2.2 Synthesis of SPF resin

The procedure for the synthesis of SPF resins are given in *Chapter 2, Section 2.2.2*.

4.1.2.3 Characterization

Characterization methods employed include FT-IR, NMR, XRD, Raman spectroscopy, FESEM and elemental analysis. The detailed procedures of all these characterizations are given in *Chapter 2, Section 2.5*.

4.1.2.4 Pyrolysis condition

For the selection of an appropriate pyrolysis condition, polymer-to-ceramic conversion of SPF was carried out at 1450°C and 1650°C separately under argon and nitrogen atmosphere. The detailed procedure for the ceramic conversion process is given in *Chapter 2, Section 2.4.3*.

4.1.3. Results and Discussion

4.1.3.1 Synthesis and characterization of SPF resin

Novel SPF resins were synthesized by reacting varying amounts of 1, 3, 5-trimethyl-1ʹ, 3ʹ, 5ʹ-trivinylcyclotrisilazane (CTS) with phenol formaldehyde (PF) resin as shown in *Chapter 2, Table 2.4*. This involves two-step reaction as shown in Figure 4.1.1. The first step involved the formation of PCTS by the reaction of CTS with DCP (Step-1 in Figure 4.1.1). Figure 4.1.2 (a) shows the FT-IR spectra of CTS and PCTS.

As expected, both showed similar spectrum, however, in the PCTS spectrum a new band corresponding to aliphatic C-H stretching appeared at 2909 cm^{-1}. Also, with the appearance of an aliphatic C-H stretching band, decrease in the band intensities of the vinyl groups at 3047 cm^{-1}, 1594 cm^{-1} and 1401 cm^{-1} was observed which indicates that vinyl polymerization has occurred partially. Additionally, broadening of the N–H stretching band (3400 cm^{-1}) as well as the Si–N–Si stretching (918 cm^{-1}) were observed which further confirms polymerization of CTS to form PCTS resin.

In the second step, formation of SPF resins occurs by the reaction of PCTS with PF (Step-2 in Figure 4.1.1). Figure 4.1.2 (b) shows FT-IR spectra of PF and silazane modified PF resins. The appearance of Si-O-C and Si-C-H bands at 1268 cm^{-1} and 1093 cm^{-1}, respectively [Figure 4.1.2 (b)], confirms the reaction proceeds through condensation reaction of PCTS with PF. Moreover, by increasing the concentration of PCTS, the intensity of Si–O–C stretching band increases which proves beyond doubt

that PCTS has chemically reacted with PF resin to form SPF resin.
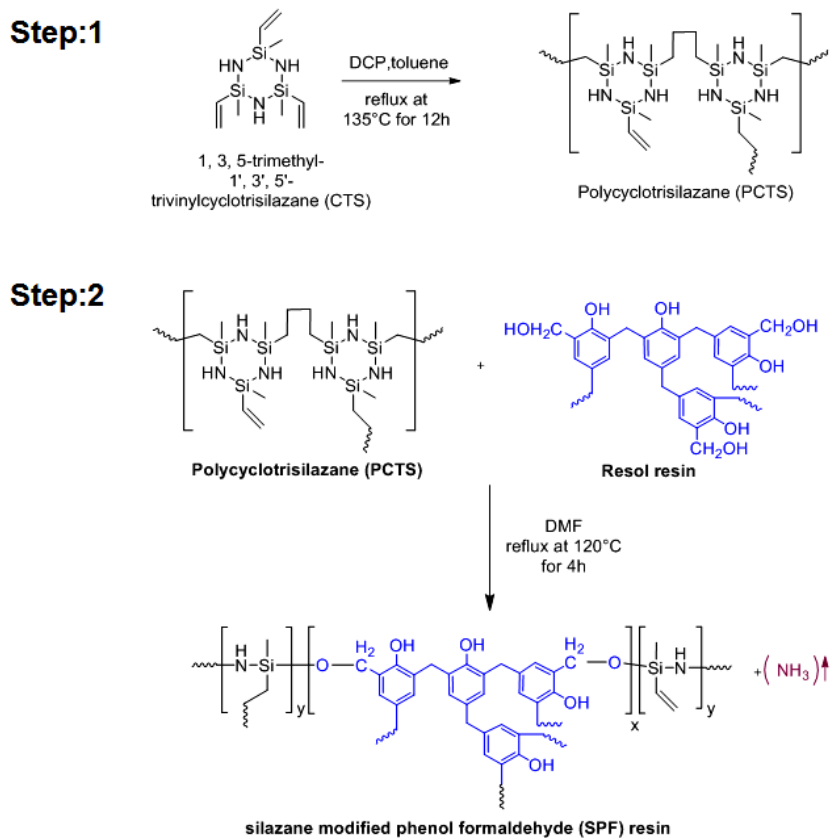
Figure 4.1.1. Synthesis of SPF resin
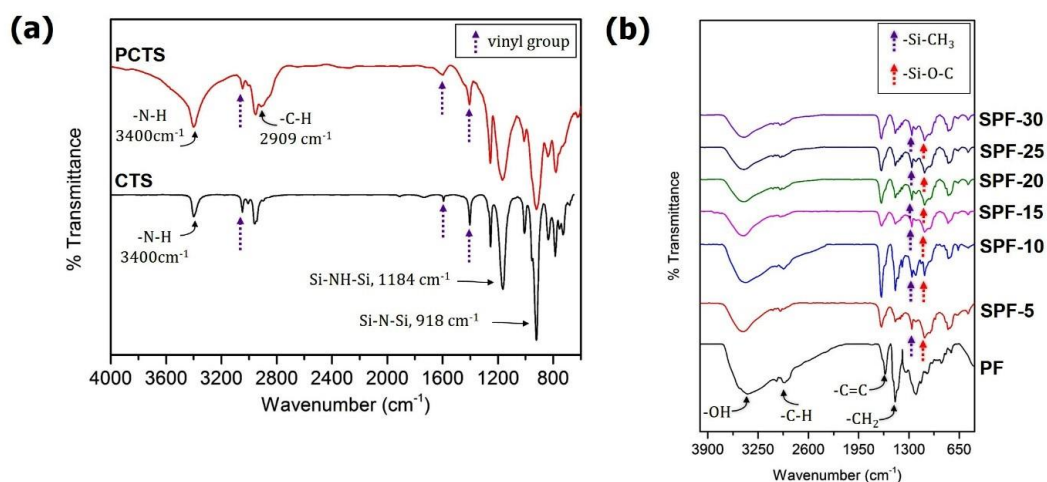
Figure 4.1.2. FT-IR spectra of (a) CTS and PCTS resin and (b) PF resin and different composition of SPF resins

Further, the detailed reaction mechanism for the formation of SPF resins was discerned through NMR analysis. Figure 4.1.3 (a), (b) and (c) shows the ^{1}H NMR spectra of PF, PCTS and SPF resins, respectively.
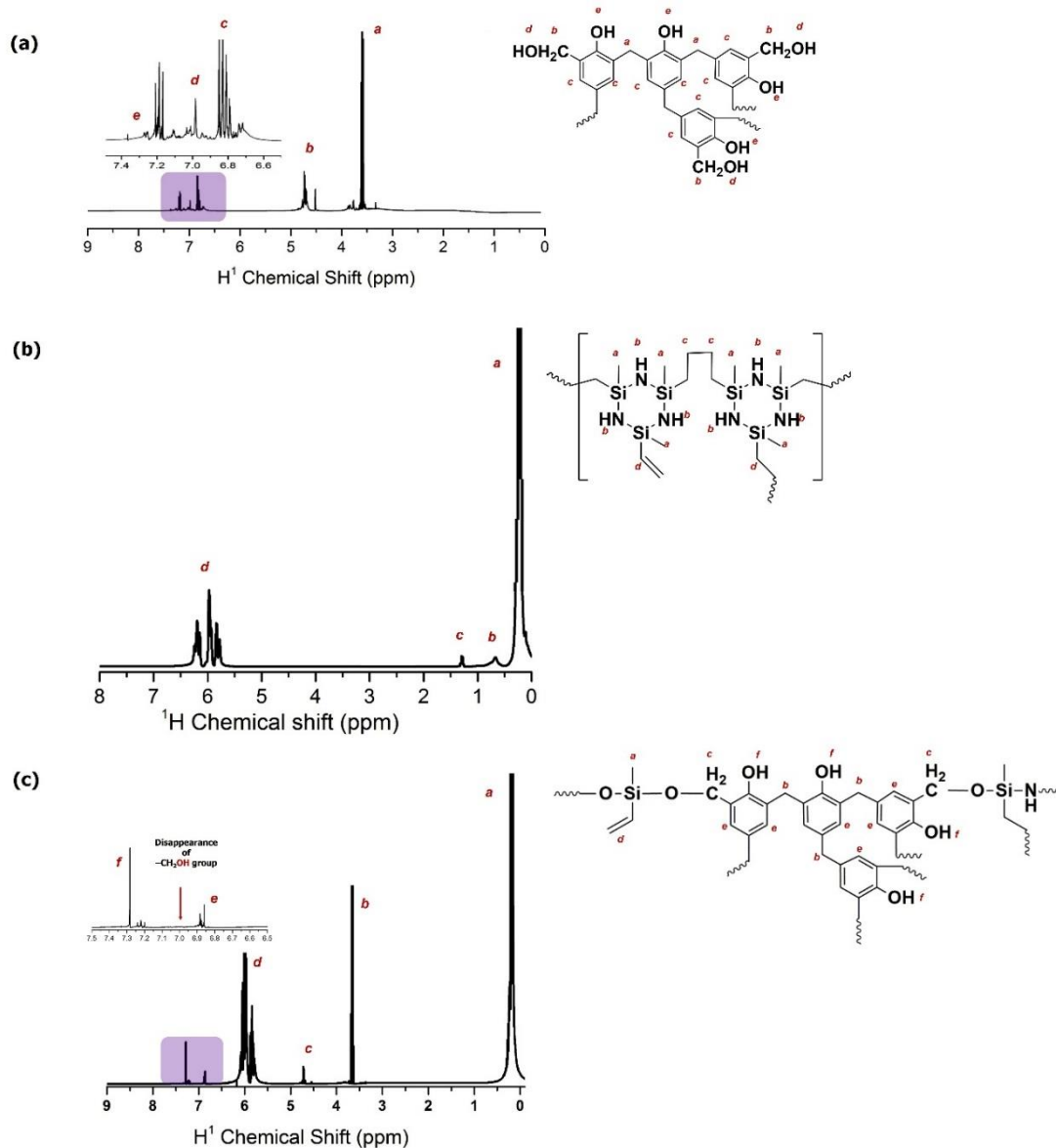
Figure 4.1.3. ^{1}H NMR spectra of (a) PF, (b) PCTS and (c) SPF

PF resin shows signals corresponding to -CH$_2$- group at δ = 3.43-3.92 ppm, methyloyl -CH$_2$- group at δ =4.80-4.76 ppm, Ar-H at δ = 6.74-6.85 ppm, methyloyl -OH group at δ = 7.03 ppm and phenolic -OH group at δ = 7.37 ppm [Figure 4.1.3 (a)]. PCTS showed signals corresponding to SiCH$_3$ group at δ = 0-0.45 ppm, N-H group at

$\delta = 0.62$ ppm, -CH$_2$-group at $\delta = 1.3$ ppm and -CH$_2$=CH- at $\delta = 5.71$–6.28 ppm [Figure 4.1.3 (b)]. SPF resin ^{1}H NMR showed characteristic signals of both PCTS and PF, with the disappearance of methyloyl -OH group at $\delta = 7.03$ ppm and N-H group at $\delta = 0.62$ ppm [Figure 4.1.3 (c)]. This confirms the reaction of PCTS with methylol -OH groups of PF which precedes over phenolic -OH groups of PF, with evolution of ammonia as shown in Figure 4.1.1.

The validation of reaction mechanism was further done through ^{29}Si NMR studies. Figure 4.1.4 (a) and (b) shows ^{29}Si NMR spectra of PCTS and SPF.
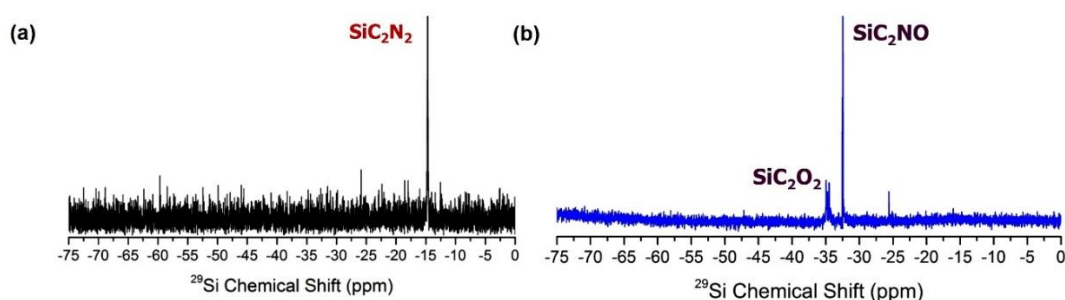
Figure 4.1.4. ^{29}Si NMR spectra of (a) PCTS and (b) SPF

PCTS showed SiC$_2$N$_2$ signal at $\delta = -14.90$ ppm, whereas in SPF no signal for SiC$_2$N$_2$ was observed. However, two new peaks at $\delta = -32.55$ ppm and $\delta = -35.02$ ppm were observed for SPF, which corresponds to SiC$_2$NO and SiC$_2$O$_2$, respectively. The formation of SiC$_2$NO and SiC$_2$O$_2$ indicates that, the reaction of PCTS with PF proceeds through a ring opening mechanism as shown in Figure 4.1.5.

The ring opening proceeds *via* condensation of one Si-NH-Si linkage of PCTS with two methyloyl -OH groups of PF which occurs in two steps. In the first step, the electrophilic attack of the hydrogen atoms of the methyloyl -OH group of PF on the nitrogen atoms of the silazane occurs to form a four centered labile complex. Formation of one Si-O-C linkage and one Si-NH$_2$ group occurs by the splitting of Si-N bond in the complex. In the second step, the formed Si-NH$_2$ group undergoes further reaction with methyloyl -OH group of PF forming another Si-O-C linkage with the evolution of NH$_3$ gas. This results in a more stable and less strained linear structured SPF resin.
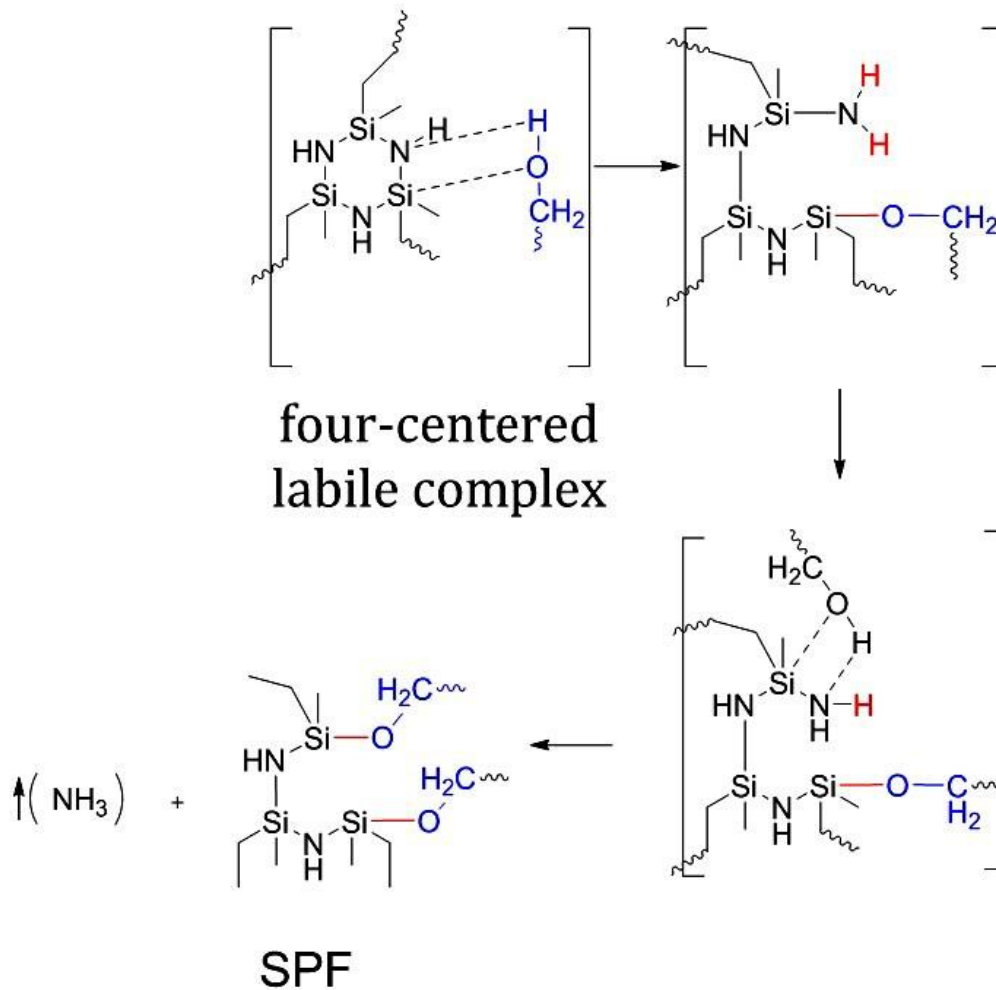
Figure 4.1.5. Proposed ring opening mechanism for the formation of SPF resin

4.1.3.2 Pyrolysis of SPF resin

To evaluate the potential of SPF resin as a preceramic polymer for high-temperature applications, studies on pyrolysis condition are mandatory. To meet this objective, Polymer-to-ceramic conversion was carried out under different pyrolysis conditions (*see Section- 2.4*). The thermal stability of the resultant ceramics in terms of thermal decomposition, crystallization, and ceramic yield under different pyrolysis condition were investigated through XRD, Raman and FESEM techniques.

4.1.3.2.1 XRD of pyrolyzed SPF resin
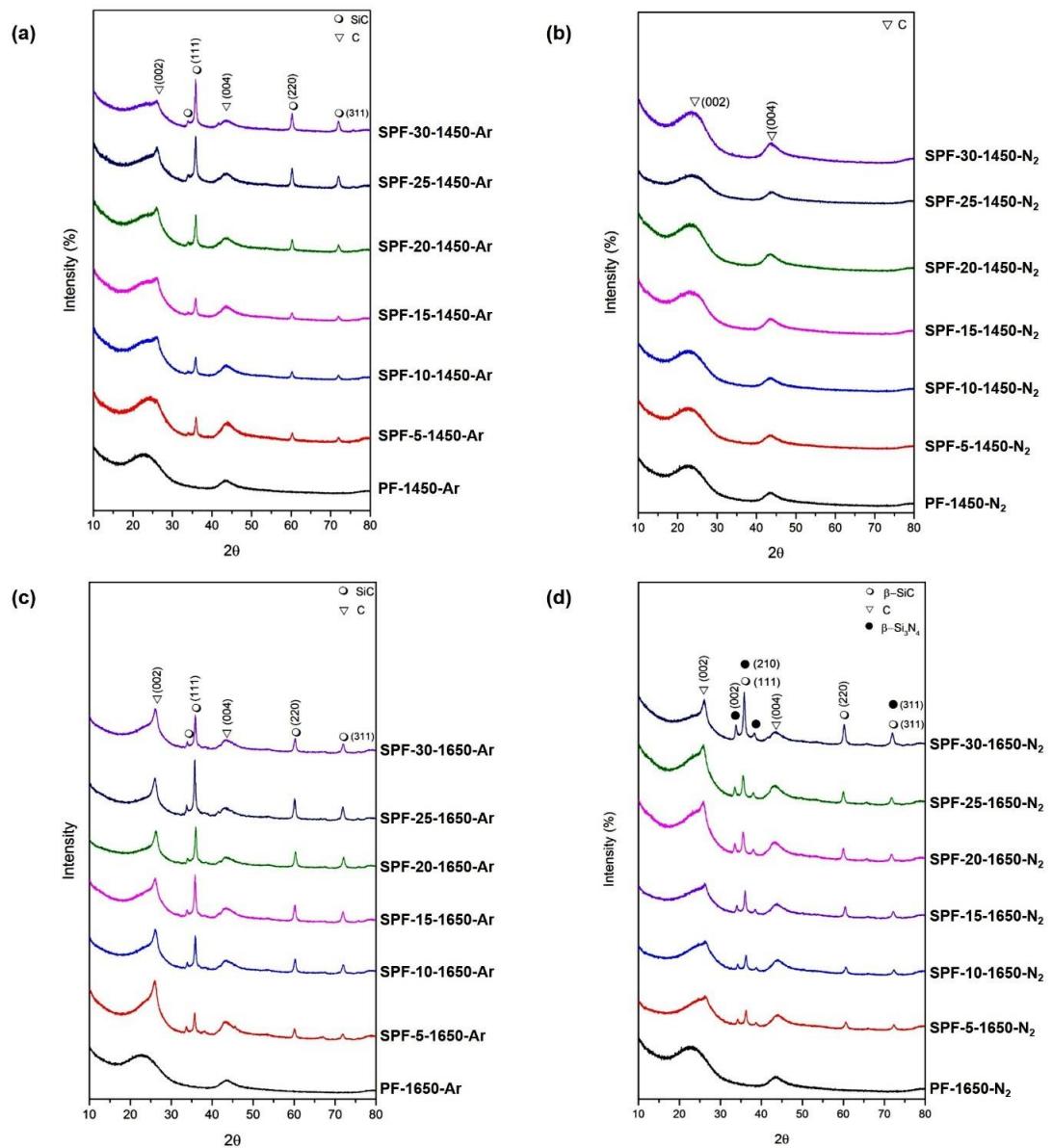
Figure 4.1.6. XRD spectra of the pyrolyzed SPF resin (a) argon atmosphere at 1450°C (b) nitrogen atmosphere at 1450°C and (c) argon atmosphere at 1650°C (d) nitrogen atmosphere at 1650°C

Figure 4.1.6 (a), (b), (c) and (d) show the XRD spectra of the pyrolyzed SPF resins at 1450°C and 1650°C under argon and nitrogen atmosphere respectively. In the case of PF resin, under different pyrolysis conditions (PF-1450-Ar, PF-1450-N_2, PF-1650-Ar and PF-1650-N_2), two broad diffraction peaks centered at $2\theta = 24.9°$ and $43.2°$

were observed, which corresponds to (002) and (004) planes respectively of glassy carbon (PDF 89-8493). For PCTS modified PF samples pyrolyzed at 1450°C and 1650°C under argon atmosphere [Figure 4.1.6 (a) and (c)], in addition to the peaks at $2\theta = 24.9°$ and $43.2°$, well defined crystalline peaks attributable to β-SiC at $2\theta = 35.6°$ (111), 41.3° (200), 59.9° (220), 71.7° (311) (PDF 74- 2307) and a small peak at $2\theta = 33.7°$ corresponding to stacking faults in β-SiC were also observed [Gosset *et al.* 2013]. Moreover, the intensity of the β-SiC peak increased with an increase in the concentration of PCTS. Interestingly, under a nitrogen atmosphere at 1450°C [Figure 4.1.6 (b)] these additional peaks [$2\theta = 35.6°$ (111), 41.3° (200), 59.9° (220), 71.7° (311), 75.4° (222)] were not observed and ceramic phase remained amorphous. This prolonged thermal stability of ceramics is known to be beneficial for high-temperature applications [Golczewski *et al.* 2004, Tang *et al.* 2016]. The prolonged thermal stability leads to desired properties like ultra-low coefficient of thermal expansion, outstanding thermal shock resistance which can be retained even to very high temperature (>1500°C). With increase in the pyrolysis temperature from 1450°C to 1650°C, along with the additional peaks observed in the case of argon atmosphere, new peaks corresponding to β-Si$_3$N$_4$ were also observed at $2\theta = 33.8°$ (002) and 38.3° (101) (PDF 33-1160) [Figure 4.1.6 (d)], which were not present in other systems. These Si$_3$N$_4$/SiC ceramic are reported to possess superior thermo-mechanical properties as compared to Si$_3$N$_4$ or SiC monolithic ceramic material [Hnatko *et al.* 2004, Schmidt *et al.* 2004] and hence are highly desired ceramic for high-temperature applications. Also these SiC/Si$_3$N$_4$ ceramics are synthesized by controlling the pyrolysis conditions which is more efficient and facile than the conventional powder route. It was also observed that the peak at $2\theta = 26.44°$ forms a shoulder peak with the main peak at $2\theta = 24.9°$ corresponding to glassy carbon in all the systems. This indicates the precipitation of graphitic carbon with increase in the concentration of PCTS. Moreover, this shoulder peak is sharper in the case of argon than nitrogen atmosphere which is supported by Raman analysis also.

4.1.3.2.2 Raman spectra of pyrolyzed SPF resin

The structural changes in the stoichiometrically excess carbon of pyrolyzed SPF resin with varying pyrolysis conditions were studied using Raman spectral analysis

[Figure 4.1.7 (a), (b), (c) and (d)].
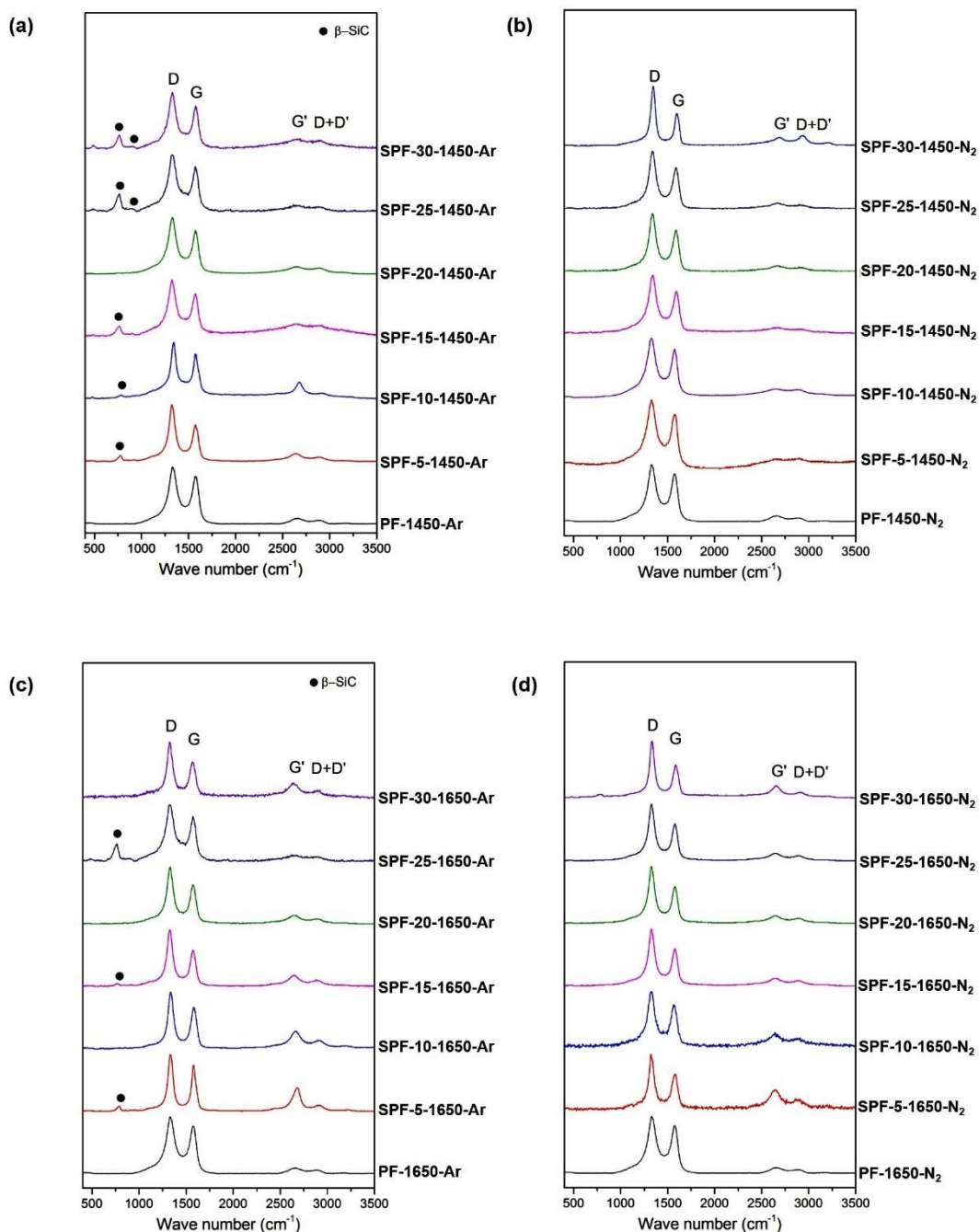
Figure 4.1.7. Raman spectra of the pyrolyzed SPF resin (a) argon atmosphere at 1450°C (b) nitrogen atmosphere at 1450°C and (c) argon atmosphere at 1650°C (d) nitrogen atmosphere at 1650°C

All the samples exhibited similar Raman spectra showing, disorder induced D and G´ bands (overtone of D band) at ~1330 cm^{-1} and 2630 cm^{-1}, G band due to in-plane bond stretching of sp^2 carbon at ~1575 cm^{-1} and combinational D+D´ band at ~2900 cm^{-1}. In addition to these peaks, some minor peaks corresponding to cubic 3C-SiC phases at 798 cm^{-1} and 930 cm^{-1} were also observed in some spectra [Figure 4.1.7 (a) and (c)]. Variations in position and intensity of D and G band, with changes in the structural organization of carbon phase in ceramics have been well reported [Traßl *et al.* 2000, Trassl *et al.* 2002, Trassl *et al.* 2002, Mera *et al.* 2010]. Hence, by evaluating these parameters, the effect of pyrolysis conditions on the structural organization of carbon phase can be thoroughly investigated. These parameters were derived using Gaussian curve fitting of the Raman bands and are listed in Table 4.1.1 and Table 4.1.2.

Table 4.1.1
Parameters derived from Raman spectra for ceramics derived from PF and SPF at 1450°C and 1650°C under argon atmosphere

| | Argon atmosphere | | | | | | | |
| | at 1450°C | | | | at 1650°C | | | |
Samples	D peak position (cm^{-1})	G peak position (cm^{-1})	I_D/I_G	La (nm)	D peak position (cm^{-1})	G peak position (cm^{-1})	I_D/I_G	La (nm)
PF	1343	1571	1.32	1.45	1340	1572	1.35	1.47
SPF-5	1335	1572	1.30	1.44	1337	1564	1.29	1.44
SPF-10	1333	1572	1.27	1.43	1332	1571	1.28	1.43
SPF-15	1330	1573	1.23	1.40	1330	1571	1.36	1.48
SPF-20	1329	1574	1.19	1.38	1329	1574	1.44	1.52
SPF -25	1325	1575	1.33	1.46	1326	1577	1.53	1.57
SPF -30	1322	1575	1.56	1.58	1324	1584	1.59	1.60

The intensity ratio of the D and G bands (I_D/I_G) can be also be used to calculate excess carbon cluster size using the formula reported by Ferrari and Robertson [Ferrari *et al.* 2004]

$$\frac{I_D}{I_G} = C'(\lambda) L_a^2 \qquad\qquad (4.1.1)$$

Where, L$_a$ is the size of carbon domains along the six-fold ring plane and C´ is

a coefficient that depends on the excitation wavelength (λ) of the laser. The value of C'
of the wavelength of 532 nm of the Nd: YAG laser used here is 0.6195 nm.

Table 4.1.2
Parameters derived from Raman spectra for ceramics derived from PF and SPF at
1450°C and 1650°C under nitrogen atmosphere

Samples	at 1450°C				at 1650°C			
	D peak position (cm^{-1})	G peak position (cm^{-1})	I_D/I_G	La (nm)	D peak position (cm^{-1})	G peak position (cm^{-1})	I_D/I_G	La (nm)
PF	1346	1574	1.29	1.44	1339	1575	1.62	1.61
SPF-5	1330	1573	1.28	1.43	1333	1563	1.61	1.61
SPF-10	1348	1600	1.26	1.42	1332	1566	1.29	1.44
SPF-15	1346	1596	1.32	1.45	1326	1568	0.88	1.19
SPF-20	1337	1588	1.23	1.4	1325	1576	1.53	1.57
SPF -25	1346	1587	1.38	1.49	1322	1579	1.67	1.64
SPF -30	1330	1573	1.36	1.48	1322	1584	1.72	1.66

Increase in the frequency of G band or a decrease in the frequency of D band
reflects the degree of orderness in carbon [Trassl *et al.* 2002]. It was observed that, for
SPF samples pyrolyzed at 1450°C and 1650°C under argon atmosphere, there was an
increase in the G band frequency and decrease in the D band frequency with increase
in PCTS concentration (Table 4.1.1). A similar trend in the D and G band frequency
was also observed for SPF samples pyrolyzed at 1650°C under nitrogen atmosphere
(Table 4.1.2). This indicates ordering of excess carbon from amorphous carbon to
crystalline graphite with increase in PCTS concentration. On the contrary, for SPF
samples pyrolyzed at 1450°C under nitrogen atmosphere (Table 4.1.2), no such trend
in the D and G band frequency with PCTS concentration was observed, indicating
insignificant effect of carbon phase at this pyrolysis temperature and gas atmosphere.
More information on structural organization of carbon was obtained by calculating L$_a$.
Figure 4.1.8 shows the variation of L$_a$ with employed pyrolysis conditions.
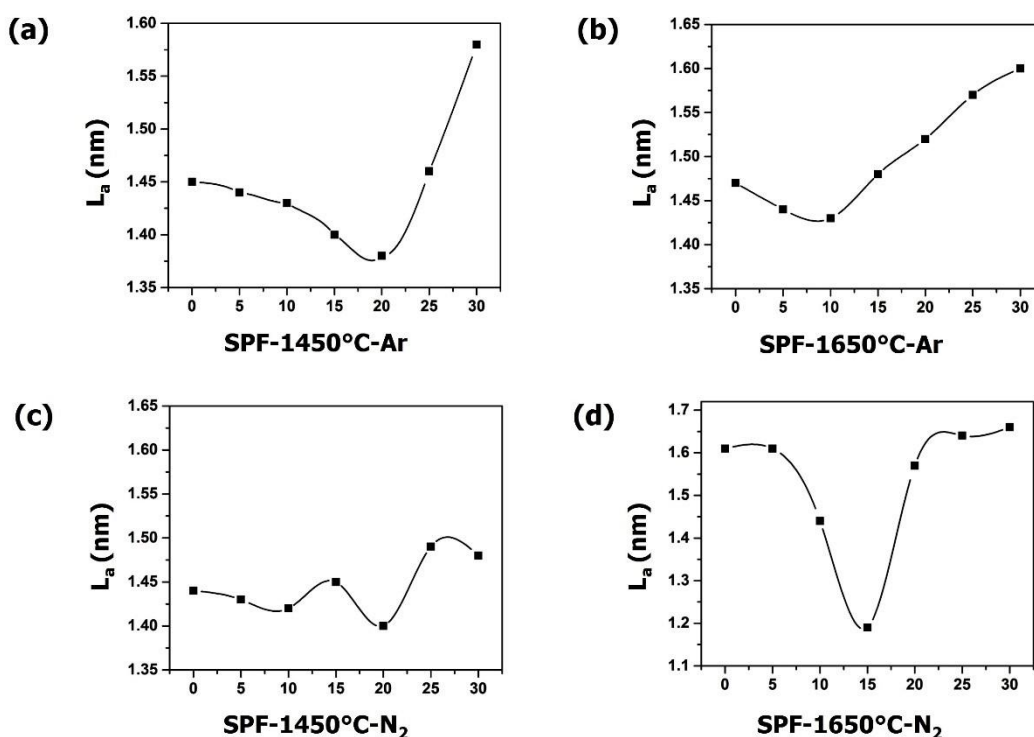
Figure 4.1.8. Variation of size in carbon domains (La) with pyrolyzed SPF at (a) 1450°C under argon atmosphere, (b) 1650°C under argon atmosphere, (c) 1450°C under nitrogen atmosphere and (d) 1650°C under nitrogen atmosphere

For SPF samples pyrolyzed under argon atmosphere at 1450°C and 1650°C, initial decrease in L_a was observed followed by subsequent increase with increase in concentration of PCTS [Figure 4.1.8 (a) & (b)]. A similar trend in L_a values with PCTS concentration was also observed for SPF samples pyrolyzed at 1650°C under nitrogen atmosphere [Figure 4.1.8 (d)]. These results are in accordance with the Ferrari model [Ferrari *et al.* 2000], which explains that, for the transformation of amorphous carbon to crystalline graphite, rearrangement of distorted aromatic rings to six-membered ring occur, which results in the shrinkage of L_a, whereas, the in-plane growth of crystalline graphite will increase the L_a value. Contrastingly, for SPF samples pyrolyzed at 1450°C under nitrogen atmosphere, no trend in L_a values with PCTS concentration was observed [Figure 4.1.8 (c)]. This indicates that, at this pyrolysis temperature and gas atmosphere, excess carbon phase does not get affected significantly, which results in the formation of amorphous carbon, as supported by XRD results [Figure 4.1.6 (b)]. Thus, XRD and Raman results, revealed the existence of a strong relationship between

crystallization of ceramics and ordering of the excess carbon phase with employed pyrolysis conditions.

4.1.3.2.3 FESEM Analysis of pyrolyzed SPF resin

XRD and Raman studies revealed that thermally more stable and desired ceramics are obtained under nitrogen atmosphere than argon atmosphere. In order to reveal the relationship between the thermal stability with employed pyrolysis conditions, morphological studies were carried out. The effect of pyrolysis conditions on the morphology of the ceramics was studied through FESEM analysis. It was observed that, the morphology of the obtained ceramics were highly sensitive to their processing pyrolysis atmospheres. The SPF samples pyrolyzed under argon atmosphere at both 1450°C and 1650°C displayed, two different morphologies viz. macro porous ceramics and nano-rod structured ceramics. These two different morphologies were obtained as a result of phase separation of ceramics under argon atmosphere. In-depth morphological investigations of these phase separated ceramics were done through FESEM and EDAX analysis. Figure 4.1.9 and Figure 4.1.10 shows the FESEM image of SPF pyrolyzed at 1450°C and 1650°C respectively, under argon atmosphere.

The formation of macro-porous ceramics can be explained by the decomposition of SiOCN ceramics [as shown in eqns. (2) to (6)] which results in local atomic rearrangement, forming a large number of Si-C enriched regions and gaseous species such as SiO, CO, N_2 and Si vapors, which are responsible for the formation of macro-pores through vapor-solid (VS) route mechanism.

$$SiC_xN_yO_{z(s)} \longrightarrow SiC_{(s)} + N_{2(g)} + NO_{(g)} + CO_{(g)} + SiO_{(g)} + Si_{(g)} \qquad (4.1.2)$$

$$Si_{(g)} + C_{(s)} \longrightarrow SiC_{(s)} \qquad (4.1.3)$$

$$2Si_{(g)} + 2CO_{(g)} \longrightarrow 2SiC_{(s)} + O_{2(g)} \qquad (4.1.4)$$

$$SiO_{(g)} + CO_{(g)} \longrightarrow SiC_{(s)} + O_{2(g)} \qquad (4.1.5)$$

$$SiO_{(g)} + C_{(s)} \longrightarrow SiC_{(s)} + CO_{(g)} \qquad (4.1.6)$$
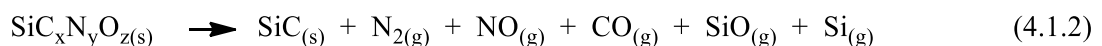
Macro porous structure
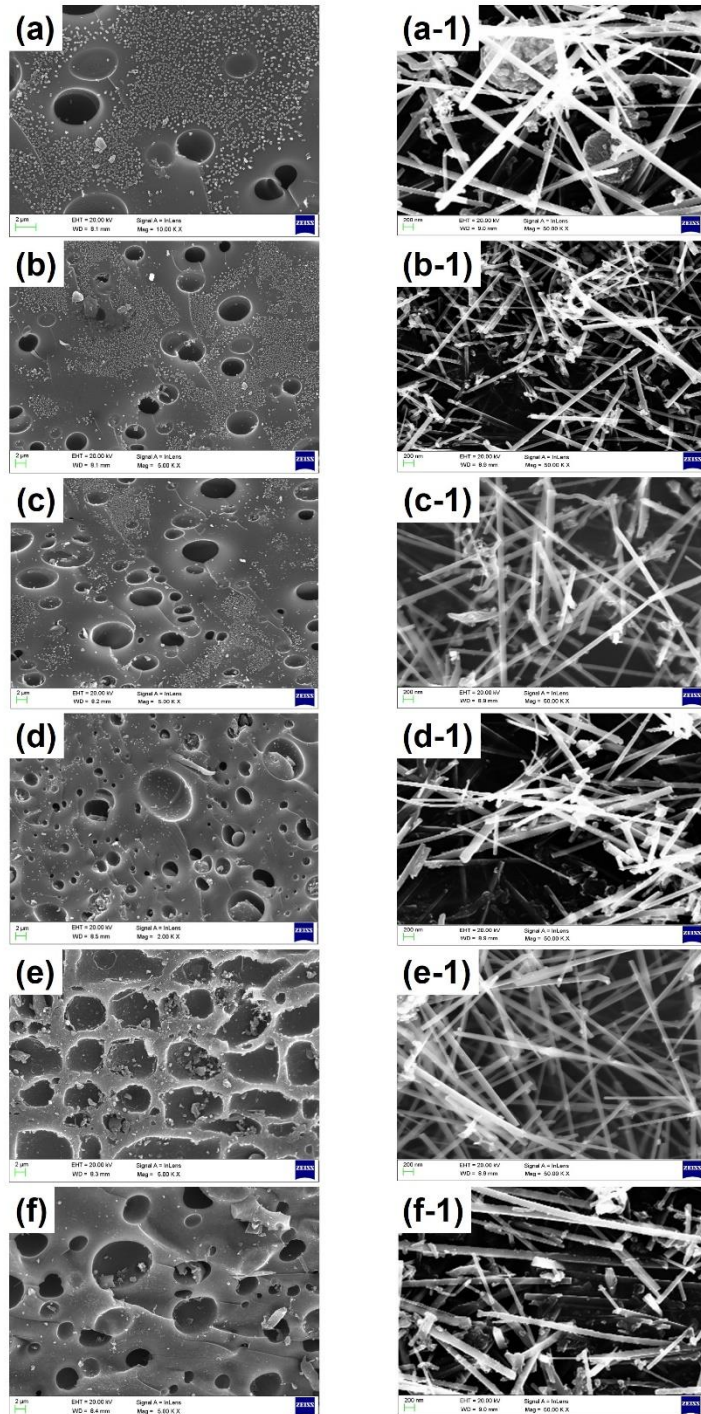
Nano-rod structure

Figure 4.1.9. FESEM image of SPF pyrolyzed at 1450°C under argon atmosphere (a) SPF-5, (b) SPF-10, (c) SPF-15, (d) SPF-20, (e) SPF-25 and (f) SPF-30

Macro porous structure
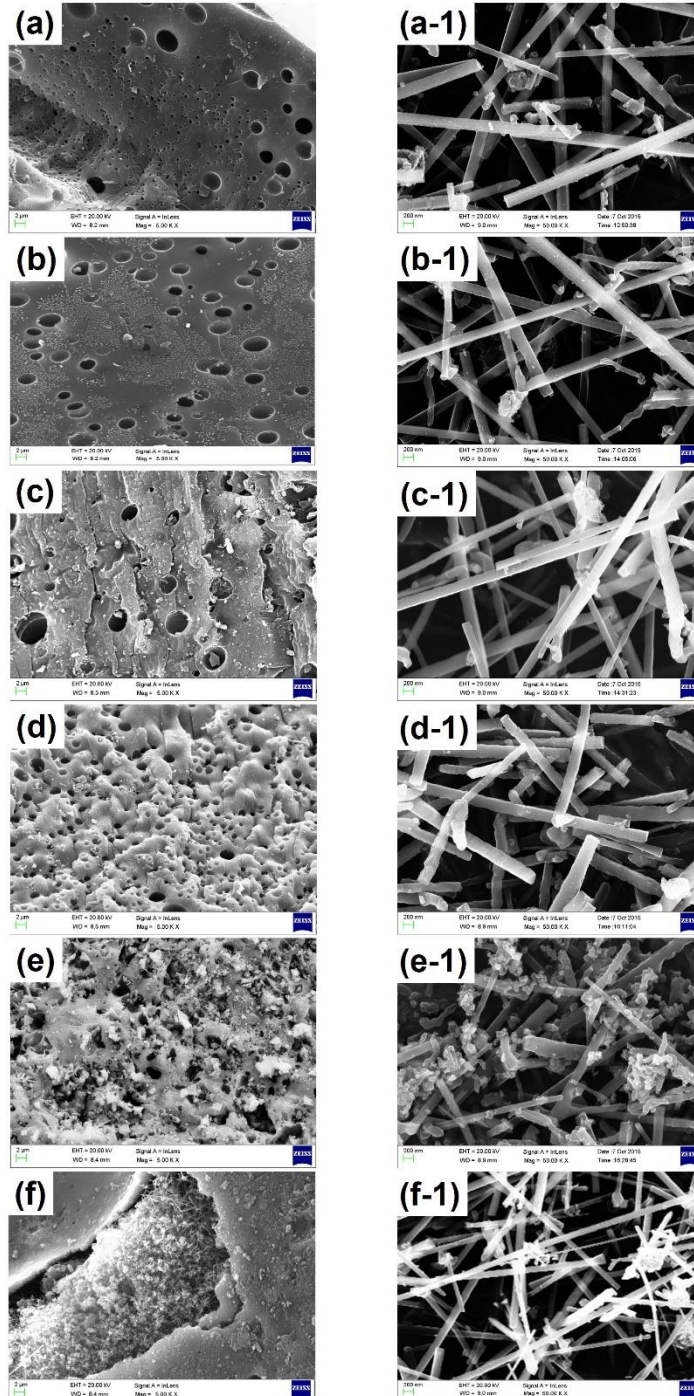
Nano-rod structure

Figure 4.1.10. FESEM image of SPF pyrolyzed under argon atmosphere at 1650°C (a) SPF-5, (b) SPF-10, (c) SPF-15, (d) SPF-20, (e) SPF-25 and (f) SPF-30

The formation of nano-rod structured ceramics was understood through elemental analysis studies. Figure 4.1.11 (a) shows the FESEM image of nano-rod structured ceramics along with its corresponding elemental composition from energy dispersive X-ray spectroscopy (EDAX).
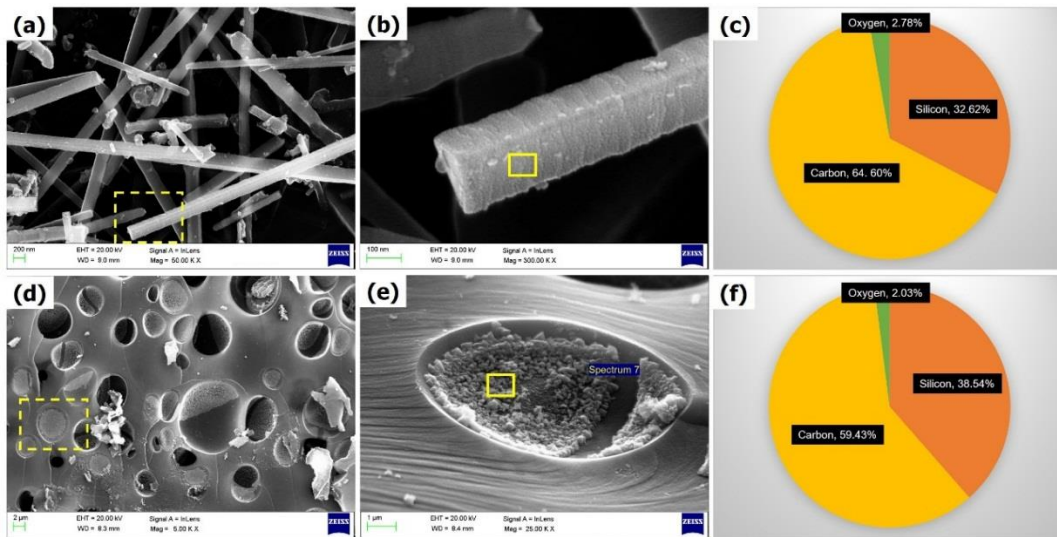
Figure 4.1.11. FESEM image, higher magnification FESEM image and corresponding EDAX spectra of SiC nano-rods (a, b and c) under argon atmosphere and nano-crystal decorated macro-porous cavity (d, e and f) under nitrogen atmosphere

FESEM image clearly revealed that, the nano-rod structures are 1D triangular shaped with edge width ranging from 20 to 200 nm and lengths of about 4 µm [Figure 4.1.11 (a) & (b)]. The corresponding EDAX spectrum showed that these nano-rods are composed of SiC ceramic [Figure 4.1.11 (c)]. This reveals that these nano-rod structured ceramics are formed by the reaction of oxygen with silicon and carbon [as shown in eqn. (4.1.4 & 4.1.5)]. This leads to the formation of SiO and CO gases which react with each other and get deposited in the form of nano-rods mainly through vapor-vapor (VV) route mechanism [Hata *et al.* , Gao *et al.* 2001, Gao *et al.* 2002]. These 1D nano-rod structured SiC ceramics are reported to have high potential in energy storage applications [Sung *et al.* 2005].

Conversely, under nitrogen atmosphere at both 1450°C and 1650°C, only macro porous ceramics were obtained with distinct variations in the morphology of the porous

cavity. At 1450°C, empty macro-porous cavities were obtained (Figures 4.1.12) whereas at 1650°C nano-crystals decorated macro-porous cavities were obtained (Figures 4.1.13).
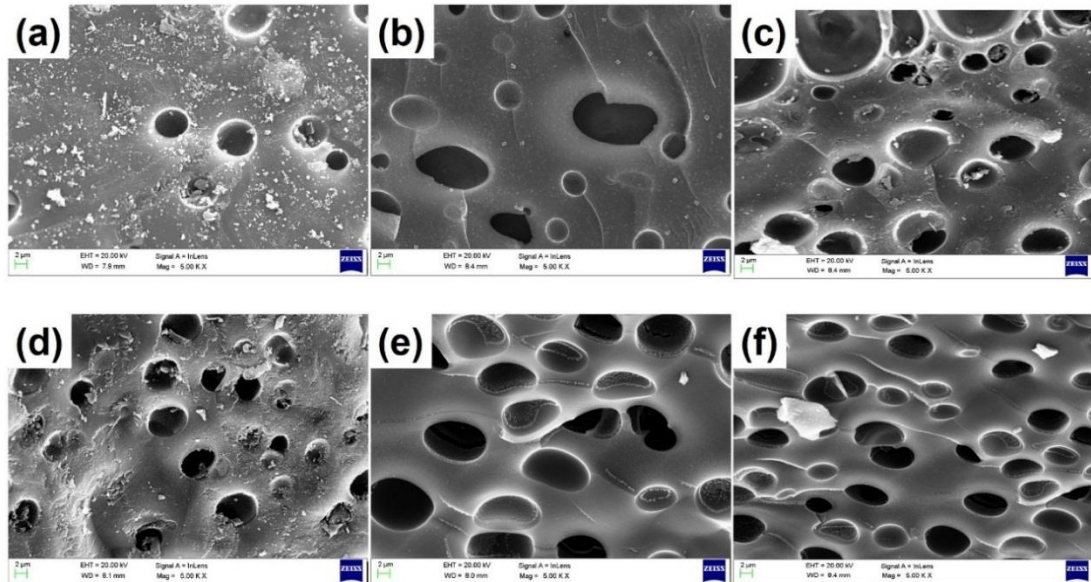
Figure 4.1.12. FESEM image of SPF pyrolyzed at 1450°C under nitrogen atmosphere (a) SPF-5, (b) SPF-10, (c) SPF-15, (d) SPF-20, (e) SPF-25 and (f) SPF-30
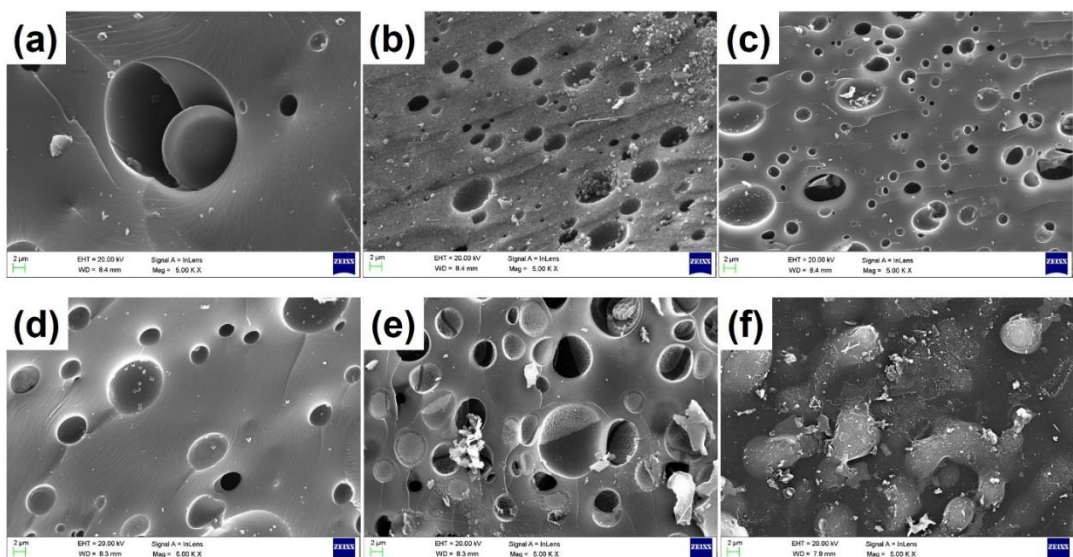
Figure 4.1.13. FESEM image of SPF pyrolyzed at 1650°C under nitrogen atmosphere (a) SPF-5, (b) SPF-10, (c) SPF-15, (d) SPF-20, (e) SPF-25 and (f) SPF-30

The formation of the macro-porous ceramics at both 1450°C and 1650°C, can be explained again by the decomposition of SiOCN ceramics [as shown in eqns. (2) to (6)] which leads to the formation of macro-pores through VS route mechanism. Whereas, at 1650°C, the formation of nano-crystals decorated macro-porous cavity occurs through VV route mechanism which was understood by EDAX studies. Figure 4.1.11 (d), (e) and (f) shows the FESEM micrograph of nano-crystal decorated macro-porous cavity ceramics with its corresponding elemental composition from EDAX. FESEM image clearly showed nano-crystals decorated macro-porous cavity formed under nitrogen atmosphere at 1650°C. The EDAX spectrum revealed that these nano-crystals are composed of SiC ceramics. These SiC nano-crystal are formed by the reaction of SiO and CO gases [as shown in eqn. (4.1.4 & 4.1.5)] which reacts with each other and gets deposited in the form of nano-crystals in macro-porous cavity through VV route mechanism as mentioned before.

Interestingly it was observed that, under argon atmosphere, the reaction of SiO and CO gases leads to the formation of nano-rod structured ceramics, whereas under nitrogen atmosphere nano-crystals decorated macro-porous cavity ceramics were formed. In order to explain this difference in morphology, detailed investigations on variation in degree of porosity with PCTS concentration and employed pyrolysis conditions is mandatory. Figure 4.1.14 shows surface porosity values computed from FESEM image using ImageJ 1.46r software [Sreekanth *et al.* 2012].

It was observed that, under argon atmosphere at both 1450°C and 1650°C [Figure 4.1.14 (a) & (b)], higher surface porosity was observed as compared to nitrogen atmosphere [Figure 4.1.14 (c) & (d)]. This clearly indicates that, the rate of decomposition of SiOCN ceramic is higher in argon atmosphere than nitrogen atmosphere. This difference in rate of decomposition of SiOCN ceramic is due to dual role of oxygen.
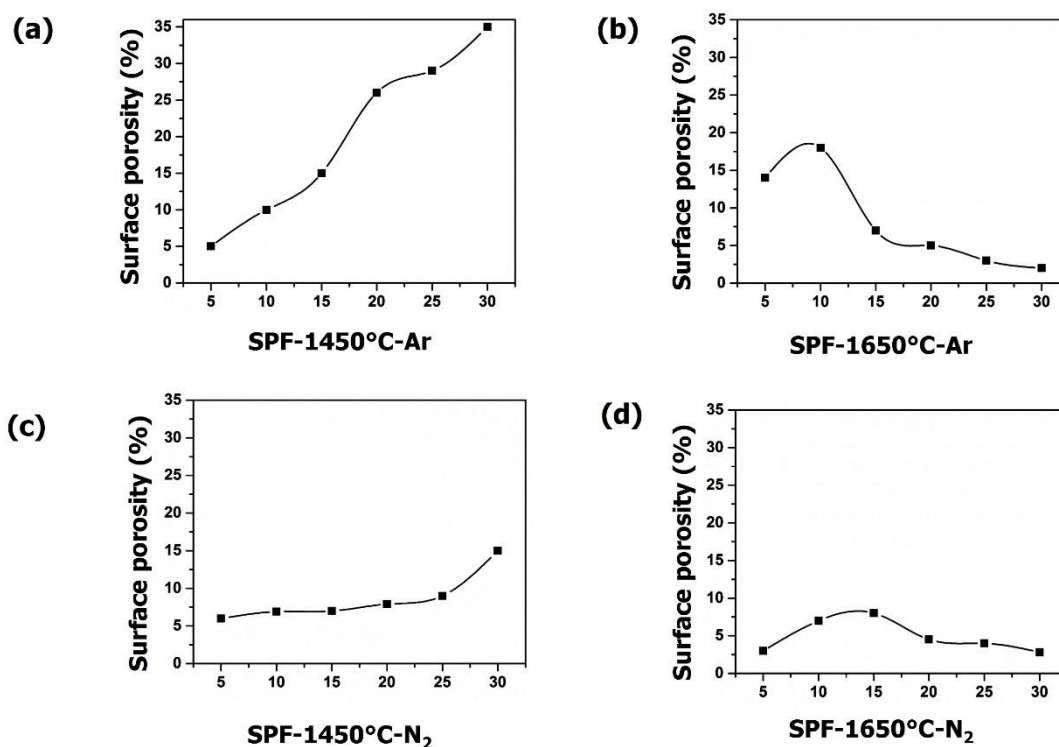
Figure 4.1.14. Variation of surface porosity with pyrolyzed SPF (a) at 1450°C under argon atmosphere, (b) at 1650°C under argon atmosphere, (c) at 1450°C under nitrogen atmosphere and (d) at 1650°C under nitrogen atmosphere

As per previously reported literature [Monthioux *et al.* 1996], oxygen can inhibit as well as promote the decomposition of SiOCN ceramics. Along with nitrogen, oxygen inhibits the generation of -SiC$_4$- aggregates, delays the formation of β-SiC crystals, and hence maintains the amorphous state of SiOCN ceramics. On the contrary, in the reaction of oxygen with silicon and carbon, oxygen promotes the formation of SiO and CO gases accelerating the decomposition of SiOCN ceramics. These two factors mutually influence the stability of amorphous SiOCN in different gas atmospheres. Under nitrogen atmosphere, the inhibition effects of oxygen and nitrogen on crystallization, play a major role in stabilization of SiOCN ceramic. While under argon atmosphere, the reaction of oxygen with silicon and carbon accelerates the vapor-phase reaction which leads to the crystallization of SiOCN ceramics. This observation falls in line with XRD and Raman results, where degree of crystallinity was more in argon atmosphere as compared to nitrogen atmosphere.

Furthermore, under argon and nitrogen atmospheres at 1450°C, surface porosity increased with increasing PCTS concentration [Figure 4.1.14 (a) & (c)]. This is due to the higher rate of decomposition of SiOCN ceramics with increase in PCTS concentration which increases the surface porosity. However, at 1650°C, surface porosity initially increased and then gradually decreased with increasing PCTS concentration [Figure 4.1.14 (b) & (d)]. This can be explained through two different path ways depending on pyrolysis atmosphere as shown in Figure 4.1.15.
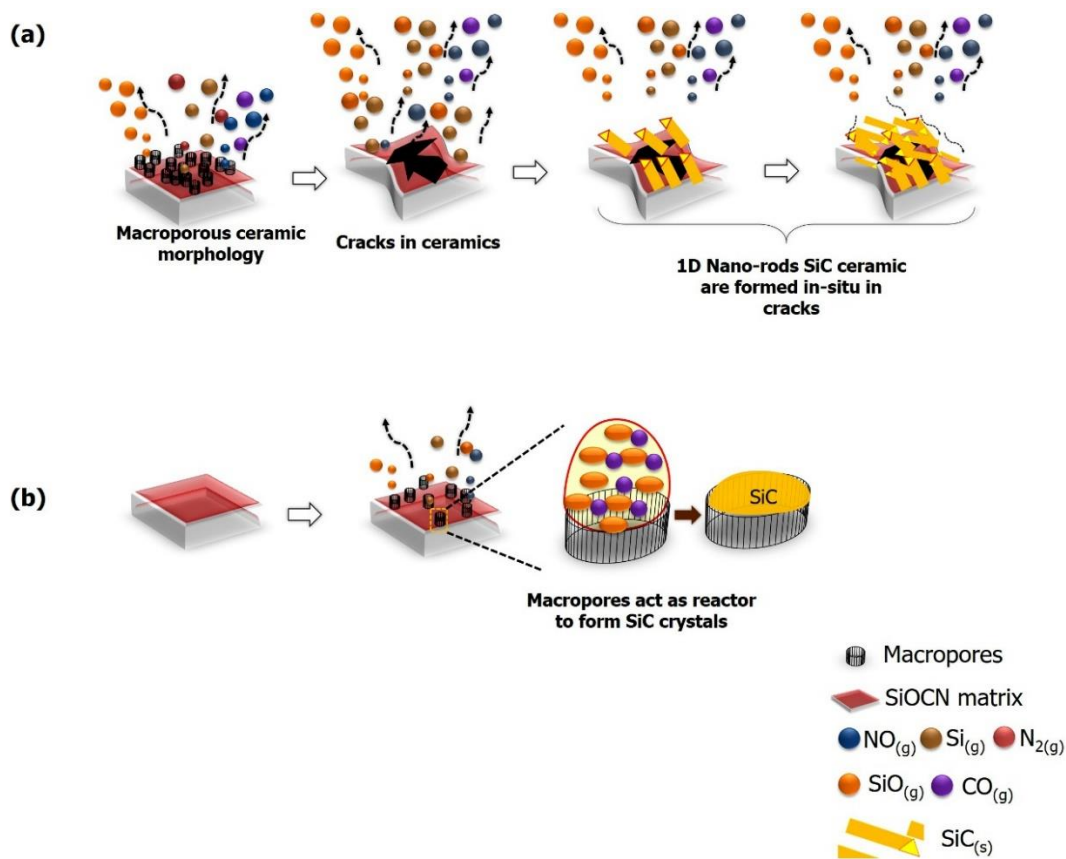
Figure 4.1.15. Mechanism for the formation (a) nano-rod structured ceramic under argon atmosphere and (b) nano-crystal decorated macro-porous cavity ceramic under nitrogen atmosphere

Under argon atmosphere at 1650°C, rate of decomposition of SiOCN ceramic is higher which results in coalescence of macro pores and leads to the formation of cracks [Figure 4.1.15 (a) & Figure 4.1.10 (f)]. This cracks form the path way for the VV mechanism which leads to *in-situ* formation of nano-rod structured SiC ceramics,

which decreases the overall porosity of the ceramics. Conversely, under nitrogen atmosphere, the rate of decomposition is relatively slow and hence results in evolution of less number of gaseous molecules. In such a situation, the macro-porous cavity acts as a reactor [Figure 4.1.15 (b) & Figure 4.1.13 (f)] for the deposition of SiC nano-crystals which decreases the overall porosity of the ceramics. This also explains the reason for the formation of nano-rod structured ceramics under argon atmosphere, whereas nano-crystals decorated macro-porous cavity ceramics under nitrogen atmosphere.

4.1.3.2.4 Elemental analysis and Ceramic yield of pyrolyzed SPF resin

In order to further ascertain the elemental compositions of as obtained ceramics, wet chemical analysis method was employed [Hilton 1966]. Table 4.1.3 and 4.1.4 shows the elemental compositions of the pyrolyzed SPF resins at 1450°C and 1650°C under argon and nitrogen atmosphere.

Table 4.1.3
Elemental composition of ceramics derived from SPF at 1450°C and 1650°C under argon atmosphere

	Argon atmosphere									
	at 1450°C					at 1650°C				
Samples	Composition (wt. %)				Empirical formula normalized on Si	Composition (wt. %)				Empirical formula normalized on Si
	Si	C	N	O		Si	C	N	O	
PF	-	100	-	-	C	-	100	-	-	C
SPF-5	10	76	0.2	13	$Si_1C_{3.3}N_{0.01}O_{1.2}$	11	77	-	11	$Si_1C_{3.05}O_{0.9}$
SPF-10	14	73	0.2	12	$Si_1C_{2.2}N_{0.01}O_{0.7}$	15	75	-	10	$Si_1C_{2.14}O_{0.58}$
SPF-15	21	69	0.3	11	$Si_1C_{1.4}N_{0.01}O_{0.4}$	21	70	-	8	$Si_1C_{1.40}O_{0.34}$
SPF-20	25	66	0.3	8	$Si_1C_{1.1}N_{0.01}O_{0.3}$	27	67	-	6	$Si_1C_{1.06}O_{0.19}$
SPF -25	28	65	0.4	7	$Si_1C_1N_{0.01}O_{0.2}$	28	66	-	5	$Si_1C_{0.99}O_{0.14}$
SPF -30	33	62	0.5	5	$Si_1C_1N_{0.01}O_{0.1}$	32	65	-	2	$Si_1C_{0.85}O_{0.05}$

Table 4.1.4
Elemental composition of ceramics derived from SPF at 1450°C and 1650°C under nitrogen atmosphere

Samples	Nitrogen atmosphere									
	at 1450°C					at 1650°C				
	Composition (wt. %)				Empirical formula normalized on Si	Composition (wt. %)				Empirical formula normalized on Si
	Si	C	N	O		Si	C	N	O	
PF	-	100	-	-	C	-	100	-	-	C
SPF-5	7	71	1.4	19	$Si_1C_4N_{0.1}O_{2.1}$	8	72	1.3	17	$Si_1C_3N_{0.11}O_{1.7}$
SPF-10	10	70	2.2	18	$Si_1C_3N_{0.1}O_{1.5}$	12	70	1.3	15	$Si_1C_2N_{0.08}O_{1.1}$
SPF-15	15	65	2.8	16	$Si_1C_2N_{0.1}O_{1.0}$	16	67	1.4	14	$Si_1C_1N_{0.06}O_{0.7}$
SPF-20	18	63	3.1	15	$Si_1C_1N_{0.1}O_{0.7}$	20	64	2.0	14	$Si_1C_1N_{0.07}O_{0.6}$
SPF -25	22	62	3.6	11	$Si_1C_1N_{0.1}O_{0.4}$	21	65	2.3	11	$Si_1C_1N_{0.08}O_{0.4}$
SPF -30	26	59	4.7	10	$Si_1C_1N_{0.1}O_{0.3}$	28	60	2.5	9	$Si_1C_1N_{0.06}O_{0.3}$

At both the pyrolysis conditions (at 1450°C and 1650°C under argon and nitrogen atmosphere), it was found that the silicon and nitrogen content increases whereas that of oxygen and carbon decreases with increase in PCTS concentration. However, there were distinct differences in nitrogen content under argon and nitrogen atmosphere. Under argon atmosphere at 1450°C only trace amount of nitrogen content was observed. With increase in pyrolysis temperature to 1650°C no nitrogen content was found (Table 4.1.3). Conversely, under nitrogen atmosphere at both 1450°C and 1650 °C, higher nitrogen content was obtained (Table 4.1.4). These differences in nitrogen content with respect to pyrolysis gas atmosphere is due to higher rate of decomposition of SiOCN ceramics under argon atmosphere than nitrogen atmosphere. These observation reveals the reason for the formation of only SiC ceramics under argon atmosphere and desired SiC/Si_3N_4 ceramics under nitrogen atmosphere. The ceramic yield of these obtained ceramics is another important criterion for high-temperature applications. Table 4.1.5 shows the variations in ceramic yield with pyrolysis condition and PCTS concentration.

Table 4.1.5
Ceramic yield of pyrolyzed SPF at 1450°C and 1650°C under argon and nitrogen atmosphere

Samples	Ceramic yield (wt. %)			
	Argon		Nitrogen	
	at 1450°C	at 1650°C	at 1450°C	at 1650°C
PF	35	32	36	33
SPF-5	37	35	43	41
SPF-10	38	36	45	43
SPF-15	39	36	49	46
SPF-20	39	37	54	52
SPF-25	42	38	57	54
SPF-30	42	40	63	60

It was observed that, at both the pyrolysis conditions (at 1450°C and 1650°C under argon and nitrogen atmosphere) ceramic yield increases with increase in PCTS concentration. Under argon atmosphere, highest ceramic residue of 42 wt. % and 40.65 wt. % for SPF-30 was obtained at 1450°C and 1650°C, respectively. While, under nitrogen atmosphere highest ceramic residue of 63 wt. % and 60.14 wt. % for SPF-30 was obtained at 1450°C and 1650°C, respectively. This shows that higher ceramic yield was achieved under nitrogen atmosphere as compared to argon atmosphere. This difference in ceramic yield is due to higher rate of decomposition of SiOCN ceramics under argon atmosphere than nitrogen atmosphere. Thus, the study reveals that under nitrogen atmosphere desired $C/SiC/Si_3N_4$ ceramics are formed with higher ceramic yield (60 wt. %), whereas under argon atmosphere only C/SiC ceramics are formed with lower ceramic yield (40 wt. %). Hence, nitrogen atmosphere is a more suitable pyrolysis gas atmosphere than argon atmosphere.

4.1.4. Conclusions

The present study reports the synthesis and pyrolysis of new class of preceramic polymer based on SPF. The thermal transformation of SPF resin to ceramics were carried out under different pyrolysis conditions (at 1450°C and 1650°C under argon and nitrogen atmosphere). Under argon atmosphere at both 1450°C and 1650°C, crystalline ceramics were obtained with only SiC as ceramic phase. Also, with increase in the concentration of PCTS, increase in degree of graphitization was observed,

indicating significant structural rearrangement of excess carbon.

Under nitrogen atmosphere at 1450°C, amorphous ceramics were obtained with no structural re-organization of carbon. While, at 1650°C crystalline SiC and Si_3N_4 ceramic phases were obtained. Also, graphitization of excess carbon from amorphous carbon to crystalline graphite occurs, showing structural re-organization of excess carbon. Moreover, under nitrogen atmosphere at both 1450°C and 1650°C, only macro-porous ceramics were formed. In contrast to nitrogen atmosphere, in argon atmosphere at both 1450°C and 1650°C, additional 1D, triangular shaped, nano-rod structured ceramics along with macro-porous structure were formed. EDAX analysis revealed that these nano-rods are composed of SiC formed through VV route mechanism.

This study demonstrates SPF as a new class of preceramic polymer for high-temperature applications. The study also reveals that nitrogen atmosphere is a more suitable pyrolysis gas atmosphere than argon atmosphere for preparation of desired $C/SiC/Si_3N_4$ ceramics with higher ceramic yield. Moreover, the work also represents an interesting and efficient route for synthesis of $C/SiC/Si_3N_4$ ceramics by controlling the pyrolysis conditions which is way more facile than the conventional powder route.

Chapter 4.2

Fabrication and characterization of CMCs using SPF as matrix resin
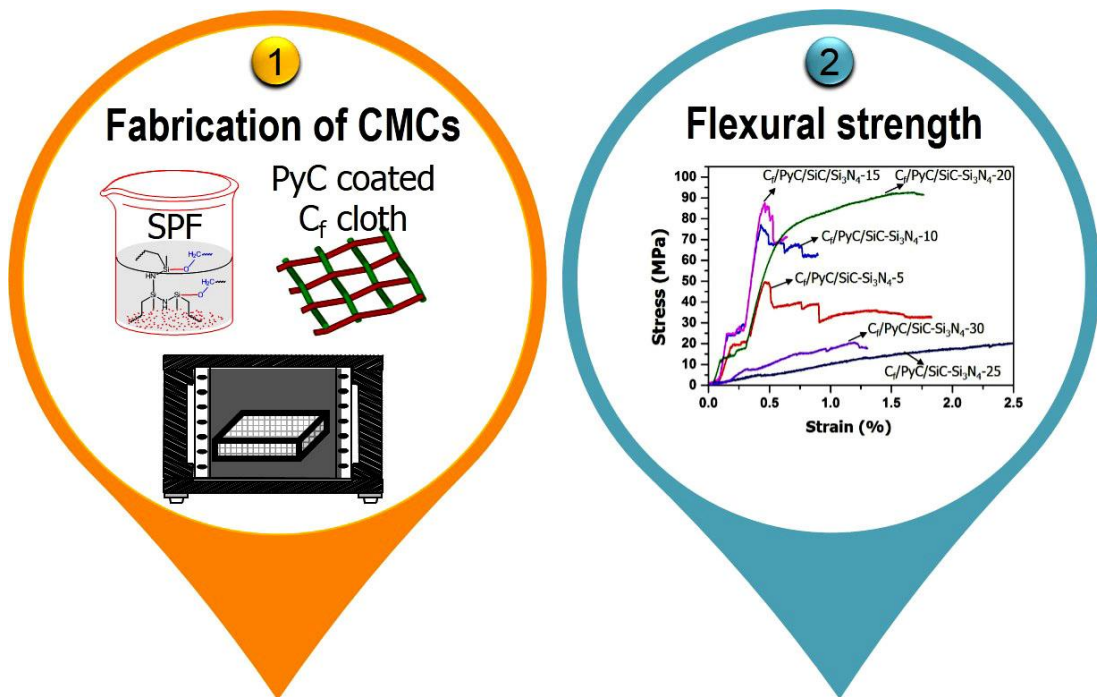
4.2.1. Introduction

Chapter 3.2, established the importance of varying F/M volume ratio and the need of PyC interphase coating to fabricate CMCs with better mechanical properties. *Chapter 4.1,* demonstrated SPF resins as a new class of preceramic polymer for the synthesis of SiCN based ceramics and revealed nitrogen atmosphere as a more suitable pyrolysis gas atmosphere than argon atmosphere for the preparation of desired SiC-Si_3N_4 ceramics with higher ceramic yield.

Hence, in this chapter, CMCs are fabricated having F/M volume ratio of 60/40, PyC as interphase coating and SPF as matrix resin *via* PIP process. The objective of the work is to assess the potential of SPF as a preceramic matrix resin for CMC applications and to select the most suitable formulation of SPF resin based on the mechanical properties of the composites.

4.2.2. Experimental

4.2.2.1 Materials

Details of the chemicals and materials are detailed in *Chapter 2, Section 2.1.*

Synthesis of SPF resins

The procedure for the synthesis of SPF resins are detailed in *Chapter 2, Section 2.2.2.*

4.2.2.2 Fabrication of C_f/PyC/SiC-Si_3N_4 composites

In order to establish SPF as potential candidate for preceramic matrix resin to achieve improved flexural properties of the composites, CMCs were fabricated as described in *Chapter 2, Section 2.6.3*. The obtained composites were finally machined to evaluate the flexural properties.

4.2.2.3 Characterization

Characterization methods employed include density and open porosity measurements, three-point-bending test, optical microscopy analysis and SEM analysis. The detailed procedures of all these characterizations are given in *Chapter 2, Section 2.5 and 2.7.*

4.2.3. Results and Discussion

4.2.3.1 Studies on C_f/PyC/SiC-Si_3N_4 composite

SPF resins were synthesized by reacting varying amounts of 1, 3, 5-trimethyl-1', 3', 5'-trivinylcyclotrisilazane (CTS) with phenol formaldehyde (PF) resin and their typical properties are shown in Table 4.2.1.

Table 4.2.1
Different formulation of SPF resin

Sl.No	Sample	Conversion of CTS to polycyclotrisilazane (PCTS)		PF-106 (g)	Ceramic yield at 1650°C	Empirical formula normalized on Si
		CTS (g)	DCP (g)			
1.	SPF-5	5	0.06	100	41.13	$Si_1C_{3.60}N_{0.11}O_{1.73}$
2.	SPF-10	10	0.12	100	43.10	$Si_1C_{2.49}N_{0.08}O_{1.09}$
3.	SPF-15	15	0.17	100	46.24	$Si_1C_{1.76}N_{0.06}O_{0.77}$
4.	SPF-20	20	0.23	100	52.12	$Si_1C_{1.37}N_{0.07}O_{0.61}$
5.	SPF-25	25	0.29	100	54.47	$Si_1C_{1.32}N_{0.08}O_{0.45}$
6.	SPF-30	30	0.35	100	60.14	$Si_1C_{0.92}N_{0.06}O_{0.28}$

It was found that, the SPF resins yield SiC-Si_3N_4 ceramics under nitrogen atmosphere at 1650°C and their formation increases with increase in the concentration of CTS as evidenced from the previous chapter (*Chapter 4.1*). Therefore, CMCs were fabricated using different composition of SPF as matrix resin (Table 4.2.2), PyC as interphase and 2D carbon fabric as reinforcement *via* PIP process at 1650°C under nitrogen atmosphere. The details of composites thus obtained are given in Table 4.2.2.

Table 4.2.2
Properties of the C_f/PyC/SiC-Si_3N_4composites

Sl. No.	Preceramic matrix resin	Sample	Open porosity (%)	Density (g/cm³)	Flexural strength (MPa)	Flexural modulus (GPa)
1.	SPF-5	C_f/PyC/SiC-Si_3N_4-5	15.0	1.38	50 ± 6	14 ± 4
2.	SPF-10	C_f/PyC/ SiC-Si_3N_4-10	13.3	1.42	75 ± 7	17 ± 7
3.	SPF-15	C_f/PyC/ SiC-Si_3N_4-15	10.6	1.44	88 ± 1	23 ± 3
4.	SPF-20	C_f/PyC/ SiC-Si_3N_4-20	9.2	1.51	92 ± 5	25 ± 5
5.	SPF-25	C_f/PyC/ SiC-Si_3N_4-25	24.1	1.28	22 ± 9	9 ± 5
6.	SPF-30	C_f/PyC/ SiC-Si_3N_4-30	28.5	1.24	21 ± 2	6 ± 3

4.2.3.1.1 Evaluation of flexural properties
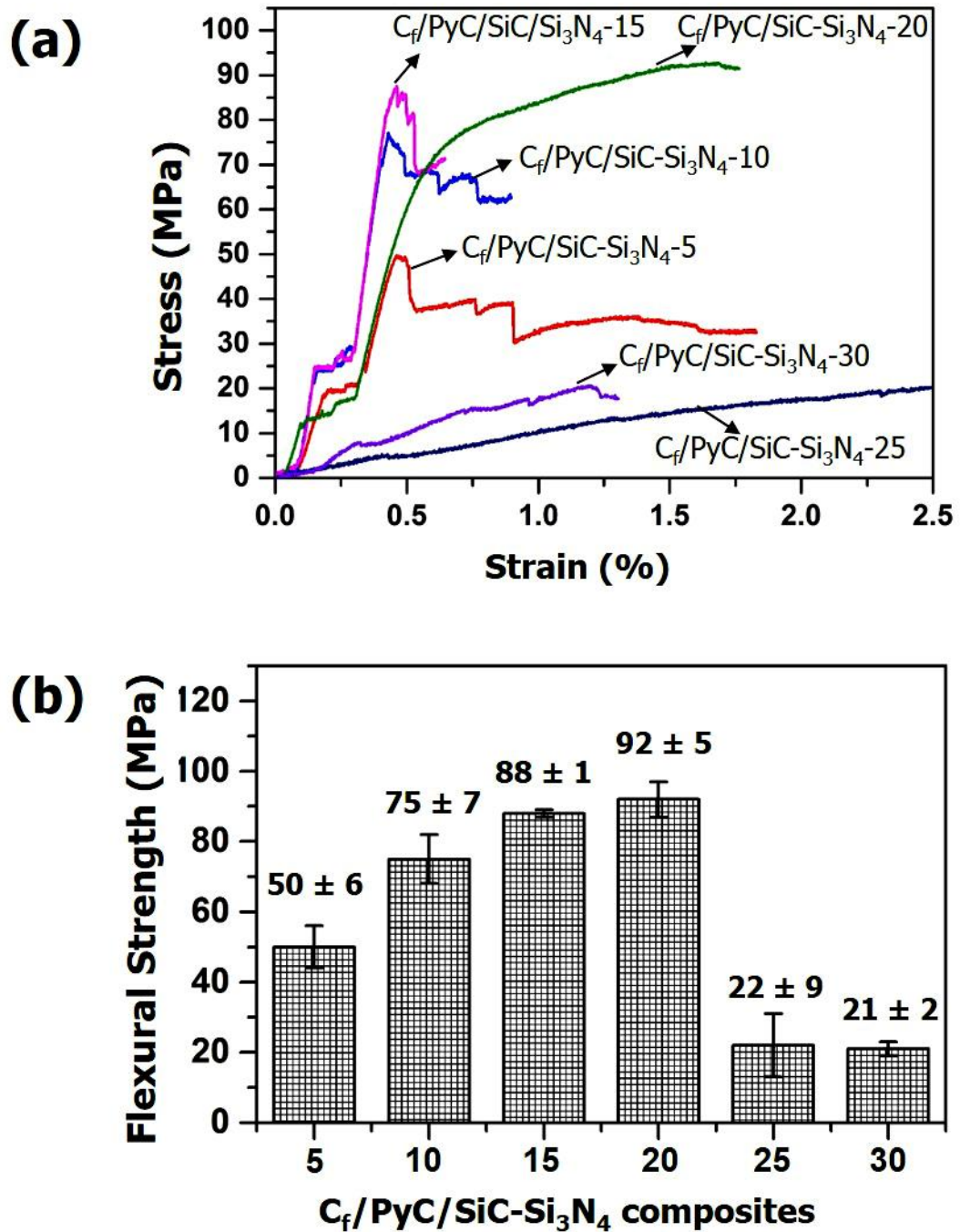
Figure 4.2.1 (a) Stress–strain-curves and (b) the average flexural strength of $C_f/PyC/SiC-Si_3N_4$ composites

The stress-strain-curves and the average flexural strength of C_f/PyC/SiC-Si_3N_4 composites are shown in Figure 4.2.1 (a) and (b), respectively. The obtained properties are summarized in Table 4.2.2. The changes in the SPF composition significantly affects the mechanical properties as shown by the changes observed in stress-strain behavior, flexural strength and flexural modulus. It is to be noted that, the composition of SiC-Si_3N_4 ceramics increases with increase in the concentration of CTS i.e., from SPF-5 to SPF-30 the concentration of SiC-Si_3N_4 ceramics gradually increases. Hence, it is expected that on increase in SiC-Si_3N_4 ceramic content and the presence of PyC as interphase will improve the flexural properties of the composites. Surprisingly, it was observed that, from C_f/PyC/SiC-Si_3N_4-5 to C_f/PyC/SiC-Si_3N_4-20 the flexural properties have gradually increased with increase in SiC-Si_3N_4 ceramic content (Table 4.2.2) and a maximum flexural strength of 92 ± 5 MPa was achieved for C_f/PyC/SiC-Si_3N_4-20 composite. However, a sudden drop in flexural properties was observed in the case of C_f/PyC/SiC-Si_3N_4-25 and C_f/PyC/SiC-Si_3N_4-30 composites (Table 4.2.2). These variations in flexural properties of C_f/PyC/SiC-Si_3N_4 composites were further understood from the stress-strain-curves which exhibited two types of fracture behavior [Figure 4.2.1 (a)].

In the first type, the stress-strain-curves of composites showed three distinctive stages. At the first stage, a linear increase in stress is observed followed by a curve at second stage and a gradual drop at the final stage. This phenomenon was observed for C_f/PyC/SiC-Si_3N_4-5, C_f/PyC/SiC-Si_3N_4-10 and C_f/PyC/SiC-Si_3N_4-15 composites as a result of weak bonding between the F/M interfaces [Babu *et al.* 2016]. As a result, the flexural properties increase with increase in SiC-Si_3N_4 ceramic content of the composites. In the second type, the stress-strain-curves exhibits a pseudo-ductile fracture behavior, which is observed in the case of C_f/PyC/SiC-Si_3N_4-20, C_f/PyC/SiC-Si_3N_4-25 and C_f/PyC/SiC-Si_3N_4-30 composites. This phenomenon is normally expected to show high flexural properties [Lamouroux *et al.* 1994] which is true only in the case of C_f/PyC/SiC-Si_3N_4-20 composite where the highest flexural strength of 92 ± 5 MPa and modulus of 25 ± 5 was observed. Whereas, C_f/PyC/SiC-Si_3N_4-25 and C_f/PyC/SiC-Si_3N_4-30 are found to have the lowest flexural strength of 22 ± 9 MPa and 21 ± 2 MPa

respectively, and modulus of 9 ± 5 GPa and 6 ± 3 GPa, respectively. With increase in SiC-Si$_3$N$_4$ composition for C$_f$/PyC/SiC-Si$_3$N$_4$composites the lack of improvement in flexural properties were understood by studying the propagation of crack and fracture surface of the composites.

The lateral view of the propagation of cracks in a flexural specimen and SEM image of the fractured surface of C$_f$/PyC/SiC-Si$_3$N$_4$ composites are shown in Figure 4.2.2 (a) and (b), respectively. The lateral view image of C$_f$/PyC/SiC-Si$_3$N$_4$ composites for all the composition of SPF showed the importance of PyC interphase coating on the carbon fiber which helps in crack propagation along 0°/90° directions [Curtin 1991]. This suggests subsistence of a weak bonding between F/M Interface leading to fiber pull-out and debonding through energy dissipative mechanism [Figure 4.2.2 (b)] [Rizvi *et al.* 2016] resulting in superior flexural properties. This was true in the case of C$_f$/PyC/SiC-Si$_3$N$_4$-5 to C$_f$/PyC/SiC-Si$_3$N$_4$-20 composites leading to increase in flexural properties.

On the contrary, the propagation of cracks and fracture surface behavior of C$_f$/PyC/SiC-Si$_3$N$_4$-25 and C$_f$/PyC/SiC-Si$_3$N$_4$-30 composites shows a partial delamination, in spite of the crack propagation along 0°/90° directions. This is due to the presence of very weak interface between F/M as indicated by arrows [Figure 4.2.2 (b)]. Hence, the structurally weak points like high propensity of cracks or pores in the matrix may lead to a premature failure of the composite and results in inferior flexural properties among other composites. It is to be noted that for achieving superior mechanical properties of CMCs, higher density and lower porosity are highly desirable [Naslain 2004]. A gradual increase in density and decrease in open porosity was observed for C$_f$/PyC/SiC-Si$_3$N$_4$-5 to C$_f$/PyC/SiC-Si$_3$N$_4$-20 composites, resulting in increase in flexural properties (Table 4.2.2). On contrary, for C$_f$/PyC/SiC-Si$_3$N$_4$-25 and C$_f$/PyC/SiC-Si$_3$N$_4$-30 composites, lowest density and highest open porosity was observed (Table 4.2.2) which resulted in lowest flexural properties among other composites. This explains the reason for highest flexural properties in the case of C$_f$/PyC/SiC-Si$_3$N$_4$-20 composite and lowest flexural properties in the case of C$_f$/PyC/SiC-Si$_3$N$_4$-30 composite. The study establishes SPF-20 as the most suitable

formulation for the fabrication of CMCs with improved mechanical properties through PIP process.
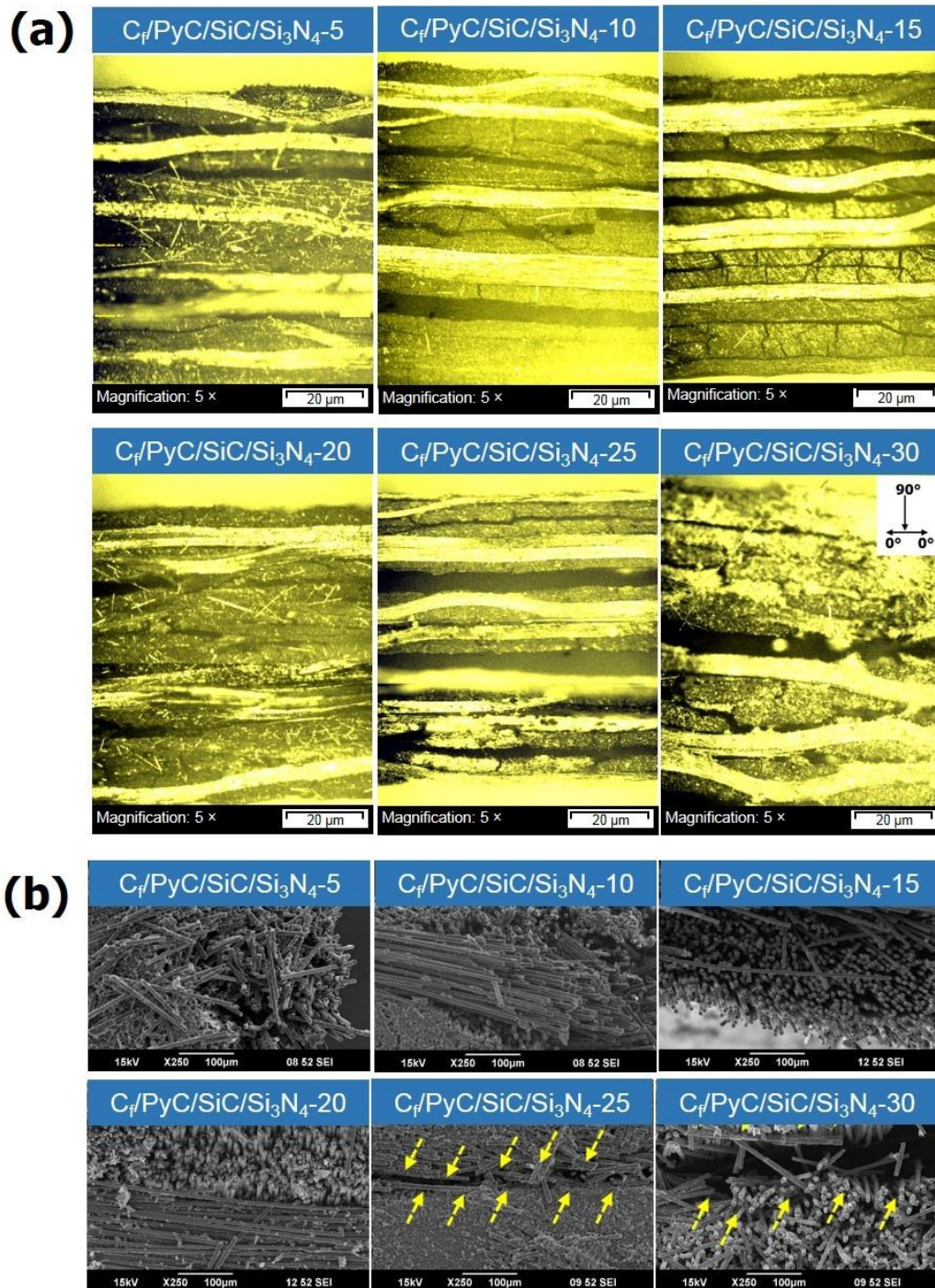
Figure 4.2.2 (a) Optical image of lateral view on the propagation of cracks in a flexural specimen and (b) SEM image of the fractured surface of C_f/PyC/SiC-Si_3N_4 composites

4.2.4. Conclusions

The present study focuses on the fabrication of C_f/PyC/SiC-Si_3N_4 composites using different composition of SPF (SPF-5 to 30) as preceramic matrix resin, PyC as interphase and 2D carbon fabric as reinforcement. The PyC interphase was deposited *via* chemical vapor infiltration (CVI) technique on the carbon fabric reinforcement and densified with matrix *via* polymer impregnation and pyrolysis (PIP) process. For C_f/PyC/SiC-Si_3N_4-5 to C_f/PyC/SiC-Si_3N_4-20 composites, gradual increase in flexural strength of 50 ± 6 MPa to 92 ± 5 MPa was obtained. On contrary, for C_f/PyC/SiC-Si_3N_4-25 and C_f/PyC/SiC-Si_3N_4-30, a sudden drop in flexural strength to 22 ± 9 and 21 ± 2 respectively, was obtained. The fractography study shows that, for C_f/PyC/SiC-Si_3N_4-5 to C_f/PyC/SiC-Si_3N_4-20 composites fiber pull-out phenomenon was observed and hence failed in a ductile manner, while C_f/PyC/SiC-Si_3N_4-25 and C_f/PyC/SiC-Si_3N_4-30 composites shows a partial delamination between F/M interface and hence, leads to premature failure of the composite. This unusual behavior of C_f/PyC/SiC-Si_3N_4-25 and C_f/PyC/SiC-Si_3N_4-30 composites is due to structurally weak points like high propensity of cracks or pores in the matrix compared to the other composites. This study establishes silazane modified phenol formaldehyde as a potential preceramic matrix resin for the fabrication of C_f/PyC/SiC-Si_3N_4 composites to achieve improved mechanical properties for thermo-structural applications. This study also demonstrated that, high density and low porosity of C_f/PyC/SiC-Si_3N_4 composites are highly essential for achieving high mechanical properties for CMCs.

Chapter 5

Studies on boron modified cyclotrisilazane (BCTS) resins as oxidation resistance coating for CMCs

In the previous chapter, SiCN based CMCs were fabricated to achieve improved mechanical properties. However, for long-term service, these composites has to be finely engineered to improve their oxidation resistance, particularly at the level of the interphase and the matrix. Hence, to have improved oxidation resistance of the matrix, synthesis of single source preceramic matrix resins containing silicon, boron and nitrogen was synthesized to obtain SiBCN based ceramics. As explained in *Chapter 1, Section 1.5.1.3,* SiBCN ceramics are commonly prepared by the pyrolysis of boron modified silazane polymer precursors such as polyorganoborosilazane [Kong *et al.* 2015, Zhang *et al.* 2017], hydridopolysilazane [Lee *et al.* 2003], silazane-substituted borazines [Luo *et al.* 2013], etc. In almost all these methods, the preparation of polymeric precursor requires several intermediate steps involving complex synthesis procedures and handling of hazardous chemicals (borane dimethyl sulfide, chlorosilanes) and their by-products (ammonium chloride) [Lee *et al.* 2003, Luo *et al.* 2013]. This makes the overall preparation of SiBCN ceramic process very complex, laborious and expensive.

In this chapter, a novel, facile and low-cost synthetic route for preparing SiBCN ceramics *via* pyrolysis of boron modified cyclotrisilazane (BCTS) is reported. This work has been divided into two parts;

- Synthesis, characterization and ceramic conversion studies of BCTS resins are discussed in detail.

- In the second part, CMCs derived from BPF and SPF resins were screened based on the mechanical properties and were infiltrated with BCTS resin *via* vacuum infiltration technique.

Chapter 5.1

Synthesis, characterization and ceramic conversion studies of BCTS resins
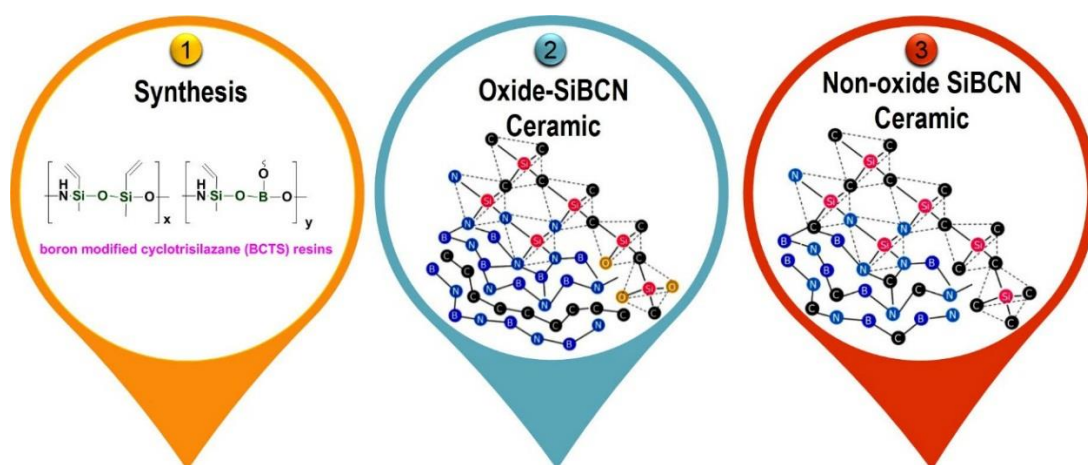
Results of this chapter has been communicated for publication:

Ganesh Babu T., Renjith Devasia, "Novel, facile and low-cost synthetic route for SiBCN ceramics from boron modified cyclotrisilazane".

5.1.1. Introduction

In this chapter, we report for the first time, synthesis and thermal transformation of BCTS and its ceramic conversion to oxide free SiBCN ceramics. To the best of our knowledge, there are no available reports on the phase evolution of SiBCN ceramics from boron modified cyclotrisilazane. Polymer to ceramic conversion of BCTS was carried out at 1450°C and 1650°C under nitrogen atmosphere. The morphology of the obtained ceramic phases and their elemental composition were thoroughly investigated through XRD, SEM and HRTEM techniques. The objective of this work is to assess BCTS resin as potential preceramic resin and to attain oxide free SiBCN ceramic.

5.1.2. Experimental

5.1.2.1. Materials

Details of the chemicals are given in *Chapter 2, Section 2.1*.

5.1.2.2. Synthesis of boron modified cyclotrisilazane (BCTS) resins

The procedure for the synthesis of BCTS resins are detailed in *Chapter 2, Section 2.2.3*.

5.1.2.3. Characterization

Characterization methods employed include GPC, FT-IR, NMR, TGA, Py-GC-MS, XRD, SEM, HRTEM and elemental analysis. The detailed procedures of all these characterizations are given in *Chapter 2, Section 2.5*.

5.1.2.4. Polymer to Ceramic conversion

Ceramic conversion studies were carried out at 1450°C or 1650°C under nitrogen atmosphere. The detailed procedure of the process is given in *Chapter 2, Section 2.4.4*.

5.1.3. Results and Discussion

5.1.3.1 Synthesis and characterization of BCTS resin

Boron modified cyclotrisilazane (BCTS) resins were synthesised by reacting

boric acid with 1, 3, 5-trimethyl-1′, 3′, 5′-trivinylcyclotrisilazane (CTS) in the molar ratio of 1:1, 1:3 and 1:5 as shown in Table 5.1.1 and Figure 5.1.1. As we intended to introduce more boron content in the synthesized polymers and to achieve oxide free ceramics, molar concentration of CTS: H_3BO_3 is not increased beyond 1:5 molar ratio. Hence, the data focused on CTS: H_3BO_3 molar ratio of 1:1, 1:3 and 1:5 compositions. In non-aqueous conditions, the reaction of CTS with boric acid does not occur because of the weak acidic behaviour of boric acid. However, in the aqueous medium, reaction of CTS with boric acid proceeds through hydrolysis and condensation mechanism. The obtained BCTS resins were liquid at room temperature and soluble in tetrahydrofuran (THF) and hence, GPC was performed to determine the molecular weight. The results of molecular weight and viscosity are summarized in Table 5.1.1 and GPC curve of CTS and BCTS resins are shown in Figure 5.1.2. It was observed that, the viscosity, molecular weight and polydispersity index decreases with increase in CTS concentration. This can be due to the formation of low molecular weight siloxane oligomers as a result of self-condensation of CTS in aqueous medium which will be discussed in detail in FTIR and NMR studies. Also, most probable molecular weight (M_p) is >5000 which states that the formed BCTS are oligomeric in nature.
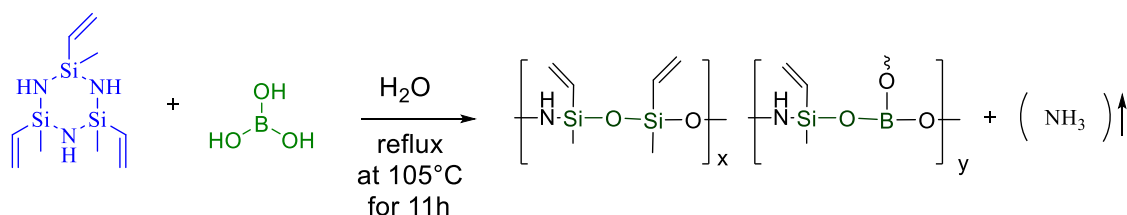
Figure 5.1.1 Synthesis of BCTS resin

Table 5.1.1
Different composition of BCTS resin with viscosity and molecular weight

SI. No.	Sample	Molar ratio of Boric acid: CTS	Viscosity at 25°C (cps)	$*\bar{M}_n$	$*\bar{M}_w$	$*\bar{M}_p$	$\dfrac{\bar{M}_w}{\bar{M}_n}$
1	CTS	-	2.3	-	-	220	-
2	BCTS11	1:1	19.6	2090	4100	4700	2
3	BCTS13	1:3	15.8	1650	2900	3100	1.8
4	BCTS15	1:5	13.0	1590	2600	2700	1.6

$*\bar{M}_n$ – number average molecular weight

$*\bar{M}_w$ – weight average molecular weight

$*\bar{M}_p$ – most probable molecular weight
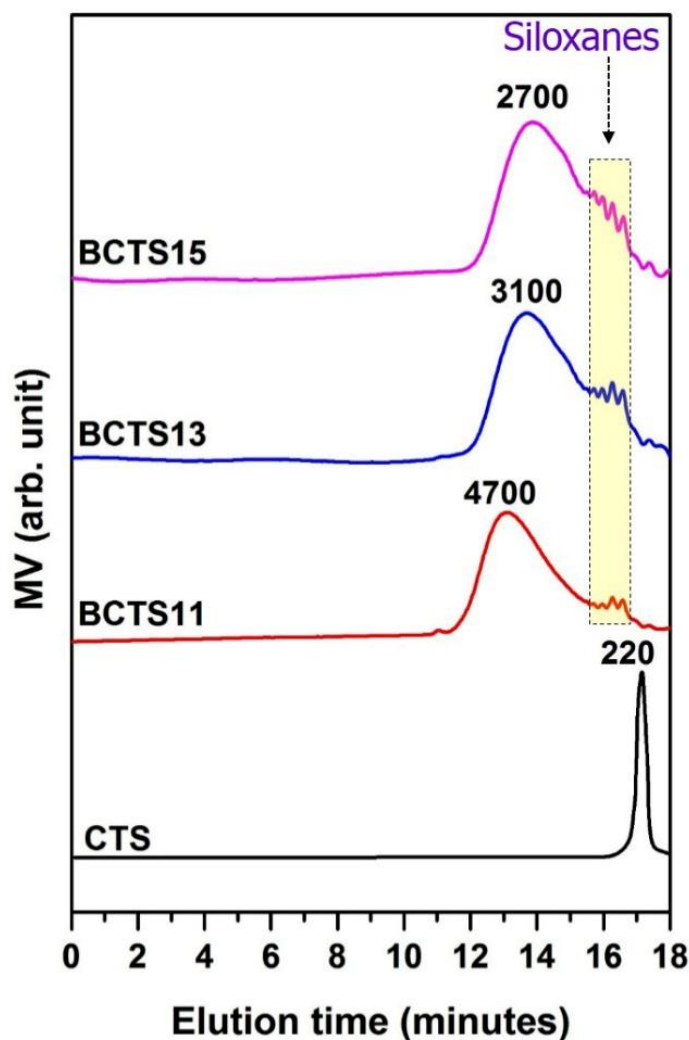
Figure 5.1.2 GPC curve of CTS and different composition of BCTS resins

To gain a better insight into the hydrolysis and condensation reaction of CTS with boric acid to form BCTS, FT-IR, liquid ^{29}Si and ^{11}B NMR studies were carried out. Figure 5.1.3 compares the FT-IR spectra of CTS and different composition of BCTS resins. The corresponding peak assignments are given in Table 5.1.2.
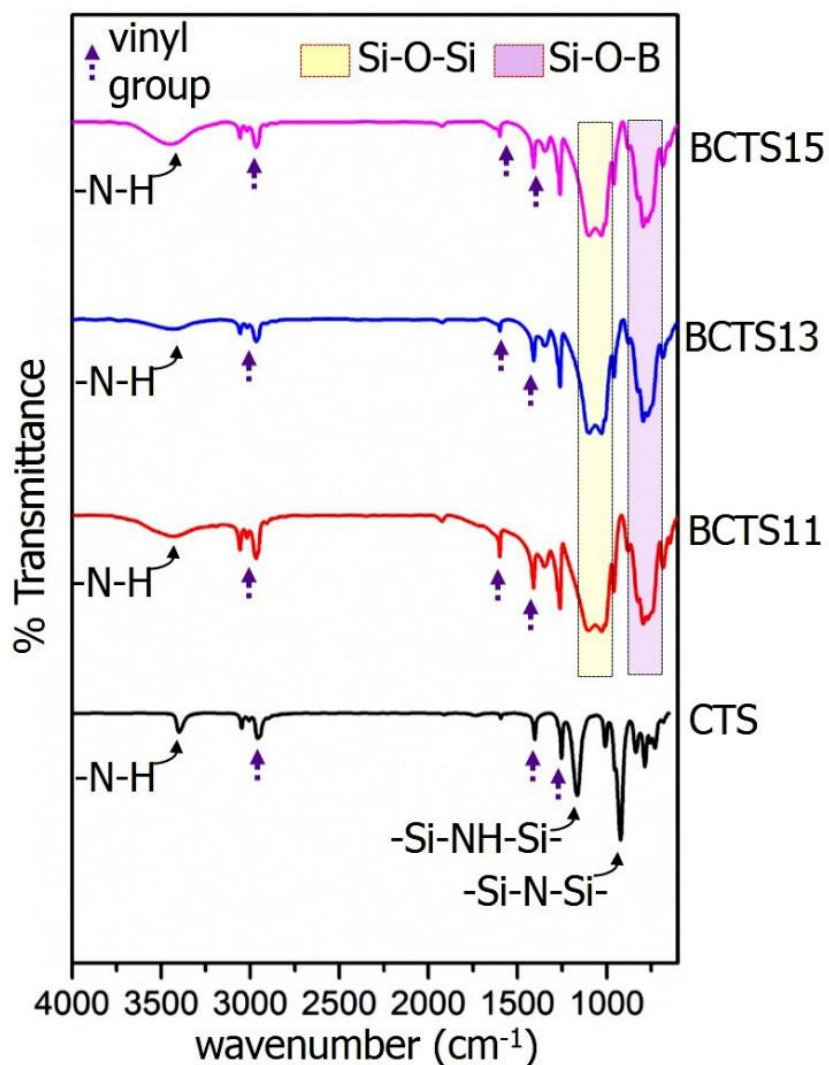
Figure 5.1.3 FT-IR spectra of CTS and different composition of BCTS resins

Table 5.1.2
Main peak assignment in FT-IR Spectrum of CTS, BCTS11, BCTS13 and BCTS15 resin

SI. No.	Wave number (cm^{-1})				peak assignment
	CTS	BCTS11	BCTS13	BCTS15	
1.	3393	3411	3413	3408	- NH stretching
2.	3057	3048	3068	3053	=CH$_2$ stretching in vinyl group
3.	2944	2963	2967	2959	-CH stretching in methyl group
4.	1599	1594	1587	1599	-CH=CH$_2$ stretching in vinyl group
5.	1405	1414	1414	1414	-Si-CH$_3$ deformation
6.	1251	1264	1264	1264	-Si-CH$_3$ stretching
7.	1163	-	-	-	-Si-NH-Si stretching
8.	-	1105	1101	1105	-Si-O-Si- symmetric stretching

9.	-	1031	1020	1023	-Si-O-Si- asymmetric stretching
10.	920	-	-	-	-Si-N-Si- stretching
11.	-	800	800	802	-Si-O-B- stretching

Similar FT-IR spectra were obtained for CTS and BCTS. However, the band at 1163 cm^{-1} and 920 cm^{-1} in CTS corresponding to Si-NH-Si and Si-N-Si bands, respectively disappears in BCTS indicating the modification of the CTS on reaction with boric acid. Also, new peaks around 1100-1020 cm^{-1} and 800 cm^{-1} corresponding to Si-O-Si and Si-O-B bands, respectively appears in the spectra which further confirms beyond doubt that the boric acid has chemically reacted with CTS forming BCTS resin. Broadening of the N–H stretching band was observed after modification of CTS with boric acid confirming the formation of BCTS resin.

The reaction mechanism for the formation of BCTS resin was elucidated through NMR analysis. Figure 5.1.4 (a), and (b) shows the liquid ^{29}Si and ^{11}B NMR analysis, respectively of CTS and BCTS15 resin.

The ^{29}Si-NMR spectrum of the CTS and BCTS15 are shown in Figure 5.1.4 (a). CTS shows signal corresponding to SiC$_2$N$_2$ group at δ = -14.90 ppm, whereas in BCTS15 no signal for SiC$_2$N$_2$ was observed. However, two new peaks at δ = -24.77 ppm and δ = -35.23 ppm were observed for BCTS15, which corresponds to SiC$_2$NO and SiC$_2$O$_2$, respectively. The formation of SiC$_2$NO and SiC$_2$O$_2$ indicates that, the reaction of CTS with boric acid, proceeds *via* a ring opening mechanism by the liberation of ammonia and water. It is to be noted that in ^{29}Si NMR, both Si-O-Si and Si-O-B exhibits similar chemical shifts around -35.23 ppm. Thus, ^{29}Si NMR is not very informative to probe the formation of a borosilicate network in BCTS, hence ^{11}B-NMR analysis was carried out to confirm the reaction of CTS with boric acid.

Figure 5.1.4 (b) shows the ^{11}B-NMR spectrum of BCTS15 resin. The spectrum of BCTS shows a broad and overlapping peak of two signals; one is due to trigonal boron connected to SiO$_4$ tetrahedra, B(OSi)$_3$ at δ = 14.16 ppm and other due to borosilicate network, B(OSi)$_{3-x}$(OB)$_x$ (x =1, 2) at δ = 15.88 ppm with a second-order quadrupolar broadening, typical for boron atoms in a trigonally coordinated configuration [Kentgens 1997]. These results confirm that a network bearing -B-O-Si-

has been formed. The characteristic peak of boric acid, $B(OH)_3$ which appears at $\delta =$ 19.6 ppm [Soraru *et al.* 1999, Soraru *et al.* 2000] was not observed indicating absence of free boric acid in BCTS resin. This decisively confirms the complete reaction of all the –OH groups in boric acid with CTS to form a highly cross-linked network structure.
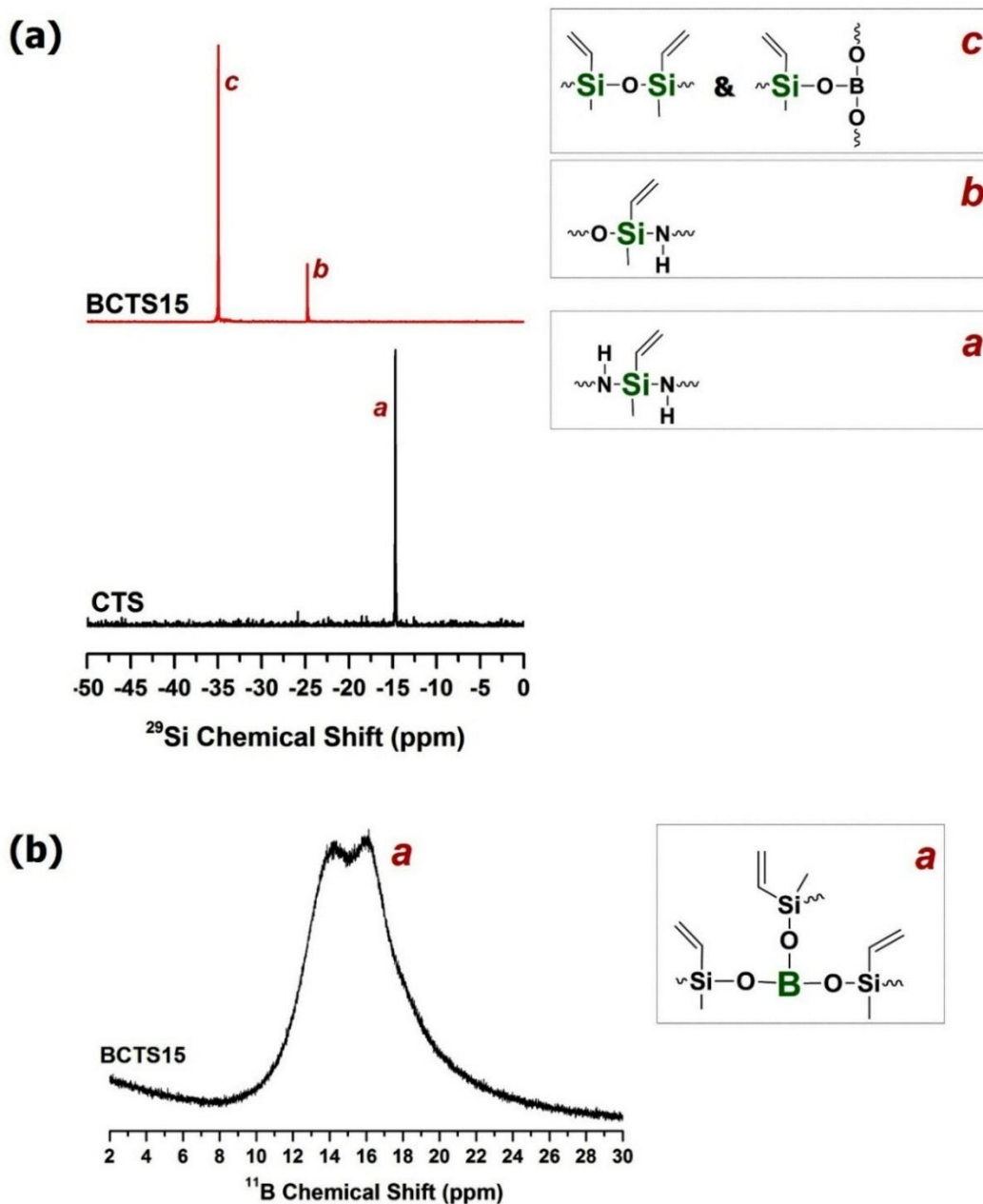
Figure 5.1.4 (a) ^{29}Si NMR spectra of CTS and BCTS15 resin and (b) ^{11}B NMR spectra of BCTS15 resin

From the FT-IR, ^{29}Si and ^{11}B NMR results, it can be inferred that the reaction of boric acid with CTS in aqueous medium proceeds *via* self-condensation of CTS and co-condensation of CTS with boric acid to form Si-O-Si and Si-O-B linkage, respectively. The self-condensation and co-condensation reaction will lead to liberation of ammonia and water by ring opening mechanism as shown in Figure 5.1.5. This results in a more stable and less strained linear structured BCTS resin containing a mixture of -Si-O-Si-, -HN-Si-O- and -Si-O-B- linkages.
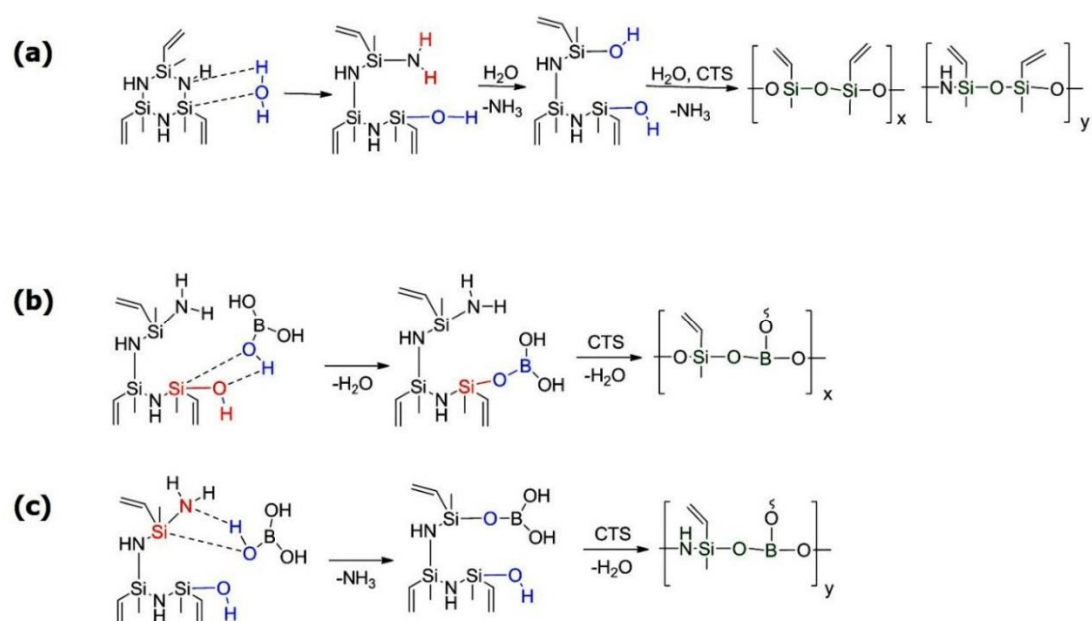
Figure 5.1.5. Proposed ring opening mechanism for the formation of BCTS resin (a) Self-condensation; (b) and (c) co-condensation

The thermal decomposition behavior of the CTS and BCTS resins were investigated through TGA analysis. Figure 5.1.6 shows the TG and its derivative curves of CTS and BCTS resins from 25°C to 1200°C under nitrogen atmosphere. The parameters derived from TG and its derivative curves are summarized in Table 5.1.3.
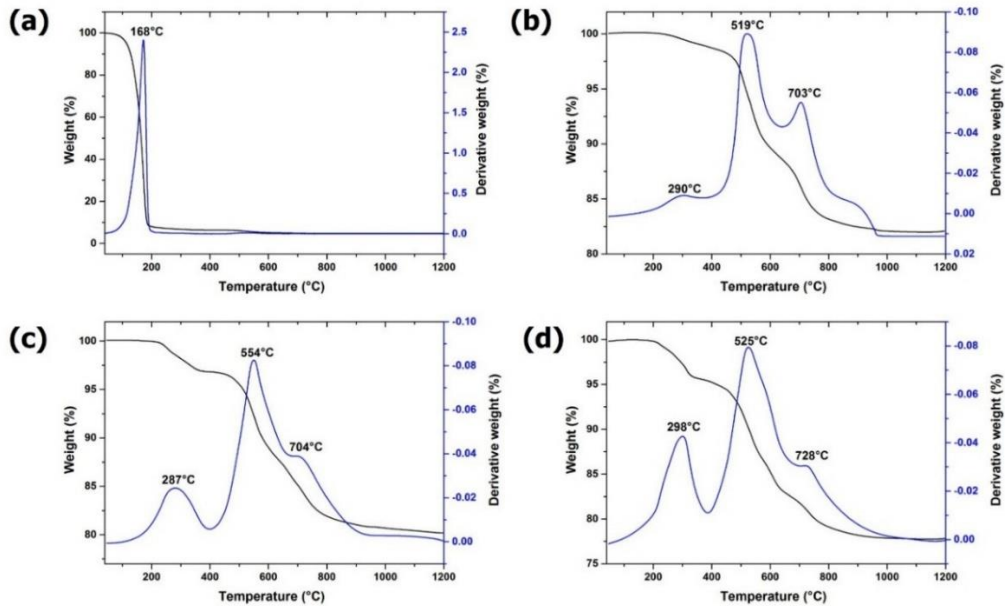
Figure 5.1.6 TG and its derivative curves of (a) CTS, (b) BCTS11, (c) BCTS13 and (d) BCTS15

Table 5.1.3
TG and its derivative data of CTS, BCTS11, BCTS13 and BCTS15 resins

Sl. No.	Sample	1st stage Decomposition				2nd stage Decomposition				3rd stage Decomposition				Ceramic yield at 1200°C (wt. %)
		Temperature (°C)			Wt. loss (%)	Temperature (°C)			Wt. loss (%)	Temperature (°C)			Wt. loss (%)	
		T_i	T_{max}	T_f		T_i	T_{max}	T_f		T_i	T_{max}	T_f		
1.	CTS	60	168	200	92.2	-	-	-	-	-	-	-	-	2.4
2.	BCTS11	216	290	344	0.7	448	519	617	6.1	639	703	835	6.3	84.6
3.	BCTS13	204	287	371	2.8	440	554	630	8.3	639	704	867	7.5	80.3
4.	BCTS15	194	298	375	4.1	437	525	635	9.2	637	728	874	8.5	77.2

T_i–Initial decomposition temperature

T_{max} – Maximum decomposition temperature

T_f – Final decomposition temperature

CTS showed single stage weight loss [Figure 5.1.6 (a)] with early decomposition, starting at 60°C (initial decomposition temperature, T_i) and continues up to 200°C (final decomposition temperature, T_f) leading to a lower ceramic residue of 2.46 wt. % at 1200°C (Table 5.1.3). The lower ceramic residue is due to evaporation of the silazanes before the ceramization process as a result of the lower molecular weight and insufficient degree of cross-linking of CTS. Conversely, the introduction of

boron in CTS resulted in three stage weight loss [Figure 5.1.6 (b), (c) and (d)] for all the composition (BCTS11, BCTS13 and BCTS15) along with distinctively shift of T_i of first stage decomposition temperature to a higher temperature regime in comparison with CTS (Table 5.1.3). The delayed initial decomposition with boron modification indicates higher thermal stability leading to higher ceramic residue (Table 5.1.3). The sudden increase in ceramic residue is attributed to enhanced thermal stability of BCTS obtained by the self-condensation and co-condensation reaction of boric acid with CTS which decreases the volatility of the oligomeric silazane and increases the degree of vinyl cross-linking (Figure 5.1.7) during ceramic conversion.

Self-condensation and Co-condensation   200°C-500°C   vinly polymerization (highly cross-linked structure)
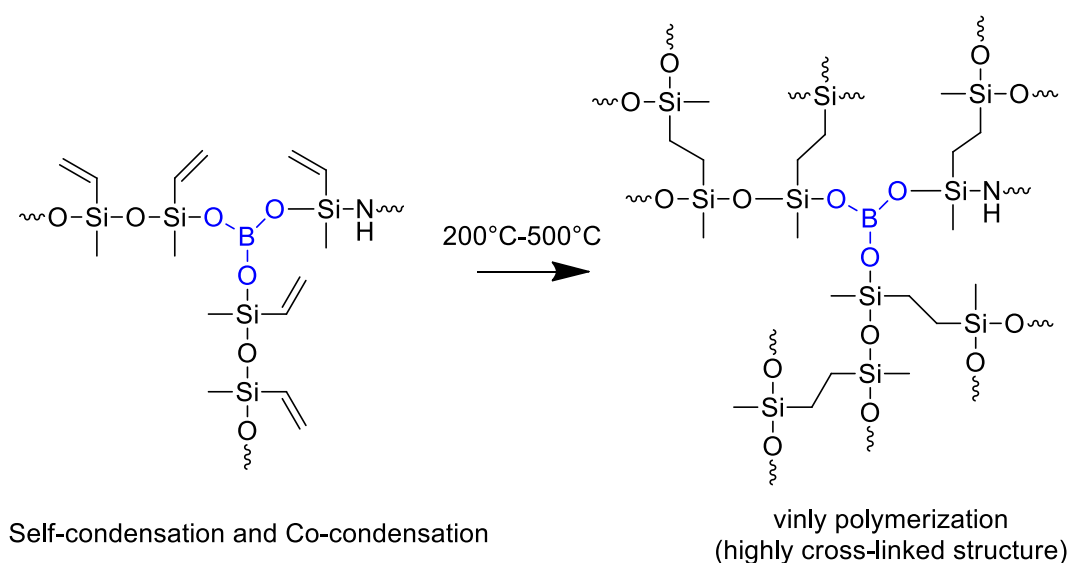
Figure 5.1.7 Schematic representation of highly cross-linked structure of BCTS

It was also observed that the composition of BCTS significantly influenced both the thermal stability (T_i) and ceramic residue. With increase in CTS: H_3BO_3 molar ratio, the weight loss in each stage increases which leads to decrease in the ceramic residue (Table 5.1.3). In order to discern these variations and three stage weight loss in BCTS sample, pyrolysis–gas chromatography–mass spectrometry (Py–GC–MS) analysis was carried out. It is to be noted that, all compositions of BCTS exhibited identical decomposition temperature regime with distinct variations in weight loss (Table 5.1.3) and amongst all, BCTS15 showed the highest percentage weight loss and hence was

selected as a typical example for better representation of the decomposition mechanism. Figure 5.1.8 shows the Py-GC-MS spectra of BCTS15 sample recorded from 25°C to 900°C.
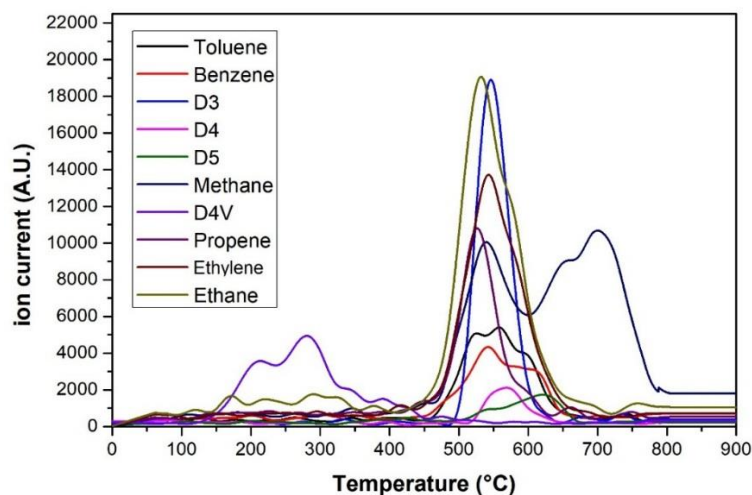
Figure 5.1.8 Py-GC-MS spectra of BCTS15 sample in the temperature range of 25°C to 900°C

The chromatogram revealed the different stages of BCTS15 decomposition. In the first stage of decomposition (190°C to 350°C), tetramethyltetravinylcyclotetrasiloxane (DV4) was volatilized, whereas in the second stage of decomposition (450°C to 640°C) ethane, ethylene, propylene, benzene, toluene, hexamethylcyclotrisiloxane (D3) and octamethylcyclotetrasiloxane (D4) were volatilized. In the final stage of decomposition (650°C to 850°C), methane and decamethylcyclopentasiloxane (D5) were volatilized. The Py-GC-MS spectra do not show any signal representing the presence of boron and nitrogen containing species which implies that -N-Si-O-B- linkage remains intact in the ceramic up to 900°C indicative of enhanced higher thermal stability. From the TGA and Py-GC-MS analysis it can be concluded that, the increase in the CTS concentration favours the formation of low molecular weight siloxanes (DV4, D3, D4 and D5) which volatilizes subsequently before the ceramization process. This leads to an increase in weight loss in each stage and decreases the ceramic yield. This explanation is further supported by decreasing trend in viscosity and molecular weight measurements (Table 5.1.2)

attributed to the formation of low molecular weight siloxanes on increasing the concentration of CTS.

5.1.3.2 Pyrolysis of BCTS resin

The above studies have demonstrated the profound effect of boron modification of CTS on resultant resin properties. It was found that, the boron modification of CTS resin resulted in desirable properties for preceramic polymers such as solubility in common solvents, processable viscosity (< 20 cps) and high ceramic yield (>80 wt. %). Such combinations of properties are quite rare with only a few known preceramic resin system and they find vast applications in ceramic processing technology [Lee *et al.* 2003, Riedel *et al.* 2006]. The principle objective of this work is to assess BCTS resin as potential preceramic resin and to attain oxide free SiBCN ceramic. In this regard, ceramic conversion studies were carried out at 1450°C and 1650°C under nitrogen atmosphere. It is to be noted that, due to the lower molecular weight and insufficient degree of crosslinking, complete evaporation of CTS occurs before the ceramization process. As a result of this, very little or no ceramic residue is left behind for further studies. Hence, the ceramic conversation studies are carried out only for BCTS resins (BCTS11, BCTS13 and BCTS15) with thorough investigations on the evolved phase evaluation, morphology, elemental analysis and ceramic yield.

5.1.3.2.1 XRD of pyrolyzed BCTS resin
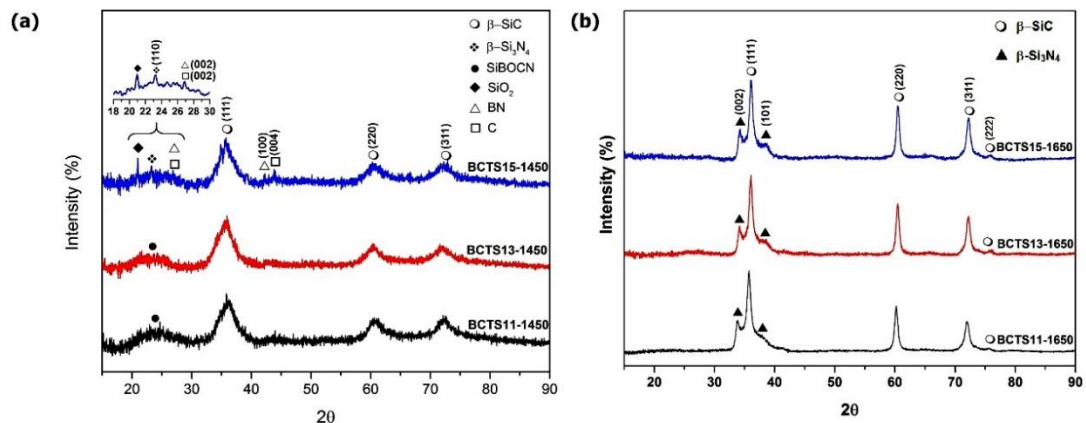
Figure 5.1.9 XRD spectra of the pyrolyzed BCTS resin (a) at 1450°C (b) at 1650°C

Figure 5.1.9 (a) and (b) shows the XRD spectra of the pyrolyzed BCTS resins at 1450°C and 1650°C, respectively. At 1450°C, XRD spectra showed broad diffraction peaks attributed to β-SiC at $2\theta = 35.9°$ (111), 60.4° (220), 72.3° (311) (PDF 74-2307) and a featureless hump around $2\theta = \sim24.3°$ corresponding to an amorphous glassy phase of SiBNC(O) [Feng *et al.* 2006, Wen *et al.* 2006]. The broad β-SiC diffraction peak indicates the nucleation of nano crystalline SiC ceramic from the amorphous SiBNC(O) phase as shown in eqn. (5.1.1) to (3). This signifies incomplete crystallization and indicates that the ceramics formed are predominantly in the amorphous phase which are well known to impart beneficial properties for their application as thermo-structural materials. This prolonged thermal stability leads to desirable properties like ultra-low coefficient of thermal expansion, outstanding thermal shock resistance which can be retained even at very high temperature (>1500°C). Remarkably, for BCTS15 sample, in addition to β-SiC, peaks corresponding to SiO_2 ($2\theta = 20.9$), h-BN ($2\theta = 26.9$ and 42.1), C ($2\theta = 26.9$ and 43.7) and Si_3N_4 ($2\theta = 23.2$) phases were also observed, which were not present in other systems. The presence of these peaks in BCTS (CTS: H_3BO_3-1:5) is due to the carbothermal reduction of amorphous SiBNC(O) ceramics as shown in eqn. (5.1.4). This is formed by the enhanced carbon concentration in BCTS15. As a result, significant increase in crystallization of the ceramic occurs with consequent decrease in oxygen content of SiBNC(O) ceramics. This explanation is further supported by the elemental and HRTEM analysis. The average crystallite sizes of β-SiC ceramics were calculated based on β-SiC (111) peak in XRD using Scherrer equation and were found to increase with increase in the concentration of CTS (Table 5.1.4) which is due to an increase in the degree of crystallization of the ceramics.

$$SiBONC(s) + C(s) \longrightarrow Si_{1-x}BO_{1-y}NC_{1-z}(s) + aSiO(g) + bCO(g) \qquad (5.1.1)$$

$$SiO(g) + CO(g) \longrightarrow SiC(nuclei) + O_2(g) \qquad (5.1.2)$$

$$O_2(g) + 2C(s) \longrightarrow 2CO(g) \qquad (5.1.3)$$

$$Si_{1-x}BO_{1-y}NC_{1-z}(s) + \text{excess } C(s) \longrightarrow aSiC + bSi_3N_4 + cSiO_2 + dBN(s) + eCO(g) \qquad (5.1.4)$$
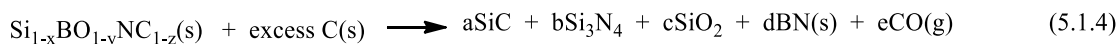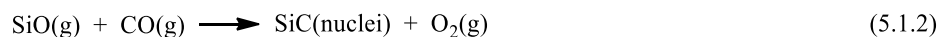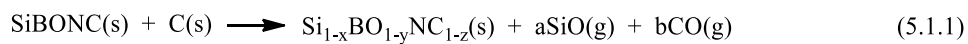
On increasing the pyrolysis temperature from 1450°C to 1650°C, similar XRD spectra were observed for all the composition of BCTS [Figure 5.1.9 (b)]. As expected,

increase in the crystallinity and crystallite size of the ceramic was observed with increase in pyrolysis temperature. Peaks corresponding to crystalline β-SiC [2θ = 35.6° (111), 41.3° (200), 59.9° (220), 71.7° (311) and 76.2° (222) (PDF 74- 2307)] and β-Si_3N_4 [2θ = 33.8° (002) and 38.3° (101) (PDF 33-1160)] were observed in the spectra. The average crystallite sizes of β-SiC (111) peak were found to increase with increase in the concentration of CTS (Table 5.1.4) and the intensity of β-SiC and β-Si_3N_4 peaks increased with increase in the concentration of CTS, indicating increase in the crystallinity of the ceramics. Surprisingly in the case of BCTS15 at 1650°C, disappearance of SiO_2, h-BN and C peaks were observed in the case of BCTS15 which were present at 1450°C. This difference in phase evolution, crystallinity and crystallite size can be attributed to the increase in the rate of carbothermal reduction of SiBNC(O) ceramic with increase in the concentration of CTS and pyrolysis temperature as shown in eqn. (5.1.5) and (5.1.6).

$$bSi_3N_4(s) + 3C(s) \longrightarrow 3SiC(s) + 2N_2 \qquad (5.1.5)$$

$$cSiO_2(g) + 3C(s) \longrightarrow SiC(s) + 2CO(g) \qquad (5.1.6)$$
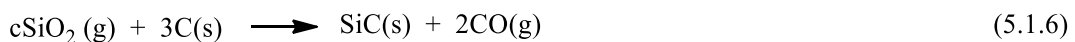
5.1.3.2.2 SEM and Elemental Analysis of pyrolyzed BCTS resin

To further understand the effect of CTS concentration and pyrolysis temperature on the morphology of the obtained ceramics, SEM investigations were carried out. It was observed that, the morphology of the obtained ceramics was highly sensitive to the boron and oxygen content.

Figure 5.1.10 shows the SEM image of the pyrolyzed BCTS resins at 1450°C and 1650°C. At 1450°C, all the BCTS composition (BCTS11, BCTS13 and BCTS15), exhibited glassy morphology [Wen *et al.* 2006] [Figure 5.1.10 (a), (b) and (c)]. This glassy nature is due to the formation of SiBNC(O) ceramics upon pyrolysis of BCTS. On increasing the pyrolysis temperature from 1450°C to 1650°C, the glassy morphology is retained in the case of BCTS11 and BCTS13 samples [Figure 5.1.10 (d) and (e)]; whereas BCTS15 sample exhibited a coarse morphology [Figure 5.1.10 (f)]. The prominent change in morphology on increasing the concentration of CTS and

pyrolysis temperature is also evident in the elemental analysis. Table 5.1.4 shows the elemental compositions and ceramic yield of the pyrolyzed BCTS resins at 1450°C and 1650°C under nitrogen atmosphere.
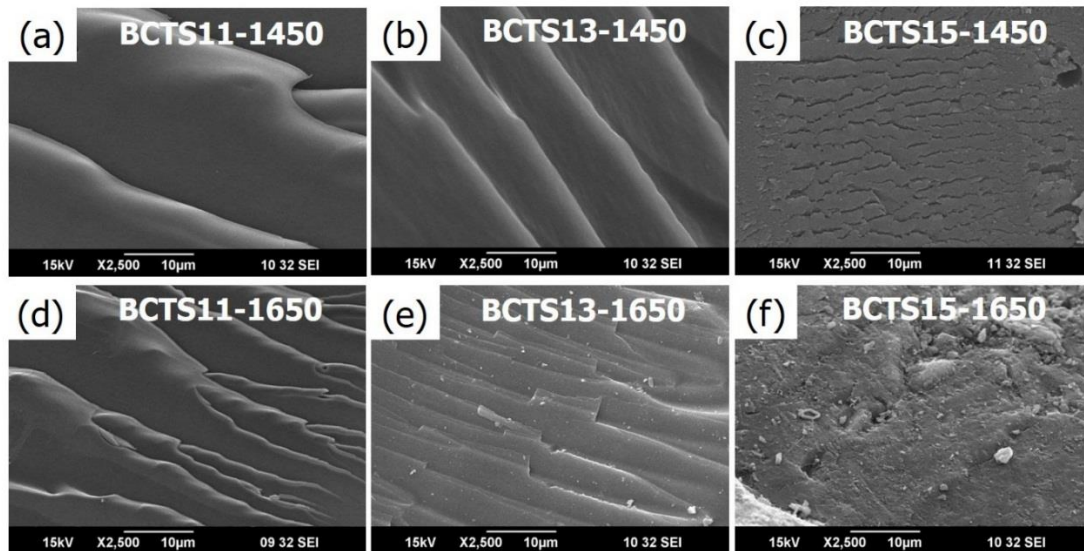
Figure 5.1.10 SEM images of BCTS pyrolyzed at (a-c) 1450°C and (d-f) 1650°C

At both the pyrolysis temperature (1450°C and 1650°C), it was found that the silicon, carbon and nitrogen content increases whereas, the boron and oxygen content decreases with increase in CTS concentration. The ceramic yield was also found to decrease with increase in CTS concentration. These variations are due to increase in the carbothermal reduction reaction [Eqn. (5.1.1) to (5.1.6)] of SiBNC(O) ceramics with increase in CTS concentration and pyrolysis temperature. As a result, the oxygen and boron content decreases with an increase in concentration of CTS [Eqn. (5.1.1) to (5.1.6)] leading to a decrease in the ceramic yield. This explains the decrease in the glassy morphology of the ceramics on increasing the concentration of CTS at both 1450°C and 1650°C (Figure 5.1.10). Finally, for BCTS15 sample at 1650°C, oxide free SiBCN ceramics were obtained explaining the resultant coarse morphology and meeting the principle objective of the work [Figure 5.1.10 (f)].

Table 5.1.4 Elemental composition and ceramic yield of ceramics derived from BCTS at 1450°C and 1650°C

SI. No.	Samples	Si	B	O	N	C	Empirical formula normalized on Si	Ceramic yield (wt. %)	Crystallite size from XRD (nm)	Crystallite size from HRTEM (nm)
							(a) at 1450°C			
1.	BCTS11-1450	48	11	17	4	20	$SiB_{0.56}O_{0.62}N_{0.16}C_{0.94}$	76	2.1	2.2±0.4
2.	BCTS13-1450	51	6	14	7	22	$SiB_{0.30}O_{0.46}N_{0.26}C_{1.01}$	75	3.2	3.3±0.2
3.	BCTS15-1450	56	4	7	6	27	$SiB_{0.18}O_{0.21}N_{0.24}C_{1.12}$	70	4.9	4.6±0.5
							(b) at 1650°C			
4.	BCTS11-1650	57	8	12	2	21	$SiB_{0.34}O_{0.38}N_{0.08}C_{0.86}$	74	7.2	7.5±0.2
5.	BCTS13-1650	61	5	5	4	25	$SiB_{0.19}O_{0.15}N_{0.12}C_{0.95}$	69	8.8	8.5±0.5
6.	BCTS15-1650	65	3	-	5	27	$SiB_{0.09}N_{0.15}C_{0.98}$	65	9.3	9.6±0.7

5.1.3.2.3 HRTEM of pyrolyzed BCTS resin

To further discern the changes observed in the crystalline structure and the morphology of the ceramics in atomic level with respect to both CTS concentration and pyrolysis temperature, HRTEM studies were carried out. Figure 5.1.11 and 5.1.12 shows the HRTEM images of the pyrolyzed BCTS resins at 1450°C and 1650°C, respectively along with their corresponding selected area electron diffraction (SAED) patterns.

At 1450°C, for all the compositions of BCTS (BCTS11, BCTS13 and BCTS15), very fine nano ceramic particles embedded in an amorphous ceramic matrix was observed with a distinct variation in their arrangement (Figure 5.1.11). It was observed that in the case of BCTS11 and BCTS13 samples, uniformly distributed nano ceramic particles were obtained [Figure 5.1.11 (a & b)]; whereas, in the case of BCTS15 sample, several nano ceramic particles coalesce to form nano ceramic clusters [Figure 5.1.11 (c)]. The corresponding SAED patterns displays a broad and diffused diffraction ring with lattice spacing measurements matching that of β-SiC (d_{111}= 0.25 nm) corroborating with the XRD results. This conclusively shows that the nano ceramic particles and nano ceramic clusters are composed of β-SiC ceramic phase embedded in amorphous SiBNC(O) ceramic matrix. The diameters of the embedded β-SiC particles

in BCTS11, BCTS13 and BCTS15 samples are given in Table 5.1.4, indicating that the particle size of β-SiC increases with increase in the concentration of CTS. This results in an increase in the rate of carbothermal reduction reaction and crystallinity of the ceramics on increasing the concentration of CTS. Interestingly, for BCTS15 sample, in addition to β-SiC, turbostatic structure corresponding to h-BN or free carbon embedded in the amorphous ceramic matrix were also evidenced in the HRTEM image [Figure 5.1.11 (c)], in line with the XRD results [Figure 5.1.9 (b)]. The evolution of the turbostatic ceramic phase only in the case of BCTS15 sample due to the removal of high concentration of oxygen in SiBNC(O) ceramics as evidenced by elemental analysis results (Table 5.1.4). This leads to a structural rearrangement of the SiBNC(O) ceramics in the atomic level to form β-SiC and h-BN ceramics. The presence of h-BN, holds great significance in the field of non-oxide CMCs. It has a layered structure very similar to that of pyrocarbon PyC) acting as a mechanical fuse (crack deflection) and exhibiting better oxidation resistance and thermo-mechanical properties compared to PyC [Li *et al.* 2016].

On increasing the pyrolysis temperature from 1450°C to 1650°C, for all BCTS composition, distinct lattice fringes were observed in the HRTEM images (Figure 5.1.12) which are attributed to the formation of highly crystalline β-SiC ceramic phases. The particle size of β-SiC ceramic in BCTS11, BCTS13 and BCTS15 samples are given in Table 5.1.4. It is observed from SAED diffraction patterns that significant variations in diffraction patterns were observed with changes in the CTS concentration. With increase in concentration of CTS, the diffraction patterns change from a faint diffuse diffraction ring to intense spotted diffraction ring. These variations in the SAED patterns and particle size is due to increase in the crystallinity of the ceramics with increase in the concentration of CTS and pyrolysis temperature. This results in an increase in the rate of carbothermal reduction reaction of SiBNC(O) ceramic which further decreases the oxygen content and finally leads to an oxide free SiBNC ceramics in the case of BCTS15 sample as evident from elemental analysis (Table 5.1.4).
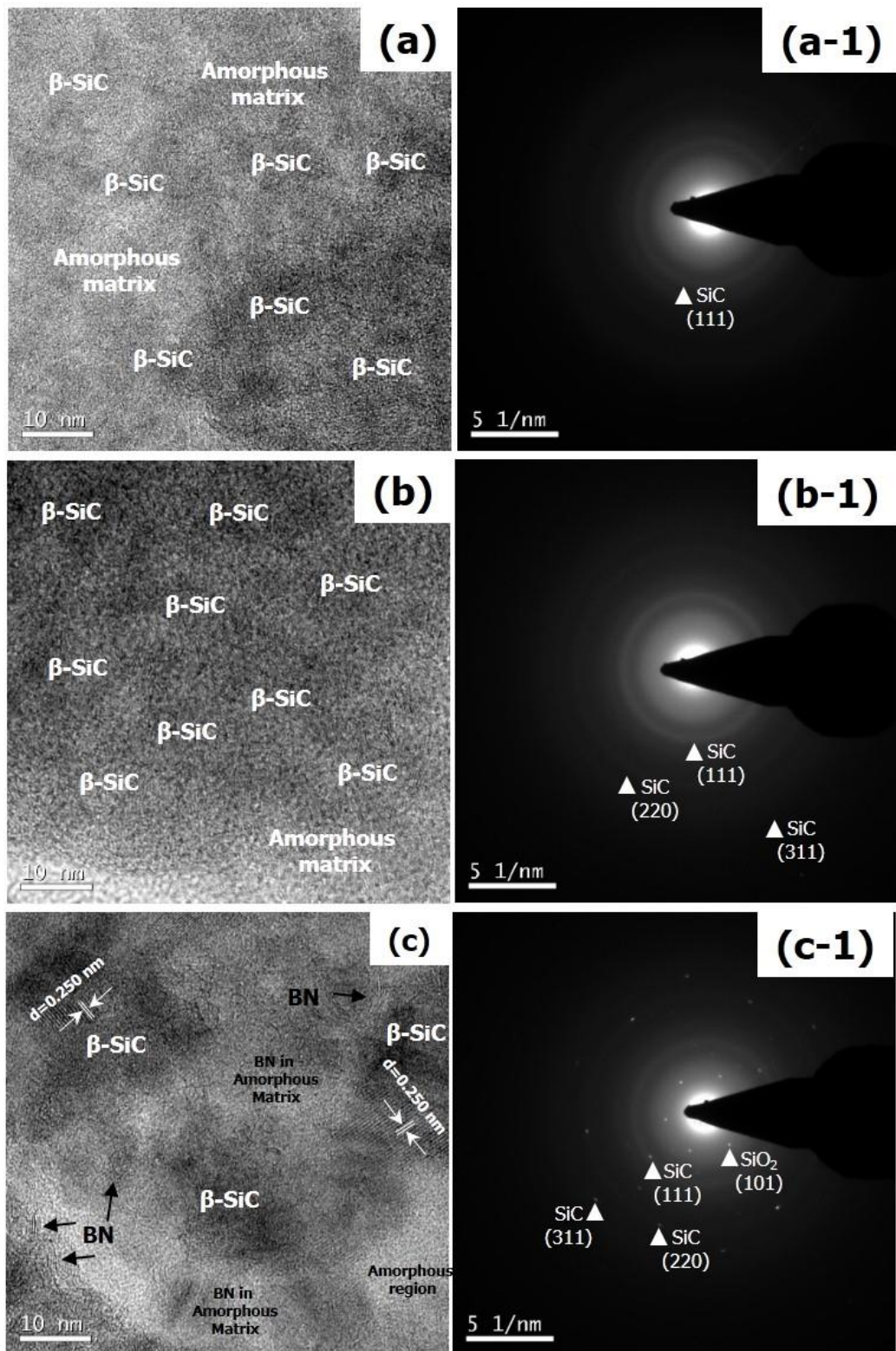
Figure 5.1.11 HRTEM image of the BCTS resin pyrolyzed at 1450°C (a) BCTS11 (b) BCTS13 and (c) BCTS15 along with their corresponding SAED pattern (a-1) BCTS11, (b-1) BCTS13 and (c-1) BCTS15
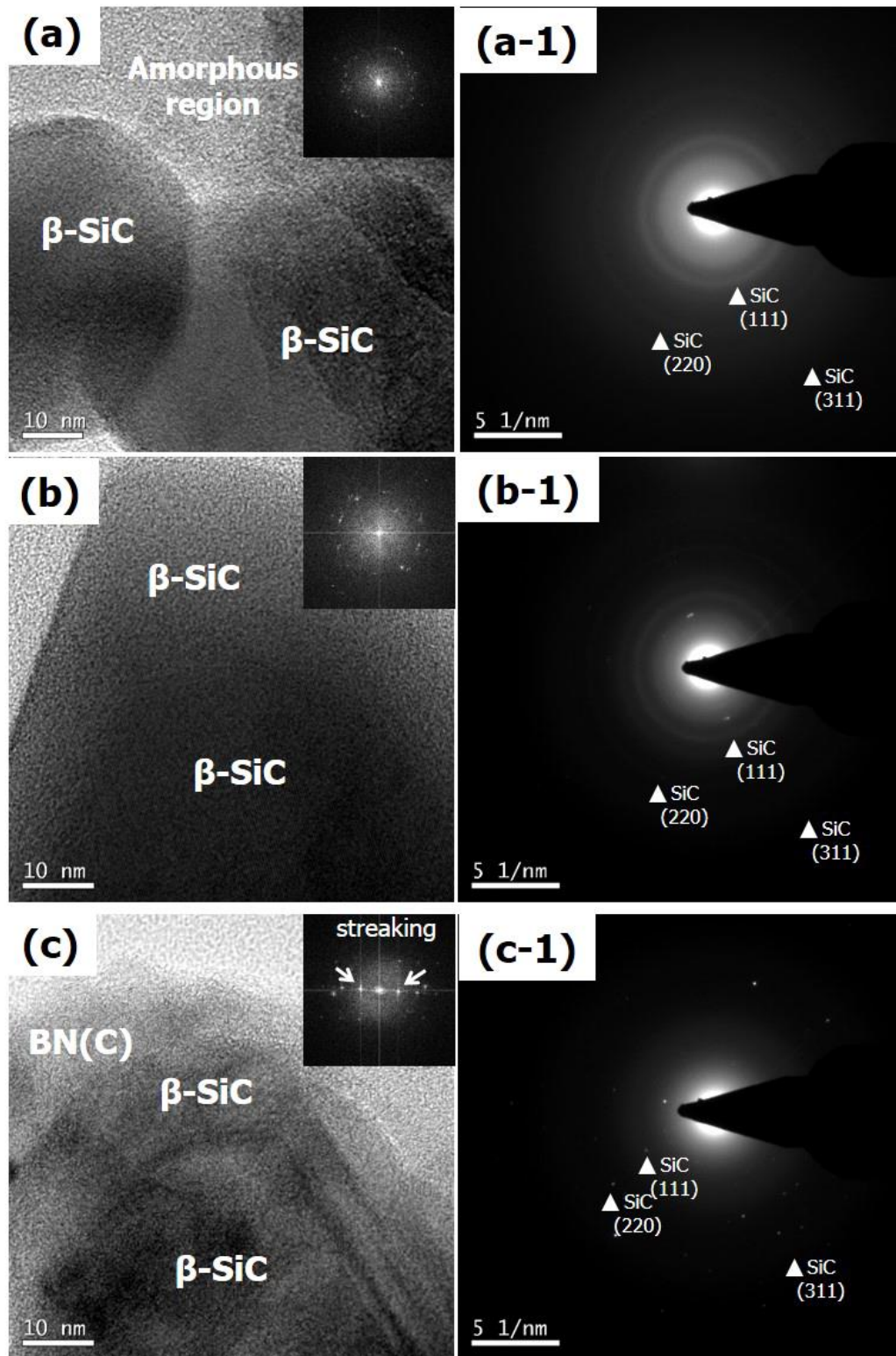
Figure 5.1.12 HRTEM image of the BCTS resin pyrolyzed at 1650°C (a) BCTS11 (b) BCTS13 and (c) BCTS15 along with their corresponding SAED pattern (a-1) BCTS11, (b-1) BCTS13 and (c-1) BCTS15

Another interesting observation was found in the case of BCTS15 sample i.e., the presence of turbostatic structure of BN(C) phase. From the XRD results of BCTS15 sample pyrolyzed at 1450°C, formation of β-SiC, h-BN, C and β-Si$_3$N$_4$ ceramics were evidenced [Figure 5.1.9 (a)]. However, upon increasing the pyrolysis temperature to 1650°C, XRD spectra showed peaks corresponding to β-SiC and β-Si$_3$N$_4$ peaks [Figure 5.1.9 (b)]. Nevertheless, the magnified HRTEM image of BCTS15 sample pyrolyzed at 1650°C [Figure 5.1.13 (b)], clearly showed the turbostatic layer of BN(C) ceramic around β-SiC crystallites.

The major reason behind the formation of BN(C) phase only in the case of BCTS15 at 1650°C was due to formation of oxide free SiBCN ceramics which results in structural rearrangement of ceramics in an atomic level. In particular, boron atom in h-BN ceramic can be easily replaced by the free carbon atom present in the ceramics by means of *bond-breaking* mechanism [Li *et al.* 2016] as shown in Figure 5.1.14. As a result, crystalline h-BN ceramic will be converted to BN(C) phase which is amorphous in nature. This explains the absence of BN(C) phase in the XRD spectrum of BCTS15 at 1650°C.
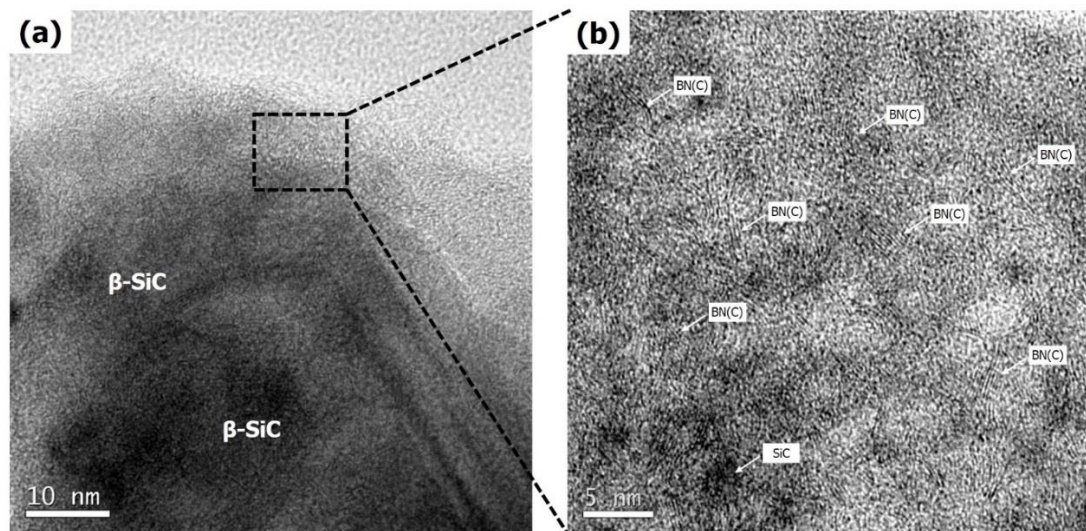
Figure 5.1.13 HRTEM image of (a) BCTS15 pyrolyzed at 1650°C (b) magnified HRTEM image of BCTS15 showing turbostatic layer of BN(C) ceramic
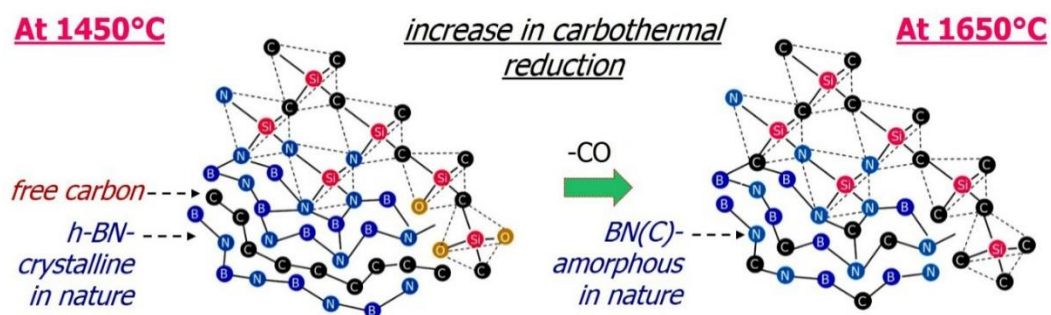
Figure 5.1.14. Schematic representation for the conversion of h-BN to BN(C) on increasing the pyrolyzed temperature from 1450°C to 1650°C in BCTS15 sample

The FFT diffraction pattern of BCTS pyrolyzed at 1650°C further confirms the presence of BN(C) only in the case of BCTS15 sample. It was observed that, in the case of BCTS11 and BCTS13 sample pyrolyzed at 1650°C shows a normal spot like FFT diffraction pattern corresponding to β-SiC ceramics [Figure 5.1.12 (a & b)]; whereas in the case of BCTS15 sample pyrolyzed at 1650°C, amorphous scattering effects are seen in the FFT diffraction patterns called as streaking phenomenon [Figure 5.1.12 (c)]. Similar streaking of diffraction spots is frequently observed in presence of turbostatic BN(C) phase embedded in SiBCN ceramics [Zhang *et al.* 2012, Li *et al.* 2016] confirming the presence of BN(C) phase in BCTS15 sample at 1650°C. The presence of BN(C) in SiBCN ceramics has major advantages in ceramic field because of their outstanding stability against crystallization and decomposition, superior mechanical properties and better creep, oxidation and thermal shock resistance [Gao *et al.* 2012, Zhao *et al.* 2017] and, thus are highly desired ceramics for thermo-structural applications. Hence, BCTS15 is the optimized composition to achieve oxide free SiBCN ceramics at 1650°C which may be utilized for thermo-structural applications such as thermal protection systems (TPS) including self-healing oxidation coatings for C/SiC and SiC/SiC ceramic matrix composites by PIP process. This aspect is being further investigated by our team and will be communicated later.

5.1.4. Conclusions

This study reports novel, facile and low-cost synthetic route for preparing SiBCN ceramics *via* pyrolysis of boron modified cyclotrisilazane (BCTS). FT-IR and

NMR investigation revealed the formation of BCTS *via* self and co-condensation reaction mechanism. This resulted in desirable properties for preceramic polymers such as solubility in common solvents, processable viscosity (< 20 cps) and high ceramic yield (>80 wt. %). The thermal transformation of BCTS resin to ceramics were carried out at 1450°C and 1650°C under nitrogen atmosphere. At 1450°C for all composition of BCTS, nano-crystallite β-SiC ceramics embedded in amorphous SiBNC(O) ceramics were formed and increases with increase in CTS concentration. However, for BCTS15, in addition to nano-crystallite β-SiC ceramics, SiO_2, h-BN, C and Si_3N_4 ceramics were also formed. The morphological studies revealed that the obtained ceramics are glassy in nature and it decrease with increase in the concentration of CTS.

At 1650°C, for all the composition of BCTS crystallinity and crystallite size of the ceramic increases with pyrolysis temperature and results in β-SiC and β-Si_3N_4 as ceramic phases. Moreover, additional turbostatic BN(C) layer was obtained with BCTS15. The morphological study showed retention of the glassy morphology in the case of BCTS11 and BCTS13 samples, whereas, the BCTS15 sample exhibited coarse morphology.

The observed changes in ceramic phases and morphology with pyrolysis temperature is attributed to increase in carbothermal reduction of SiBNC(O) ceramic which result in decrease in oxygen content with increase in CTS concentration leading to the formation of oxide free SiBCN ceramics for BCTS15 sample at 1650°C. This study demonstrates BCTS15 as the suitable preceramic polymer to attain oxide free SiBCN ceramics. This novel class of preceramic polymer opens up a new way for the fabrication of high temperature thermal protection systems (TPS) including self-healing oxidation coatings for C/SiC and SiC/SiC ceramic matrix composites by PIP process.

Chapter 5.2

Fabrication of CMCs with improved oxidation stability using BCTS as matrix resin
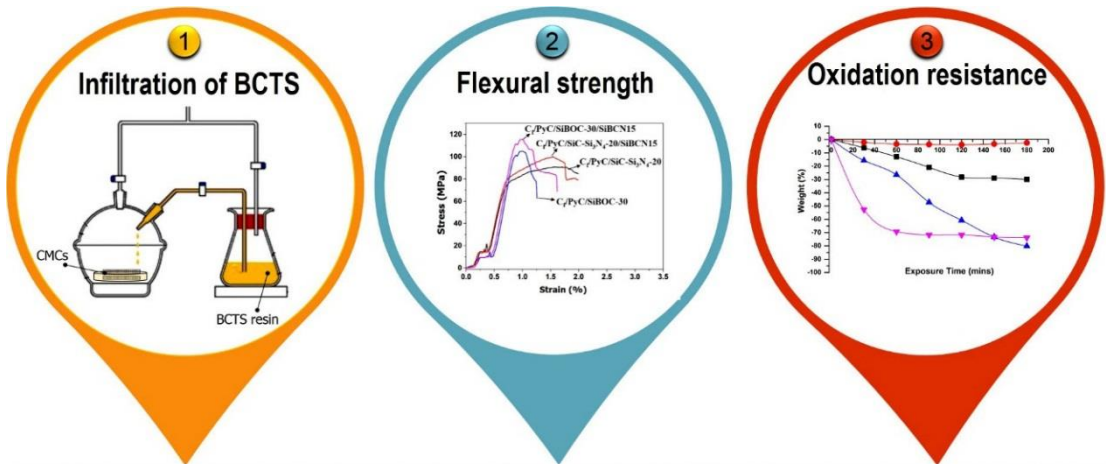
5.2.1 Introduction

Chapter 5.1, demonstrated a novel, facile and low-cost synthetic route for preparing SiBCN ceramics *via* pyrolysis of BCTS resin. The study revealed BCTS resin synthesized with the molar ratio of 1:5 (boric acid: CTS) as a potential preceramic polymer to attain oxide free SiBCN ceramics [SiC, β-Si_3N_4 and BN(C)]. As explained in *Chapter 1, Section 1.5.1.3,* presence of BN(C) in SiBCN ceramics imparts desirable properties for oxidation protection coating.

Hence, in the present Chapter, BCTS with the molar ratio of 1:5 (BCTS15) was used as oxidation protection coating to improve the lifetime of the CMCs. Toward this, two CMC were selected from the previous Chapters *(Chapter 3.2 and Chapter 4.2),* namely C_f/PyC/SiBOC-30 and C_f/PyC/SiC-Si_3N_4-20 composites due to their better mechanical properties as compared to the other composites (Table 5.2.1). The screened CMCs are infiltrated with BCTS15 resin *via* vacuum infiltration technique and their oxidation resistance property is thoroughly investigated.

Table 5.2.1
Properties of the CMCs derived from BPFSi and SPF resins

Sl. No.	Preceramic matrix resin	Samples	Open Porosity (%)	Density (g/cm^3)	Flexural strength (MPa)	Flexural Modulus (GPa)
(a) CMCs derived from boron modified phenol formaldehyde						
1.	BPFSi-10	C_f/PyC/SiBOC-10	30.9	1.40	33 ± 11	9 ± 3
2.	BPFSi-15	C_f/PyC/SiBOC-15	23.4	1.56	87 ± 3	23 ± 3
3.	BPFSi-30	C_f/PyC/SiBOC-30	21.8	1.59	102 ± 11	26 ± 3
(b) CMCs derived from silazane modified phenol formaldehyde						
4.	SPF-5	C_f/PyC/SiC-Si_3N_4-5	15.0	1.38	50 ± 6	14 ± 4
5.	SPF-10	C_f/PyC/ SiC-Si_3N_4-10	13.3	1.42	75 ± 7	17 ± 7
6.	SPF-15	C_f/PyC/ SiC-Si_3N_4-15	10.6	1.44	88 ± 1	23 ± 3
7.	SPF-20	C_f/PyC/ SiC-Si_3N_4-20	9.2	1.51	92 ± 5	25 ± 5
8.	SPF-25	C_f/PyC/ SiC-Si_3N_4-25	24.1	1.28	22 ± 9	9 ± 5
9.	SPF-30	C_f/PyC/ SiC-Si_3N_4-30	28.5	1.24	21 ± 2	6 ± 3

5.2.2 Experimental

5.2.2.1 Materials

Details of the chemicals and materials are detailed in *Chapter 2, Section 2.1.*

5.2.2.2 Synthesis of BCTS resin with the molar ratio of 1:5 (BCTS15)

The procedure for the synthesis of BCTS15 (molar ratio of 1:5) resin was detailed in *Chapter 2, Section 2.2.3*.

5.2.2.3 Fabrication of C_f/PyC/SiBOC-30 composites

C_f/PyC/SiBOC-30 composite was fabricated according to the procedure detailed in *Chapter 2, Section 2.6.2* and their properties are given in Table 5.2.1.

5.2.2.4 Fabrication of C_f/PyC/SiC-Si_3N_4-20 composites

C_f/PyC/SiC-Si_3N_4-20 composite was fabricated according to the procedure detailed in *Chapter 2, Section 2.6.3* and their properties are given in Table 5.2.1.

5.2.2.5 Infiltration of C_f/PyC/SiBOC-30 and C_f/PyC/SiC-Si_3N_4-20 composites with BCTS15 resin

In order to establish BCTS as potential oxidation protection coating to improve the lifetime of the composites, C_f/PyC/SiBOC-30 and C_f/PyC/SiC-Si_3N_4-20 composites were infiltrated with BCTS15 resin *via* standard vacuum infiltration technique as described in *Chapter 2, Section 2.6.4*. Thus obtained CMCs were named as C_f/PyC/SiBOC-30/SiBCN15 and C_f/PyC/SiC-Si_3N_4-20/SiBCN15 composites.

5.2.2.6 Oxidation tests

The detailed procedure for the oxidation test and the calculation of change in weight and oxidation rate of the CMCs are given in *Chapter 2, Section 2.7.5*.

5.2.2.7 Characterization

Characterization methods employed include density and open porosity measurements, three-point-bending test, optical microscopy analysis, SEM analysis and oxidation resistance test. The detailed procedures of all these characterizations are given in *Chapter 2, Section 2.5 and 2.7*.

5.2.3 Results and discussion

5.2.3.1 Evaluation of density and open porosity

The changes in density and open porosity of C_f/PyC/SiBOC-30 and

C_f/PyC/SiC-Si_3N_4-20 composites before and after the infiltration are given in Table 5.2.2.

Table 5.2.2
Properties of the C_f/PyC/SiBOC-30, C_f/PyC/SiC-Si_3N_4-20, C_f/PyC/SiBOC-30/SiBCN15 and C_f/PyC/SiC-Si_3N_4-20/SiBCN15 composites

Sl. No.	Infiltration of BCTS15 resin	Samples	Open Porosity (%)	Density (g/cm³)	Flexural strength (MPa)	Flexural Modulus (GPa)
1.	CMCs without infiltration	C_f/PyC/SiBOC-30	21.8	1.59	102 ± 11	26 ± 3
2.		C_f/PyC/SiC-Si_3N_4-20	9.2	1.51	92 ± 5	25 ± 5
3.	CMCs with infiltration	C_f/PyC/SiBOC-30/SiBCN15	10.5	1.63	114 ± 2.2	28 ± 1.3
4.		C_f/PyC/SiC-Si_3N_4-20/SiBCN15	1.3	1.56	100 ± 1.1	26 ± 1.4

It was observed that, the infiltration of CMCs (C_f/PyC/SiBOC-30/SiBCN15 and C_f/PyC/SiC-Si_3N_4-20/SiBCN15), have resulted in increase of density and subsequent decrease in open porosity of the composite as compared to CMCs without infiltration (C_f/PyC/SiBOC-30 and C_f/PyC/SiC-Si_3N_4-20). This shows that, the BCTS resin has efficiently infiltrated into the pore-channels of the composite, which upon pyrolyzing leads to filling of the pore-channels by the SiBCN based ceramic [SiC, β-Si_3N_4 and BN(C)]. As a result, C_f/PyC/SiBOC-30/SiBCN15 and C_f/PyC/SiC-Si_3N_4-20/SiBCN15 composites have exhibited low porosity with higher density (Table 5.2.2). However, C_f/PyC/SiBOC-30/SiBCN15 and C_f/PyC/SiC-Si_3N_4-20/SiBCN15 showed some residual porosity of 9.2 vol. % and 1.3 vol. % due to the pyrolysis of the polymer precursor which is an inherent property of the polymer derived ceramic matrix. The surface morphology of the composite before and after infiltration were studied through SEM analysis.
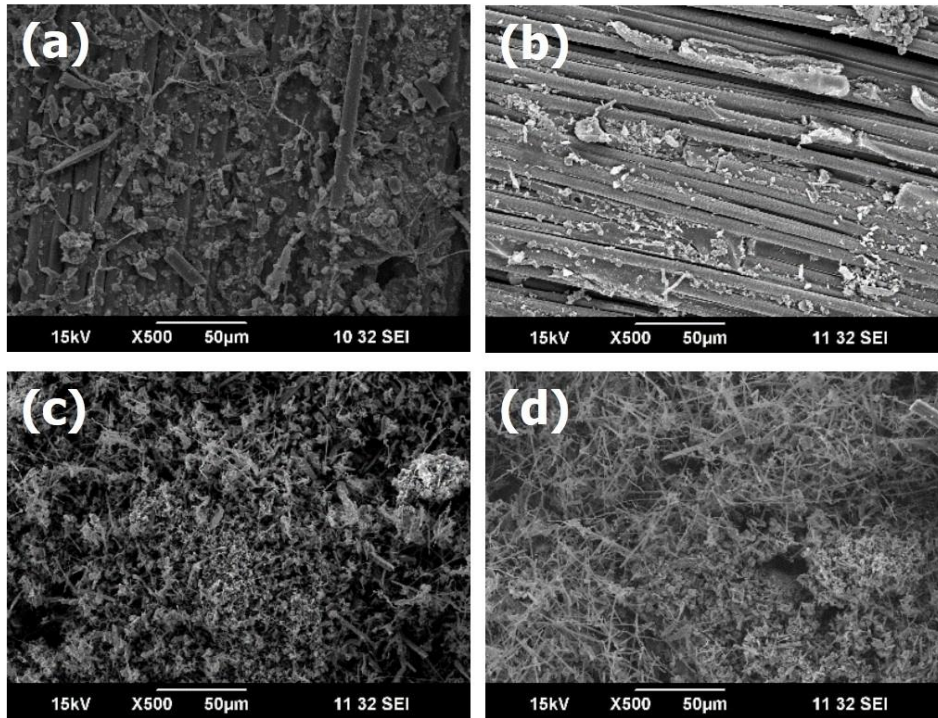
Figure 5.2.1 SEM image of (a) C_f/PyC/SiBOC-30, (b) C_f/PyC/SiC-Si_3N_4-20 (c) C_f/PyC/SiBOC-30/SiBCN15 and (d) C_f/PyC/SiC-Si_3N_4-20/SiBCN15

Figure 5.2.1 (a), (b), (c) and (d) shows SEM image of C_f/PyC/SiBOC-30, C_f/PyC/SiC-Si_3N_4-20, C_f/PyC/SiBOC-30/SiBCN15 and C_f/PyC/SiC-Si_3N_4-20/SiBCN15 composites, respectively. In the case of C_f/PyC/SiBOC-30 and C_f/PyC/SiC-Si_3N_4-20 composites, carbon fibers are exposed to the atmosphere [Figure 5.2.1 (a) and (b)], whereas in the case of C_f/PyC/SiBOC-30/SiBCN15 and C_f/PyC/SiC-Si_3N_4-20/SiBCN15 composites, the carbon fibers are covered homogenously by the SiBCN based ceramic matrix showing effective infiltration of BCTS in the pore-channels of the CMCs [Figure 5.2.1 (c) and (d)]. This explains the increase in density and decrease in porosity after infiltration process of CMCs.

5.2.3.2 Evaluation of flexural strength
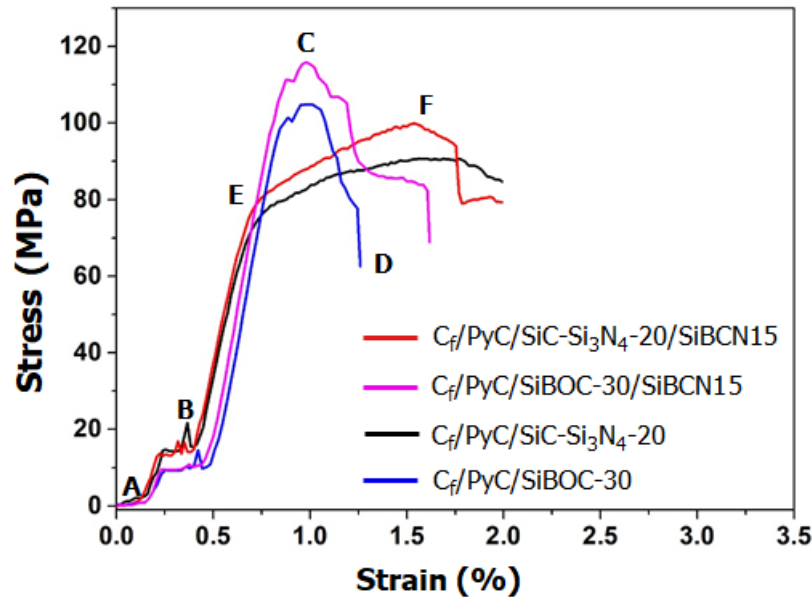
Figure 5.2.2 Stress-strain-curves of CMCs before and after infiltration with BCTS resin.

The different regions of the stress-strain curve of C_f/PyC/SiBOC-30, C_f/PyC/SiC-Si$_3$N$_4$-20, C_f/PyC/SiBOC-30/SiBCN15 and C_f/PyC/SiC-Si$_3$N$_4$-20/SiBCN15 composites have been taken into consideration and explained in the revised thesis as suggested by the examiner.

For all the composition, the initial region of the stress-strain curve (A to B) corresponds to the pre-loading stress that the CMCs samples are subjected to during the flexural testing. Such stress-strain curve characteristics in the initial region is typical feature for CMCs laminates. Hence, the actual stress-strain curves start from the B-region onwards. The stress-strain-curves of the CMCs [Figure 5.2.2] showed two types of fracture behavior irrespective of the infiltration process. The first type of the stress-strain-curves showed three distinctive stages, which are marked as B, C and D. In the first stage (B), a linear increase in stress is observed followed by a curve at the second stage (C) and a gradual drop at the final stage (D). This phenomenon was observed for the CMCs with SiBOC as ceramic matrix i.e., C_f/PyC/SiBOC-30 and C_f/PyC/SiBOC-

30/SiBCN15 composites. On the contrary, the second type of the stress-strain-curves exhibits a pseudo-ductile fracture behavior (B, E and F), which is observed for the CMCs with SiCN as ceramic matrix i.e., C_f/PyC/SiC-Si_3N_4-20 and C_f/PyC/SiC-Si_3N_4-20/SiBCN15 composites.

Table 5.2.3
Elemental composition of the ceramic matrix

Sl. No.	Sample	Ceramic matrix	Composition (mass %)					
			Si	B	C	O	N	Empirical formula normalized on Si
1.	BPFSi-30-1450	SiBOC	39	33	16	11	-	$Si_1B_{0.8}O_{0.2}C_{0.4}$
2.	SPF-20-1650	SiCN	28	-	60	9	3	$Si_1C_{0.92}N_{0.06}O_{0.28}$
3.	BCTS15-1650	SiBCN	62	3	27	-	5	$SiB_{0.09}N_{0.15}C_{0.98}$

This difference is due to the variation in the elemental composition of the ceramic matrix (Table 5.2.3). In the case of SiBOC based ceramic matrix, the elemental composition is found to be as $Si_1B_{0.8}O_{0.2}C_{0.4}$, whereas in the case of SiCN based ceramic matrix the elemental composition is found to be as $Si_1C_{0.92}N_{0.06}O_{0.28}$. This reveals that the CMCs made from SiCN matrix [C_f/PyC/SiC-Si_3N_4-20 and C_f/PyC/SiC-Si_3N_4-20/SiBCN15] is rich in carbon content as compare to that of CMCs made from SiBOC matrix [C_f/PyC/SiBOC-30 and C_f/PyC/SiBOC-30/SiBCN15]. This high carbon content enhances the ductility of the composite which normally exhibits high flexural properties [Liu *et al.* 2017]. It is to be noted that, increasing the carbon content will decrease the density of composite, which decreases the mechanical properties [Krenkel 2004]. Hence, high carbon content in CMCs will show ductile facture behavior with a moderate flexural strength. This phenomenon is called pseudo-ductile behavior. Therefore, the CMCs derived from SiBOC based ceramic matrix [C_f/PyC/SiBOC-30 and C_f/PyC/SiBOC-30-SiBCN15] have shown better mechanical properties as compared to the CMCs derived from SiCN based composite [C_f/PyC/SiC-Si_3N_4-20 and C_f/PyC/SiC-Si_3N_4-20-SiBCN15]. To gain insight of the failure mechanism of the CMCs, studies on crack propagation and fracture behavior of the composites were carried out.
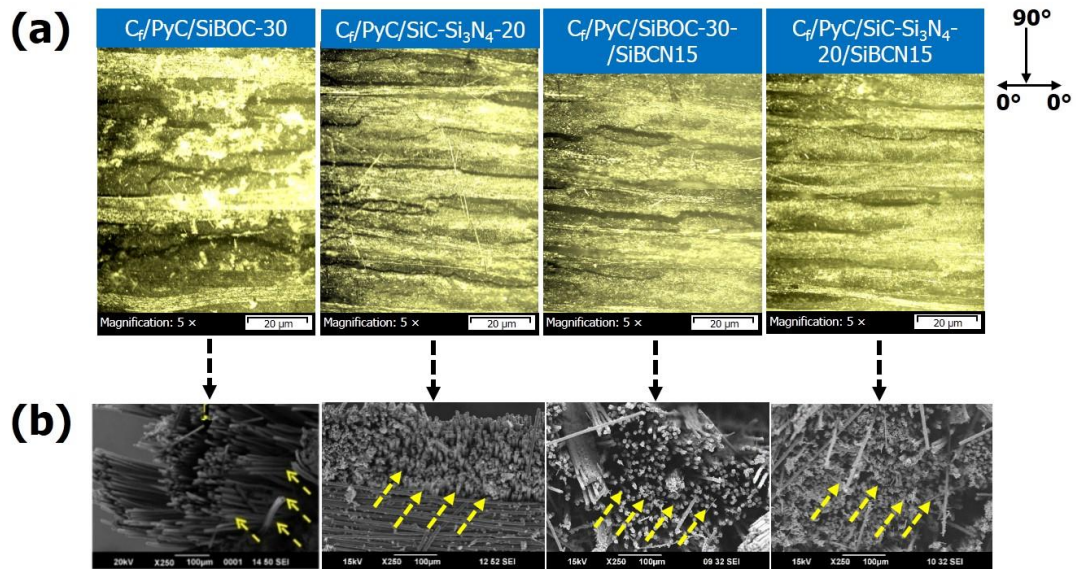
Figure 5.2.3 (a) Optical Image of lateral view on the development of cracks in a flexural specimen and (b) SEM image of the fractured surface of CMCs before and after infiltration

Figure 5.2.3 (a) and (b) shows the lateral view of the propagation of cracks in a flexural specimen and SEM image of the fractured surface, respectively of C_f/PyC/SiBOC-30, C_f/PyC/SiC-Si$_3$N$_4$-20, C_f/PyC/SiBOC-30/SiBCN15 and C_f/PyC/SiC-Si$_3$N$_4$-20/SiBCN15 composites. The lateral view image of all the CMCs showed the importance of PyC interphase coating on the carbon fiber which helps in crack propagation along 0°/90° directions. This suggests existence of a weak bonding between F/M interface leading to fiber pull-out and de-bonding through energy dissipative mechanism [Figure 5.2.3 (b)] [Rizvi *et al.* 2016] resulting in increase in flexural properties. Although, all the CMCs have shown energy dissipative mechanism, infiltrated CMCs exhibit high flexural property as compare to that of non-infiltrated CMCs. It is to be noted that for achieving superior mechanical properties of CMCs, apart from energy dissipative mechanism, it should have higher density and lower porosity [Naslain 2004]. Hence, infiltrated CMCs has shown better mechanical properties due to its high density and lower porosity as compared to that of non-infiltrated CMCs (Table 5.2.2).

5.2.3.3 Evaluation of oxidation resistance

As the objective of the work is to establish BCTS as potential oxidation resistance coating to improve the lifetime of the CMCs, C_f/PyC/SiBOC-30 and C_f/PyC/SiC-Si$_3$N$_4$-20 composites were infiltrated with BCTS and evaluated their oxidation resistance property was evaluated. Both the CMCs before infiltration (C_f/PyC/SiBOC-30 and C_f/PyC/SiC-Si$_3$N$_4$-20) and after infiltration (C_f/PyC/SiBOC-30-SiBCN15 and C_f/PyC/SiC-Si$_3$N$_4$-20-SiBCN15) is subjected to isothermal oxidation at three different temperatures 1000°C, 1250°C and 1500°C in raising hearth furnace at the flow rate of air 100 cm^3/min for 3h with 30 mins intervals. The weight change and oxidation rate were calculated as given in *Chapter 2, Section 2.7.5*.

Figure 5.2.4 (a) and (b) shows the percentage weight loss and oxidation rate of the oxidized CMCs, respectively at 1000°C. In the case of CMCs before infiltration, C_f/PyC/SiBOC-30 composite, shows a small weight loss of 12 %, whereas C_f/PyC/SiC-Si$_3$N$_4$-20 composite shows a huge weight loss of 80 % [Figure 5.2.4 (a)]. The insignificant weight loss in C_f/PyC/SiBOC-30 composite is attributed to the presence of boron in the matrix, which form a borosilicate glassy phase [B$_2$O$_3$.xSiO$_2$] during the oxidation of CMCs as per the eqn. 5.2.2 and 5.2.4.

$$C + O_2 \xrightarrow{400°C} 2CO \qquad\qquad (5.2.1)$$

$$SiB_{4(s)} + 4O_{2(g)} \xrightarrow{400°C-1000°C} B_2O_{3(l)} + xSiO_{2(l)} \qquad (5.2.2)$$

$$Si_xB_yC_zN_{u(s)} + (x+0.75y+0.5z)O_2 \xrightarrow{600°C-1000°C}$$
$$xSiO_{2(l)} + y/2B_2O_{3(l)} + z/2CO_{(g)} + u/2N_{2(g)} \qquad (5.2.3)$$

$$B_2O_{3(l)} + xSiO_{2(l)} \xrightarrow{1000°C} B_2O_3.xSiO_{2(l)} \qquad\qquad (5.2.4)$$
$$\textit{borosilicate glass}$$
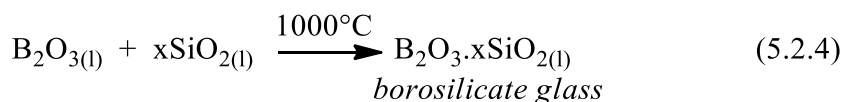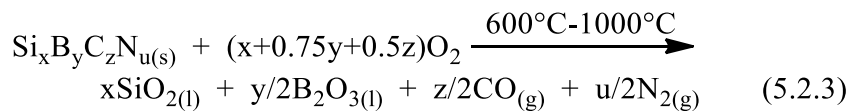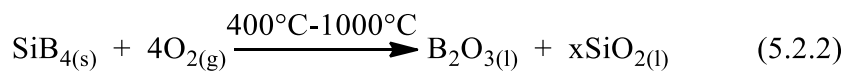
Figure 5.2.4 Isothermal oxidation at 1000°C in air for 3h, showing (a) Percentage weight loss of CMCs and (b) oxidation rate of CMCs

This will slow down the in-depth diffusion of oxygen imparting *self-healing* property and protects the carbon fiber from oxidative atmosphere. However, in C_f/PyC/SiC-Si_3N_4-20 composite, no such reactions are possible due to the absence of boron in the matrix, resulting in massive weight loss due to the oxidation of carbon phase as shown

in the eqn. (5.2.1). Interestingly, in the case of CMCs after infiltration, C_f/PyC/SiBOC-30/SiBCN15 composite shows increase in weight by 3 %, whereas C_f/PyC/SiC-Si_3N_4-20/SiBCN15 composite shows weight loss of 50 %. The increase in weight for C_f/PyC/SiBOC-30/SiBCN15 composite is due to the presence boron in both the ceramic matrix (SiBOC and SiBCN). As a result, the overall concentration of boron increases which enhances the formation of borosilicate glassy phase ($B_2O_3.xSiO_2$) as shown in eqn. (5.2.2) to (5.2.4). This leads to increase in weight [Figure 5.2.4 (a)] and decrease in oxidation rate of the C_f/PyC/SiBOC-30/SiBCN15 composite [Figure 5.2.4 (b)], indicating the carbon fibers are protected from the oxidation. Whereas, in the case of C_f/PyC/SiC-Si_3N_4-20/SiBCN15 composite, although boron contain ceramic matrix (SiBCN) was present, weight loss of 50 % of was observed. This is due to SiCN based ceramic matrix which is not capable of producing *self-healing* matrix at relatively low temperature i.e., at 1000°C, hence the weight loss is most predominant for C_f/PyC/SiC-Si_3N_4-20/SiBCN15 composite due to oxidation of carbon phase. This observation is further evidenced from the SEM image of the oxidized CMCs [Figure 5.2.5], where the carbon fibers are protected by the formation of borosilicate glassy phase [$B_2O_3.xSiO_2$] in the case of C_f/PyC/SiBOC-30 and C_f/PyC/SiBOC-30/SiBCN15 composites. While in C_f/PyC/SiC-Si_3N_4-20 and C_f/PyC/SiC-Si_3N_4-20/SiBCN15 composites the carbon fibers are completely oxidized, indicating the importance of boron in protecting the CMCs at relatively lower temperature.
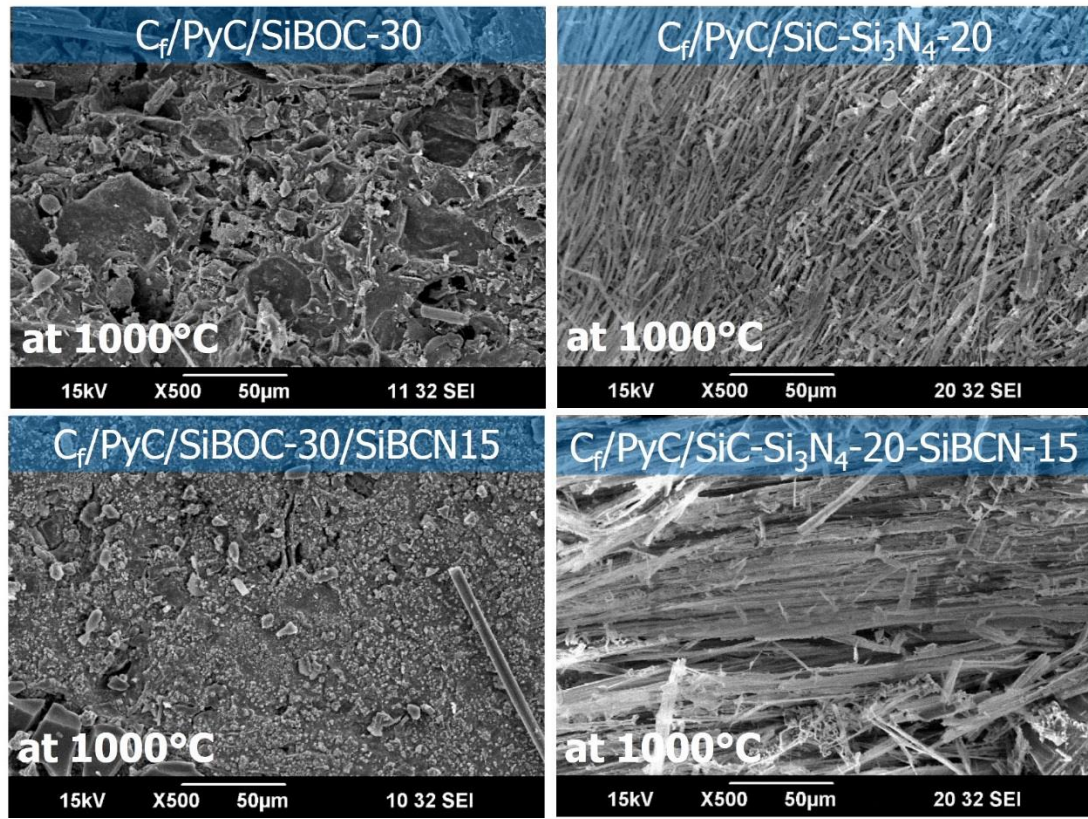
Figure 5.2.5 SEM image of oxidized CMCs at 1000°C in air for 3h

Further to test the oxidation resistance skill of these composites, the oxidation test was performed at higher temperature (1250°C and 1500°C) as well. Figure 5.2.6 (a) and (b) shows the percentage weight loss and oxidation rate of the oxidized CMCs, respectively at 1250°C. In the case of CMCs before infiltration, C_f/PyC/SiBOC-30 and C_f/PyC/SiC-Si_3N_4-20 composite shows a weight loss of 15 % and 80 %, respectively. This difference is due to the same reason as explained in the case of 1000°C, where the C_f/PyC/SiBOC-30 composite is well protected from the oxidative atmosphere by boron containing *self-healing* matrix (SiBOC). However, at 1250°C SiCN based ceramic matrix in C_f/PyC/SiC-Si_3N_4-20 composite, are capable of forming SiO_2 layer as per the eqn. (5.2.5) and (5.2.6), which can act as *self-healing* matrix to protect the carbon fiber from oxidation.

$$Si_3N_{4(s)} + 3O_{2(g)} \xrightarrow{>1100°C} SiO_{2(l)} + 2N_{2(g)} \qquad (5.2.5)$$

$$SiC(s) + 3/2O_{2(g)} \xrightarrow{>1100°C} SiO_{2(l)} + CO_{(g)} \qquad (5.2.6)$$
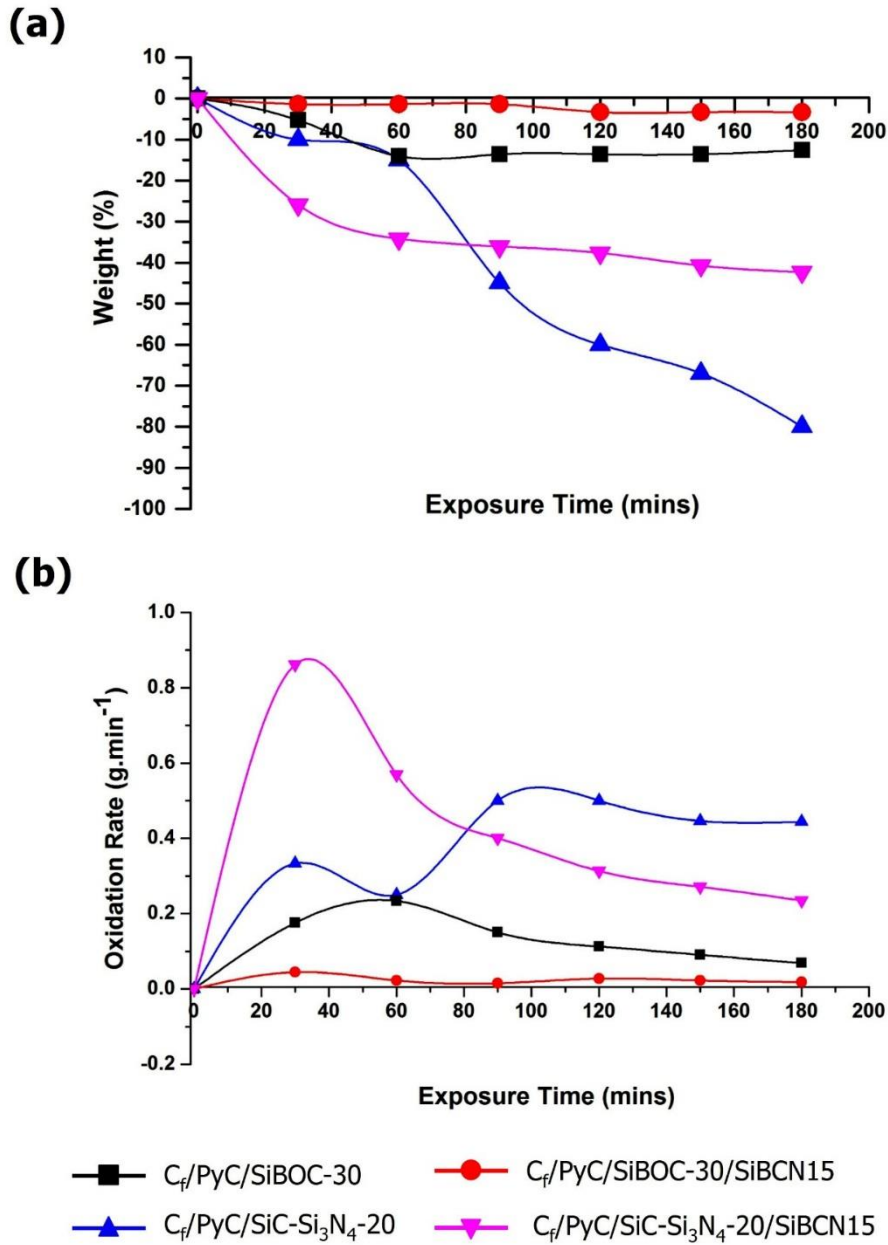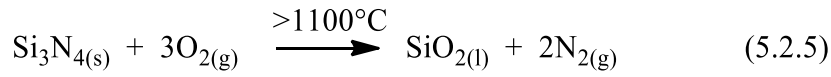
Figure 5.2.6 Isothermal oxidation at 1250°C in air for 3h, showing (a) Percentage weight loss of CMCs and (b) oxidation rate of CMCs

However, weight loss of 80 % was observed, indicating that the voids formed at 1000°C due to the oxidation of carbon fibers have become a path way for the oxygen to enter into the CMCs, contributing to further weight loss [Figure 5.2.6 (a)] and increasing the oxidation rate [Figure 5.2.6 (b)] at 1250°C. The same observation is reflected in the case of CMCs after infiltration as well, C_f/PyC/SiC-Si_3N_4-20/SiBCN15 composite shows the weight loss of 35% although SiBCN ceramic matrix were present. However, compare to the weight loss of 50 % observed at 1000°C [Figure 5.2.4 (a)], the weight loss of the C_f/PyC/SiC-Si_3N_4-20/SiBCN15 composite decreased to 35 % at 1250°C [Figure 5.2.6 (a)]. This is due to the oxidation of SiCN based ceramics and SiBCN based ceramics which results in the formation of two kinds of *self-healing* matrix *viz.* borosilicate ($B_2O_3.xSiO_2$) and silica (SiO_2), respectively as shown in eqn. (5.2.3) to (5.2.6). Conversely, C_f/PyC/SiBOC-30/SiBCN15 composite shows negligible weight loss of 2% owing to its higher boron concentration, establishing it as better composite compare to the other composites.
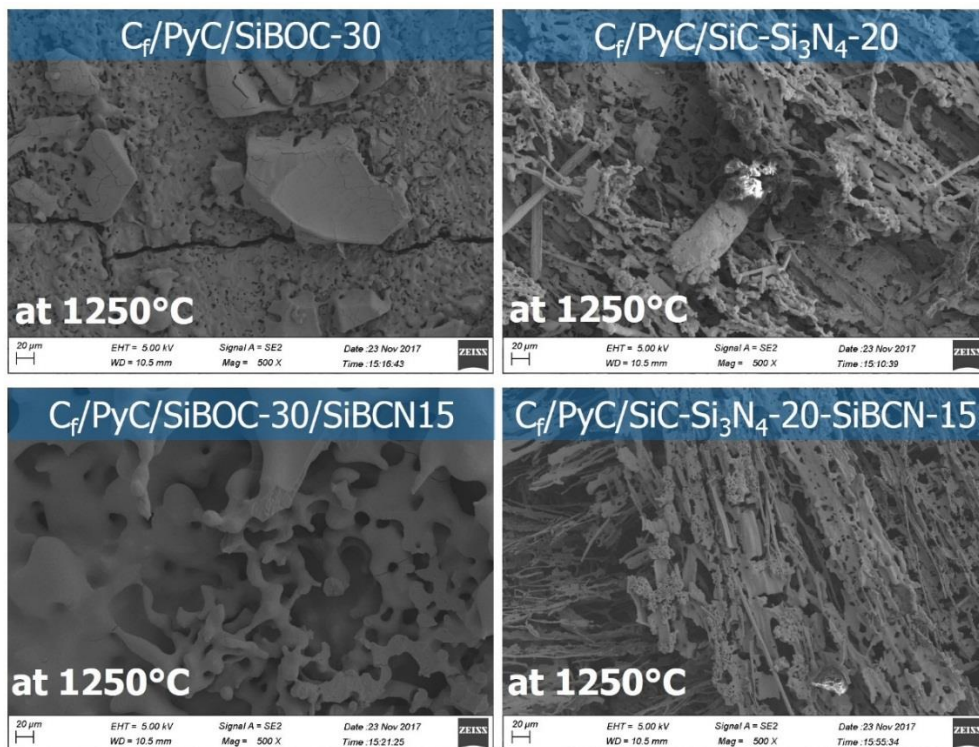
Figure 5.2.7 SEM image of oxidized CMCs at 1000°C in air for 3h

This observation is further supported by the SEM image of the oxidized CMCs [Figure 5.2.7], showing the same results as that of 1000°C [Figure 5.2.5]. In the case of C_f/PyC/SiBOC-30 and C_f/PyC/SiBOC-30/SiBCN15 composites, the carbon fibers are protected by the formation of borosilicate glassy phase [$B_2O_3.xSiO_2$], whereas in the case of C_f/PyC/SiC-Si_3N_4-20 and C_f/PyC/SiC-Si_3N_4-20/SiBCN15 composites the carbon fibers were completely oxidized.

(a)

(b)

Legend:
- C_f/PyC/SiBOC-30
- C_f/PyC/SiBOC-30/SiBCN15
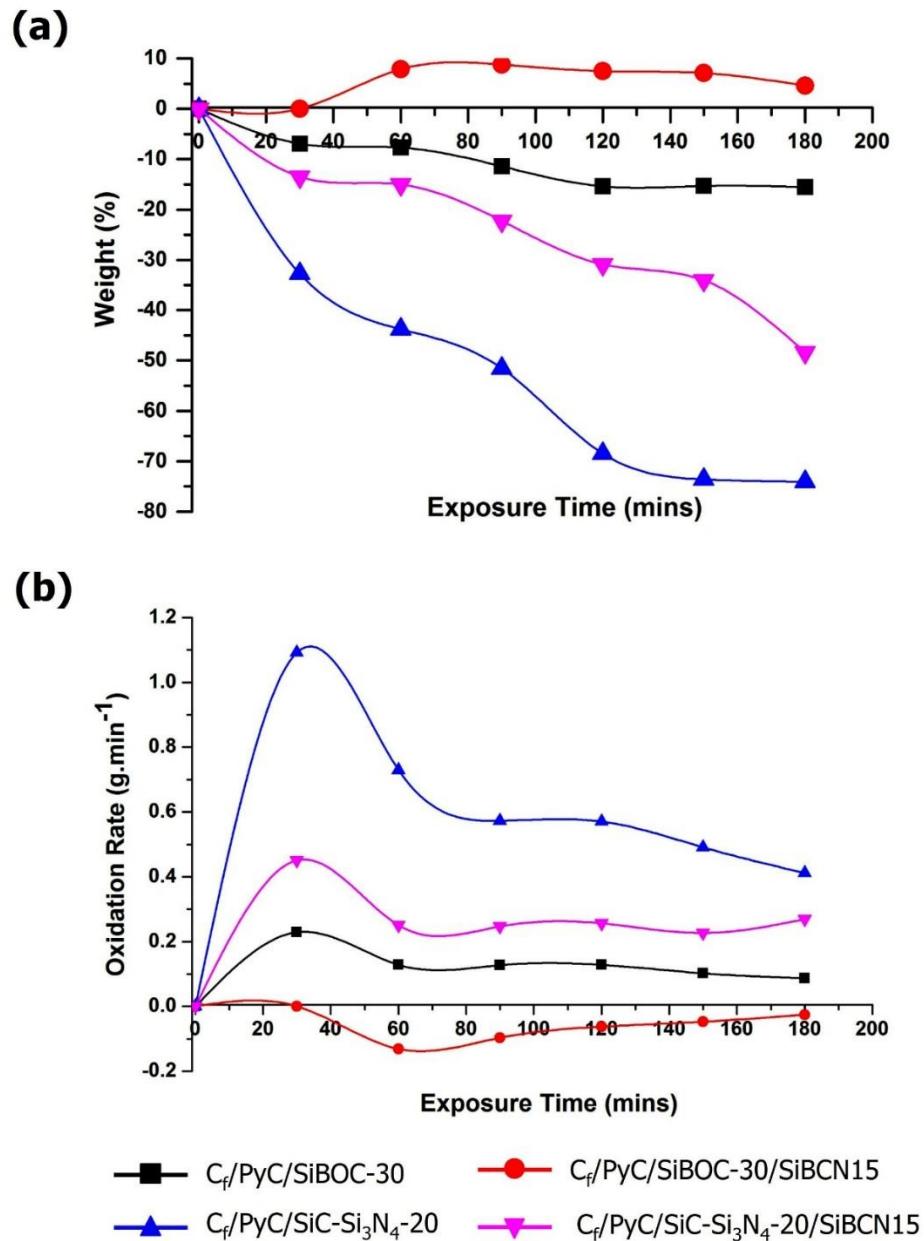- C_f/PyC/SiC-Si_3N_4-20
- C_f/PyC/SiC-Si_3N_4-20/SiBCN15
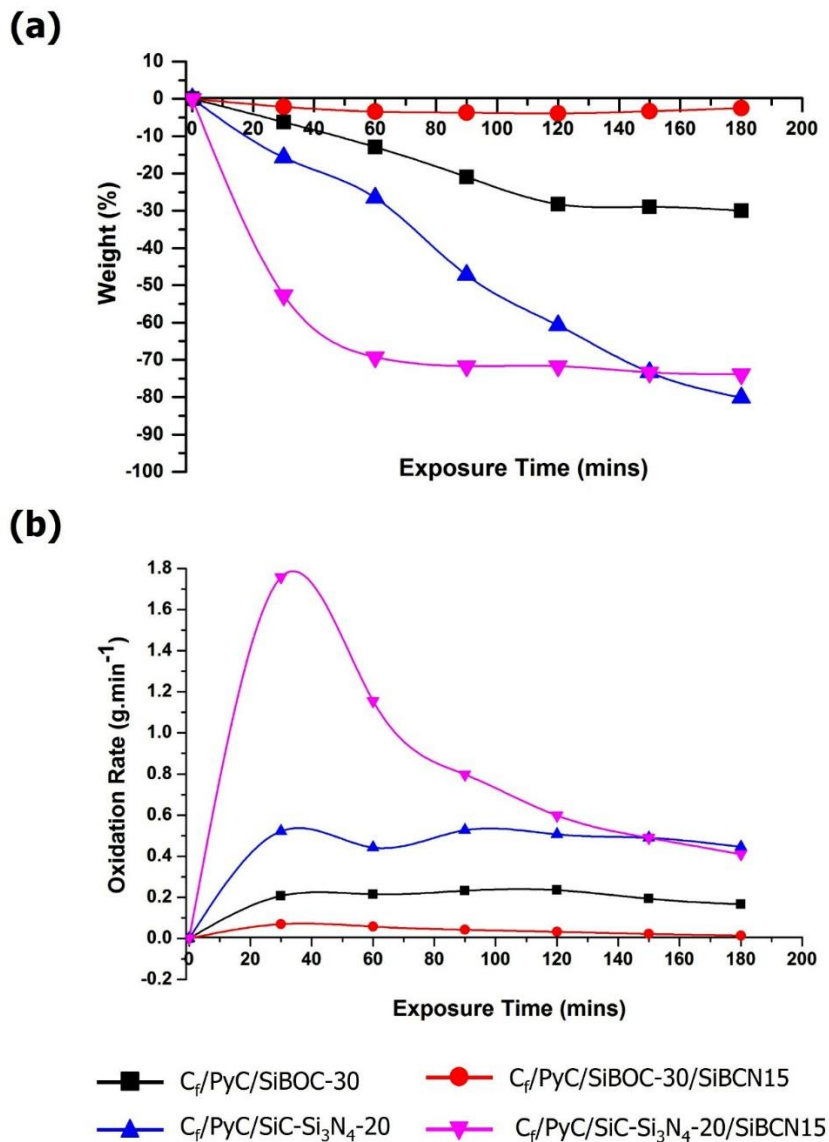
Figure 5.2.8 Isothermal oxidation at 1500°C in air for 3h, showing (a) Percentage weight loss of CMCs and (b) oxidation rate of CMCs

Figure 5.2.8 (a) and (b) shows the percentage weight loss and oxidation rate of the oxidized CMCs, respectively at 1500°C. The weight loss for C_f/PyC/SiBOC-30, C_f/PyC/SiC-Si$_3$N$_4$-20, C_f/PyC/SiBOC-30/SiBCN15 and C_f/PyC/SiC-Si$_3$N$_4$-20/SiBCN15 composites are 40 %, 80 %, 2 % and 75 %, respectively. It is interesting to note that, C_f/PyC/SiBOC-30 composite exhibiting better results at 1000°C and 1250°C has failed drastically at 1500°C. This is due to the evaporation of B_2O_3 phase in $B_2O_3.xSiO_2$ ceramic phase at 1500°C as shown in eqn. (5.2.7). As a result, the voids are formed in the ceramic matrix which becomes a path way for the oxygen to enter into the composite and oxidize the carbon fiber.

$$B_2O_3.xSiO_{2(l)} \xrightarrow{>1300°C} B_2O_{3(g)} + xSiO_{2(s)} \qquad (5.2.7)$$
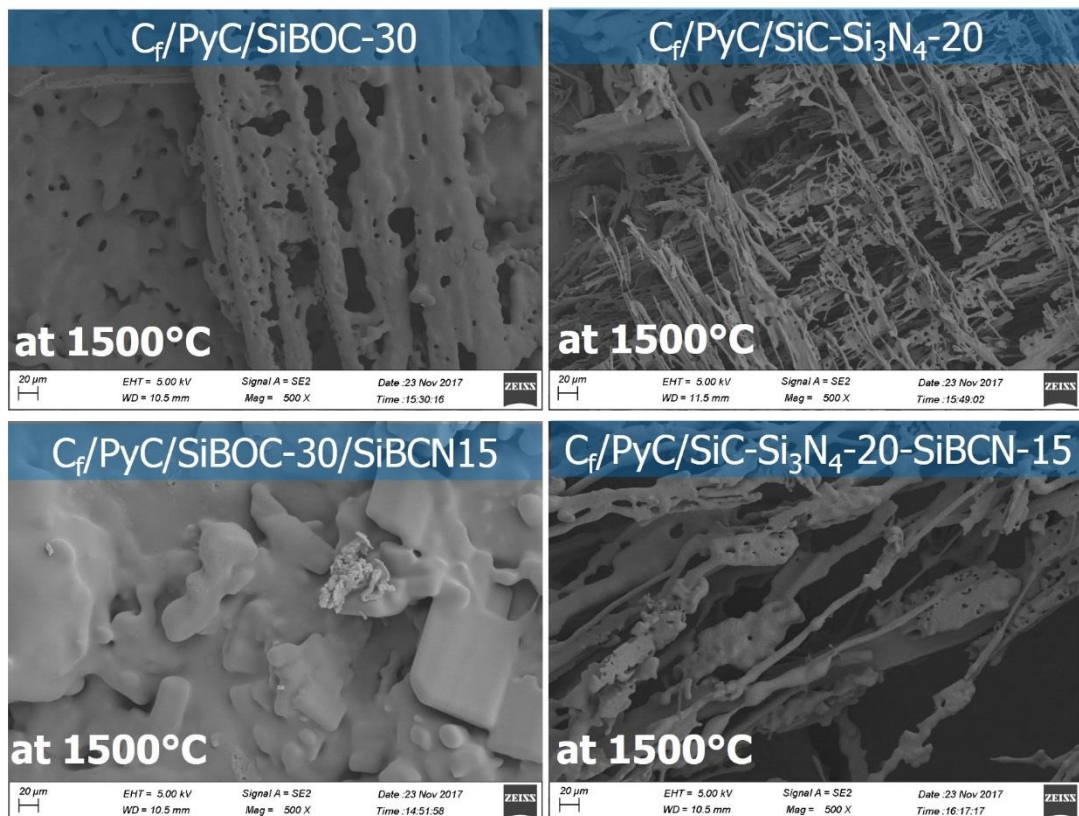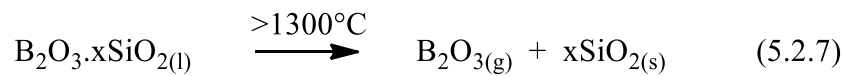
Figure 5.2.9 SEM image of oxidized CMCs at 1000°C in air for 3h

The SEM image of the oxidized CMCs also shows that, the carbon fibers are oxidized in the case of C_f/PyC/SiBOC-30, C_f/PyC/SiC-Si_3N_4-20 and C_f/PyC/SiC-Si_3N_4-20/SiBCN15 composites [Figure 5.2.9]. Conversely, C_f/PyC/SiBOC-30/SiBCN15 composite shows that, the carbon fibers were completely protected by the formation of $B_2O_3.xSiO_2$ which is retained even at 1500°C [Figure 5.2.9]. This prolonged stability of the $B_2O_3.xSiO_2$ is due to the presence of BN(C) ceramic phase in SiBCN ceramic matrix, which prevents the decomposition and crystallization of the $B_2O_3.xSiO_2$ ceramics [Li *et al.* 2017] and hence, imparting the extended *self-healing* property. This demonstrates the potential of BCTS as oxidation resistance coating for improving the life-time of CMCs in oxidative atmosphere and established C_f/PyC/SiBOC-30/SiBCN15 composites as the better composite compare to other composites.

5.2.4 Conclusions

The present study focused on the improvement of oxidation resistance of C_f/PyC/SiBOC-30 and C_f/PyC/SiC-Si_3N_4-20 composites. For this, BCTS resin was infiltrated into the C_f/PyC/SiBOC-30 and C_f/PyC/SiC-Si_3N_4-20 composites *via* vacuum infiltration technique (denoted as C_f/PyC/SiBOC-30/SiBCN15 and C_f/PyC/SiC-Si_3N_4-20/SiBCN15) and their oxidation resistance property was investigated at three different temperatures *viz.* 1000°C, 1250°C and 1500°C. The results clearly revealed the changes observed in the weight loss, oxidation rate and the morphology of CMCs before and after the infiltration. At 1000°C and 1250°C, C_f/PyC/SiBOC-30 and C_f/PyC/SiBOC-30/SiBCN15 composites showed better oxidation resistance due to the formation of $B_2O_3.xSiO_2$ phase, whereas in the case of C_f/PyC/SiC-Si_3N_4-20 and C_f/PyC/SiC-Si_3N_4-20/SiBCN15 composites complete oxidation of carbon fibers were observed, indicating the importance of boron in protecting the CMCs at relatively lower temperature. Surprisingly, on increasing the oxidation temperature to 1500°C, except C_f/PyC/SiBOC-30/SiBCN15 composite, all other CMCs resulted in the oxidation of carbon fibers. This prolonged stability of C_f/PyC/SiBOC-30/SiBCN15 composite is attributed to the presence of BN(C) ceramic phase in SiBCN ceramic matrix, which prevented the decomposition of $B_2O_3.xSiO_2$ phase imparting the extended *self-healing*

property. This demonstrated the potential of BCTS as oxidation resistance coating for improving the life-time of CMCs in oxidative atmosphere and established C_f/PyC/SiBOC-30/SiBCN15 composites as the better composite compare to other composites. This study opens up a new way for the fabrication of cost-effective CMCs with improved mechanical and oxidation resistance properties for the long-term thermo-structural applications.

Chapter 6

Summary and Conclusions

1. Studies on BPF as preceramic matrix resin for CMCs
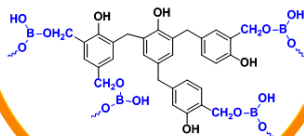
2. Studies on SPF as preceramic matrix resin for CMCs
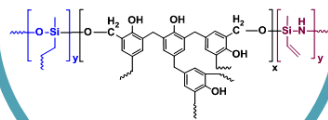
3. Studies on BCTS resin as oxidation resistance coating for CMCs
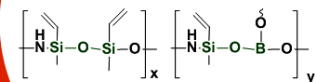
This chapter summarizes the findings of the present investigation together with concluding remarks and scope for future work.

T his research was aimed at developing a new class of cost effective preceramic matrix resins for CMCs with *self-healing* properties and to investigate their effect on the mechanical properties. Covering these aspects, the work was divided into the following chapters:

(i)   Studies on boron modified phenol-formaldehyde (BPF) as preceramic matrix resin for CMCs

(ii)   Studies on silazane modified phenol-formaldehyde (SPF) as preceramic matrix resin for CMCs

(iii)   Studies on boron modified cyclotrisilazane (BCTS) resin as oxidation resistance coating for CMCs

The most important findings and conclusions of the present investigation are given below:

Studies on BPF as preceramic matrix resin for CMCs

This chapter is comprised of two parts;

➢ In the first part, synthesis, characterization and ceramic conversion of BPF resins were investigated. BPF resins were synthesized by reacting various amount of boric acid [5, 10, 15, 20, 25 and 30 pph w.r.t PF] with PF resin. The concentration of boric acid could not be increased beyond 30 pph as it precipitated in the reaction medium. FTIR studies revealed that, boric acid has chemically reacted with PF resin to form BPF resin *via* condensation reaction mechanism. The ceramic conversion of BPF resins were carried out at 1450°C under argon atmosphere, with and without elemental silicon as reactive additive. The structural evolution of the resultant ceramics were investigated using XRD, Raman and HRTEM techniques. XRD studies of the ceramics revealed that, in the case of BPF resin, without silicon additive, carbon and B_4C ceramic phases were obtained; whereas, in the case of BPF resin with silicon additive, SiC and SiB_4 ceramic phases were obtained. This difference is attributed to the reaction of 'Si' atoms with 'C' atoms in the C–B–C chain of B_4C icosahedron, leading to SiC and SiB_4 ceramic phases. The nature of free carbon in the ceramics derived from BPF resins were

understood using Raman and HRTEM analysis. In the case of PF resin, free carbon was found to exist as fine ribbon like structures corresponding to glassy carbon; whereas, on incorporating boron to PF resin, the structure of free carbon has transformed from glassy carbon to graphitic carbon following the sequence:

glassy carbon [PF] → amorphous carbon [BPF-10 (boric acid 10 pph w.r.t. PF)] → turbostatic carbon [BPF-15 (boric acid 15 pph w.r.t. PF)] → graphitic carbon [BPF-30 (boric acid 30 pph w.r.t. PF)].

This sequential transformation of carbon through various intermediate phases were attributed to the catalytic effect of boron. Hence, among various compositions of BPF resins, BPF-10, BPF-15 and BPF-30 were chosen for further studies.

The objective of the second part of the study was to assess BPF resin as a *self-healing* matrix resin for CMC. In this regard, CMCs were fabricated using 2D carbon fabric as reinforcement and a slurry containing BPF with silicon (BPFSi) as matrix resin. The CMCs thus obtained were evaluated for the flexural strength and oxidation resistance properties. The obtained properties were compared with CMC derived from a slurry containing PF with silicon (PFSi) as matrix resin. The flexural strength of BPFSi derived CMCs showed a marginal improvement (46 ± 1.6 MPa) as compared to PFSi derived CMCs (42 ± 2.2 MPa). This was attributed to the damage of carbon fiber on reaction with molten silicon to form a thin polycrystalline SiC layer. The evaluation of oxidation resistance properties for CMCs demonstrated improved oxidation resistance of BPFSi derived CMCs in comparison to PFSi derived CMCs. This was due to the formation of a borosilicate glassy layer on BPFSi derived CMCs which slowed down the in-depth diffusion of oxygen, imparting *self-healing* property for CMCs. This study demonstrated BPF as a potential *self-healing* matrix resin for CMCs. The next section focuses on the attempts made to improve the mechanical properties of the CMCs.

➤ The mechanical properties of CMCs are greatly influenced by the proper design of Fiber/Matrix (F/M) interface. In this section, an attempt was made to study the effect of F/M volume ratio and the influence of interphase coating on the flexural properties

of the CMCs. To understand the effect of F/M volume ratio on the flexural properties of the composites, three types of CMCs were fabricated using PFSi as matrix resin, varying the F/M volume ratio *viz.* 40/60, 50/50 and 60/40 (wt.%). The percentage of fiber content could not be increased beyond 60 vol. % due to delamination of the composite. The results revealed increase in the flexural strength from 25 ± 3.9 MPa (F/M-40/60) to 63 ± 9.9 MPa (F/M-60/40) on increasing the fiber vol. %. Additionally, CMCs having F/M volume ratio of 40/60 and 50/50 had failed in a brittle manner while CMC having F/M volume ratio of 60/40 exhibited a ductile fracture leading to fiber bundle pull-out. This revealed that increasing the 'C' fiber vol. % was effective in preventing catastrophic fracture. Hence, F/M volume ratio of 60/40 was chosen for all further studies.

To investigate the significance of an interphase coating, CMCs were fabricated using F/M volume ratio of 60/40, PyC as interphase coating (thickness 0.2-0.5 μm) and different composition of BPFSi (BPFSi-10, BPFSi-15, BPFSi-20 and BPFSi-30) as preceramic matrix resin. The CMCs thus obtained were evaluated for the flexural properties. The obtained properties were compared with CMC fabricated without an interphase. CMCs with PyC interphase showed improvement in flexural strength from 32.86 ± 10.7 MPa (BPFSi-10 derived CMCs) to 102 ± 11.5 MPa (BPFSi-30 derived CMCs), while CMCs without interphase showed no improvement in flexural properties and exhibited maximum flexural strength of 38 ± 4.4 MPa (BPFSi-30 derived CMCs). The fractograph of CMCs without interphase showed no fiber pull-out, indicating a strong fiber-matrix bonding; while CMCs with PyC interphase coating exhibited fiber pull-out phenomenon and hence failed in a ductile manner. The study demonstrated the importance of optimization of F/M volume ratio and the necessity of an interphase coating to fabricate CMCs with better mechanical properties. However, the limitation created by the silicon as additive still persists. Hence, an attempt was made in the next chapter, to incorporate silicon as back bone of PF resin and investigate it as preceramic matrix resin for CMCs.

Studies on SPF as preceramic matrix resin for CMCs

This chapter is comprised of two parts;

➢ In the first part, synthesis, characterization and ceramic conversion of SPF resins were investigated. SPF resins were synthesized by reacting varying amounts of CTS [5, 10, 15, 20, 25 and 30 pph w.r.t PF] with PF resin. The concentration of CTS could not be increased beyond 30 pph due to incomplete reaction of CTS with PF resulting in the formation of separate phase in the reaction medium. FTIR and NMR analysis revealed that, CTS chemically reacted with PF resin to form SPF resin *via* ring opening mechanism. To evaluate the potential of SPF as a preceramic matrix resin, studies on pyrolysis condition are mandatory. To meet this objective, ceramic conversion studies were carried out at 1450°C and 1650°C under argon and nitrogen atmosphere. The structural evolution of the resultant ceramics were investigated through XRD, Raman and FESEM techniques. Under argon atmosphere both at 1450°C and 1650°C, SPF yield SiC ceramic phases only. While, at 1450°C under nitrogen atmosphere, amorphous ceramics were obtained and at 1650°C, crystalline SiC and Si_3N_4 ceramic phases were obtained. Moreover, under nitrogen atmosphere both at 1450°C and 1650°C, only macro-porous ceramics were formed. Surprisingly, under argon atmosphere both at 1450°C and 1650°C, additional 1D, triangular shaped, nano-rod structured ceramics along with macro-porous structure were formed. EDX analysis revealed that, these nano-rods are composed of SiC ceramics and are formed through vapor-vapor mechanism. This study demonstrated SPF as a new class of preceramic polymer and revealed that nitrogen atmosphere was more suitable as a pyrolysis gas atmosphere than argon for preparation of SiC/Si_3N_4 ceramics with enhanced ceramic yield.

➢ In the second part of the investigation, CMCs were fabricated using F/M volume ratio of 60/40, PyC as interphase coating and different composition of SPF (SPF-5 to 30) as preceramic matrix resin *via* polymer infiltration and pyrolysis (PIP) process. For C_f/PyC/SiC-Si_3N_4-5 (SPF-5 derived CMCs) to C_f/PyC/SiC-Si_3N_4-20 (SPF-20 derived CMCs) composites, gradual increase in flexural strength of 50 ± 6 MPa to 92 ± 5 MPa was obtained. On the contrary, for C_f/PyC/SiC-Si_3N_4-25 (SPF-25 derived CMCs) and

C_f/PyC/SiC-Si_3N_4-30 (SPF-30 derived CMCs), a sudden drop in flexural strength to 22 ± 9 MPa and 21 ± 2 MPa respectively, was obtained. The fractograph of CMCs showed fiber pull-out phenomenon for C_f/PyC/SiC-Si_3N_4-5 to C_f/PyC/SiC-Si_3N_4-20 composites and hence failed in a ductile manner. In the case of C_f/PyC/SiC-Si_3N_4-25 and C_f/PyC/SiC-Si_3N_4-30 composites, partial delamination between F/M interface was observed which led to premature failure of the composite. This unusual behavior of C_f/PyC/SiC-Si_3N_4-25 and C_f/PyC/SiC-Si_3N_4-30 composites was attributed to structurally weak points like high propensity of cracks or pores in the matrix compared to the other composites. This study demonstrated that, high density and low porosity of C_f/PyC/SiC-Si_3N_4 composites are highly suitable for achieving high mechanical properties for CMCs. The study established SPF-20 as the most suitable formulation for the fabrication of CMCs with improved mechanical properties by PIP process.

Studies on BCTS resin as oxidation resistance coating for CMCs

In the previous chapter, SPF based CMCs were fabricated to achieve improved mechanical properties. However, for the long-term service life, these composites have to be highly engineered in order to improve their oxidation resistance and *self-healing* behaviour. Hence, to have improved oxidation resistance as well, synthesis of a single source preceramic matrix resin containing silicon, boron and nitrogen was attempted to get SiBCN based ceramics.

This chapter is comprised of two parts;

➢ In the first part, studies on synthesis, characterization and ceramic conversion of BCTS resins were carried out. BCTS resins were synthesized by reacting boric acid with CTS in the molar ratio of 1:1, 1:3 and 1:5. FT-IR and NMR investigations revealed the formation of BCTS *via* self and co-condensation reaction mechanism. This resulted in optimum properties for preceramic polymers such as solubility in common solvents, processable viscosity (< 20 cps) and high ceramic yield (>80 wt. %). The polymer to ceramic conversion was carried out at 1450°C and 1650°C under nitrogen atmosphere. The study revealed that changes in CTS concentration and pyrolysis temperatures significantly affected the evolution of ceramic phases, morphology and elemental

composition which were thoroughly investigated through XRD, SEM and HRTEM techniques. The increase in the CTS concentration and pyrolysis temperature resulted in an increase of carbothermal reduction of SiBNC(O) ceramic. As a result, BCTS with the molar ratio of 1:1 and BCTS with the molar ratio of 1:3 led to the formation of β-SiC, β-Si_3N_4 and oxide ceramic phases. In the case of BCTS with the molar ratio of 1:5, oxide free β-SiC, β-Si_3N_4 and turbostatic BN(C) ceramics were obtained. In this study, we report the synthesis of a new, low viscous preceramic polymer with high ceramic yield (>80 wt. %). BCTS with the molar ratio of 1:5 was demonstrated as a suitable preceramic polymer to attain oxide free SiBCN ceramics.

➢ In the second part of the investigation, BCTS with the molar ratio of 1:5 (BCTS15) was used as an oxidation protection coating to improve the lifetime of the CMCs. Towards this, two CMC were selected from the previous chapters, namely C_f/PyC/SiBOC-30 (BPFSi-30 derived CMCs) and C_f/PyC/SiC-Si_3N_4-20 (SPF-20 derived CMCs) composites due to their better mechanical properties as compared to the other composites. These CMCs were infiltrated with BCTS15 resin *via* vacuum infiltration technique (denoted as C_f/PyC/SiBOC-30/SiBCN15 and C_f/PyC/SiC-Si_3N_4-20/SiBCN15) and their oxidation resistance property was investigated at three different temperatures *viz.* 1000°C, 1250°C and 1500°C. The results clearly revealed significant changes in the weight loss, oxidation rate and the morphology of CMCs before and after the infiltration. At 1000°C and 1250°C, C_f/PyC/SiBOC-30 and C_f/PyC/SiBOC-30/SiBCN15 composites showed better oxidation resistance due to the formation of $B_2O_3.xSiO_2$ phase; whereas, in the case of C_f/PyC/SiC-Si_3N_4-20 and C_f/PyC/SiC-Si_3N_4-20/SiBCN15 composites complete oxidation of carbon fibers were observed, indicating the importance of boron in protecting the CMCs at relatively lower temperature. Surprisingly, on increasing the oxidation temperature to 1500°C, except C_f/PyC/SiBOC-30/SiBCN15 composite, all other CMCs resulted in the oxidation of carbon fibers. This prolonged stability of C_f/PyC/SiBOC-30/SiBCN15 composite is attributed to the presence of BN(C) ceramic phase in SiBCN ceramic matrix, which prevented the decomposition of $B_2O_3.xSiO_2$ phase imparting the extended *self-healing* property. The study demonstrated the capability of BCTS as oxidation protection

coating for improving the life-time of CMCs in an oxidative atmosphere.

To summarize,

(i) A new class of cost effective preceramic polymers based on phenol-formaldehyde resin and single source preceramic polymer resin containing silicon, boron, carbon and nitrogen was developed.

(ii) The preceramic polymers showed optimum properties such as solubility in common solvents, good processablity and moderately high ceramic residue (> 60 wt.%).

(iii) The preceramic polymers as matrix resin for CMCs showed moderate mechanical properties with excellent self-healing properties.

Future Perspectives

Based on the present results, the future perspectives of this research work are:

(i) The present study showed moderate mechanical properties. Further, investigation can be extended on the improvement of their mechanical properties by fabricating CMCs with high strength (T300J) and high modulus (M40J) carbon fibers as reinforcement.

(ii) The present study showed high temperature (1500°C) applicability of developed ceramics. Further, investigations can be extended on the improvement of their operating temperature (>2000°C) through chemical modification of the preceramic polymer with metal [Ti, Zr, Hf, etc.,] alkoxides to form ultra-high temperature ceramics.

(iii) Investigation of the SPF derived SiCN and BCTS derived SiBCN ceramics as potential electrode active materials for energy storage applications.

References

(1966). "Encyclopedia of industrial chemical analysis. Vol. 1, General Techniques A-E. Edited by F. D. Snell and C. L. Hilton. Interscience Publishers, a div. of John Wiley & Sons., Inc., 605 Third Ave., New York, N. Y. 10016, 1966. xv + 763 pp. 18.5 × 26 cm. Price $35.00 per copy with subscription. $45.00 per single copy." *Journal of Pharmaceutical Sciences,* **55**(9): 993-994.

Abdalla M. O., Ludwick A. and Mitchell T. (2003). "Boron-modified phenolic resins for high performance applications." *Polymer,* **44**(24): 7353-7359.

Agarwal B. D., Broutman L. J. and Chandrashekhara K. (2017). *Analysis and performance of fiber composites*, John Wiley & Sons.

Al Nasiri N., Patra N., Ni N., Jayaseelan D. D. and Lee W. E. (2016). "Oxidation behaviour of SiC/SiC ceramic matrix composites in air." *Journal of the European Ceramic Society,* **36**(14): 3293-3302.

Babu T. G. and Devasia R. (2016). "Boron Modified Phenol Formaldehyde Derived Cf/SiBOC Composites with Improved Mechanical Strength for High Temperature Applications." *Journal of Inorganic and Organometallic Polymers and Materials,* **26**(4): 764-772.

Bahloul D., Pereira M. and Goursat P. (1993). "Preparation of silicon carbonitrides from an organosilicon polymer: II, thermal behavior at high temperatures under argon." *Journal of the American Ceramic Society,* **76**(5): 1163-1168.

Bahloul D., Pereira M., Goursat P., Yive N. and Corriu R. J. (1993). "Preparation of Silicon Carbonitrides from an Organosilicon Polymer: I, Thermal Decomposition of the Cross-linked Polysilazane." *Journal of the American Ceramic Society,* **76**(5): 1156-1162.

Baldus P., Jansen M. and Sporn D. (1999). "Ceramic fibers for matrix composites in high-temperature engine applications." *Science,* **285**(5428): 699-703.

Bansal N. P. (2006). *Handbook of ceramic composites*, Springer Science & Business Media.

Barros P. M., Yoshida I. V. P. and Schiavon M. A. (2006). "Boron-containing poly (vinyl alcohol) as a ceramic precursor." *Journal of non-crystalline solids,* **352**(32): 3444-3450.

Bertrand R., Henne J.-F., Camus G. and Rebillat F. (2017). "Influence of the Cooling Temperature on the Mechanical Behavior of an Oxidized Self-Healing Ceramic Matrix Composite." *Oxidation of Metals,* **88**(3-4): 237-246.

Brennan J. J. and Prewo K. M. (1982). "Silicon carbide fibre reinforced glass-ceramic matrix composites exhibiting high strength and toughness." *Journal of Materials Science,* **17**(8): 2371-2383.

Buckley J. D. and Edie D. D. (1993). *Carbon-carbon materials and composites*, William Andrew.

Budiansky B., Hutchinson J. W. and Evans A. G. (1986). "Matrix fracture in fiber-

reinforced ceramics." *Journal of the Mechanics and Physics of Solids,* **34**(2): 167-189.

Buet E., Sauder C., Sornin D., Poissonnet S., Rouzaud J.-N. and Vix-Guterl C. (2014). "Influence of surface fibre properties and textural organization of a pyrocarbon interphase on the interfacial shear stress of SiC/SiC minicomposites reinforced with Hi-Nicalon S and Tyranno SA3 fibres." *Journal of the European Ceramic Society,* **34**(2): 179-188.

C1341 A. (2013). "Standard Test Method for Flexural Properties of Continuous Fiber-Reinforced Advanced Ceramic Composites, ASTM International, West

Conshohocken, PA, 2013." *www.astm.org*.

Camus G., Guillaumat L. and Baste S. (1996). "Development of damage in a 2D woven C/SiC composite under mechanical loading: I. Mechanical characterization." *Composites Science and Technology,* **56**(12): 1363-1372.

Cao X., Vassen R. and Stoever D. (2004). "Ceramic materials for thermal barrier coatings." *Journal of the European Ceramic Society,* **24**(1): 1-10.

Cao X., Yin X., Fan X., Cheng L. and Zhang L. (2014). "Effect of PyC interphase thickness on mechanical behaviors of SiBC matrix modified C/SiC composites fabricated by reactive melt infiltration." *Carbon,* **77**: 886-895.

Carrère N., Martin E. and Lamon J. (2000). "The influence of the interphase and associated interfaces on the deflection of matrix cracks in ceramic matrix composites." *Composites Part A: Applied Science and Manufacturing,* **31**(11): 1179-1190.

Carrère P. and Lamon J. (2003). "Creep behaviour of a SiC/Si-BC composite with a self-healing multilayered matrix." *Journal of the European Ceramic Society,* **23**(7): 1105-1114.

čerović L. S., Milonjić S. and Bibić N. (1995). "Influence of boric acid concentration on silicon carbide morphology." *Journal of materials science letters,* **14**(15): 1052-1054.

Chamberlain A. L. and Lazur A. J. (2014). Sic based ceramic matrix composites with layered matrices and methods for producing sic based ceramic matrix composites with layered matrices, Google Patents.

Chand S. (2000). "Review carbon fibers for composites." *Journal of Materials Science,* **35**(6): 1303-1313.

Chawla K. K. (1998). Ceramic matrix composites. *Composite Materials*, Springer**:** 212-251.

Chermant J., Boitier G., Darzens S., Farizy G., Vicens J. and Sangleboeuf J.-C. (2002). "The creep mechanism of ceramic matrix composites at low temperature and stress, by a material science approach." *Journal of the European Ceramic Society,* **22**(14): 2443-2460.

Chiang C.-L. and Ma C.-C. M. (2004). "Synthesis, characterization, thermal properties and flame retardance of novel phenolic resin/silica nanocomposites." *Polymer Degradation and Stability,* **83**(2): 207-214.

Chongjun L., Boxin M., Xiaoxu H. and Zhibiao H. (1997). "The Catalytic Graphitization Effects of B_4C in C/C Composites [J]." *AEROSPACE MATERIALS & TECHNOLOGY,* **5**: 007.

Christin F. (2002). "Design, fabrication, and application of thermostructural composites (TSC) like C/C, C/SiC, and SiC/SiC composites." *Advanced engineering materials,* **4**(12): 903-912.

Cluzel C., Baranger E., Ladevèze P. and Mouret A. (2009). "Mechanical behaviour and lifetime modelling of self-healing ceramic-matrix composites subjected to thermomechanical loading in air." *Composites Part A: Applied Science and Manufacturing,* **40**(8): 976-984.

Conde O., Silvestre A. and Oliveira J. (2000). "Influence of carbon content on the crystallographic structure of boron carbide films." *Surface and Coatings Technology,* **125**(1): 141-146.

Curtin W. A. (1991). "Theory of mechanical properties of ceramic-matrix composites." *Journal of the American Ceramic Society,* **74**(11): 2837-2845.

Di Salvo D., Sackett E., Johnston R., Thompson D., Andrews P. and Bache M. (2015). "Mechanical characterisation of a fibre reinforced oxide/oxide ceramic matrix composite." *Journal of the European Ceramic Society,* **35**(16): 4513-4520.

Ding J., Huang Z., Qin Y., Luo H. and Mao J. (2015). *The effect of boron incorporation on the thermo-oxidative stability of phenol-formaldehyde resin and its pyrolyzate phase*. 2015 International Conference on Materials, Environmental and Biological Engineering, Atlantis Press.

Domnich V., Reynaud S., Haber R. A. and Chhowalla M. (2011). "Boron carbide: structure, properties, and stability under stress." *Journal of the American Ceramic Society,* **94**(11): 3605-3628.

Dong-Xiao H. (2006). "Review of the Application of Advanced Composite in Aviation and Aerospace [J]." *Hi-Tech Fiber & Application,* **2**: 002.

Draper A. B. and Owusu Y. A. (1976). *Role of Carbonaceous Materials at the Mold-metal Interface: Final Report Submitted to American Foundrymen's Society*, Pennsylvania State University, College of Engineering.

Evans A. G. and Marshall D. B. (1989). "Overview no. 85 The mechanical behavior of ceramic matrix composites." *Acta Metallurgica,* **37**(10): 2567-2583.

Feng L., Guangwu W. and Zhaoxiang H. (2006). "Thermal Stability and Crystallization Process of SiBONC Ceramics Derived from Polymeric Precursors." *Rare Metal Materials and Engineering,* **35**: 228.

Feng L., Li K., Xue B., Fu Q. and Zhang L. (2017). "Optimizing matrix and fiber/matrix interface to achieve combination of strength, ductility and toughness in carbon nanotube-reinforced carbon/carbon composites." *Materials & Design,* **113**: 9-16.

Ferrari A. C. and Robertson J. (2000). "Interpretation of Raman spectra of disordered and amorphous carbon." *Physical review B,* **61**(20): 14095.

Ferrari A. C. and Robertson J. (2004). "Raman spectroscopy of amorphous,

nanostructured, diamond–like carbon, and nanodiamond." *Philosophical Transactions of the Royal Society of London A: Mathematical, Physical and Engineering Sciences,* **362**(1824): 2477-2512.

Ferrari A. C. and Robertson J. (2004). "Raman spectroscopy of amorphous, nanostructured, diamond–like carbon, and nanodiamond." *Philosophical Transactions of the Royal Society of London. Series A: Mathematical, Physical and Engineering Sciences,* **362**(1824): 2477-2512.

Figueiredo J. L., Bernardo C., Baker R. and Hüttinger K. (2013). *Carbon fibers filaments and composites*, Springer Science & Business Media.

Fitzer E. (1987). "The future of carbon-carbon composites." *Carbon,* **25**(2): 163-190.

Fitzer E. (1989). "Pan-based carbon fibers—present state and trend of the technology from the viewpoint of possibilities and limits to influence and to control the fiber properties by the process parameters." *Carbon,* **27**(5): 621-645.

Flores O., Bordia R. K., Nestler D., Krenkel W. and Motz G. (2014). "Ceramic fibers based on SiC and SiCN systems: Current research, development, and commercial status." *Advanced Engineering Materials,* **16**(6): 621-636.

Frank E., Ingildeev D. and Buchmeiser M. (2016). "High-performance PAN-based carbon fibers and their performance requirements." *Structure and Properties of High-Performance Fibers*: 7.

Ganesh Babu T. and Devasia R. (2016). "Boron-modified phenol formaldehyde resin-based self-healing matrix for Cf/SiBOC composites." *Advances in Applied Ceramics,* **115**(8): 457-469.

Ganesh Babu T. and Devasia R. (2016). "Boron-modified phenol formaldehyde resin-based self-healing matrix for Cf/SiBOC composites." *Advances in Applied Ceramics*: 1-13.

Gao J. G., Lin H. J. and Ma Y. Y. (2011). *Systhesis, Curing and Thermal Propertied of Boron-Containing o-Cresol-Formaldehyde Resin*. Advanced Materials Research, Trans Tech Publ.

Gao Y., Bando Y., Kurashima K. and Sato T. (2001). "The microstructural analysis of SiC nanorods synthesized through carbothermal reduction." *Scripta materialia,* **44**(8): 1941-1944.

Gao Y., Bando Y., Kurashima K. and Sato T. (2002). "SiC nanorods prepared from SiO and activated carbon." *Journal of materials science,* **37**(10): 2023-2029.

Gao Y., Mera G., Nguyen H., Morita K., Kleebe H.-J. and Riedel R. (2012). "Processing route dramatically influencing the nanostructure of carbon-rich SiCN and SiBCN polymer-derived ceramics. Part I: Low temperature thermal transformation." *Journal of the European Ceramic Society,* **32**(9): 1857-1866.

Gay D. (2014). *Composite materials: design and applications*, CRC press.

Gibson R. F. (2010). "A review of recent research on mechanics of multifunctional composite materials and structures." *Composite structures,* **92**(12): 2793-2810.

Golczewski J. A. and Aldinger F. (2004). "Thermodynamic modeling of amorphous Si–C–N ceramics derived from polymer precursors." *Journal of non-crystalline solids,* **347**(1): 204-210.

Golovko É., Makarenko G., Voitovich R. and Fedorus V. (1994). "Oxidation of boron silicide and materials based on it." *Powder Metallurgy and Metal Ceramics,* **32**(11-12): 917-920.

Gosset D., Colin C., Jankowiak A., Vandenberghe T. and Lochet N. (2013). "X-ray Diffraction Study of the Effect of High-Temperature Heat Treatment on the Microstructural Stability of Third-Generation SiC Fibers." *Journal of the American Ceramic Society,* **96**(5): 1622-1628.

Hackemann S., Flucht F. and Braue W. (2010). "Creep investigations of alumina-based all-oxide ceramic matrix composites." *Composites Part A: Applied Science and Manufacturing,* **41**(12): 1768-1776.

Hagio T., Nakamizo M. and Kobayashi K. (1987). "Thermal conductivities and Raman spectra of boron-doped carbon materials." *Carbon,* **25**(5): 637-639.

Halbig M. C., Jaskowiak M. H., Kiser J. D. and Zhu D. (2013). *Evaluation of ceramic matrix composite technology for aircraft turbine engine applications*. 51st AIAA Aerospace Sciences Meeting including the New Horizons Forum and Aerospace Exposition.

Hata T., Bonnamy S., Bronsveld P., Castro V., Fujisawa M., Kikuchi H. and Imamura Y. "SiC Nanorods grown on SiC coated Wood Charcoal."

Hilton F. D. S. a. C. L. (1966). "Encyclopedia of industrial chemical analysis. Vol. 1, General Techniques A-E. Edited by F. D. Snell and C. L. Hilton. Interscience Publishers, a div. of John Wiley & Sons., Inc., 605 Third Ave., New York, N. Y. 10016, 1966. xv + 763 pp. 18.5 × 26 cm. Price $35.00 per copy with subscription. $45.00 per single copy." *Journal of Pharmaceutical Sciences,* **55**(9): 993-994.

Hnatko M., Galusek D. and Šajgalík P. (2004). "Low-cost preparation of Si 3 N 4–SiC micro/nano composites by in-situ carbothermal reduction of silica in silicon nitride matrix." *Journal of the European Ceramic Society,* **24**(2): 189-195.

Hsiue G. H., Shiao S. J., Wei H. F., Kuo W. J. and Sha Y. A. (2001). "Novel phosphorus-containing dicyclopentadiene-modified phenolic resins for flame-retardancy applications." *Journal of applied polymer science,* **79**(2): 342-349.

Hynes J. T., Hynes B. J., Jackson T. B. and Hon W. (2016). Polymer matrix-ceramic matrix hybrid composites for high thermal applications, Google Patents.

Inagaki M., Tachikawa H., Nakahashi T., Konno H. and Hishiyama Y. (1998). "The chemical bonding state of nitrogen in kapton-derived carbon film and its effect on the graphitization process." *Carbon,* **36**(7): 1021-1025.

Ionescu E., Kleebe H.-J. and Riedel R. (2012). "Silicon-containing polymer-derived ceramic nanocomposites (PDC-NCs): preparative approaches and properties." *Chemical Society Reviews,* **41**(15): 5032-5052.

Jacobson N. S. and Curry D. M. (2006). "Oxidation microstructure studies of reinforced

carbon/carbon." *Carbon,* **44**(7): 1142-1150.

Jiménez C., Mergia K., Lagos M., Yialouris P., Agote I., Liedtke V., Messoloras S., Panayiotatos Y., Padovano E. and Badini C. (2016). "Joining of ceramic matrix composites to high temperature ceramics for thermal protection systems." *Journal of the European Ceramic Society,* **36**(3): 443-449.

Jones R., Szweda A. and Petrak D. (1999). "Polymer derived ceramic matrix composites." *Composites Part A: Applied Science and Manufacturing,* **30**(4): 569-575.

Kalaiyarasan A., Ramesh P. and Paramasivam P. (2016). "Study of Advanced Composite Materials in Aerospace Application."

Kalpakjian S. and Schmid S. R. (2014). *Manufacturing engineering and technology*, Pearson Upper Saddle River, NJ, USA.

Kawamoto A. M., Pardini L. C., Diniz M. F., Lourenço V. L. and Takahashi M. F. K. (2010). "Synthesis of a boron modified phenolic resin." *Journal of Aerospace Technology and Management,* **2**(2): 169-182.

Kentgens A. (1997). "A practical guide to solid-state NMR of half-integer quadrupolar nuclei with some applications to disordered systems." *Geoderma,* **80**(3-4): 271-306.

Kerans R. J., Hay R. S., Pagano N. J. and Parthasarathy T. (1989). "The role of the fiber-matrix interface in ceramic composites." *American Ceramic Society Bulletin,* **68**(2): 429-442.

Kerans R. J., Hay R. S., Parthasarathy T. A. and Cinibulk M. K. (2002). "Interface Design for Oxidation-Resistant Ceramic Composites." *Journal of the American Ceramic Society,* **85**(11): 2599-2632.

Kiser J. D., Grady J. E., Bhatt R. T., Wiesner V. L. and Zhu D. (2016). "Overview of CMC (Ceramic Matrix Composite) Research at the NASA Glenn Research Center."

Knop A. and Pilato L. A. (2013). *Phenolic resins: chemistry, applications and performance*, Springer Science & Business Media.

Knop A. and Scheib W. (1979). *Chemistry and application of phenolic resins*, Springer.

Kong J., Wang M., Zou J. and An L. (2015). "Soluble and meltable hyperbranched polyborosilazanes toward high-temperature stable SiBCN ceramics." *ACS applied materials & interfaces,* **7**(12): 6733-6744.

Krenkel W. (2004). "Carbon Fiber Reinforced CMC for High-Performance Structures." *International Journal of applied ceramic technology,* **1**(2): 188-200.

Krenkel W. (2008). *Ceramic matrix composites: fiber reinforced ceramics and their applications*, John Wiley & Sons.

Krenkel W. (2009). *Cost effective processing of CMC composites by melt infiltration (LSI-process)*. Ceramic Engineering and Science Proceedings.

Krenkel W. and Berndt F. (2005). "C/C–SiC composites for space applications and advanced friction systems." *Materials Science and Engineering: A,* **412**(1): 177-181.

Krenkel W., Heidenreich B. and Renz R. (2002). "C/C-SiC Composites for Advanced

Friction Systems." *Advanced Engineering Materials,* **4**(7): 427-436.

Kumar Mandal A. (2010). *Standard Test Method for Apparent Porosity, Water Absorption, Apparent Specific Gravity and Bulk Density of Burned Refractory Brick and Shapes by Boiling Water, ASTM C 20–92.*

Lamouroux F., Bertrand S., Pailler R., Naslain R. and Cataldi M. (1999). "Oxidation-resistant carbon-fiber-reinforced ceramic-matrix composites." *Composites science and technology,* **59**(7): 1073-1085.

Lamouroux F., Steen M. and Valles J. (1994). "Uniaxial tensile and creep behaviour of an alumina fibre-reinforced ceramic matrix composite: I. Experimental study." *Journal of the European Ceramic Society,* **14**(6): 529-537.

Lee J. and Baney R. (2003). Process for SiBCN based preceramic polymers and products derivable therefrom, Google Patents.

Lee S. H., Weinmann M. and Aldinger F. (2008). "Processing and properties of C/Si–B–C–N fiber–reinforced ceramic matrix composites prepared by precursor impregnation and pyrolysis." *Acta Materialia,* **56**(7): 1529-1538.

Lee Y. K., Kim D. J., Kim H. J., Hwang T. S., Rafailovich M. and Sokolov J. (2003). "Activation energy and curing behavior of resol-and novolac-type phenolic resins by differential scanning calorimetry and thermogravimetric analysis." *Journal of applied polymer science,* **89**(10): 2589-2596.

Levi C. G., Yang J. Y., Dalgleish B. J., Zok F. W. and Evans A. G. (1998). "Processing and Performance of an All-Oxide Ceramic Composite." *Journal of the American Ceramic Society,* **81**(8): 2077-2086.

Li C., Ma Z., Zhang X., Fan H. and Wan J. (2016). "Silicone-modified phenolic resin: Relationships between molecular structure and curing behavior." *Thermochimica Acta,* **639**: 53-65.

Li D., Yang Z., Jia D., Duan X., Wang S., Zhu Q., Miao Y., Rao J. and Zhou Y. (2017). "Effects of boron addition on the high temperature oxidation resistance of dense sSiBCN monoliths at 1500° C." *Corrosion Science*.

Li D., Yang Z., Jia D., Wu D., Zhu Q., Liang B., Wang S. and Zhou Y. (2016). "Microstructure, oxidation and thermal shock resistance of graphene reinforced SiBCN ceramics." *Ceramics International,* **42**(3): 4429-4444.

Li S., Chen F., Zhang B., Luo Z., Li H. and Zhao T. (2016). "Structure and improved thermal stability of phenolic resin containing silicon and boron elements." *Polymer degradation and stability*.

Liu C., Lin Y., Zhou Z. and Li K.-Y. (2017). "Dual phase amorphous carbon ceramic achieves theoretical strength limit and large plasticity." *Carbon,* **122**: 276-280.

Liu J., Li J. and Xu C. (2014). "Interaction of the cutting tools and the ceramic-reinforced metal matrix composites during micro-machining: a review." *CIRP Journal of Manufacturing Science and Technology,* **7**(2): 55-70.

Longbiao L., Yingdong S. and Youchao S. (2013). "Estimate interface shear stress of unidirectional C/SiC ceramic matrix composites from hysteresis loops." *Applied*

Composite Materials, **20**(4): 693-707.

Low I.-M. (2014). *Advances in ceramic matrix composites*, Woodhead Publishing.

Luan X. g., Liu Y., Yang W., Peng Y., Zhang L. and Cheng L. (2016). "Stressed oxidation behaviors of 2D C/SiC-BC x composite under wet oxygen atmosphere." *Journal of the European Ceramic Society,* **36**(11): 2673-2678.

Luo L., Ge M. and Zhang W. (2013). "Pyrolysis synthesis of Si–B–C–N ceramics and their thermal stability." *Ceramics International,* **39**(7): 7903-7909.

Luo L., Wang Y., Liu L., Zhao X., Lu Y. and Wang G. (2017). "Carbon fiber reinforced silicon carbide composite-based sharp leading edges in high enthalpy plasma flows." *Composites Part B: Engineering.*

Magnant J., Maillé L., Pailler R., Ichard J.-C., Guette A., Rebillat F. and Philippe E. (2012). "Carbon fiber/reaction-bonded carbide matrix for composite materials– manufacture and characterization." *Journal of the European Ceramic Society,* **32**(16): 4497-4505.

Matsushita J.-I. and Sawada Y. (1997). "Oxidation resistance of silicon tetra boride powder." *Nippon Seramikkusu Kyokai Gakujutsu Ronbunshi(Journal of the Ceramic Society of Japan)(Japan),* **105**(1226): 922-924.

Matsushita J. and Komarneni S. (2001). "High temperature oxidation of silicon hexaboride ceramics." *Materials research bulletin,* **36**(5): 1083-1089.

Mera G., Tamayo A., Nguyen H., Sen S. and Riedel R. (2010). "Nanodomain Structure of Carbon-Rich Silicon Carbonitride Polymer-Derived Ceramics." *Journal of the American Ceramic Society,* **93**(4): 1169-1175.

Miller R. A. (1997). "Thermal barrier coatings for aircraft engines: history and directions." *Journal of thermal spray technology,* **6**(1): 35-42.

Mondal S. and Banthia A. K. (2005). "Low-temperature synthetic route for boron carbide." *Journal of the European Ceramic Society,* **25**(2): 287-291.

Monthioux M. and Delverdier O. (1996). "Thermal behavior of (organosilicon) polymer-derived ceramics. V: Main facts and trends." *Journal of the European Ceramic Society,* **16**(7): 721-737.

Morrison J. (2010). Method for forming interphase layers in ceramic matrix composites, Google Patents.

Morrison J. A., Campbell C., Merrill G. B., Lane J. E., Thompson D. G., Albrecht H. A. and Shteyman Y. P. (2004). Ceramic matrix composite gas turbine vane, Google Patents.

Mouritz A., Gellert E., Burchill P. and Challis K. (2001). "Review of advanced composite structures for naval ships and submarines." *Composite structures,* **53**(1): 21-42.

Nair C. R. (2004). "Advances in addition-cure phenolic resins." *Progress in Polymer Science,* **29**(5): 401-498.

Najafi A., Golestani-Fard F. and Rezaie H. (2015). "Improvement of SiC nanopowder synthesis by sol–gel method via TEOS/resin phenolic precursors." *Journal of Sol-Gel Science and Technology,* **75**(2): 255-263.

Naslain R. (1993). "Fibre-matrix interphases and interfaces in ceramic matrix composites processed by CVI." *Composite Interfaces,* **1**(3): 253-286.

Naslain R. (1999). "Materials design and processing of high temperature ceramic matrix composites: state of the art and future trends." *Advanced composite materials,* **8**(1): 3-16.

Naslain R. (2004). "Design, preparation and properties of non-oxide CMCs for application in engines and nuclear reactors: an overview." *Composites Science and Technology,* **64**(2): 155-170.

Naslain R., Dugne O., Guette A., Sevely J., Brosse C. R., Rocher J. P. and Cotteret J. (1991). "Boron Nitride Interphase in Ceramic-Matrix Composites." *Journal of the American Ceramic Society,* **74**(10): 2482-2488.

Naslain R., Guette A., Rebillat F., Pailler R., Langlais F. and Bourrat X. (2004). "Boron-bearing species in ceramic matrix composites for long-term aerospace applications." *Journal of Solid State Chemistry,* **177**(2): 449-456.

Naslain R., Langlais F. and Fedou R. (1989). "The CVI-processing of ceramic matrix composites." *Le Journal de Physique Colloques,* **50**(C5): C5-191-C195-207.

Naslain R. R. (1998). "The design of the fibre-matrix interfacial zone in ceramic matrix composites." *Composites Part A: Applied Science and Manufacturing,* **29**(9): 1145-1155.

Naslain R. R. (2005). "SiC-Matrix Composites: Nonbrittle Ceramics for Thermo-Structural Application." *International Journal of Applied Ceramic Technology,* **2**(2): 75-84.

Nason H. K. (1939). Silicon modified phenolic resins and process for producing same, Google Patents.

Niihara K. (1991). "New design concept of structural ceramics." *Journal of the Ceramic Society of Japan,* **99**(1154): 974-982.

Noparvar-Qarebagh A., Roghani-Mamaqani H. and Salami-Kalajahi M. (2016). "Novolac phenolic resin and graphene aerogel organic-inorganic nanohybrids: High carbon yields by resin modification and its incorporation into aerogel network." *Polymer degradation and stability,* **124**: 1-14.

Odeshi A., Mucha H. and Wielage B. (2006). "Manufacture and characterisation of a low cost carbon fibre reinforced C/SiC dual matrix composite." *Carbon,* **44**(10): 1994-2001.

Ohnabe H., Masaki S., Onozuka M., Miyahara K. and Sasa T. (1999). "Potential application of ceramic matrix composites to aero-engine components." *Composites Part A: Applied Science and Manufacturing,* **30**(4): 489-496.

Peebles Jr L. (1995). "Carbon fibers, formation, structure and properties." *CRC Press, Inc, 2000 Corporate Blvd, NW, Boca Raton, FL 33431, USA, 1995. 224.*

References

Peters S. T. (2013). *Handbook of composites*, Springer Science & Business Media.

Quemard L., Rebillat F., Guette A., Tawil H. and Louchet-Pouillerie C. (2007). "Self-healing mechanisms of a SiC fiber reinforced multi-layered ceramic matrix composite in high pressure steam environments." *Journal of the European Ceramic Society,* **27**(4): 2085-2094.

Rajan V. P. and Zok F. W. (2014). "Matrix cracking of fiber-reinforced ceramic composites in shear." *Journal of the Mechanics and Physics of Solids,* **73**: 3-21.

Raman V., Parashar V. and Bahl O. (1997). "Influence of boric acid on the synthesis of silicon carbide whiskers from rice husks and polyacrylonitrile." *Journal of materials science letters,* **16**(15): 1252-1254.

Riedel R., Mera G., Hauser R. and Klonczynski A. (2006). "Silicon-based polymer-derived ceramics: synthesis properties and applications-a review dedicated to Prof. Dr. Fritz Aldinger on the occasion of his 65th birthday." *Journal of the Ceramic Society of Japan (日本セラミックス協会学術論文誌),* **114**(1330): 425-444.

Rizvi R., Anwer A., Fernie G., Dutta T. and Naguib H. (2016). "Multifunctional Textured Surfaces with Enhanced Friction and Hydrophobic Behaviors Produced by Fiber Debonding and Pullout." *ACS Applied Materials & Interfaces,* **8**(43): 29818-29826.

Rosso M. (2006). "Ceramic and metal matrix composites: Routes and properties." *Journal of Materials Processing Technology,* **175**(1): 364-375.

Ruggles-Wrenn M. and Jones T. (2013). "Tension–compression fatigue of a SiC/SiC ceramic matrix composite at 1200° C in air and in steam." *International Journal of Fatigue,* **47**: 154-160.

Sambell R., Bowen D. and Phillips D. (1972). "Carbon fibre composites with ceramic and glass matrices." *Journal of Materials Science,* **7**(6): 663-675.

Sanchez J. E. R., Riccione M. A. and Glispin J. C. (2013). Attaching ceramic matrix composite to high temperature gas turbine structure, Google Patents.

Schmidt H., Borchardt G., Müller A. and Bill J. (2004). "Formation kinetics of crystalline Si3N4/SiC composites from amorphous Si–C–N ceramics." *Journal of Non-Crystalline Solids,* **341**(1–3): 133-140.

Schmidt S., Beyer S., Knabe H., Immich H., Meistring R. and Gessler A. (2004). "Advanced ceramic matrix composite materials for current and future propulsion technology applications." *Acta Astronautica,* **55**(3): 409-420.

Shanyi D. (2007). "Advanced composite materials and aerospace engineering [J]." *Acta Materiae Compositae Sinica,* **1**: 000.

Shi F., Yin X., Fan X., Cheng L. and Zhang L. (2010). "A new route to fabricate SiB 4 modified C/SiC composites." *Journal of the European Ceramic Society,* **30**(9): 1955-1962.

Sommers A., Wang Q., Han X., T'Joen C., Park Y. and Jacobi A. (2010). "Ceramics and ceramic matrix composites for heat exchangers in advanced thermal systems—A

review." *Applied Thermal Engineering,* **30**(11): 1277-1291.

Soraru G. D., Babonneau F., Gervais C. and Dallabona N. (2000). "Hybrid RSiO1. 5/B2O3 gels from modified silicon alkoxides and boric acid." *Journal of sol-gel science and technology,* **18**(1): 11-19.

Soraru G. D., Dallabona N., Gervais C. and Babonneau F. (1999). "Organically Modified SiO2− B2O3 Gels Displaying a High Content of Borosiloxane (B− O− Si∶) Bonds." *Chemistry of materials,* **11**(4): 910-919.

Sreekanth D., Rameshbabu N. and Venkateswarlu K. (2012). "Effect of various additives on morphology and corrosion behavior of ceramic coatings developed on AZ31 magnesium alloy by plasma electrolytic oxidation." *Ceramics International,* **38**(6): 4607-4615.

Su J.-m., Cui H., SU Z.-a., GUO C., LI R.-z., LI Y.-d. and ZHOU S.-j. (2004). "RESEARCH OF 4D C/C COMPOSITE MATERIAL THROAT INSERT BY MIX WEAVED WITH CARBON FIBRE AND AXIAL CARBON ROD." *Carbon,* **1**: 002.

Sun J., Deemer C., Ellingson W. and Wheeler J. (2006). "NDT technologies for ceramic matrix composites: Oxide and nonoxide." *Materials evaluation,* **64**(1): 52-60.

Sung I. K., Christian, Mitchell M., Kim D. P. and Kenis P. J. A. (2005). "Tailored Macroporous SiCN and SiC Structures for High-Temperature Fuel Reforming." *Advanced Functional Materials,* **15**(8): 1336-1342.

Takeda M., Sakamoto J., Saeki A., Imai Y. and Ichikawa H. (2009). *High performance silicon carbide fiber Hi-Nicalon for ceramic matrix composites.* 19th Annual Conference on Composites, Advanced Ceramics, Materials, and Structures-A: Ceramic Engineering and Science Proceedings, Volume 16, John Wiley & Sons.

Tang B., Zhang Y., Hu S. and Feng B. (2016). "A dense amorphous SiBCN (O) ceramic prepared by simultaneous pyrolysis of organics and inorganics." *Ceramics International,* **42**(4): 5238-5244.

Tong C., Cheng L., Yin X., Zhang L. and Xu Y. (2008). "Oxidation behavior of 2D C/SiC composite modified by SiB 4 particles in inter-bundle pores." *Composites Science and Technology,* **68**(3): 602-607.

Toreki W., Batich C. D., Sacks M. D. and Morrone A. A. (1990). *Synthesis and applications of a vinylsilazane preceramic polymer.* 14th Annual Conference on Composites and Advanced Ceramic Materials, Part 2 of 2: Ceramic Engineering and Science Proceedings, Volume 11, Issue 9/10, Wiley Online Library.

Trassl S., Kleebe H. J., Störmer H., Motz G., Rössler E. and Ziegler G. (2002). "Characterization of the Free-Carbon Phase in Si-C-N Ceramics: Part II, Comparison of Different Polysilazane Precursors." *Journal of the American Ceramic Society,* **85**(5): 1268-1274.

Trassl S., Motz G., Rössler E. and Ziegler G. (2002). "Characterization of the Free-Carbon Phase in Precursor-Derived Si-C-N Ceramics: I, Spectroscopic Methods." *Journal of the American Ceramic Society,* **85**(1): 239-244.

Traßl S., Suttor D., Motz G., Rössler E. and Ziegler G. (2000). "Structural

characterisation of silicon carbonitride ceramics derived from polymeric precursors." *Journal of the European Ceramic Society,* **20**(2): 215-225.

Tressler R. E. (1999). "Recent developments in fibers and interphases for high temperature ceramic matrix composites." *Composites Part A: Applied Science and Manufacturing,* **30**(4): 429-437.

Triantou K., Mergia K., Perez B., Florez S., Stefan A., Ban C., Pelin G., Ionescu G., Zuber C. and Fischer W. (2017). "Thermal shock performance of carbon-bonded carbon fiber composite and ceramic matrix composite joints for thermal protection re-entry applications." *Composites Part B: Engineering,* **111**: 270-278.

Triantou K., Perez B., Marinou A., Florez S., Mergia K., Vekinis G., Barcena J., Rotärmel W., Zuber C. and de Montbrun À. (2017). "Performance of cork and ceramic matrix composite joints for re-entry thermal protection structures." *Composites Part B: Engineering,* **108**: 270-278.

Tuinstra F. and Koenig J. L. (1970). "Raman spectrum of graphite." *The Journal of Chemical Physics,* **53**(3): 1126-1130.

Wang H., Guo Q., Yang J., Liu Z., Zhao Y., Li J., Feng Z. and Liu L. (2013). "Microstructural evolution and oxidation resistance of polyacrylonitrile-based carbon fibers doped with boron by the decomposition of B4C." *Carbon,* **56**(0): 296-308.

Wang L., Cheng J., Qiao Z., Yang J. and Liu W. (2017). "Tribological behaviors of in situ TiB 2 ceramic reinforced TiAl-based composites under sea water environment." *Ceramics International,* **43**(5): 4314-4323.

Wang Z., Dong S., He P., Gao L., Zhou H., Yang J. and Jiang D. (2010). "Fabrication of carbon fiber reinforced ceramic matrix composites with improved oxidation resistance using boron as active filler." *Journal of the European Ceramic Society,* **30**(3): 787-792.

Wen G., Li F. and Song L. (2006). "Structural characterization and mechanical properties of SiBONC ceramics derived from polymeric precursors." *Materials Science and Engineering: A,* **432**(1): 40-46.

Wilson D., Withers J., Safadi B., Kowbel W., Loutfy R., Schetanov B., Kablov E., Scheglova T., Ulyanova T. and Titova L. (2001). "High temperature ceramic matrix composites."

Yajima S., Hayashi J. and Omori M. (1978). Silicon carbide fibers having a high strength and a method for producing said fibers, Google Patents.

Yu J., Ma X., Song Q., Zhao Y., Cao J. and Chen X. (2015). "The effect of B4C on the properties of graphite foam prepared by template method." *Materials Research Innovations,* **19**(S5): S5-118-S115-122.

Zhang C., Han K., Liu Y., Mou S., Chang X., Zhang H., Ni J. and Yu M. (2017). "A novel high yield polyborosilazane precursor for SiBNC ceramic fibers." *Ceramics International.*

Zhang C., Zhang Y., Zhao D., Hu H. and Zhang Z. (2013). "Mechanism of ablation of

3D C/ZrC–SiC composite under an oxyacetylene flame." *Corrosion Science,* **68**: 168-175.

Zhang P., Jia D., Yang Z., Duan X. and Zhou Y. (2012). "Progress of a novel non-oxide Si-BCN ceramic and its matrix composites." *Journal of Advanced Ceramics,* **1**(3): 157-178.

Zhang Y., Shen S. and Liu Y. (2013). "The effect of titanium incorporation on the thermal stability of phenol-formaldehyde resin and its carbonization microstructure." *Polymer degradation and stability,* **98**(2): 514-518.

Zhao H., Chen L., Luan X., Zhang X., Yun J. and Xu T. (2017). "Synthesis, pyrolysis of a novel liquid SiBCN ceramic precursor and its application in ceramic matrix composites." *Journal of the European Ceramic Society,* **37**(4): 1321-1329.

Zhao J.-C. and Westbrook J. H. (2003). "Ultrahigh-temperature materials for jet engines." *MRS bulletin,* **28**(9): 622-630.

Zhong D., Sano H., Zheng G.-B. and Uchiyama Y. (2005). "Graphitization behavior of the boron-containing carbon film derived from polyimide." *長崎大学工学部研究報告 ,* **35**(64): 63-67.

Zhou M., Lin T., Huang F., Zhong Y., Wang Z., Tang Y., Bi H., Wan D. and Lin J. (2013). "Highly conductive porous graphene/ceramic composites for heat transfer and thermal energy storage." *Advanced Functional Materials,* **23**(18): 2263-2269.

Zmihorska-Gotfryd A. (2006). "Phenol-formaldehyde resols modified by boric acid." *Polimery,*(5): 386-388.

List of Publications

a) Publications in International Journals

1. **Ganesh Babu T.**, Renjith Devasia "Boron-modified phenol formaldehyde resin-based self-healing matrix for C_f/SiBOC composites." **Advances in Applied Ceramics (2016): 1-13.**

2. **Ganesh Babu T.**, Renjith Devasia "Boron Modified Phenol Formaldehyde Derived C_f/SiBOC Composites with Improved Mechanical Strength for High Temperature Applications." **Journal of Inorganic and Organometallic Polymers and Materials (2016): 1-9.**

3. **Ganesh Babu T.**, Anil Painuly, Renjith Devasia "Novel silazane modified phenol formaldehyde derived C_f/PyC/SiC-Si_3N_4 composites with improved mechanical strength for thermo-structural applications" **[paper accepted in Material Today Proceedings, 2017].**

4. **Ganesh Babu T.**, Bhuvaneswari S, Renjith Devasia "Synthesis and ceramic conversion of novel silazane modified phenol formaldehyde resin" **[Under Review].**

5. **Ganesh Babu T.**, Renjith Devasia, "Novel, facile and low-cost synthetic route for SiBCN ceramics from boron modified cyclotrisilazane" **[communicated].**

6. Sandha G. Nair, K.J. Sreejith, S. Packrisamy, **Ganesh Babu T.**, "Polymer derived PyC interphase coating for C/SiBOC composites". **Material Chemistry and Physics 204 (2018) 179-186.**

b) Papers presented in conferences and seminars

1. **Poster presentation** on "Novel silazane modified phenol formaldehyde derived C_f/PyC/SiC-Si_3N_4 composites with improved mechanical strength for thermo-structural applications", International Conference on Advances in Materials and Manufacturing Applications [IConAMMA 2017], Amrita University, August 17-19 2017, Bangalore, India.

2. **Oral presentation** on "Boron Modified Phenol Formaldehyde derived C_f/SiBOC composites with improved mechanical strength for high temperature applications" at material research society of India-2016, IIST, Trivandrum, India.

3. **Oral presentation** on "Investigation on Boron Modified Phenol Formaldehyde Resin as Ceramic Precursors for C_f/SiC composites" at International Conference on Ceramic & Advanced Materials for Energy and Environment, December 14-17 2015, Bangalore, India.

4. **Poster presentation** on "Self-healing Si-B-C ceramics from boron modified phenolic resin for high temperature applications" presented at National conference on Recent Trends in Materials Science and Technology. Dated: 28-30th July 2014, IIST, Trivandrum, India.

Ganesh Babu T.

🏠 Senior Research Fellow
Ceramic Matrix Products Division,
Propellants, Polymers, Chemicals &
Materials Entity,
Vikram Sarabhai Space Centre,
Indian Space Research Organisation,
Thiruvananthapuram 695 022
Kerala, India.

☎ +91-9710235276
   +91-8157902274

✉ ganeshbabut@gmail.com

I. Personal Information:

Father's name	:	Thiyagarajan M.
Birth Date	:	15th September 1988
Gender	:	Male
Marital Status	:	Single
Languages Known	:	Tamil, Telugu, Malayalam and English
Nationality	:	Indian

II. Education:

Bachelor of Chemistry : University of Madras, Chennai, Tamilnadu, India
2009, 1st class (76.00 %) with Distinction

Master of Chemistry : Anna University, Chennai, Tamilnadu, India
2011, 1st class (CGPA 8.4/10).

Ph.D. in Chemistry : Cochin University of Science and Technology,
Cochin, Kerala, India, 2013- Cont.,
Thesis titled "Studies on polymer derived SiC
based ceramics and ceramic matrix composites
for high temperature applications".

III. Research Interests:

- Polymer derived ceramics
- High temperature and Ultra high temperature ceramic materials

- Ceramic matrix composites
- High temperature oxidation resistant coatings
- Porous ceramic materials
- Ceramic materials for energy storage applications
- Organic Inorganic hybrid materials
- Super-hydrophobic materials

IV.   Research Experience:

- 2013- Cont.   :   ISRO Research Fellow,
  Vikram Sarabhai Space Centre,
  Thiruvananthapuram, Kerala, India.

- 2011-2013   :   Junior Executive in R&D,
  Susira Industries,
  Chennai, Tamilnadu, India.

- 2011   :   M.Sc., Project
  Titled "Development of organic-inorganic hybrid membrane" Anna University, Chennai, Tamilnadu, India

V.   Fellowship:

- Indian Space Research Organisation Fellowship for Ph. D. research (2013-Cont.).

VI.   Research publications and Conferences

a) Publications in International Journals

1. **Ganesh Babu T.,** Renjith Devasia "Boron-modified phenol formaldehyde resin-based self-healing matrix for C_f/SiBOC composites." **Advances in Applied Ceramics (2016): 1-13.**

2. **Ganesh Babu T.,** Renjith Devasia "Boron Modified Phenol Formaldehyde Derived C_f/SiBOC Composites with Improved Mechanical Strength for High Temperature Applications." **Journal of Inorganic and Organometallic Polymers and Materials (2016): 1-9.**

3. **Ganesh Babu T.,** Anil Painuly, Renjith Devasia "Novel silazane modified phenol formaldehyde derived C_f/PyC/SiC-Si_3N_4 composites with improved mechanical strength for thermo-structural applications" **[paper accepted in Material Today Proceedings, 2017].**

4. **Ganesh Babu T.,** Bhuvaneswari S, Renjith Devasia "Synthesis and ceramic conversion of novel silazane modified phenol formaldehyde resin" **[Under Review].**

5. **Ganesh Babu T.,** Renjith Devasia, "Novel, facile and low-cost synthetic route for SiBCN ceramics from boron modified cyclotrisilazane" **[Communicated].**

6. Sandha G. Nair, K.J. Sreejith, S. Packrisamy, **Ganesh Babu T.,** "Polymer derived PyC interphase coating for C/SiBOC composites". **Material Chemistry and Physics 204 (2018) 179-186.**

b) Papers presented in conferences and seminars

1. **Poster presentation** on "Novel silazane modified phenol formaldehyde derived C_f/PyC/SiC-Si_3N_4 composites with improved mechanical strength for thermo-structural applications", International Conference on Advances in Materials and Manufacturing Applications [IConAMMA 2017], Amrita University, August 17-19 2017, Bangalore, India.

2. **Oral presentation** on "Boron Modified Phenol Formaldehyde derived C_f/SiBOC composites with improved mechanical strength for high temperature applications" at material research society of India-2016, IIST, Trivandrum, India.

3. **Oral presentation** on "Investigation on Boron Modified Phenol Formaldehyde Resin as Ceramic Precursors for C_f/SiC composites" at International Conference on Ceramic & Advanced Materials for Energy and Environment, December 14-17 2015, Bangalore, India.

4. **Poster presentation** on "Self-healing Si-B-C ceramics from boron modified phenolic resin for high temperature applications" presented at National conference on Recent Trends in Materials Science and Technology. Dated: 28-30th July 2014, IIST, Trivandrum, India.

This bio-data is a true and accurate declaration of my activities and accomplishments. I certify that the information furnished in this bio-data is true to the best of my knowledge and belief.

Place: Thiruvananthapuram, Kerala   Ganesh Babu T.